EXPERIMENTAL STUDIES OF ATMOSPHERIC CHANGES (ESAC)

BELGISCH INSTITUUT VOOR RUIMTE AERONOMIE
Ringlaan 3
B-1180 BRUSSEL
M. DE MAZIÈRE (coordinator CG/DD/01A)

UNIVERSITÉ LIBRE DE BRUXELLES
LABO. DE CHIMIE PHYSIQUE MOLÉCULAIRE
Avenue F.D. Roosevelt 50 CP 160/09
B-1050 BRUXELLES
R. COLIN (promoter CG/DD/01B)

KONINKLIJK METEOROLOGISCH INSTITUUT VAN BELGIË
Ringlaan 3
B-1180 BRUSSEL
D. DE MUER (promoter CG/DD/01C)

UNIVERSITÉ DE LIÈGE
INSTITUT D'ASTROPHYSIQUE ET DE GÉOPHYSIQUE
Avenue de Cointe 5
B-4000 LIEGE
R. ZANDER (promoter CG/DD/01D)

TABLE OF CONTENTS

ABSTRACT

This document is the final scientific report for the project ESAC, Experimental Studies of Atmospheric Changes, a project contributing to the Global Change and Sustainable Development Programme of the Belgian Prime Minister's Services - Federal Offices for Scientific, Technical and Cultural Affairs. It integrates the achievements obtained during the project (1/12/1996- 31/5/2001) by all four partners collaborating in the project. They are the Belgian Institute for Space Aeronomy (BIRA-IASB), the Laboratoire de Chimie Physique Moléculaire of the Université Libre de Bruxelles (LCPM-ULB), the Royal Meteorological Institute of Belgium (KMI-IRM), and the Institut d'Astrophysique et de Géophysique of the Université de Liège (ULg).

The project aims at a better understanding of the Earth atmospheric composition and chemical processes, from ground level up to the stratosphere, and at an assessment of the atmosphere's actual state and evolution. To achieve this goal, ESAC relies on the acquisition, analysis and geophysical interpretation of atmospheric data. Data are collected at four European stations that belong to the Network for the Detection of Stratospheric Change, and are complemented with *in situ* and satellite data, campaign observations, and model simulations. The four stations are Ukkel (Belgium, 50.5°N, 4.3°E), Jungfraujoch in the Swiss Alps (46.5°N, 8°E), Harestua (Norway, 60.2°N, 10.7°E), and Observatoire de Haute Provence (France, 44°N, 6°E). Studies concerning the consistency between the various data sets have been performed to enable synergistic use of all the data.

Starting from state of the art experimental techniques and numerical models, more performant instruments, advanced data acquisition and analysis methods, and new modelling activities have been developed. Particular progress has been made in tropospheric composition measurements, including the development of vertical inversion algorithms, and in the investigations of fast twilight photochemistry of species like OClO.

Existing time series of atmospheric species concentrations and of UV spectral irradiances have been improved for quality and consistency, and have been updated with four and a half years of data. The actual extent of the time series has allowed to identify and quantify changes in the rates of increase for some gases and families, an issue that is of special importance to assess the effectiveness and further requirements of international regulations like the Montreal Protocol and its successive Amendments, and the Kyoto Protocol. For example for inorganic chlorine above the Jungfraujoch, the turnover time of maximum abundance has been observed around 1998 ; it has been evaluated against the expected evolution when

taking into account the gradual phase out of chlorine-bearing emissions. Height-resolved trends of ozone above Ukkel have been updated, based on a homogenized and validated time series of soundings since 1969.

Particular events have been investigated, such as the impact of the Mt. Pinatubo eruption of summer 1991 on the evolution of the NO_2 abundance above the Jungfraujoch. Tropospheric process studies have been made, including an evaluation of the boundary layer O_3 budget and measurements of pollution in Brussels.

A reanalysis of all occultations performed with the Atmospheric Trace Molecule Spectroscopy (ATMOS) instrument during 4 shuttle-based space missions has allowed to produce an improved "Version 3" set of geophysical data for over 30 atmospheric species. This has resulted in volume mixing ratio profiles now extending throughout the entire stratosphere and further down into the free troposphere, thus demonstrating that infrared remote sensing from space can be used to consistently investigate the exchanges between the upper troposphere and lower stratosphere

The field measurements are supported by high-quality laboratory experiments. New and/or improved spectroscopic parameters for a number of atmospherically relevant species (NO_2, O_2, H_2O, some HCFC, ...) have been obtained and provided to the community.

The achievements made in ESAC have been valorised on a national and international level, through many communications, publications, participations to symposia, working groups and assessment efforts, through contributions to European research projects and international programmes, and through the dissemination of results and the submission of data to international databases. The public has been informed through participation to colloquia and expositions for a large audience, and the distribution of brochures. During ESAC, the procedure for UV index forecasting has been established and implemented, and the daily publication of the UV index has been initiated.

This report provides an extensive overview of the achievements made by the ESAC consortium during the project. It reviews and completes the previously submitted yearly reports, at the end of 1997, 1998 and 1999.

1. OVERALL CONTEXT AND GENERAL OBJECTIVES OF ESAC

The composition of the Earth's atmosphere is changing as the concentrations of a number of radiatively and chemically active atmospheric constituents emitted at the surface are rapidly increasing, mainly due to man-made activities. These increased emissions influence atmospheric ozone, the Earth's radiative balance, hence climate, and modify the oxidising capacity of the atmosphere. It has become clear also that the upper troposphere / lower stratosphere is a region of high interest, because it controls the exchange of gases between the troposphere, where the sources are, and the stratosphere, and it controls to a great extent the radiative balance of the atmosphere.

A better knowledge of atmospheric composition and chemical processes, from ground level up to the stratosphere, is fundamental to assess the present state and changes and predict the future evolution of the Earth's environment, so that regulatory decisions about mankind practices can be identified on the basis of firm scientific grounds. This can only be achieved by a comprehensive series of complementary measurements including ground-based observations, aeroplane and balloon-borne campaigns, and global satellite missions, by improving the probing capabilities in the troposphere, and by comparing and integrating the observational data with numerical models.

In the field of atmospheric chemistry three main objectives can be identified:

- Long-term global monitoring of key stratospheric and tropospheric species such as ozone, halogen and nitrogen compounds, and the radiatively active gases or so-called 'greenhouse' gases[#]
- Advance knowledge of processes that control the chemical behaviour of the stratosphere and the troposphere, as determined from the observed spatial and temporal variability of trace species. The UV spectral irradiance is an important parameter in these processes.
- Identification of sources and sinks of primary species, and of their spatial and temporal variability.

ESAC contributes to the objectives of investigating the behaviour of ozone and many key stratospheric and tropospheric species at four stations in Europe, complemented by global satellite observations. This investigation includes long-term monitoring and the evaluation of radiative, dynamical, and chemical mechanisms underlying the observed variabilities and changes. The four stations are Ukkel (Belgium, 50.5°N, 4.3°E), Jungfraujoch (ISSJ) in the Swiss Alps (46.5°N, 8°E), Harestua (Norway, 60.2°N, 10.7°E), and Observatoire de Haute Provence (OHP, France, 44°N, 6°E);

they are part of the international Network for Detection of Stratospheric Change (NDSC). Additionally it was tasked to improve the acquisition of tropospheric data, and in particular, to pursue the analysis of earlier ATMOS/Shuttle observations to assess the possibilities to study the upper troposphere by infrared remote sensing from space. Long-term monitoring of the spectral UV irradiance is performed at Ukkel, in compliance with the international quality standards. The atmospheric observations are supported by numerical modelling of the atmosphere and by laboratory experiments that provide the fundamental spectroscopic and radiative data needed in the models and in the spectral data analyses.

ESAC is linked to international research activities, in particular to projects funded within the EC Environment Programme and EUROTRAC. Its results contribute to international research programmes like SPARC/WCRP (Stratospheric Processes and Their Role on Climate/ World Climate Research Programme) and NDSC/GAW/WMO (Network for Detection of Stratospheric Change / Global Atmosphere Watch / World Meteorological Organisation), and to international assessment studies, in support of environmental policies and the Montreal and Kyoto Protocols, aiming at preserving the Earth's environment from threats resulting from mankind's activities. Resulting data are archived for further exploitation in local and international databases.

2. METHODOLOGY: STATE OF THE ART TECHNIQUES

The research carried out in ESAC relies on the acquisition, analysis and geophysical interpretation of atmospheric data. The acquisition is performed with a suite of state of the art spectrometric instruments, and the spectral analysis is done with appropriate retrieval algorithms. Performant numerical models of the atmosphere are used for comparison and integration with observational data, to support the geophysical interpretation of the experimental data. Once validated, they can be used to make predictions of the future evolution of the atmosphere.

Both for the analysis of spectral observations of the atmosphere as well as in chemical-dynamical-radiative modelling of the atmosphere, one needs the spectroscopic and radiative parameters of the atmospheric absorbers and scatterers with high accuracy: they are obtained in laboratory experiments tailored to these needs.

It must be emphasized that the remote sensing measurements carried out in ESAC are part of the NDSC. They are complementary to atmospheric composition measurements from space and balloons. Therefore, part of the activities in ESAC concerns satellite data validation using NDSC ground-based data, and the

geophysical interpretation of the data is mostly done making synergistic use of the network, satellite and model data.

Although attention is paid to particular stratospheric and tropospheric process studies (see, chapters 4.1 and 4.3), mainly in the context of campaign measurements, the continuity of the measurements is of utmost importance for addressing the global change issues. Instrument maintenance and calibration, data verification and validation, and homogenisation of long-term time series represent major efforts in this field of research. Examples are given throughout Chapter 4.

Qualified data series are stored locally and in international databases, in particular HITRAN/GEISA for spectroscopic data, and NADIR (NILU's Interactive Database for Atmospheric Retrieval) at NILU (Norway) and the NDSC database at NOAA for the geophysical data. The Ukkel soundings are transmitted to WMO and ECMWF (European Centre for Meteorology and Weather Forecasting).

More details about the instruments and techniques used in ESAC are given in the following subsections (2.1 to 2.5).

2.1 Remote sensing by optical spectrometry

2.1.1 UV-visible differential optical absorption spectrometry (DOAS)

The DOAS instruments operated in ESAC at the Jungfraujoch, Harestua and OHP observatories are spectrographs with linear photodiode arrays or CCD arrays; they are operated automatically. The Jungfraujoch instrument is a commercial SAOZ (Système d'Analyse par Observations Zénithales), the other ones have been built at BIRA-IASB. The DOAS method is based on spectral measurements of the solar light in the UV and/or visible range (300-600 nm) of the spectrum that is diffused by the atmosphere at the zenith or at another angle with respect to the zenith ('off-axis' measurement). The spectrum is analysed for its high frequency structures (resolution $\cong$ 0.5 nm) that are representative of the atmospheric molecular absorptions. Measurements can be performed irrespective of the weather conditions. The technique is capable of detecting and quantifying the total column abundances of O_3, NO_2, OClO, BrO, H_2CO (O_4 and H_2O).

2.1.2 Fourier transform spectrometry

High resolution Fourier transform spectrometry (FTS) is based on the principle of Michelson interferometry. In ESAC, FTS are used in the UV-visible and infrared spectral range. The technique allows the recording of absorption spectra over a large spectral range, carrying many absorption signatures simultaneously; mostly the individual absorption lines can be resolved.

Currently the Fourier transform infrared (FTIR) measurements are performed at the Jungfraujoch, in the 2 to 15 μm region, with a maximum resolution of order 0.003 cm^{-1}. Two FTIR instruments have been operational: a commercial Bruker 120 HR and a home-made spectrometer built at the University of Liège. An important list of atmospheric species can be detected and their total column abundances determined: CO_2, CH_4, N_2O, CO, O_3, NO, NO_2, HNO_3, HNO_4, $CFCl_3$, CF_2Cl_2, CHF_2Cl, HCl, HF, $ClONO_2$, COF_2, SF_6, C_2H_2, C_2H_6, OCS, HCN, H_2CO. The measurements require clear-sky conditions and are not automatic. Table I illustrates the species currently monitored at the Jungfraujoch, including (between parentheses) an estimate of the precisions of the retrieved total column abundances.

A mobile Bruker 120 M FTS, with a maximum resolution of 0.008 cm^{-1}, has been operated in the UV-visible for horizontal long-path measurements of atmospheric pollutants (O_3, NO_2, SO_2, C_2H_6, H_2CO,...) at the ULB campus in Brussels, and in the infrared range for field experiments in the Jungfraujoch area (see chapter 4.3).

Table I: *List of Molecules Studied in FTIR Solar Observations at the Jungfraujoch. The relative precisions, in percentage, with which the total column abundances can be derived routinely from typical individual observations are given between parentheses for each species. Species that are primarily stratospheric are listed in italic, the other ones are primarily tropospheric; species under evaluation are put between square brackets.*

Reference gas:	N_2(≈1%)
Minor constituents:	CO_2(<2%), N_2O(≤2%), CH_4(≈2%), CO(≤4%), O_3(≤5%), [H_2O]
Trace constituents:	
Halogenated species:	*HCl*(≤4%), *$ClONO_2$*(≈ 20%), CCl_2F_2(≤4%), $CHClF_2$(≤6%), *HF*(≤3%), *COF_2*(≤20%), SF_6(≈30%)
Nitrogenated species:	*NO*(≤6%), *NO_2*(≤10%), *HNO_3*(≈5%), *HNO_4* (monthly avg.)
Others:	C_2H_2(≈20%), C_2H_6(≤6%), HCN(≤8%), OCS(≤8%), H_2CO(≥monthly avg.), [H_2CO_2, CH_3Cl, CCl_4, CCl_3F,...];
Various isotopes	

2.2 In situ Ozone soundings

Ozone soundings are based on a reduction reaction in an electro-chemical cell, carried by a small balloon to about 35 km altitude. Currently at Ukkel (since 1997) they are performed with Z-ECC type sondes; before Brewer-Mast type cells were used. Vertical profiles of ozone concentrations can be measured with a very high vertical resolution, of order 100 m, from ground to the burst altitude of the balloon.

2.3 UV-visible spectral radiometry

Spectral monitoring of the solar irradiance in the UV and visible is performed with radiometrically calibrated instruments of different types. The core instruments at Ukkel are a Brewer Mk II spectrophotometer (280-325 nm) at KMI-IRM, and a double modified HD10 Jobin-Yvon monochromator at BIRA-IASB. Additional instruments are 3 filter radiometers and 4 pyranometers. Together, they allow measurements of the total and direct and diffuse components of the solar irradiance; complementary information on the ozone total column and aerosol optical depth can be extracted. The spectral range of the core instruments covers the UVA to UVC (280 nm - 600 nm).

2.4 Laboratory experiments

Laboratory experiments are performed with similar Fourier transform instruments as the ones mentioned above, coupled to long path absorption cells with known gas concentrations inside. The cells are temperature and pressure controlled. The gas pressure, temperature and concentration in the cell must be varied, to mimic the atmospheric conditions. In ESAC, laboratory experiments are performed in collaboration with the Laboratoire de Spectrométrie Moléculaire et Atmosphérique (GSMA) of the Université de Reims, where cells with optical path lengths up to 2 km and temperature cooling down to 220 K are available.

2.5 Numerical modelling

In the ESAC project, we have used various radiative transfer (RT) and UV models, 1-dimensional chemical box models, and 3-dimensional chemistry-transport models (3D CTM). Most of them were developed in the consortium. Moreover several statistical models and empirical regression models have been developed for analysis of experimental data and time series.

3. METHODOLOGY: NEW DEVELOPMENTS AND IMPROVEMENTS AS TO INSTRUMENTS, ALGORITHMS AND DATA ANALYSIS TOOLS

3.1 DOAS Off-axis instruments

The DOAS technique is configured commonly for observations of the solar light scattered at zenith, the so-called zenith-sky viewing geometry. However, one can also apply the technique to the off-axis viewing geometry, i.e., the collected light comes from a scattering point at a large angle with respect to the zenith). A combination of measurements successively performed in zenith-sky and off-axis geometries allows to derive the tropospheric content of the measured species, in a relatively thin layer (2-3 km) above the earth surface. The principle of the method is schematically outlined in Figure 1, where typical ray-paths corresponding to both viewing geometries are represented. Off-axis and zenith-sky rays being scattered at approximately the same altitude, their difference is mainly sensitive to the region below the scattering altitude (which roughly corresponds to the location of the planetary boundary layer PBL).

The zenith-sky UV-visible spectrometer in operation at Observatoire de Haute Provence has been modified in December 2000 to include an off-axis mode where the scattered light is measured in a quasi-horizontal direction (see Figure 2). Located a few meters above the ground, the spectrometer benefits from an unobstructed field of view down to the horizon in all directions. The similar transformation of the Harestua instrument (off-axis measurement mode) is planned for late 2001.

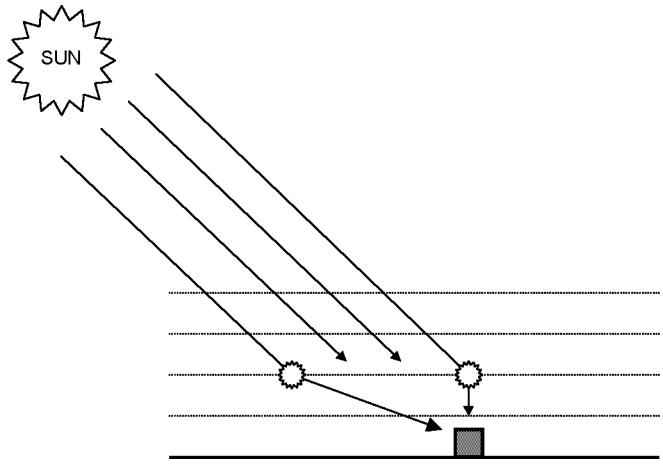

Figure 1: *Schematic drawing comparing typical ray-paths for zenith-sky and off-axis viewing geometries. Paths before the scattering altitude are similar in both geometries.*

Figure 2: *BIRA-IASB UV-visible spectrometer operated at OHP. Alternate observations of the zenith-sky and of the "off-axis" scattered light (10° above horizon) are obtained by means of a rotating mirror installed in a quartz dome on top of the box.*

Figure 3 displays preliminary results obtained using the OHP instruments on January 16, 2001. The spectral analysis of zenith-sky and off-axis observations performed around noon within a few minutes of interval reveals significant differences in the absorption of O_3, NO_2, BrO and formaldehyde (HCHO), thus providing evidence for the presence of these species in the troposphere. These promising results confirm the potential of off-axis measurements for tropospheric investigations. Quantitative interpretation will be the subject of algorithm developments planned in the near future.

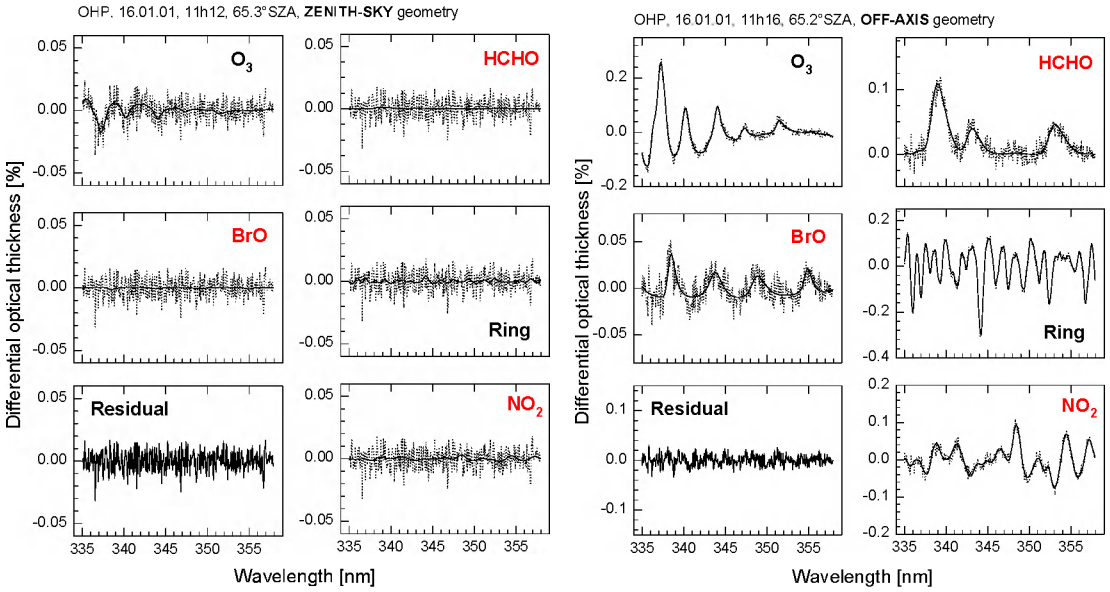

Figure 3: *Results of DOAS fitting procedures applied to zenith-sky and off-axis spectra measured quasi-simultaneously at noon with the OHP spectrometer on 16 January 2001. The increased absorption of O_3, HCHO, BrO and NO_2 in the off-axis geometry compared to the zenith-sky geometry is a signature of the presence of these species in the troposphere. Further developments of the analysis algorithms are still needed for a quantitative interpretation.*

In addition to the modification of the OHP spectrometer, a new instrument was built to enable combined measurements under different viewing geometries. The instrument consists of a commercial ARC Spectra-Pro 150-S spectrometer equipped with a grating of 1200 l/mm and a cooled CCD from Princeton Instrument. The whole spectrometer is mounted on a BRUSAG solar tracker allowing for precise pointing in any direction, including towards the sun and the moon. The spectral range covered by the instrument extends from 300 nm to 650 nm (in 3 independent spectral windows), with a resolution of about 0.7 nm full width half maximum (FWHM).

A preliminary version of this instrument was used for the first time during a campaign at the University of Reims during the solar eclipse of 11 August 1999, inside the zone of total occultation. The total eclipse was observed at 12h25 local time during 2 minutes, while the complete phase of occultation lasted 2h40m. The instrument was set up to allow measurements of O_3 and NO_2 stratospheric and tropospheric columnar abundances from the observation of the scattered skylight in the UV-visible spectral region.

The large differences between the NO_2 slant columns observed in both observation geometries were a clear indication for the presence of large amounts of NO_2 in the

planetary boundary layer (PBL) in the few hours that followed the eclipse. The data showed a large increase in the NO_2 content just after the eclipse, and later again around 14 UT.
This instrument will be used in the future for campaign observations in the context of the Network for the Detection of Stratospheric Change (NDSC).

3.2 WinDOAS

The SAOZ and DOAS data processing have been improved in the course of the ESAC project duration (see section 4.1). Moreover, the spectral analysis tools have been extended to include the analysis of DOAS spectra taken in zenith and off-axis geometries, from balloon (e. g., the SAOZ balloon spectra from Service d'Aéronomie du CNRS) and space (e.g., GOME). An operational version of the data processing algorithm has been implemented under Windows '98, called WinDOAS (Van Roozendael et al., 1999), that integrates all algorithm improvements and various analysis options, with a user-friendly graphical interface as illustrated in Figure 4. WinDOAS is already used by about 11 research groups in- and outside Europe, and still broader distribution is expected in the near future.

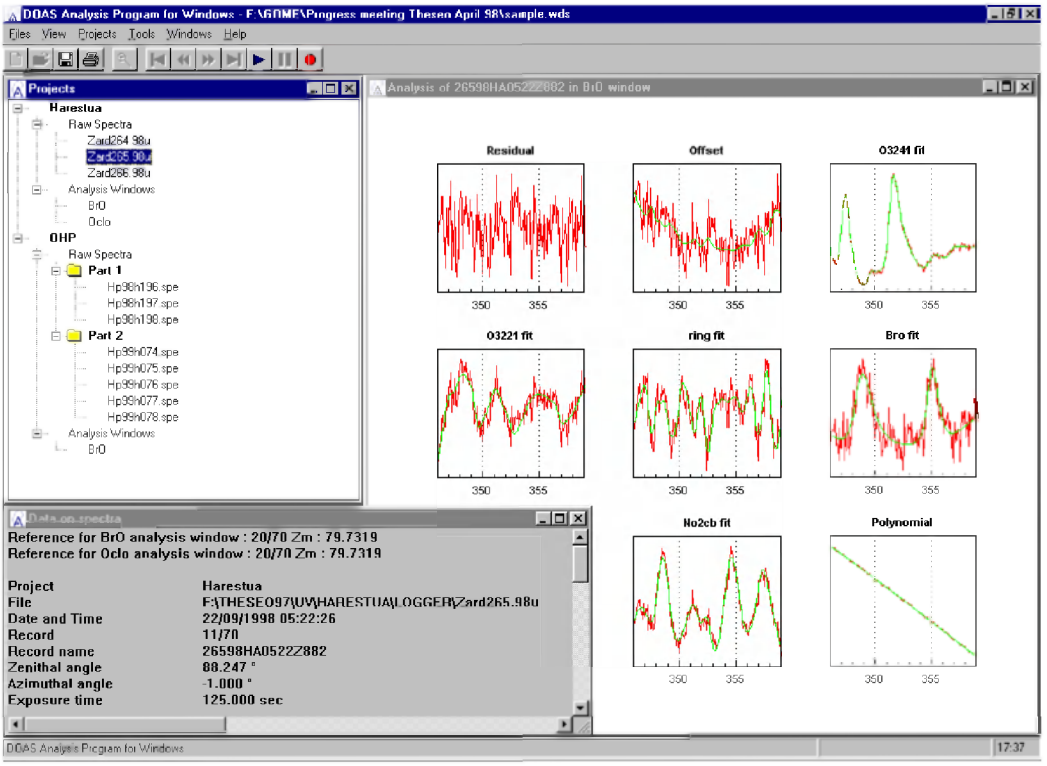

Figure 4: *The graphical user interface of the BIRA-IASB DOAS analysis software package (Windoas).*

3.3 PSCBOX, a coupled photochemical box-/radiative transfer model

Model packages based on coupled 1D photochemical box-/radiative transfer models and initialised by chemical fields from 3D chemical transport models (3D CTM) enable the simulation with full diurnal cycle of slant column densities (SCDs) of stratospheric constituents. A model package of this kind called PSCBOX has been developed at BIRA-IASB primarily for modelling SCDs of fast diurnally varying species such as BrO, OClO or NO_2, for both nadir and zenith observation geometries. These simulations are being used to interpret SCDs measured by the DOAS instruments at the three ground-based stations Harestua, OHP, and Jungfraujoch.

3.3.1 Model package description

The model package PSCBOX consists of the stacked version of the trajectory box-model PSCBOX (Fonteyn et al., 2000) coupled to a radiative transfer (RT) model. PSCBOX includes 48 variable species, 104 gas-phase and 27 photolysis reactions. Treatment of heterogeneous chemistry reactions on liquid sulfuric acid aerosols and on PSC particles is included also; more details about this can be found in Fonteyn et al. (2000). The model makes neither family nor photochemical equilibrium assumptions. Updated kinetic and photochemical data are taken from the JPL 2000 compilation (Sander et al., 2000). Photolysis rates are computed off-line by using the RT scheme developed by Toon et al. (1989). This scheme includes multiple scattering and a pseudo-spherical geometry approximation. PSCBOX is initialised with 12h UT pressure, temperature, and chemical species fields from the 3D CTM SLIMCAT (Chipperfield, 1999). Pressure and temperature fields used in SLIMCAT are taken from UKMO (UK Meteorological Office) meteorological analyses.

Two kinds of RT models have been used to generate slant columns from the box-model outputs: (1) a single scattering ray tracing model (Van Roozendael et al., 1998) and (2) the model S-DISORT/UVspec (Kylling, 1995). (1) calculates the rays in a full spherical geometry using the appropriate local concentration of the absorbing species along the light path. O_3 absorption, Mie scattering (stratospheric background conditions), and refraction can also be included. (2) solves the RT equation by the discrete ordinate method and includes full treatment of multiple scattering in pseudo-spherical geometry (direct beam only), Mie scattering, ground albedo, and refraction. The program has been modified in order to take into account the variation of the concentration of the absorbing species along the light path with varying solar zenith angle (direct beam only).

3.3.2 Model package validation

PSCBOX has been validated through an intercomparison exercise with two other similar packages including a stacked 1D photochemical box-model and a single scattering ray tracing model (Hendrick et al., 2000): SLACO (IFE Bremen) and SLIMCAT1D (University of Leeds). During the intercomparison the consistency between the three packages has been verified through comparison of model results obtained using common initialisation data. Calculated BrO differential slant column densities (DSCDs) have been also compared to ground-based zenith-sky DOAS measurements for the following locations and days: Bremen (53°N, 8.8°E), 4/3/97 (outside polar vortex scenario) and Ny-Ålesund (79°N, 11.9°E), 19/3/97 (inside polar vortex scenario). The adopted approach included three comparison tests:

Test 1 ("blind test"): Initialisation of the photochemical models with common SLIMCAT 12h UT profiles for the above-mentioned locations and days. The photochemical models keep their own reaction schemes and kinetic and photochemical data (also for the heterogeneous chemistry processes). The settings of the RT models are let free.

Test 2: Similar reactions scheme and rate constants based on the JPL97 compilation (DeMore et al., 1997) are now implemented in the three photochemical models and the settings of the RT models are imposed (except the BrO fields which are provided by each box-model).

Test 3: Verification of the consistency between the three RT models through their initialisation with identical parameters including the BrO fields (from SLIMCAT1D).

Modelled BrO DSCDs resulting from Test 1 are compared to measurements in Figure 5. Considering the quite large uncertainties of the measurements, the three models capture reasonably well the observations for Ny-Ålesund and Bremen. However, for both scenarios, discrepancies are observed between modelled BrO DSCDs, especially at large SZAs. SLIMCAT1D values are generally larger than PSCBOX and SLACO ones. These discrepancies could be due to differences in the photochemical models outputs but also in the settings of the ray tracing models.

Results from Test 2 as well as from sensitivity tests to the inclusion of Mie scattering, O_3 absorption, and refraction in the RT calculations show that a large part of the discrepancies obtained in the blind test is due to differences in the conditions of initialisation of the ray tracing models. This highlights the importance of defining appropriate settings for the radiative transfer part of the slant column interface.

A detailed comparison of the photochemical models outputs from Test 2 also reveals significant discrepancies which points to differences in the calculations of photolysis rates and in the treatment of heterogeneous chemistry processes (the only parameters not set up in a common way in this test). This is illustrated in Figures 6 and 7 where the volume mixing ratio of BrO, HOBr, $BrONO_2$, BrCl, OClO, and NO_2 calculated at 20 km for the Bremen scenario are plotted as a function of the SZA respectively for both cases with and without heterogeneous chemistry processes taken into account. Note the severe discrepancies observed above 80° SZA for HOBr, $BrONO_2$ and BrCl, when the heterogeneous chemistry processes are switched on. As to be expected, a significant improvement of the agreement between the model outputs is obtained when switching off the heterogeneous chemistry processes (Figure 7). Remaining discrepancies are likely to be due to differences in the calculation of photolysis rates that was not constrained in this comparison test.

Finally, Test 3 has revealed that significant discrepancies between modelled BrO DSCDs are still observed when the ray tracing models are identically initialised. Differences found are in the range 5-10 %, which is larger than reported in previous intercomparison exercises (e.g. Sarkissian et al., 1995) and is probably related to differences in the way the 2-dimensional BrO concentration matrices are handled in each model.

To summarize, this intercomparison exercise shows that the three model packages reproduce reasonably well the measurements for the selected days and locations. However, comparisons for more than two days are needed to conclude on the agreement between measurements and models. Discrepancies have been observed between modelled BrO DSCDs and can be attributed to differences between the ray tracing models and especially to their conditions of initialisation. The comparison of photochemical model outputs also reveals significant differences in the treatment of heterogeneous chemistry processes and in the calculation of the photolysis rates. These differences will be further investigated.

An example of the exploitation of PSCBOX for comparison with observational data is given in section 4.1.2.

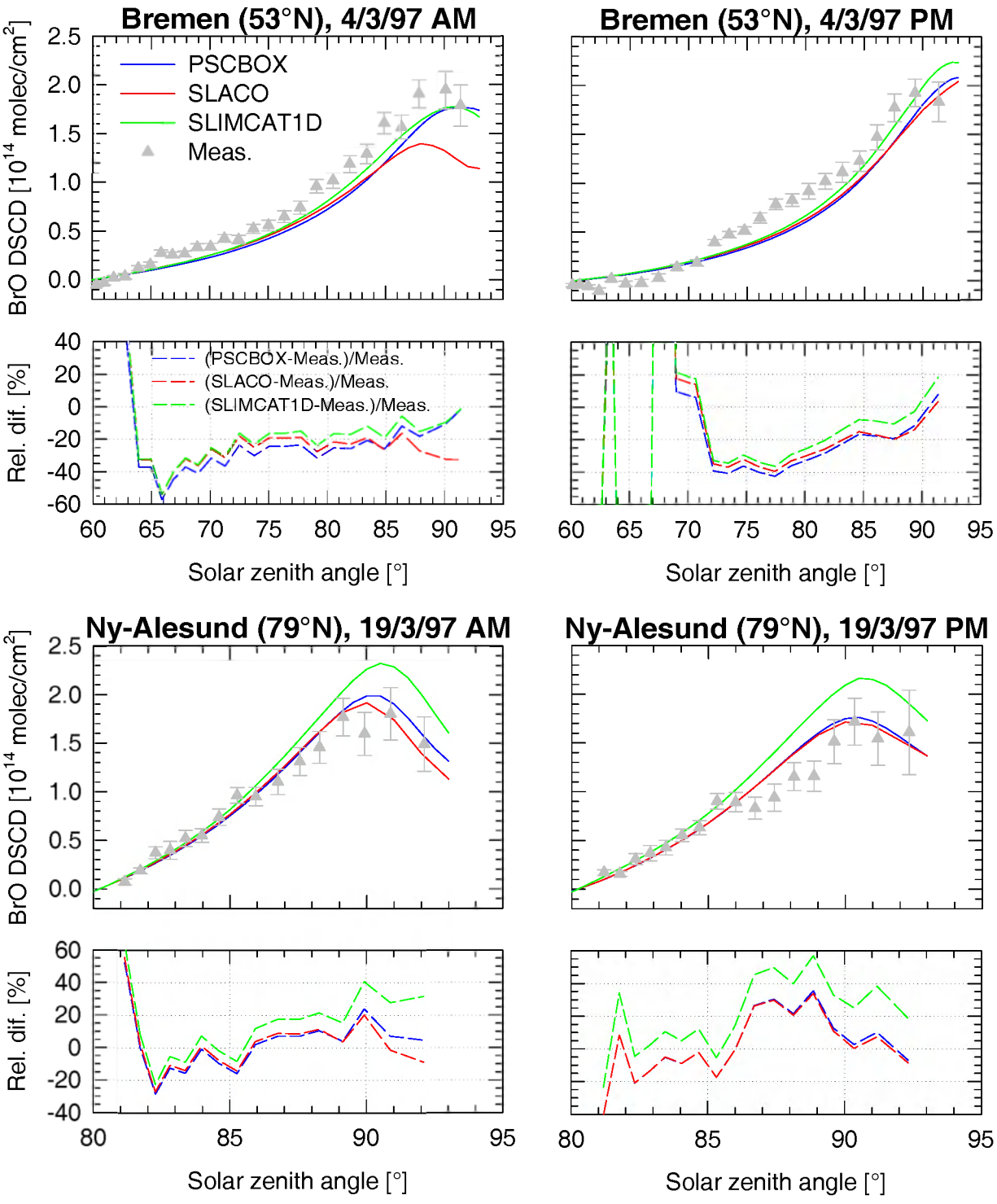

Figure 5: *Comparison between measured and modeled BrO DSCDs resulting from Test 1. The DSCDs are relative to the local noon.*

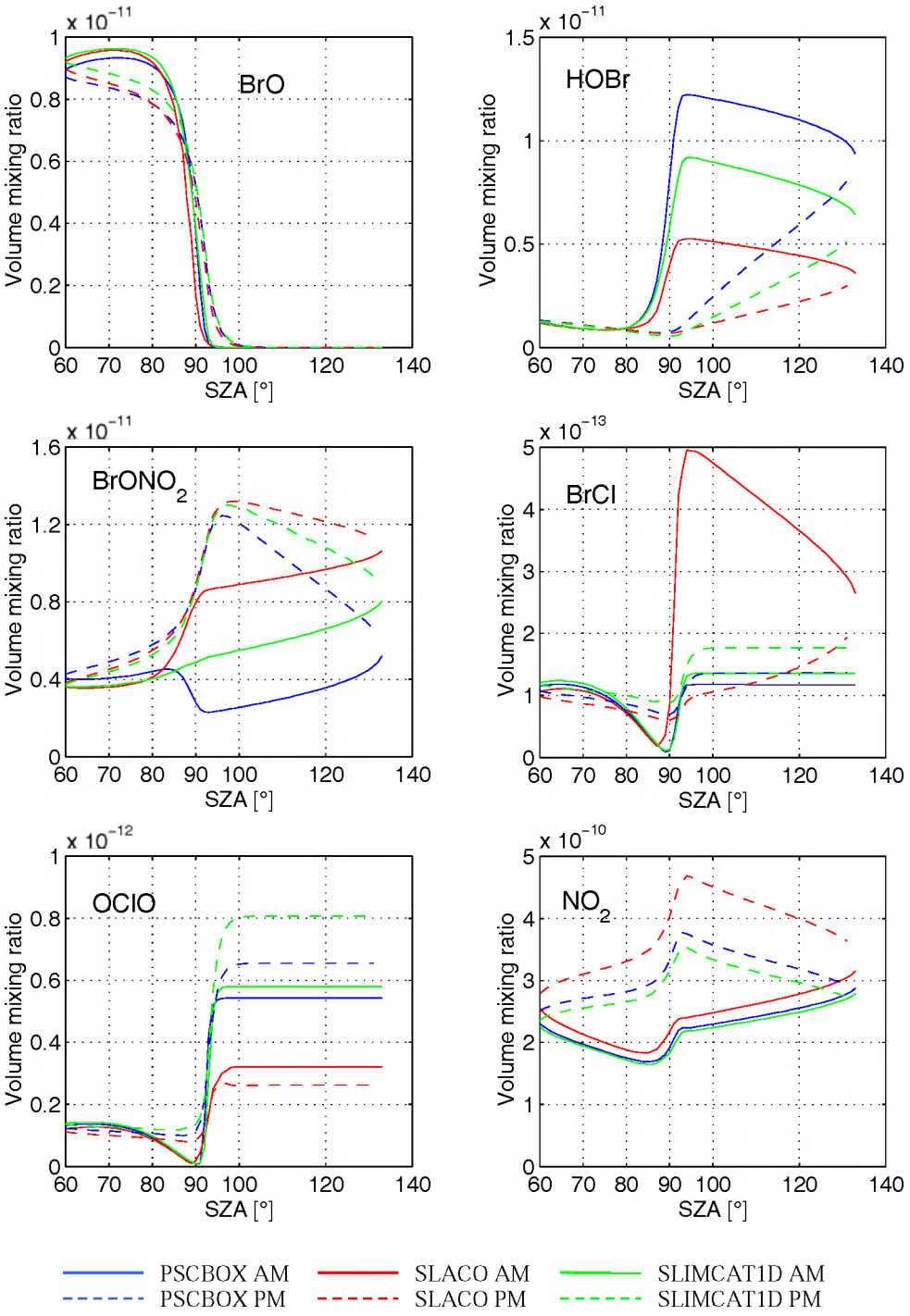

Figure 6: *Comparison between photochemical models outputs for BrO, HOBr, $BrONO_2$, BrCl, OClO, and NO_2 at 20km of altitude for the Bremen scenario resulting from Test 2. Heterogeneous chemistry processes are switched ON.*

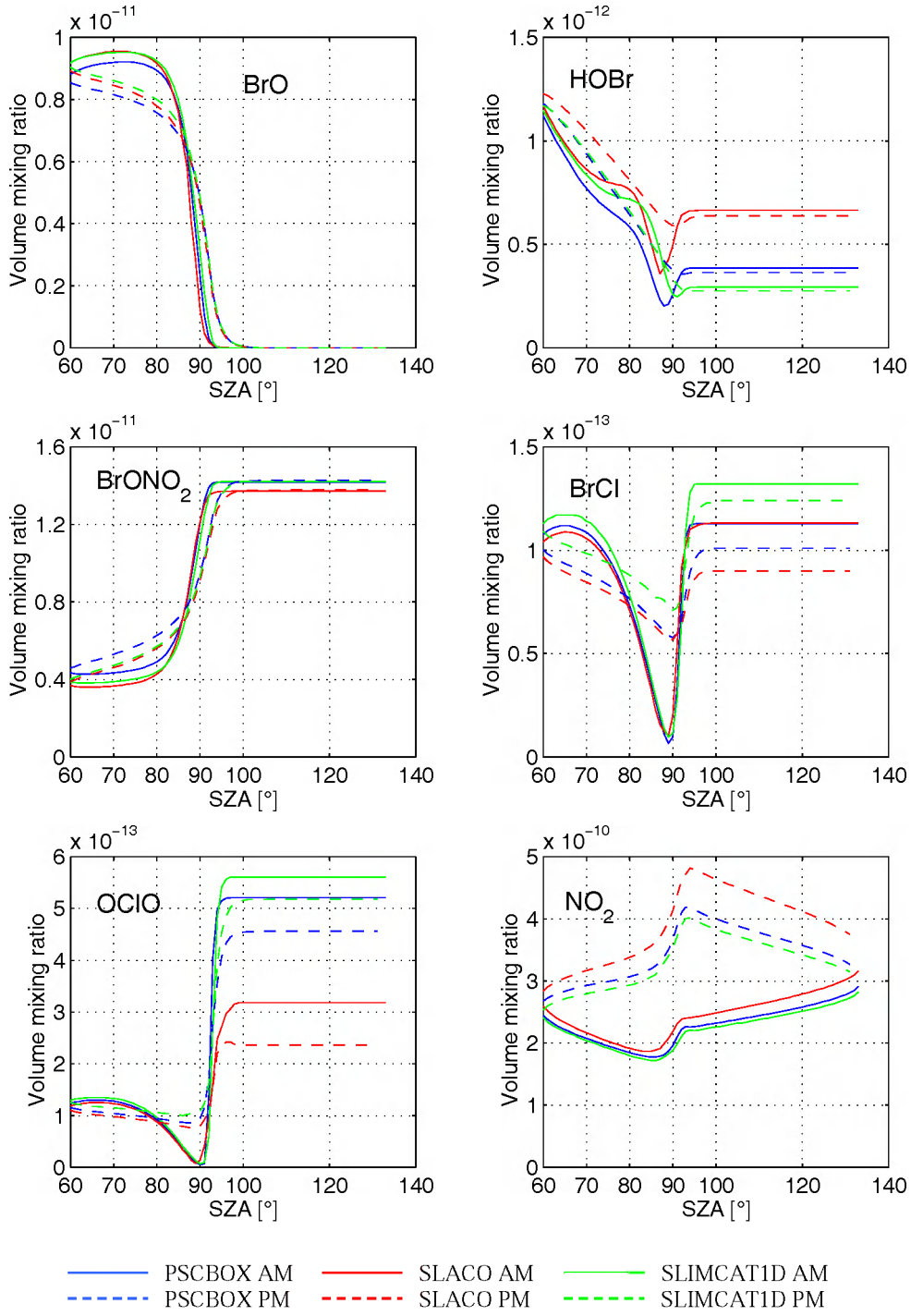

Figure 7: *Comparison between photochemical models outputs for BrO, HOBr, $BrONO_2$, BrCl, OClO, and NO_2 at 20km of altitude for the Bremen scenario resulting from Test 2. Heterogeneous chemistry processes are switched OFF.*

3.4 Altitude-Differential column measurements

In a search for distinguishing contributions from different altitude ranges in the atmosphere from ground-based FTIR measurements, an original method of altitude-differential measurements was tested during a campaign in summer 1998 in the Jungfraujoch area. The idea is as follows: two similar FTIR instruments are operated simultaneously at two different altitudes, making observations of the same species. The differences between the column abundances measured at both sites represent the amount of the species that is present in the height range between the two observation altitudes. To validate the technique, both instruments were operated initially side-by-side at one location (on top of the Jungfraujoch), to verify that they made consistent measurements. After that initial period, one instrument (the Bruker 120M) was moved down to the valley, in Grindelwald, at an altitude of 1070 m asl., while the other one (the Bruker 120 HR) continued its measurements at the Jungfraujoch observatory, at an altitude of 3580 m asl. The geophysical results of the campaign are discussed briefly in Chaper 4.

The method has proven valid and worth for the measurements of column measurements in the lower troposphere and planetary boundary layer of species like CO, CH_4, N_2O, C_2H_6 ... for which the distribution with altitude in the troposphere is badly known. It may be repeated on the purpose of validation of tropospheric satellite measurements like MOPITT.

3.5 Advanced FTIR spectral analysis algorithms

In the consortium, two state of the art algorithms are used for retrieval of vertical column abundances of atmospheric absorbers from high resolution FTIR solar absorption spectra, namely SFIT (Rinsland et al., 1984) and SFSP (Synthspec & Fitspec, a home-made code from BIRA-IASB). In both codes an a priori profile shape of the target species is adopted; a scaling factor of the profile is adjusted by least squares minimisation of the difference between the observed spectrum and the corresponding synthetic one, using a Levenberg-Marquardt procedure. Part of the uncertainty in the resulting column abundance therefore originates in the choice of the a priori profile.

In a first step (section 3.5.1), the a priori profile was replaced by a 'model' of profiles to better represent the actual state of the atmosphere: this has been developed and implemented for the retrieval of ozone. In a second step (section 3.5.2), profile retrieval has been implemented.

3.5.1 O_3 vertical column abundance retrieval including a daily, tropopause dependent climatological model

The geophysical model that was developed for the O_3 vertical distribution model is based on local meteorological/dynamical parameters, namely the local tropopause height, and on a climatology for the seasonal variation of O_3.
The model is meant to replace the single standard a priori profile in spectral data analyses, in particular of FTIR spectra, with the purpose of optimizing the retrieved ozone column abundance. At the same time, in the FTIR spectral fit procedure, it attempts to eliminate or reduce the importance of the effective apodization parameter (EAP). The effective apodisation is an ad hoc fit parameter to compensate for any discrepancies of instrumental or geophysical origin between reality and its parametrized representation in the retrieval process.

The model is based on the following known facts: (i) the ozone column abundance is correlated positively with the local tropopause pressure, (ii) there exists some correlation between the ozone vertical profile and the tropopause parameters at least in the lowest stratosphere, up to about 22 to 25 km, and (iii), the tropopause changes capture only part of the observed ozone total column changes that are also influenced by longer-lasting perturbations such as the annual cycle, planetary waves, etc. Trials with a model which introduces a seasonal variation only in the upper part of the O_3 profile, above 25 km, have shown that hereby the seasonal O_3 variation is not adequately represented. Therefore, a climatology as to ozone vertical profiles has been constructed as follows: the ozone sonde data at Uccle (Belgium) since 1969 from the Royal Meteorological Institute have been sorted according to 4 seasons and 9 tropopause height classes, from (7.0 $\pm$ 0.5) km to (15.0 $\pm$ 0.5) km. Above 25 km the profiles have been extended with the CIRA '86 ozone seasonal model data for the 40°-50° latitude band. Figure 8 is an example set, showing some model profiles for the most frequently occurring tropopause heights, for each season. The most important model characteristics are the following. The altitude of the ozone concentration maximum (AOCM) increases when the tropopause rises, and the value of the ozone concentration at AOCM concurrently decreases. The increase of AOCM with rising tropopause is most evident in winter and spring. The less systematic relationship observed in summer and fall originates in the fact that for these seasons the peak in the ozone profile is wider along the vertical, and therefore the location of the ozone maximum is less precise. There is a remarkable difference of about 20% between the higher values of the ozone concentration maximum in winter and spring on the one hand, and the lower ones in summer and fall on the other hand. The appearance of a secondary maximum in the ozone concentration vertical profiles

between 10 and 15 km altitude becomes more pronounced as the tropopause altitude goes down, and is most evident in summer and spring.

It has been demonstrated that the above O_3 vertical profile climatology based on Uccle data is representative of the Jungfraujoch as well, from comparisons with sonde and microwave observations at Payerne and Bern, respectively, which are both within 100 km of the Jungfraujoch.

For evaluation of the appropriateness of the model, the model has been implemented for the selection of the a priori profile in SFIT and SFSP. ISSJ Bruker IR O_3 spectra for 1995 to 1997 have been analysed with the SFIT algorithm, once using a standard O_3 profile, and a second time using the new O_3 vertical profile model as the a priori, keeping all other parameters identical. It has been demonstrated that the use of the O_3 a priori vertical profile model significantly improves the agreement between the FTIR and SAOZ time series at the Jungfraujoch: the agreement gets as close as the one between O_3 data obtained with different UV/visible DOAS spectrometers and well calibrated Dobson and Brewer spectrophotometers - see also section 3.5.2.2. and Figures 12 and 13. It has been demonstrated also that the model addresses most of the atmospheric changes that are otherwise dissimulated by an ad hoc adjustment of the EAP. Nevertheless, even with this new profile model, an additional adjustment of the EAP in the fit procedure is still beneficial to improve the accuracy of the retrieved ozone column amounts, by accounting for some systematic discrepancies between observed and calculated spectra.

More details can be found in De Mazière et al. (1999).

The development and evaluation of the O_3 vertical distribution model have been conducted for the FTIR ozone measurements at Jungfraujoch, but the concept holds at all midlatitude locations, and it can be applied probably also to space-borne nadir looking observations (thermal infrared emission). It has also been implemented in the analysis of the Jungfraujoch SAOZ data as a test case in validation exercises (see section 3.5.2.2).

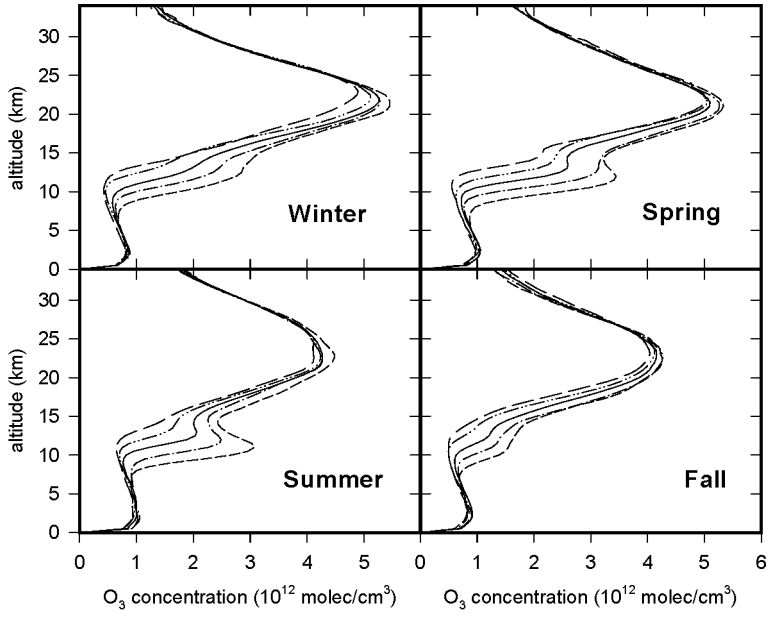

Figure 8: *Example profiles from the climatological O_3 a priori profile model for each season, for tropopause heights of 9 km (short-dashed line), 10 km (dash-dotted line), 11 km (solid line), 12 km (dash-double-dotted line), and 13 km (long-dashed line).*

3.5.2 Vertical inversion algorithms for FTIR spectra: SFSP upgraded to SFSP2, and SFIT2

3.5.2.1 The Optimal Estimation Method and its application for inversion of FTIR spectra

In the spectral analysis retrieval algorithms, a forward model F describes how the measurement vector I_m (measured spectrum) depends on the state vector x (molecular profiles, additional parameters to be fitted) and on a model parameters vector b (spectral line data...) :

$$\mathbf{I}_m = \mathbf{F}(\mathbf{x},\mathbf{b}) + \varepsilon_I$$

where ε_I is the vector of direct measurement errors (noise).

In order to obtain information about the height profiles, the optimal estimation method (OEM) (Rodgers 1976) has been implemented in the retrieval algorithm. This method is based on a statistical approach in which the solution is a weighted average of the measurements and the a priori information. The a priori information consists of a virtual measurement of the height profile x_a together with its covariance matrix S_a that

is supposed to reproduce the variability of the profile. The measurements consist of a measured spectrum I_m together with a covariance matrix S_I. This matrix is diagonal with the inverse of the squared signal-to-noise ratio (S/N) on the diagonal.

OEM requires the linearisation of the forward model about the a priori state vector

$$\mathbf{I_m} = \mathbf{F}(\mathbf{x_a}, \mathbf{b}) + \frac{\partial \mathbf{F}}{\partial \mathbf{x}}(\mathbf{x} - \mathbf{x_a}) = \mathbf{F}(\mathbf{x_a}, \mathbf{b}) + \mathbf{K}(\mathbf{x} - \mathbf{x_a})$$

The measured spectrum can be converted into a measured profile $K^{-1}I_m$ with covariance matrix $K^T S_I^{-1} K$.

In a linear case the weighted profile average is given by :

$$\bar{\mathbf{x}} = (\mathbf{S_a^{-1}} + \mathbf{K}^T \mathbf{S_I^{-1}} \mathbf{K})^{-1} (\mathbf{S_a^{-1}} \mathbf{x_a} + \mathbf{K}^T \mathbf{S_I^{-1}} \mathbf{I_m})$$

while in a non-linear case the estimation is made iteratively with the (n+1)st iterate given by :

$$\mathbf{x_{n+1}} = \mathbf{x_a} + (\mathbf{S_a^{-1}} + \mathbf{K_n^T} \mathbf{S_I^{-1}} \mathbf{K_n})^{-1} \mathbf{K_n^T} \mathbf{S_I^{-1}} \left[(\mathbf{I_m} - \mathbf{I_n}) - \mathbf{K_n} (\mathbf{x_a} - \mathbf{x_n}) \right]$$

This method also provides the uncertainty covariance matrix of the result profile

$$\bar{\mathbf{S}} = (\mathbf{S_a^{-1}} + \mathbf{K}^T \mathbf{S_I^{-1}} \mathbf{K})^{-1}$$

We have implemented OEM in SFSP, and we call this new upgraded version SFSP2. Analogously, SFIT2 is a version of SFIT in which OEM was implemented in a collaboration between NIWA and LaRC. We verified that SFSP2 and SFIT2 produce similar results if used in common conditions.

An example of some O_3 profiles retrieved from spectra in the 3039 cm^{-1} microwindow recorded at ISSJ in March 1996 is shown in Figure 9. The profile of March 29 represents a situation where the polar vortex moved close to the Jungfraujoch.

Preliminary analyses of various FTIR time series recorded at the Jungfraujoch are discussed hereinafter.

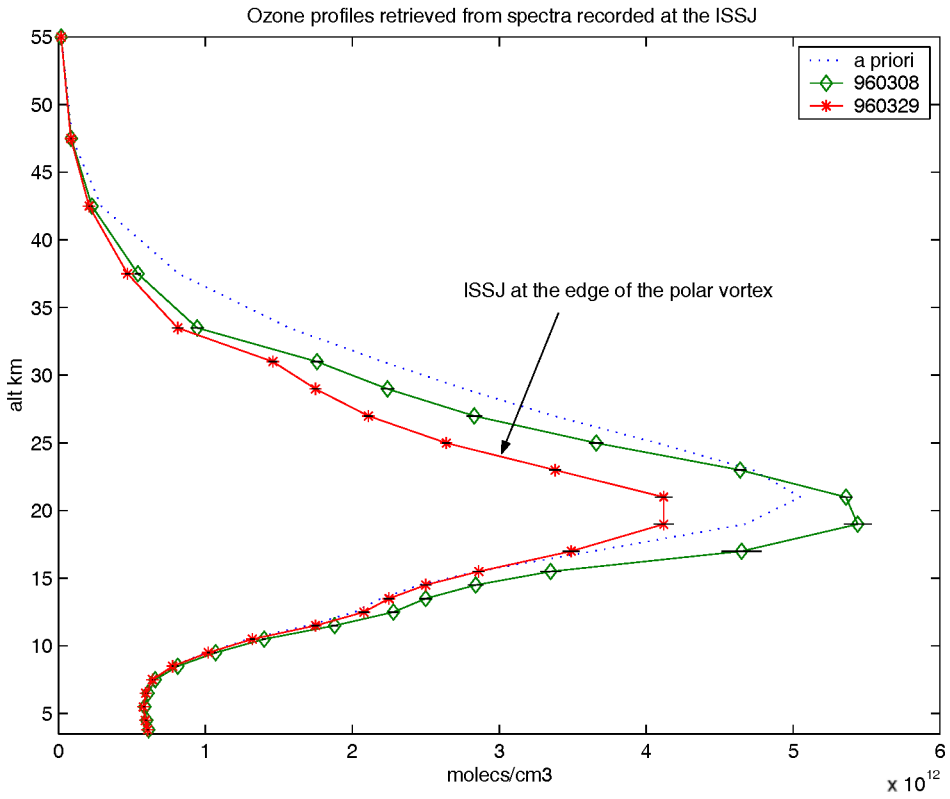

Figure 9: *O_3 profiles on March 8 and 29, 1996 (solid green and red lines, respectively), retrieved from FTIR spectra recorded at ISSJ. The profiles are daily means; error bars represent the standard deviation throughout the day. The dotted line represents the a priori profile used in the retrieval procedure.*

3.5.2.2 Preliminary results for O_3, HCl and HF vertical profiles retrieved from ISSJ FTIR spectra

The vertical distributions of O_3, HCl and HF have been retrieved using SFIT2 from high resolution FTIR solar spectra recorded at the Jungfraujoch. When available, the results have been compared to correlative measurements. The HF vertical distributions retrieved from the spectra recorded between November 1995 and January 1997 have been compared to correlative measurements from the HALOE instrument on board the UARS satellite. The ozone profiles retrieved from FTIR spectra recorded from June 1997 to June 2000 have been compared to correlative profiles measured by the ozone soundings from Payerne. For the three molecules, the stratospheric columns have been compared to correlative results of the SLIMCAT Chemistry Transport Model for the winter 1999-2000.

Ozone profiles

To enhance the sensitivity to the troposphere, vertical inversions for ozone have been performed in the 1003 cm^{-1} window (1002.6 – 1003.2 cm^{-1}), a window which was already chosen by Pougatchev et al. (1995, 1996) for that reason. The tropospheric sensitivity is indeed apparent in the averaging kernel for this window shown in Figure 10, calculated for conditions that are characteristic of the Jungfraujoch FTIR spectra. The kernels indicate a vertical resolution of order 10km FWHM for the retrieved profiles. Figure 11 shows retrieved daily mean partial column abundances in 3 distinct layers, up to 30km altitude (the mean altitude range of the sondes), in comparison with sonde data, for coincident measurement days, integrated over the same altitude range. The plots include also running averages over 15 days of the sonde data. A very good agreement is observed between the individual sonde and FTIR observations, in all layers. We also checked the derived total column abundances in comparison with Arosa Dobson data for the same period. The agreement is excellent, with a bias of –1.6%, and a dispersion (1 sigma standard deviation) of 2.3%. An interesting point to note is that particular ozone sonde profiles are well captured by the FTIR data. For example, on February 12, 1999, the vortex came over the Jungfraujoch, the tropopause lowered to 9 km, and the integrated ozone amount was particularly high, well above the associated running average. The FTIR data are still in very good agreement with coincident sonde data. For each layer the mean and standard deviation of the differences between both data sets have been calculated (see plot). One sees some underestimation by FTIR in the troposphere (3.58-14 km layer) and some overestimation by FTIR in the next layer, just above the tropopause (14-24 km layer). Both compensate each other in the integrated amount, where a mean difference of 2.5% ($\pm$2.9%) between both datasets is obtained. In a subsequent step, a better quantification of the associated error budget will be attempted.

Ozone total columns: improved consistency between various data sets

The successive advances in the ozone retrieval procedures from FTIR spectra have resulted in significant improvements in the agreement of the FTIR total column ozone data with correlative data, in particular with the co-located SAOZ data, TOMS overpass data and Dobson data from Arosa. Figures 12 and 13 show the intercomparisons between successive versions of the FTIR and SAOZ daily mean ozone data (see also section 4.1.1) and the TOMS and Dobson data. The successive versions of the FTIR data are: (i) the common SFIT retrieved data, using a fixed a priori profile, annotated 'FTIR-noclim', (ii) the SFIT retrieved data using the climatological tropopause dependent model for the a priori profiles, annotated 'FTIR-

clim' (cf. section 3.5.1), and (iii), the FTIR total column data obtained from a vertical inversion with SFIT2 as discussed above, annotated 'FTIR-SFIT2'. As to the SAOZ data, successive versions are : (i) the SAOZ vertical column data based on a climatological sine-like air mass factor, annotated SAOZ-sine, (ii) the SAOZ vertical column data based on an air mass factor that is calculated using the above mentioned climatological model for the ozone profiles, annotated 'SAOZ-clim', and (iii), the actual new SAOZ homogenised time series as described in section 4.1.1 that uses again the sine-like air mass factor, annotated as 'new SAOZ-sine'. Figures 12 and 13 plot relative differences (in percentage) between the various data sets, and indicate the mean and standard deviation (between parentheses) over the respective time series. The period before April 1992 is eliminated from the evaluation of the mean and standard deviation, because of known biases in the data caused by the Pinatubo aerosol loading in the atmosphere. Also the SAOZ-sine and SAOZ-clim data beyond 1998 shouldn't be considered because they are obtained with the upgraded instrument, before revision and homogenisation of the whole time series (see section 4.1.1). It must be noticed that Dobson and TOMS data have not been corrected for the differential ozone column between the altitude of the Jungfraujoch and that of Arosa and ground-level, respectively, which explains part of the observed biases.

It clearly appears in the various graphs that there is a seasonal variation in the relative differences with FTIR-noclim data, and that the amplitude of this sine-like variation decreases upon use of the climatological model for the a priori profiles (FTIR-clim). This decrease is most significant in the intercomparison between FTIR-clim and SAOZ-clim data. If however the vertical profiles are really retrieved (FTIR-SFIT2), then the consistency with the TOMS and Dobson data becomes very good : the standard deviation of the difference, which is a measure of the scatter, decreases to about 2%, to be compared with 3 and 5% in the former cases for the comparison with TOMS and Dobson, respectively. There appears a change in behaviour in the FTIR-SFIT2 versus TOMS and Dobson intercomparison around mid-1997 : this is explained by a realignment of the FTIR instrument at the Jungfraujoch, making the retrievals before the realignment less reliable. We also see that the scatter of the newSAOZ-sine data with respect to TOMS and Dobson data (of order 4.5%) is larger than that observed for the FTIR-SFIT2 data with respect to these data (of order 2%), proving that the reduction of uncertainties in the vertical distribution obtained with the FTIR inversion is worth the effort even for total column determinations. This is illustrated very clearly in early 1999, when exceptionally high ozone columns were observed : FTIR-SFIT2 catches the high values and therefore the high discrepancies observed in this period in the intercomparisons with other FTIR data sets (Figure 13, upper 2 plots) disappear. Climatological approaches, like the one adopted for the

SAOZ air mass factors, cannot compensate sufficiently for day-to-day variations. This latter point is confirmed by the fact that the scatter of the FTIR-SFIT2 data is higher with respect to the new SAOZ-sine data than with respect to the TOMS and Dobson data, despite the fact that the SAOZ data should better correlate because of the closer co-location of the sampled airmasses. Overall the agreement between the latest versions of all ozone data sets is within 3% (±5%).

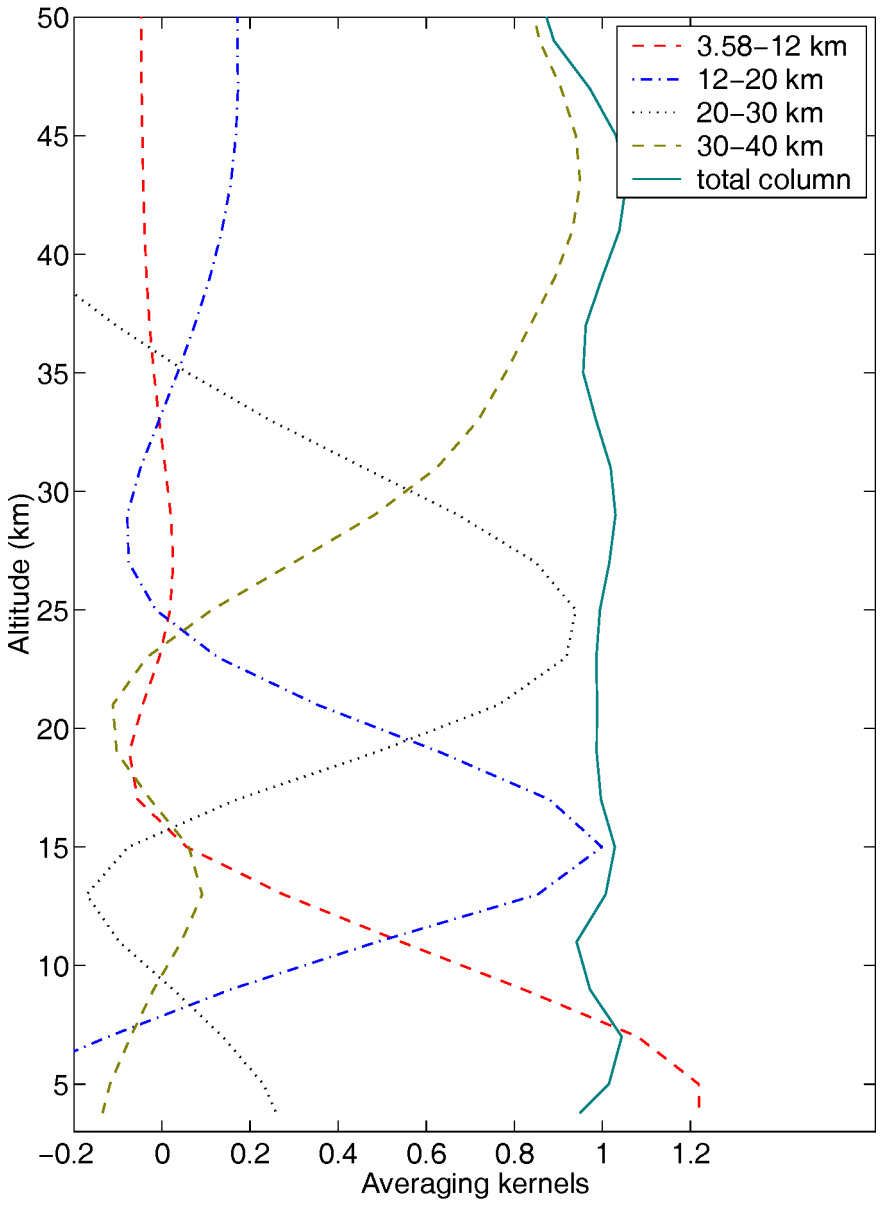

Figure 10: *Averaging kernels for ozone profile retrieval in the 1002.6-1003.3 cm^{-1} for spectral characteristics typical of the Jungfraujoch FTIR solar spectra. Layer averaging kernels are represented corresponding to the 4 independent information elements (see legend on top), as well as the averaging kernel for the total column (solid line).*

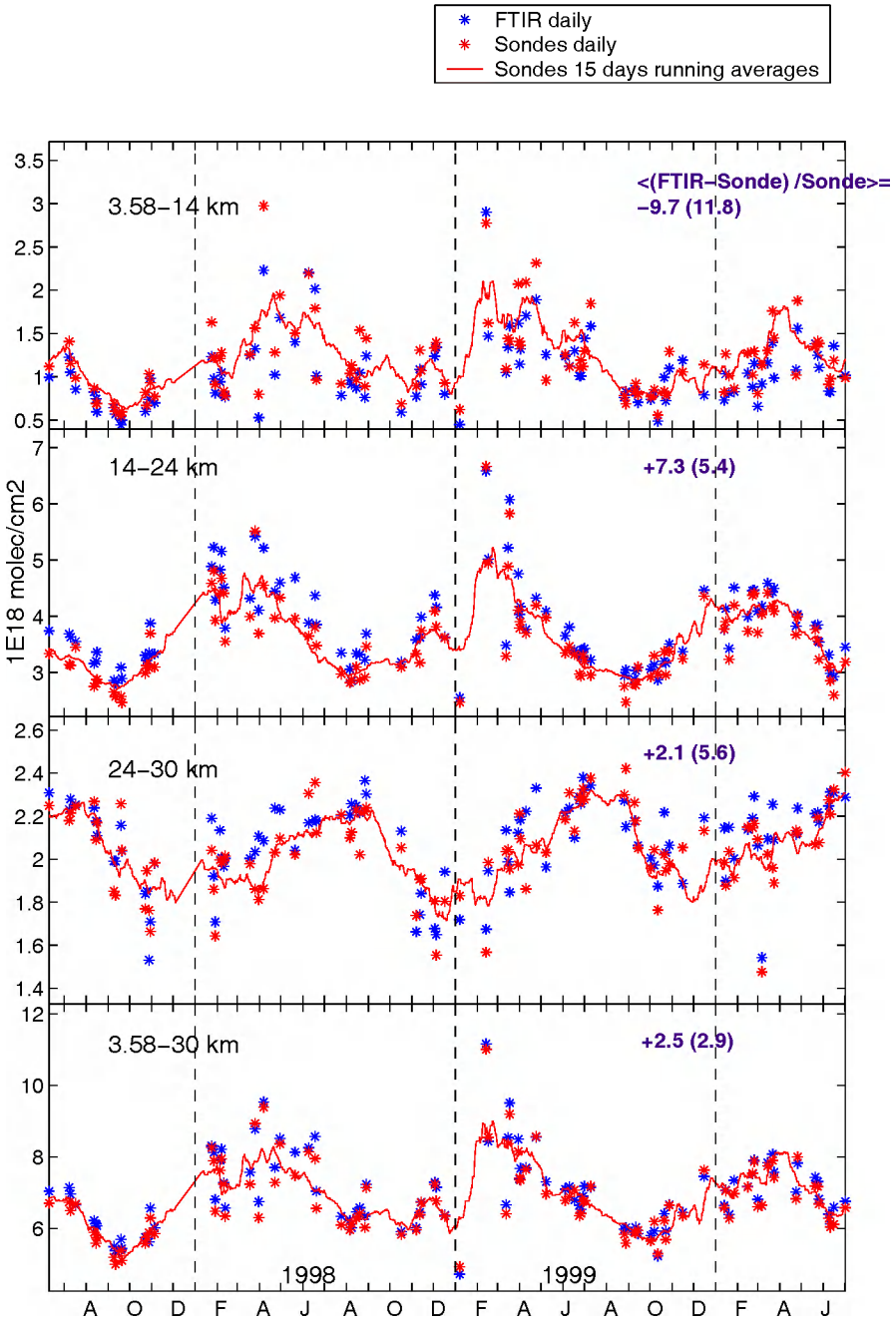

Figure 11: *Comparison between ozone partial column abundances retrieved from FTIR spectra at the Jungfraujoch (black asterisks) and from ozone soundings at Payerne (daily values: grey asterisks; 15-days running means: solid line). The layers are, from top to bottom, 3.58-14 km, 14-24 km, 24-30 km, and the total range covered by the soundings (above the Jungfraujoch altitude) 3.58-30 km. In the upper right corner of each plot is given the mean relative difference (in percentage) between FTIR and sonde data and its corresponding standard deviation (in parentheses).*

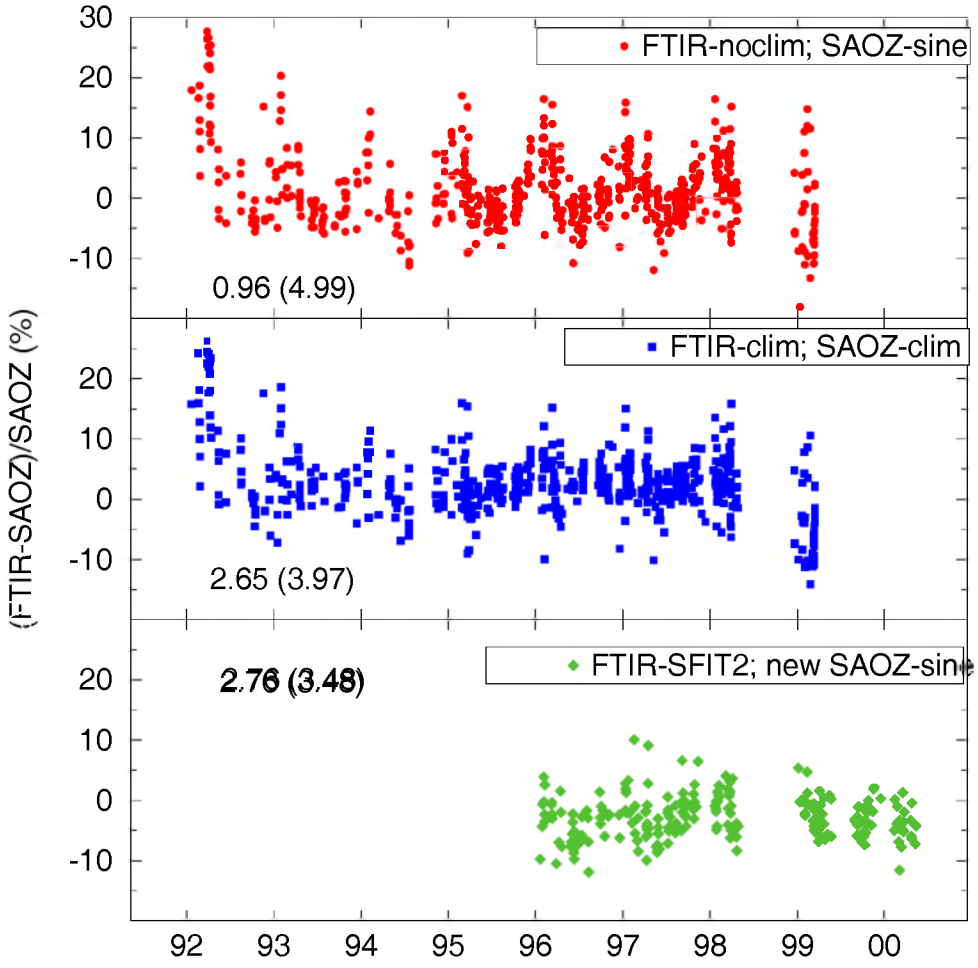

Figure 12: *Relative differences, in percentage, between different sets of correlative data for total ozone measured above the Jungfraujoch. For identification of the various data sets: see text.*

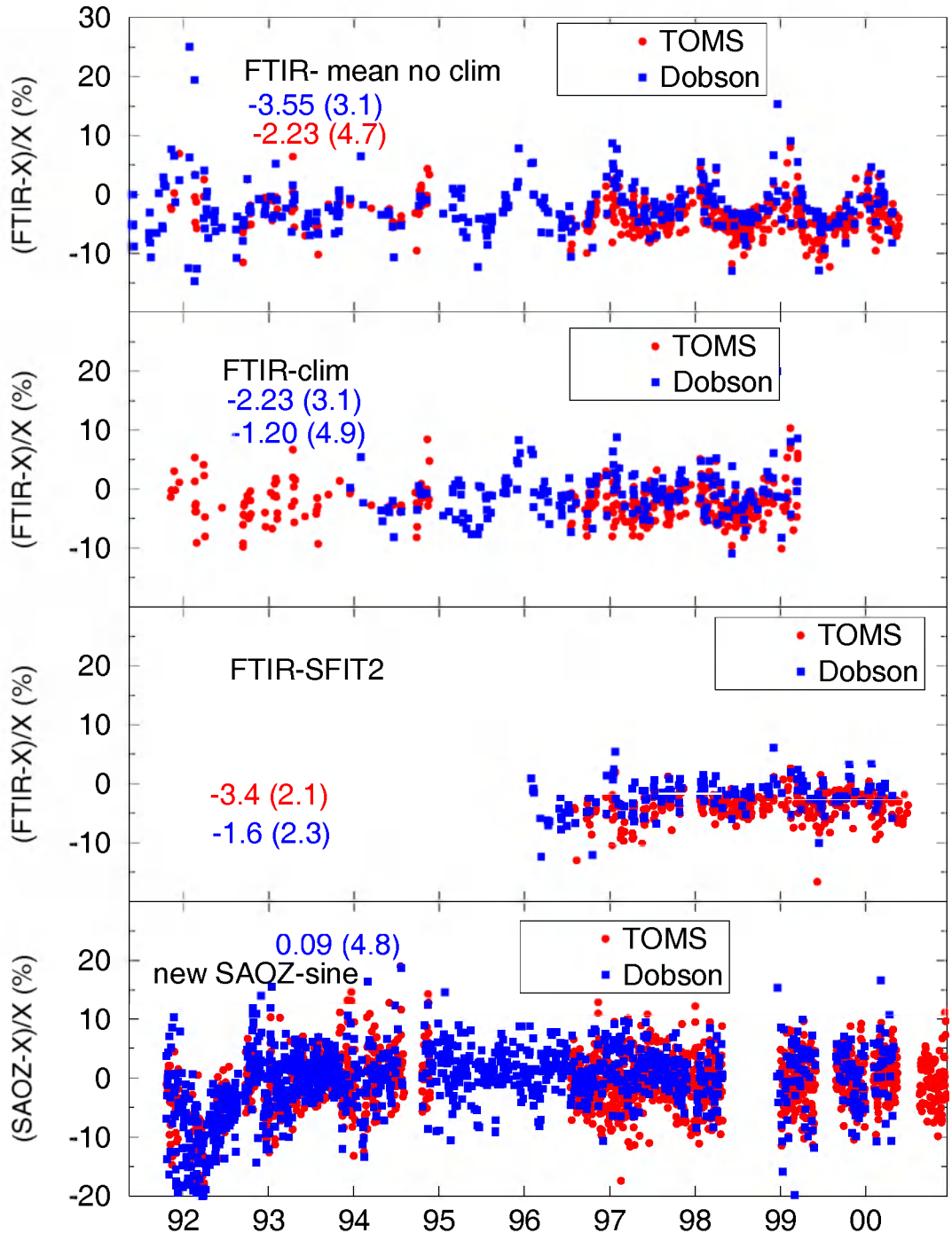

Figure 13: *Similar to Figure 12, but for other total ozone data sets.*

HF profile inversion and comparison with HALOE

HF profiles were retrieved from the spectral microwindow from 4037.8 to 4039.1 cm^{-1} for a 14 months record between November 1995 and January 1997. Comparisons with HALOE overpass profiles were performed in 2 layers from 20 to 28 km and from 28 to 40 km (Figure 14). In the bottom layer, the FTIR results are higher than HALOE (<HALOE-FTIR> = -11.1±10.1%) while they are lower in the top layer (11.6 ± 9.0%). Both layer biases compensating each other, the agreement is very good in the total layer (-2.4 ± 6%). Two reasons can explain this lack of height resolution. The averaging kernels for the two layers are not well separated and the ILS could not be retrieved in this spectral domain. During the intrusion of HF-rich polar air masses in mid April 1996 (PV at 475K of 38 PVU on April the 18th 1996) a very good agreement was found between the space-based and ground-based instruments in the 20 to 28 km layer.

These results were presented at the Quadrennial Ozone Symposium - Sapporo 2000.

Comparison of stratospheric O_3, HF and HCl with the 3D CTM SLIMCAT for the 1999-2000 winter

The vertical distributions of O_3, HF and HCl were retrieved from the Jungfraujoch FTIR spectra for the winter 1999-2000. For O_3 and HF, the same microwindows as above were used, while the spectral interval 2925.69 to 2926.21 cm-1 was used for the retrieval of the HCl vertical distribution. The results of the retrievals were compared to the results of a run of the 3D CTM model SLIMCAT for the location of the Jungfraujoch. For O_3 (Figure 16, lower plot) and HCl (Figure 15, lower plot), the modelled integrated stratospheric columns (from 12 to 55 km) are in very good agreement with the FTIR measurements. For HF, the measured stratospheric columns are systematically 30% lower than the modelled ones (Figure 15, upper plot). This effect is due to a tuning of the CFC and HFC´s emissions in the model, which does not reproduce the absolute stratospheric HF quantity. Concerning the vertical profiles, except for O_3, the discrepancies are high between the model and the measurements. For HCl and HF, the profiles retrieved from the FTIR spectra have systematically lower values than the modelled profiles in the lower stratosphere (below 20 to 24 km) and higher ones in the middle to upper stratosphere. The explanations for these discrepancies have not yet been studied in detail and require a better characterisation of the retrievals. The situation is better for ozone, for which one does not observe systematic oscillations between the measured and the modelled profiles. The O_3 partial columns between 12 and 28 km (Figure 16, upper

plot) observed by both the ozone sondes and the FTIR spectrometer are in good agreement with the model except in March and April 2000 with both techniques measuring values lower than the modelled ones suggesting a problem in the modelisation of midlatitudinal ozone for this period. Also for HCl, discrepancies between FTIR and model data seem to be larger in April than in the earlier part of the winter.

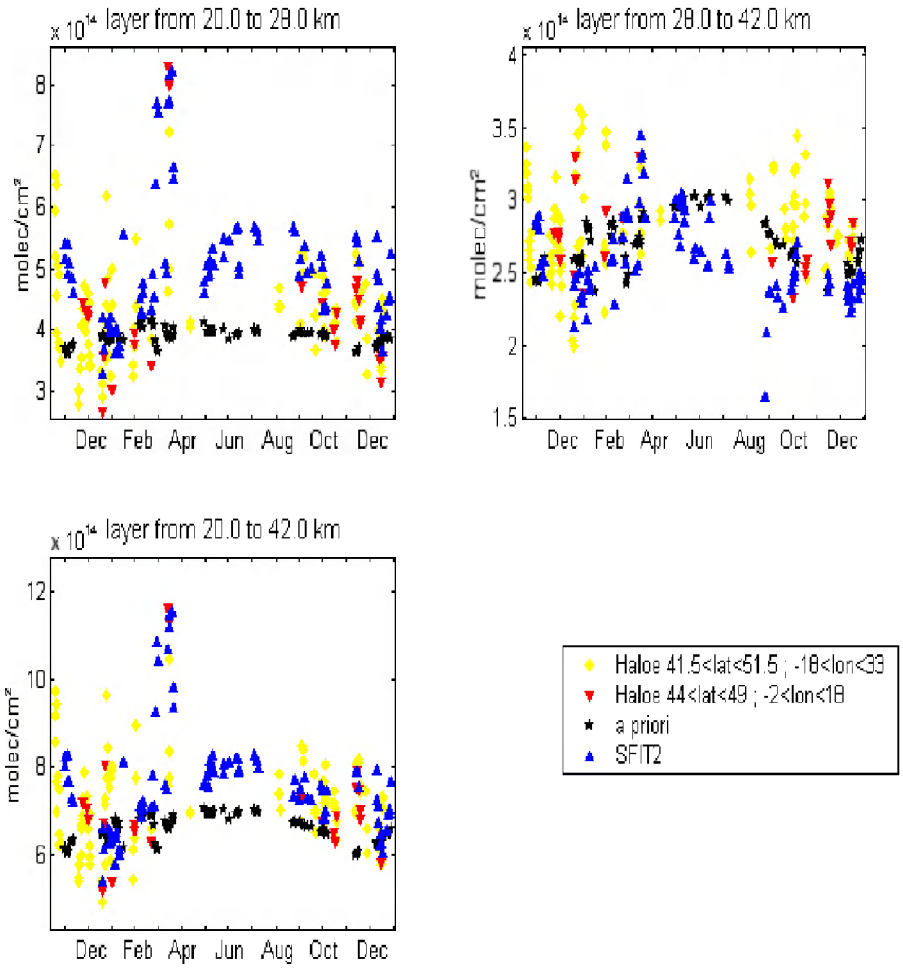

Figure 14: *Comparison between HF partial column abundances from FTIR measurements at ISSJ (SFIT2, blue upward triangles) and correlative HALOE observations (yellow diamonds and red downward triangles, for more or less restricted spatial coincidence, respectively), in 2 stratospheric layers (upper left: 20-28 km, and upper right: 28-42 km) and for the total layer between 20 and 42 km (lower left).*

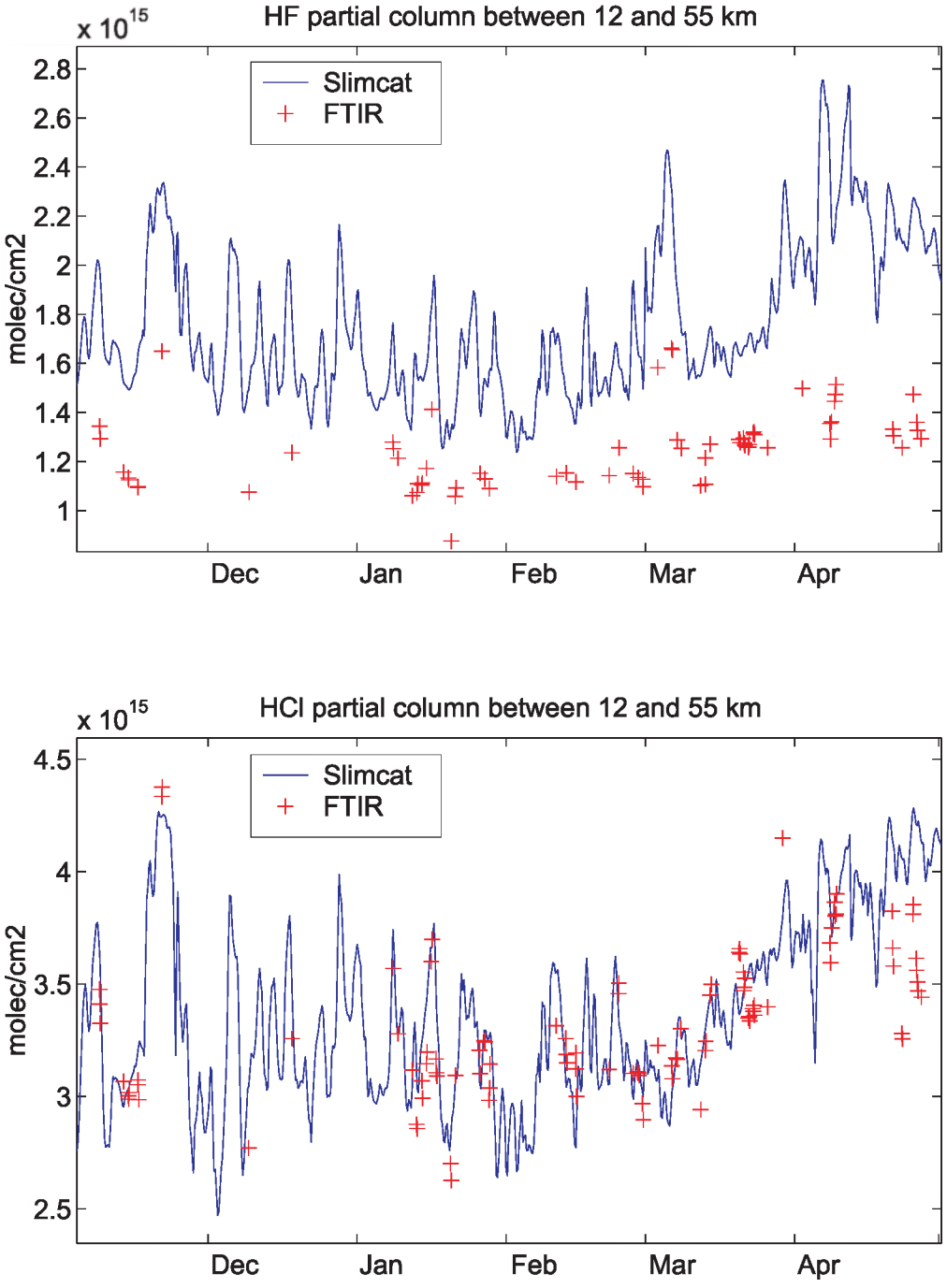

Figure 15: *Comparison between HF (top) and HCl (bottom) stratospheric column (12-55 km) data retrieved from FTIR spectra at the Jungfraujoch (+) and corresponding data from the 3D CTM SLIMCAT model (solid lines).*

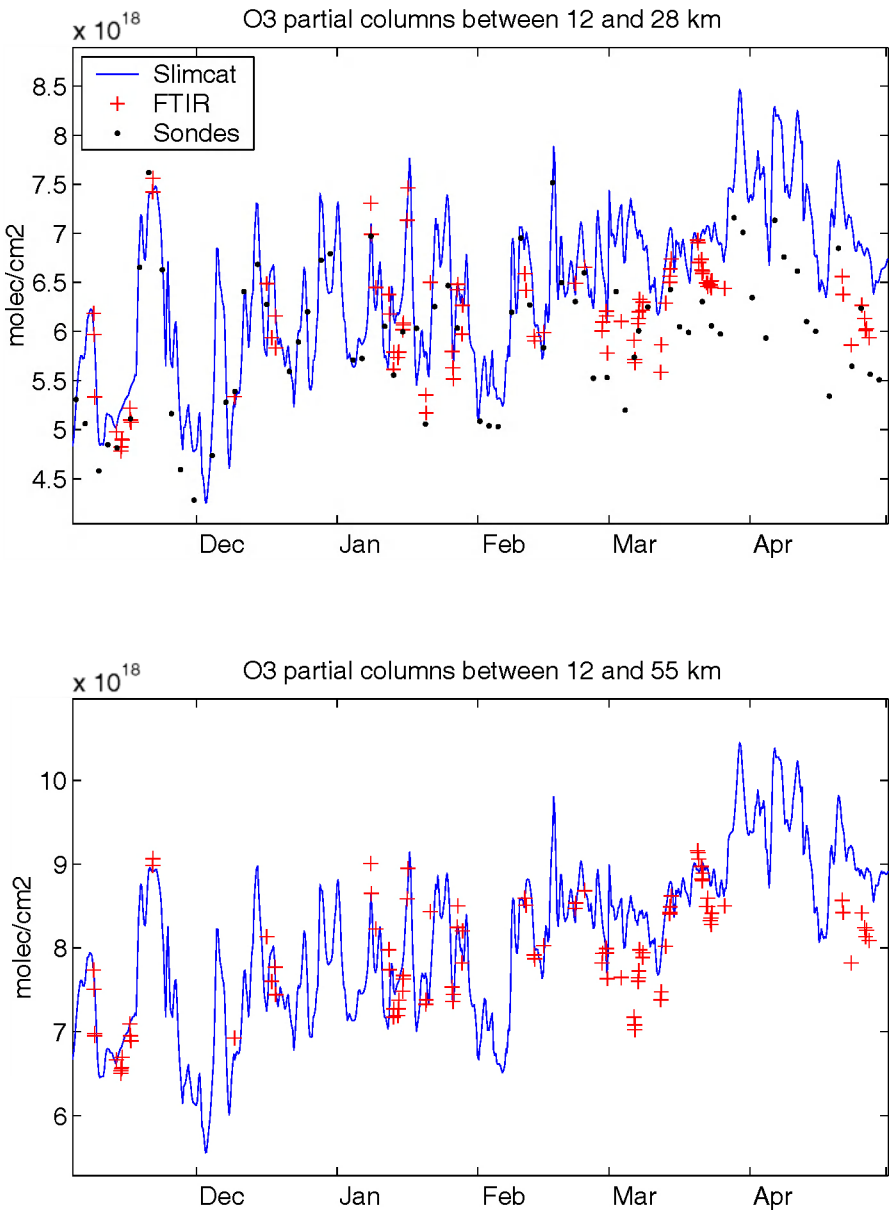

Figure 16: *Similar to Figure 15 but for ozone. Upper plot: partial columns between 12 and 28 km, with in addition sonde data from Payerne (•); lower plot: stratospheric columns (12-55 km).*

3.6 Wspectra and bFit

The analysis of reference spectra recorded in the laboratory under strictly controlled conditions must be of the best possible precision. Therefore analysis programs that are capable of retrieving highly accurate intensity and profile parameters of the absorption or emission lines of the atmospherically relevant molecules are required. Two computer programs – WSpectra and bFit – have been developed to satisfy this requirement.

WSpectra is a Windows 32 bit program developed to view, find, manipulate and, most importantly, measure the line parameters of high-resolution FT spectra. Measuring spectral lines parameters consists in a process done in two consecutive steps.

The first step consists of automatically finding all the lines in a spectrum. It is done by determining the zero-crossing points of the first and second derivatives of the spectrum. The finding procedure is followed by a second step in which each found line is, in turn, fitted by least squares to a theoretical line profile that provides the searched parameters. In Wspectra, the theoretical line profile can be a simple Voigt profile taking into account the temperature and pressure effects, or the more sophisticated Rautian-Sobelman and Galatry profiles that refine the profile by modelling the effect of molecular collisions. Wspectra is capable of measuring isolated absorption lines with a precision on the line position as good as 5 10^{-6} cm^{-1}, and a precision on the absorbed light intensity better than 0.5%.

bFit, also running under the Microsoft Windows operating system, measures absorption line parameters by adjustment of a synthetic spectrum to an observed spectrum, using a Levenberg-Marquardt least squares fitting procedure. The synthetic spectrum is calculated by convolution of a monochromatic Voigt transmission spectrum with an instrument line shape function, which includes the effects of the finite maximum optical path difference and the finite entrance aperture in the interferometer (Birk et al., 1996). Any number of lines (limited by available memory) can be fitted simultaneously. Adjustable parameters include the position, the intensity, the Gaussian width, the pressure self- and air-broadening parameters of each line, the diameter of the entrance aperture of the interferometer and the background level (modelled by a second order polynomial expansion).

The user has full control on the choice of parameters to fit.

3.7 New correction procedures for the pump efficiency of Ozone sondes

The vertical distribution of ozone is measured at RMI since 1969 with the Brewer-Mast (BM) ozonesondes. For various reasons it was decided to change to the Z-ECC type of ozonesonde in 1997. To assure the homogeneity of the long-term data series it was necessary to have good information on possible systematic differences between data obtained with both types of ozone sensors. Results of international intercomparisons found in the literature were not conclusive, and not applicable to our station. Therefore a campaign of double soundings, carrying both types of sonde on the same balloon was started in October 1996. By the end of 1997, 23 successful pairs were available for intercomparison.

Figure 17 shows that with the standard operational procedures there is a systematic, altitude dependent difference between both types of profiles. Near the ground the BM sondes measure on average up to 15% more ozone than the Z-ECC sondes. Around the 40 hPa level (which is near the mean level of the ozone maximum at 22 km) the agreement is excellent, but at higher levels the BM sondes underestimate the ozone amounts, ending by about -5 % at the highest level of the soundings. The differences are statistically significant in the whole troposphere and above the ozone maximum. An earlier intercomparison of the Brewer-Mast ozone profiles in Uccle with ECC profiles measured in De Bilt (NI) showed similar deviations. From those results, it was suspected that an underestimation of the decrease of the pump efficiency with decreasing pressure of the BM sondes causes these discrepancies.

In addition to the double soundings the efficiency of the pumps of both types of sondes was tested in a vacuum chamber at different pressures and temperatures before launch. From the results of these extensive measurements, a new altitude dependent correction profile was proposed. When it is applied the two types of ozonesondes agree to within 3 % (see thick line in Figure 17), while the differences are statistically insignificant over nearly the whole altitude range (0-32 km). The standard deviation of the differences is also lower, suggesting that part of the instrumental noise in the differences has been removed.

Detailed results of this study are reported in De Backer et al. (1998).

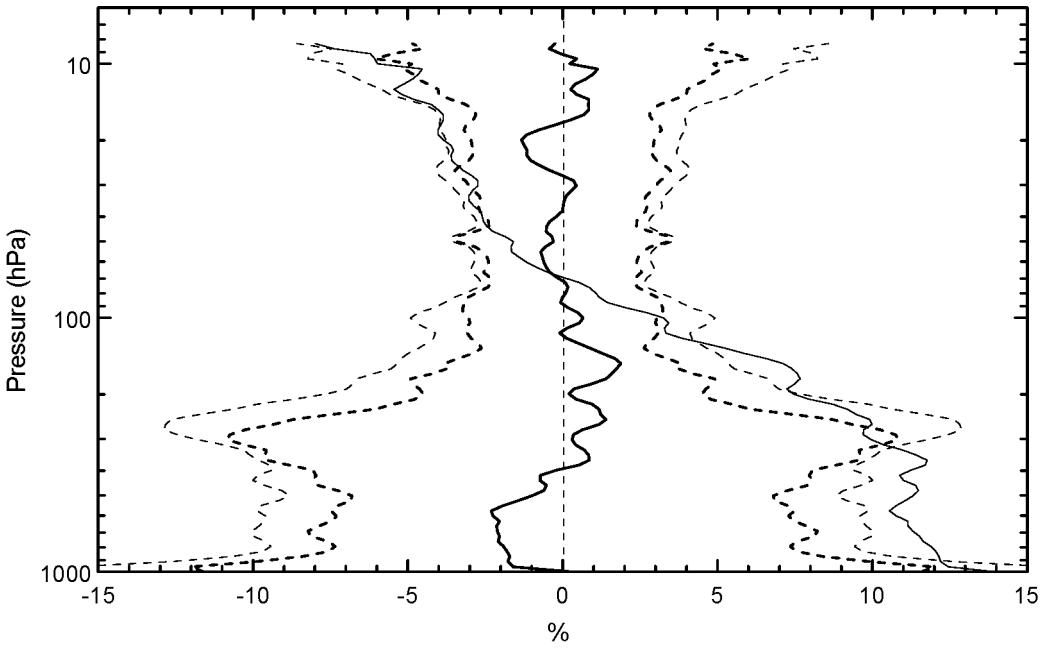

Figure 17: *Mean percentage differences between ozone profiles obtained from simultaneous measurements with Brewer-Mast and Z-ECC sondes with the standard (thin solid line) and the newly proposed (thick solid line) correction procedures in Uccle. The thin and thick dashed lines give the standard deviation of the differences, with the standard and new correction procedures respectively.*

4. RESULTS OF GEOPHYSICAL RELEVANCE

4.1 Evaluation of long-term atmospheric chemistry data. Variability and global changes of the atmospheric composition

The long-term monitoring performed at the four stations of the Jungfraujch, Harestua, OHP and Uccle contributes to the NDSC programme (Uccle has been recognised officially as a secondary NDSC station by the end of 2000). The NDSC was incepted in the mid-1980s, in response to the need for the scientific community to identify, document and understand atmospheric composition and climate changes. The NDSC dual goal of observation and understanding, as well as its task of establishing the links between stratospheric changes, ultraviolet radiation at the ground, and tropospheric chemistry and climate, requires the investigation of key stratospheric species resulting from manmade source gas emissions at the ground and affecting the stability of the ozone layer. They include HCl, OClO, $ClONO_2$, HNO_3, NO_2, and NO, which along with O_3 allow to investigate the relative impact of chlorine- and nitrogen-bearing species upon the ozone erosion via the Cl_x and NO_x catalytic cycles, and additional constituents among which species such as BrO, HF and COF_2, as well as source gases and tracers of atmospheric circulation and dynamics (e.g., N_2O).

The data obtained during the ESAC project have been merged with previous results, in order to build long-term data bases and draw conclusions concerning the long-term behaviour of stratospheric and tropospheric constituents and to distinguish it from short-term (daily, seasonal and interannual) variabilities. Attention has been paid to the long-term homogenisation of the various time series, by internal consistency checks and verifications with respect to correlative data. Validated time series have been submitted to international databases, in particular NADIR/NILU (http://www.nilu.no/projects/nadir) and the NDSC database at NOAA (http://www.ndsc.ws).

4.1.1 Long-term data at the Jungfraujoch

Already in 1989 (Kurylo and Solomon, 1989), the NDSC selected the Jungfraujoch as part of its northern hemisphere mid-latitude "Primary Alpine Station", on the basis of infrared solar observations and related monitoring activities performed successfully by the "Groupe Infra-Rouge de Physique Atmosphérique et Solaire" (GIRPAS) of the University of Liège (ULg) during previous years. BIRA-IASB has added a SAOZ UVVis instrument at the Jungfraujoch in 1990. At present, the responsibilities for the long-term data at the Jungfraujoch lie with GIRPAS (ULg) for the FTIR data, in collaboration with KSB-ORB and BIRA-IASB, and with BIRA-IASB for the SAOZ UV-Vis data.

During the period covered by this contract (1/12/1996 to 5/31/2001), solar FTIR observations have been performed on 555 clear sky days which are reported by month in Table II; this required the presence at the site of observers from ULg, IASB/BIRA and ORB/KSB during more than 1100 days. Overall, the FTIR monitoring activities conducted consistently at ISSJ primarily cover the period from 1985 to present, with some investigations reaching back to the mid-1970s, even to 1950 (e.g., Zander et al., 1994).

Since 1991, climatological observations of NO_2 and O_3 total columns at morning and evening twilight have been performed at the Jungfraujoch station using the SAOZ instrument. In early 1998 the original instrument has been irreversibly damaged; it has been replaced by a new version in late 1998. During this project, the homogeneity of the complete time-series of observations has been verified. The whole data set has been reprocessed using the latest version of the data analysis programme including most recent updates on laboratory data and corrections for seasonal drifts in instrumental slit functions previously identified. O_3 columns were

retrieved using climatological air mass factors as described in Van Roozendael et al. (1998). The complete time-series has been submitted to the NDSC data base.

Table II: *Number of days per month with FTIR observations at the Jungfraujoch.*

Month	1996	1997	1998	1999	2000	2001	TOTAL
JANUARY	9	17	13	9	15	10	**73**
FEBRUARY	6	8	17	6	8	1	**46**
MARCH	15	6	14	14	14	7	**70**
APRIL	9	12	9	13	9	8	**60**
MAY	7	16	12	5	10	15	**65**
JUNE	15	10	13	18	7		**63**
JULY	12	10	13	10	8		**53**
AUGUST	6	8	16	12	9		**51**
SEPTEMBER	10	20	9	9	12		**60**
OCTOBER	8	10	5	15	10		**48**
NOVEMBER	7	13	8	7	12		**47**
DECEMBER	4	2	12	4	1		**23**
TOTAL	**108**	**132**	**141**	**122**	**115**	**41**	**659**

The consistency of the O_3 time-series has been checked by comparison with TOMS and Dobson measurements as well as co-located FTIR measurements (see section 3.5.2.2). The systematic differences between these data sets are found to be smaller than 3%. Similarly the NO_2 time-series has been compared with HALOE and FTIR measurements (see Figure 18). This comparison reveals a systematic bias between the data sets. The FTIR instrument measures NO_2 columns in average 15% larger than the SAOZ, while HALOE measurements are approximately 10% smaller than SAOZ ones. Part of the discrepancy between SAOZ and HALOE can be explained by the tropospheric part of the NO_2 column not measured by the satellite. More work planned in the near future is needed to understand the origin of the differences between FTIR and SAOZ results.

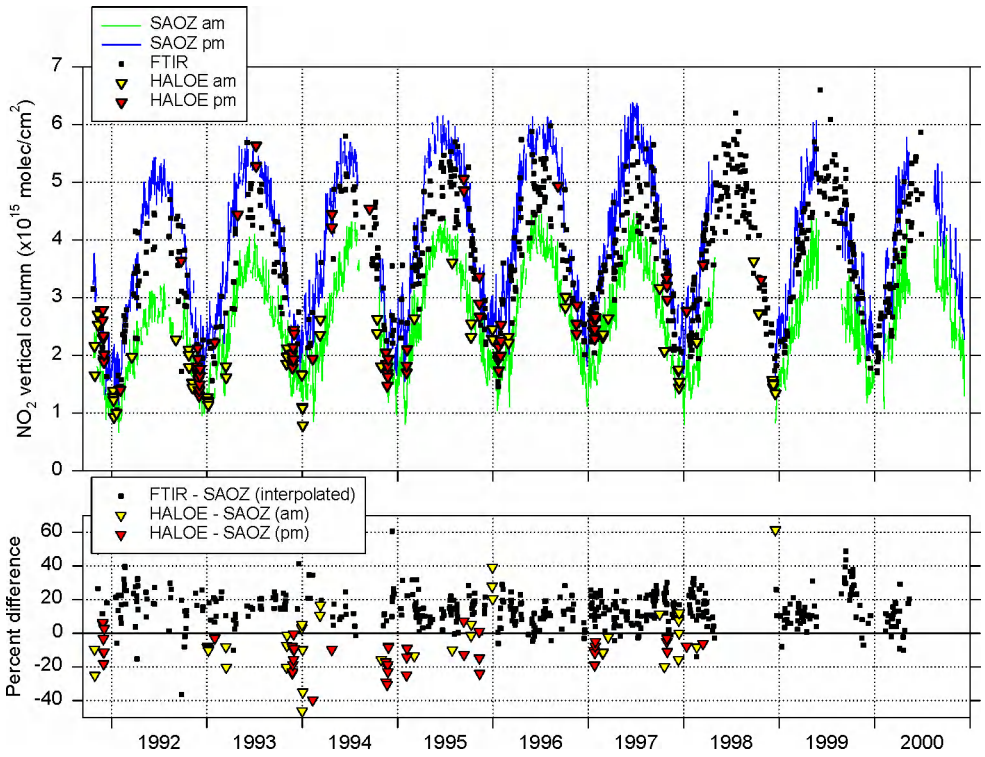

Figure 18: *NO_2 total column measurements by SAOZ, FTIR and HALOE instruments above the Jungfraujoch between November 1991 and December 2000 (upper plot). The relative differences between the various data sets and SAOZ measurements are displayed in the lower plot.*

Figure 19 reproduces the FTIR 1990-2001 daily mean vertical column abundance data sets of the key stratospheric species mentioned in the previous paragraph, as well as the long-lived N_2O and HF tracers. They all show noticeable seasonal variations (primarily resulting from the annual change in solar irradiance which affects photo-chemistry, temperature gradients and the tropopause height) as well as strong short-term variability during the winter-spring seasons (which is associated to enhanced meridional circulation and local dynamics), often superimposed on long-term rates of change (which essentially reflect the secular evolution of related source gas emissions at the ground). Consequently, mean secular trend characteristics can only be derived when the time bases are sufficiently long, so that short-term changes can be properly identified and be dealt with in a quantified way. Further noticeable in Figure 19 is the fact that short-term variability occurs primarily during the winter-spring months (December to May), so that secular trend determinations often are better defined by considering only summer-fall (June to November) measurements. In addition, monthly mean columns are often considered in trend evaluations, in order to attenuate the impact of months with different observation densities. With these considerations in mind (which may slightly affect mass loadings, but not trends), the following sections will deal with specific investigations involving various data sets of Figure 19 as well as additional ones of relevance within the ESAC context.

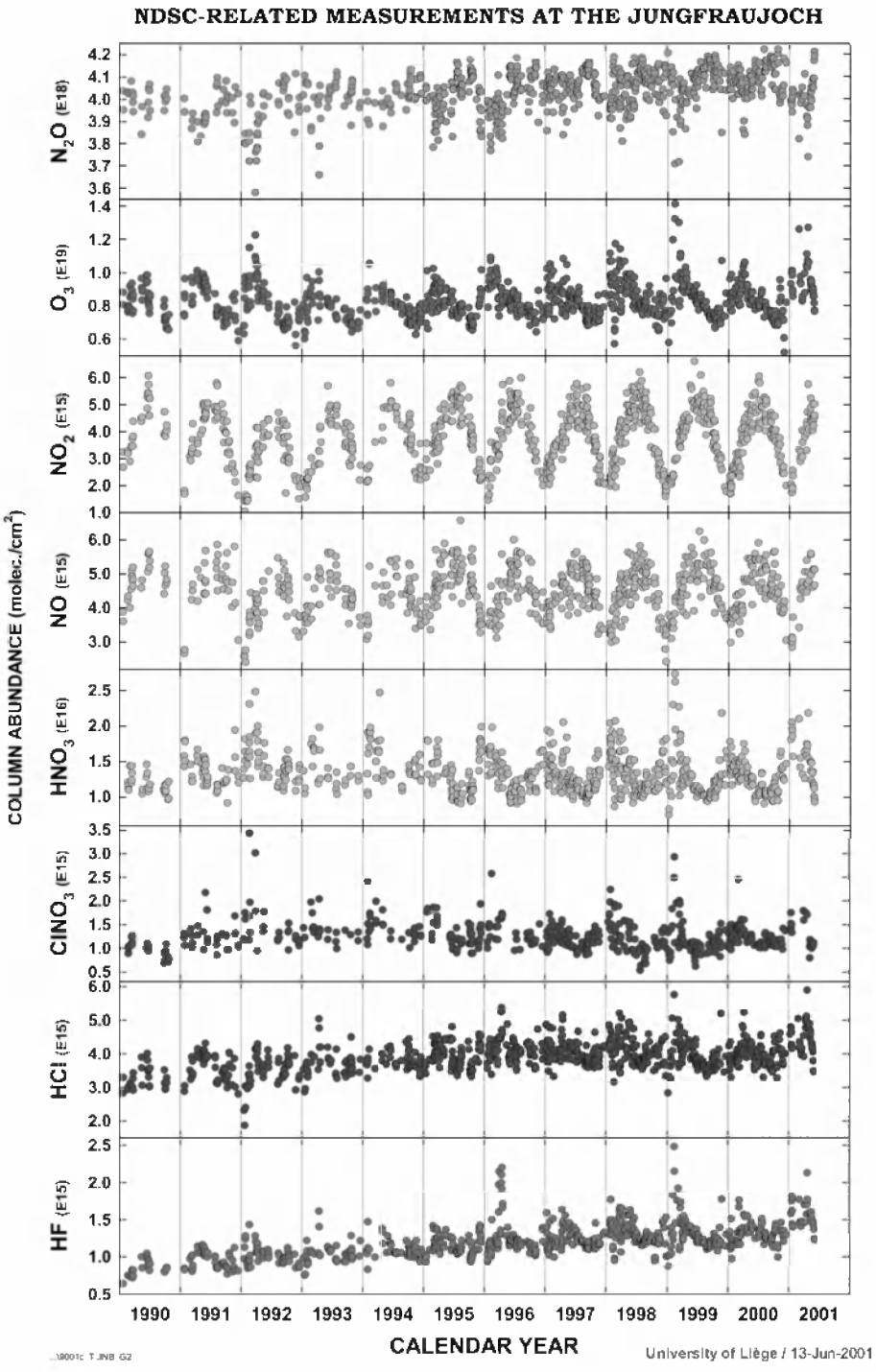

Figure 19: *An excerpt of daily mean vertical column abundances derived consistently from Jungfraujoch FTIR solar observations since the mid-1980s. The 8 molecules shown here are key species allowing to study the chemistry and dynamics of the stratosphere within the frame of the ULg commitment towards the international Network for the Detection of Stratospheric Change (NDSC).*

The following sections deal with specific research activities and findings related to these data sets.

4.1.1.1 Evolution of the budget of inorganic chlorine (Cly) above ISSJ

Inorganic chlorine primarily results from organic chlorine-bearing source gases released at the ground and sufficiently long-lived that they can be transported into the stratosphere and be broken apart by photolysis and reactions with OH and $O(^1D)$. Based on our current knowledge of inorganic chlorine partitioning in the stratosphere, total Cl_y is defined as follows:

$$Cl_y = [HCl] + [ClONO_2] + [ClO] + [OClO] + 2[ClOOCl] + [HOCl] + [ClONO] + [COClF] + [Cl] + 2[Cl_2] + [BrCl] \quad (1)$$

where the brackets indicate the vertical column abundances of each reported compound. In this evaluation, the dominant species present under normal background conditions at mid-latitudes are the two reservoirs HCl and $ClONO_2$ which can be measured and monitored in FTIR remote observations. They account, indeed, for over 92% of the total inorganic Cl_y loading (Zander et al., 1992) and their sum can be considered as a good Cl_y surrogate.

Figure 20 reproduces the monthly mean vertical column abundance measurements above the Jungfraujoch of HCl (circles) between 1977 and present, and of $ClONO_2$ (triangles) from 1986 to present. The full symbols correspond to the months of June to November, whereas the open symbols refer to the winter-spring months of December to May. Summing on the polynomial curves fitted to the summer-fall data points (full symbols; to avoid significant variability during the winter-spring time) gives the upper thick black curve labeled Cl_y which extends over the common time interval of 1986 to present. Inspection of the latter indicates that the growth rate of inorganic chlorine loading at northern mid-latitudes has progressively slowed down during the 1990s: it was equal to (4.4 ± 0.3) %/yr. between 1986-90, reaching zero sometimes during 1997-1998.

Discrete column changes (expressed in molec./cm^2/yr and in % of total column) for HCl, $ClONO_2$ and Cl_y are given in Table III.

When accounting for a mixing time of 3 to 5 years for long-lived chlorine-bearing source gases to reach mid-latitude stratospheric altitudes and decompose into inorganic compounds, the timely occurrence of this maximum Cl_y loading is in line

with the peaking of total organic chlorine (CCl_y) in the lower troposphere that occurred between mid-1992 and mid-1994 as found by two *in situ* global measurement networks, namely AGAGE (Advanced Global Atmospheric Gases Experiment) and NOAA/CMDL (National Oceanic and Atmospheric Administration/Climate Monitoring and Diagnostics Laboratory) (Montzka et al., 1999). As can be seen in Figure 20, the timely evolution of CCl_y resulting from AGAGE measurements (orange curve referred to the right hand volume mixing ratio scale) had to be shifted by +4.0 years for its peak to best match the maximum occurrence of the Cl_y loading above the Jungfraujoch. This result further agrees satisfactorily with model calculations (e.g., +3.7 years found by D. Considine at NASA-Goddard Space Center, Greenbelt, MD, USA; private communication, 2000) based on the scenario of chlorine-bearing source gas emissions controlled by the Montreal Protocol and its subsequent Amendments and Adjustments (WMO Report Nr.44, 1999).

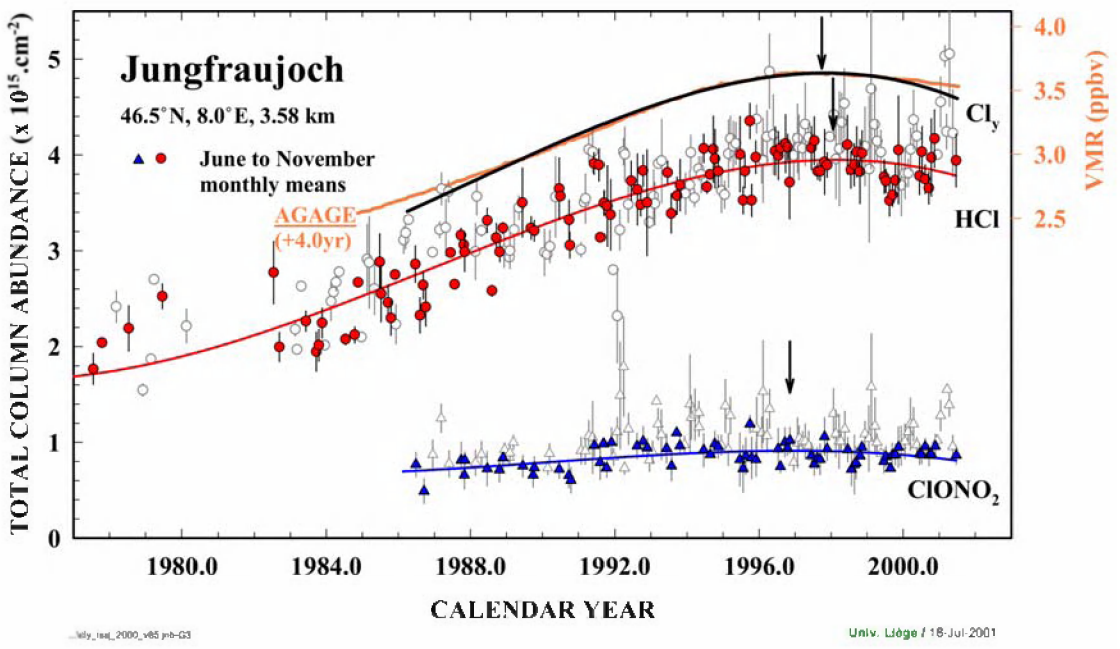

Figure 20: *The timely evolution of inorganic chlorine (Cl_y) above the Jungfraujoch based on monthly mean vertical column abundances of HCl and $ClONO_2$. The maximum Cl_y loading is found here to have occurred near the end of 1997, about 4 years after the load of organic chlorine peaked in the troposphere.*

Table III: *Typical column changes per year for species of relevance to Cl_y and F_y*

Species	**1987**	**1992**	**1997**	**2000**
HCl (x10^{14} molec/cm^2/yr)	1.50 (5.20%)	1.14 (3.20%)	0.17 (0.44%)	-0.7 (-1.8%)
$ClONO_2$ (x10^{14} - - -)	0.23 (3.10%)	0.23 (2.74%)	-0.05 (-0.55%)	-0.36 (- 4.24%)
Cl_y (x10^{14} - - -)	1.73 (4.80%)	1.37 (3.10%)	0.12 (0.25%)	-1.07 (-2.3%)
HF (x10^{13} - - -)	3.84 (5.12%)	5.51 (5.54%)	4.52 (3.60%)	2.61 (1.91%)
COF_2 (x10^{13} - - -)	0.41 (2.05%)	1.06 (4.40%)	0.47 (1.66%)	-0.50 (-1.75%)
F_y (x10^{13} - - -)	5.38 (4.68%)	7.26 (4.90%)	5.55 (3.06%)	2.75 (1.41%)
CFC-12 (x10^{14} - - -)	2.06 (3.70%)	1.33 (2.06%)	0.59 (0.85%)	0.15 (0.21%)
HCFC-22 (x10^{13} - - -)	0.73 (7.10%)	0.82 (5.80%)	0.91 (4.93%)	0.96 (4.53%)

The vertical arrows in Figure 20 correspond to the turnover times of the various curves, i.e., 1996.9 for $ClONO_2$, 1998.1 for HCl, and 1997.8 for the resulting Cl_y curve. The difference of over one year between the $ClONO_2$ and the HCl peak occurrences is definitely within the uncertainty of the peak determinations which have been estimated at ± 1.5 years for the former and ± 1.0 year for the latter at the 90% confidence level; these large uncertainties are due to the very slow rates of change observed in both the HCl and $ClONO_2$ columns, as well as their associated variabilities and measurement precisions. It should be further noted here that the interannual variations observed recently (e.g., the minimum during 1999 and the enhanced columns during winter-spring of 2000-2001 in the HCl data base) render the peak determinations uncertain. This has been raised by Anderson et al. (2000) and by Waugh et al. (2001) who have critically discussed the evolution of the HCl concentration near 55 km altitude as measured since October 1991 to present by the HALOE experiment aboard the UARS satellite. In particular, the latter concluded that the turnover time of HCl in the lower mesosphere, found by the former to occur as early as at the start of 1997 could not be explained by any model hypotheses that rather predicted late 1999. In our present research, it ought to be stressed that we are dealing with the integrated Cl_y columns and that its maximum occurrence in late

1997 is in much better agreement with the Waugh et al (2001) model calculations (D. Considine, private communication, 2000). To statistically improve the moment of the Cl_y peak occurrence, it is important to continue measurements during the next years and to combine a multi-station approach; this latter task has been initiated during the past months and involves 7 NDSC sites equipped with FTIR instruments and located in both hemispheres. Beside the Jungfraujoch, however, only two of these have sufficiently long observational time bases (Kitt Peak, USA and Lauder, New-Zealand) to contribute to improving the Cl_y issue as reported above; the other sites (Ny Ålesund, Spitzbergen; Zugspitze, Germany; Mauna Loa, Hawaii; Wollongong, Australia) have shorter data sets only allowing to assess the post-maximum evolution. Related findings will be presented by C.P. Rinsland (from NASA-Langley Research Center, Hampton, VA, USA) at the September 2001 NDSC Symposium to be held in Arcachon, France.

It should be noted here that we have tested and adopted an improved set of spectroscopic line parameters for $ClONO_2$ (Birk and Wagner, 2000), which leads to lower column abundances by about 10-15 % with respect to those reported earlier using the Bell et al. (1992) linelist. This partly accounts for discrepancies generally noted between observations and model calculations.

Once the Cl_y column decrease has been observed unambiguously, it will be important to correlate its rate of decrease with any subsequent change in the ozone layer, and estimate the time of full ozone recovery.

During the past three decades, the predominant chlorine-bearing source gases responsible for the increase of Cl_y in the stratosphere have been the anthropogenic CFCs and HCFCs. The Montreal Protocol (1987) was enacted and subsequently amended and adjusted in order to progressively and efficiently reduce the production and release to the atmosphere of those source gases with large ozone depletion potentials (ODP; see WMO Report No. 44 (1999)) thus causing significant threat to the stratospheric ozone layer.

While all source gase concentrations with noticeable ODPs are being monitored at the ground by *in situ* techniques and related to industrial production inventories and to protocol restrictions, it was thought useful to monitor the total column abundances above the Jungfraujoch of a couple of them, in order to have a quantitative link between Cl_y and CCl_y. CFC-12 (CCl_2F_2) and HCFC-22 ($CHClF_2$) were chosen, because of their clear and well defined absorption signatures in infrared solar spectra.

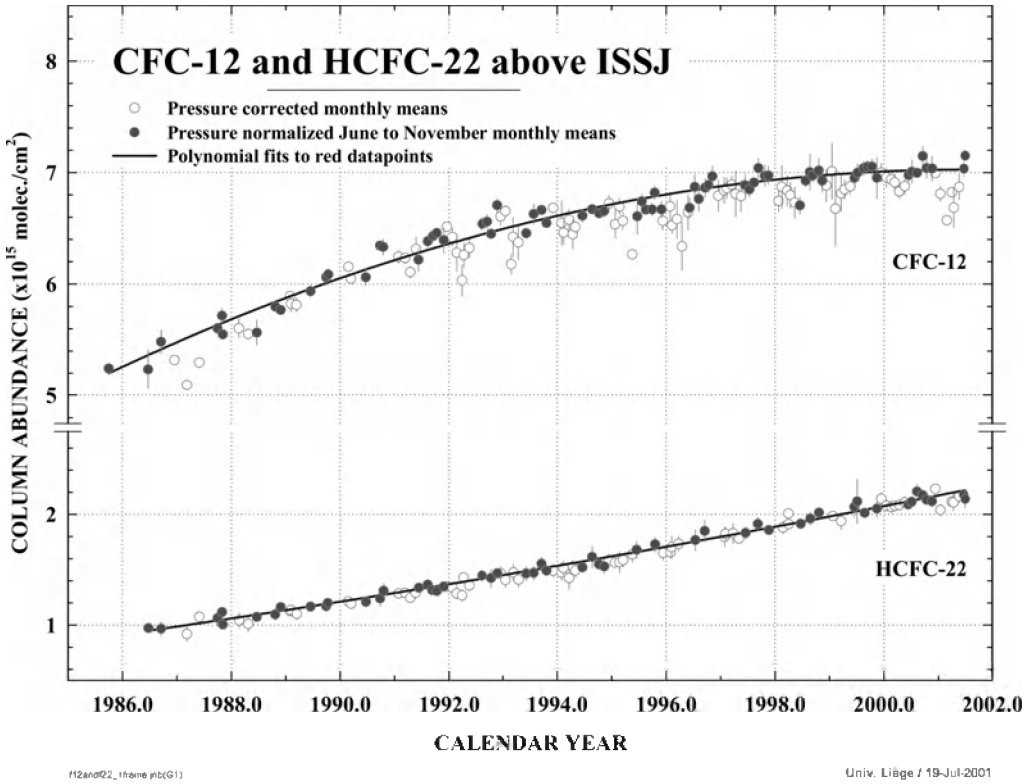

Figure 21: *The timely evolution above the Jungfraujoch of the column abundances of CFC-12 (CCl_2F_2) and HCFC-22 ($CHClF_2$) which are two important source gases contributing to the budget of Cl_y in the stratosphere. The former has been progressively phased out by the Montreal Protocol and subsequent Amendments, while the latter is not yet regulated.*

Figure 21 displays the monthly mean column abundances of CFC-12 and HCFC-22 as determined above ISSJ from the mid-1980s to present. Only the data points corresponding to the quietest June to November months have been considered in the polynomial curve fitting process for reasons already evoked before. While the rate of increase of the regulated CFC-12 has definitely slowed during the 1990s, it has not yet reached its maximum loading despite its production and consumption having been phased out to 100% in the developed countries in 1996 (WMO Nr. 44, 1999); this behaviour mirrors the evolution of CFC-12 observed at the ground (S. Montzka, NOAA, Boulder,CO, USA; private communication, 2001) and is indicative of the CFC-12 long lifetime (~ 100 years), applications with time-delayed releases (e.g., refrigeration, cellular foam blowing) and small consumption in developing countries.
On the other hand, the columns of $CHClF_2$ (HCFC-22; which is not yet regulated), have increased steadily; this increase is the consequence of this compound being used in various applications as a substitute for the banned CFC-11 and –12. Notice that HCFC-22 has a lifetime of 12 years and thus will be removed from the atmosphere much faster than CFC-12 after its phase out has begun in 2004.

Discrete column increases for CFC-12 and HCFC-22 are reported in Table 3; they have been compared with increases measured at the ground by *in situ* techniques and found in excellent agreement (WMO Report Nr 44, 1999).

4.1.1.2 Evolution of the budget of inorganic fluorine (F_y) above ISSJ

Inorganic fluorine does not contribute to stratospheric ozone depletion (Stolarski and Rundel, 1975). However, the evaluation of its loading provides an independent check regarding the anthropogenic contribution to chlorine loading by CFCs and HCFCs because, thus far, the latter have also been the predominant sources of inorganic fluorine-bearing compounds in the stratosphere. Total inorganic fluorine, F_y, can be defined as:

$$F_y = [HF] + 2[COF_2] + [COClF] \quad (2)$$

Based on earlier fluorine budget evaluations from ATMOS measurements (Zander et al., 1992) and by MarkIV-balloon observations (Sen et al., 1996), HF and COF_2 account for some 98% of the total F_y column. Therefore, the combination as per equation (2) of the HF and COF_2 vertical column abundances measured above the Jungfraujoch is an excellent surrogate of the total inorganic F_y loading and its timely evolution.

The lower part of Figure 22 displays the monthly mean vertical column abundances of HF and COF_2 observed above ISSJ between 1985 and present. Their mean timely evolution is reproduced by polynomial curves fitted to all data points (all months were included here, as HF is a good tracer of meridional transport and dynamics/subsidence). Until the mid-1990s, both species showed relatively monotonous column increases which were in agreement with the continued emission increases of their principal parent source gases CFC-11, CFC-12 and HCFC-22 (Mahieu et al., 1998; Mélen et al., 1998). Subsequently, the fitted curves reveal a weak slowing down in the rate of increase of HF after about 1996, as well as a levelling off for COF_2 around 1997 and a subsequent slight decrease which, however, is not yet significant at the 90% confidence level. Further noticeable are the low columns observed for both species during 1999-2000 as well as enhanced columns measured during the first months of 2001. Whether this 2-year minimum is related to some special atmospheric circulation behaviour or special chemistry will have to await near future observations (it needs to be investigated in parallel with the 1999-2001 behaviour of HCl mentioned in Section 4.1.1.1.

The upper curve of Figure 22 reproduces the inorganic F_y atom total vertical column abundance evolution above ISSJ resulting from the combined contributions of HF and COF_2 as per equation (2). Here, data points have been displayed for months during which both HF and COF_2 measurements were available; the continuous curve corresponds to the best polynomial fit to all these points. Rates of column abundance changes for HF, COF_2 and F_y are also provided in Table III. The F_y rates of change are consistent with those found for the organic fluorine (CF_y) loading in the troposphere by the *in situ* networks AGAGE and NOAA/CMDL (WMO Report Nr. 44, 1999).

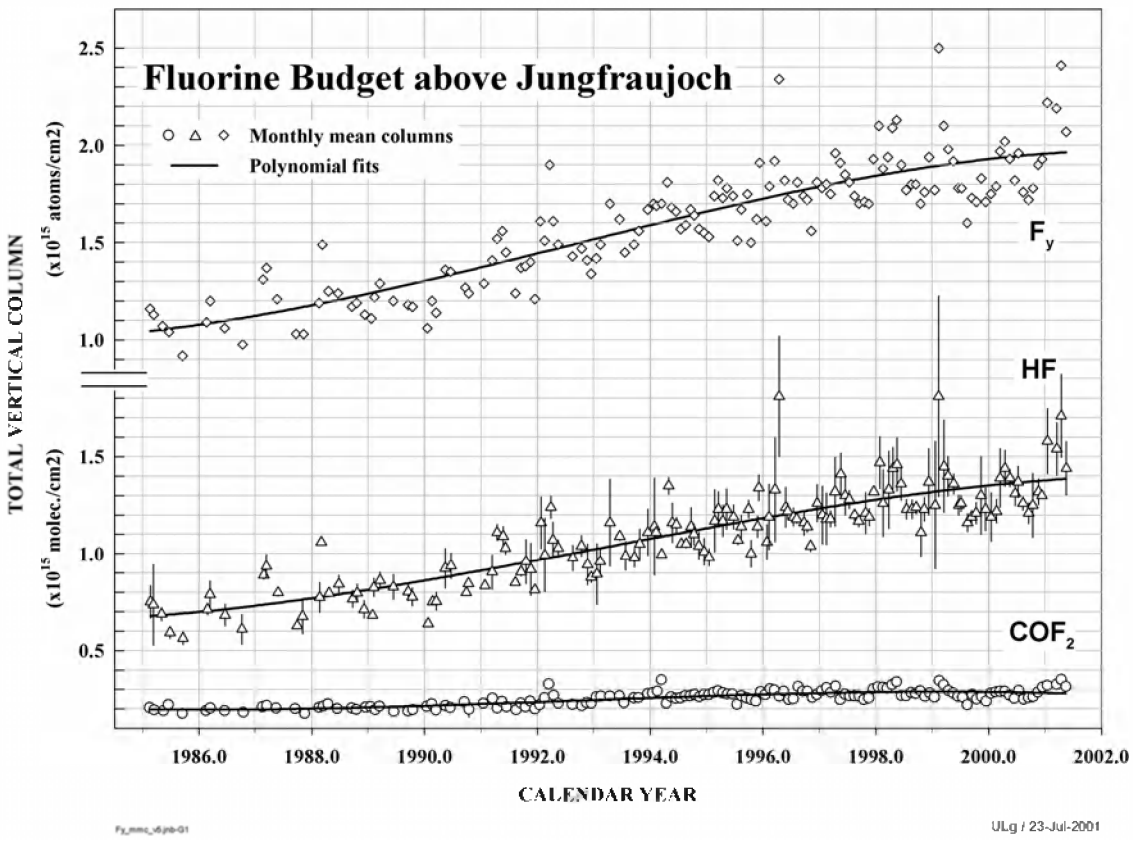

Figure 22: *The timely evolution of inorganic fluorine (F_y) above the Jungfraujoch obtained by combining the column abundances of HF and COF_2. The slowing down of the F_y rate of increase observed since the late 1990s results from the mixed use of regulated CFCs and substituted HFCs and FCs (WMO Report Nr. 44, 1999).*

The evolution of F_y observed here contrasts with that of the Cl-atom loading mentioned in the previous paragraph. It is further in disagreement with findings by Considine et al. (1997) who report a slowing in the rate of increase of HF above 55 km altitude, in a manner consistent with the tropospheric loadings and trends of CCl_3F and CCl_2F_2 in the early 1990s (Montzka et al., 1996); these findings were based on HALOE observations of HF volume mixing ratio profiles over the 50°N to

50°S latitude band. Contacts with modelers have been initiated to understand and quantify the above problem and with colleagues involved in *in situ* measurements to relate the observed F_y changes with CF_y loadings in the troposphere.

4.1.1.3 The evolution of HCl/HF

Beside long-term background column evolutions described in this report, related effects of atmospheric transport have also been investigated and identified, generally involving correlations with long lived tracers. Here, as HF is chemically stable in the stratosphere, any change in its column abundance will reflect some special circulation that brings masses of air above the Jungfraujoch having different latitudinal origins. Figure 23 displays the ratios of the HCl over the HF daily mean column abundances observed above the site on same days since 1991 (all circles).

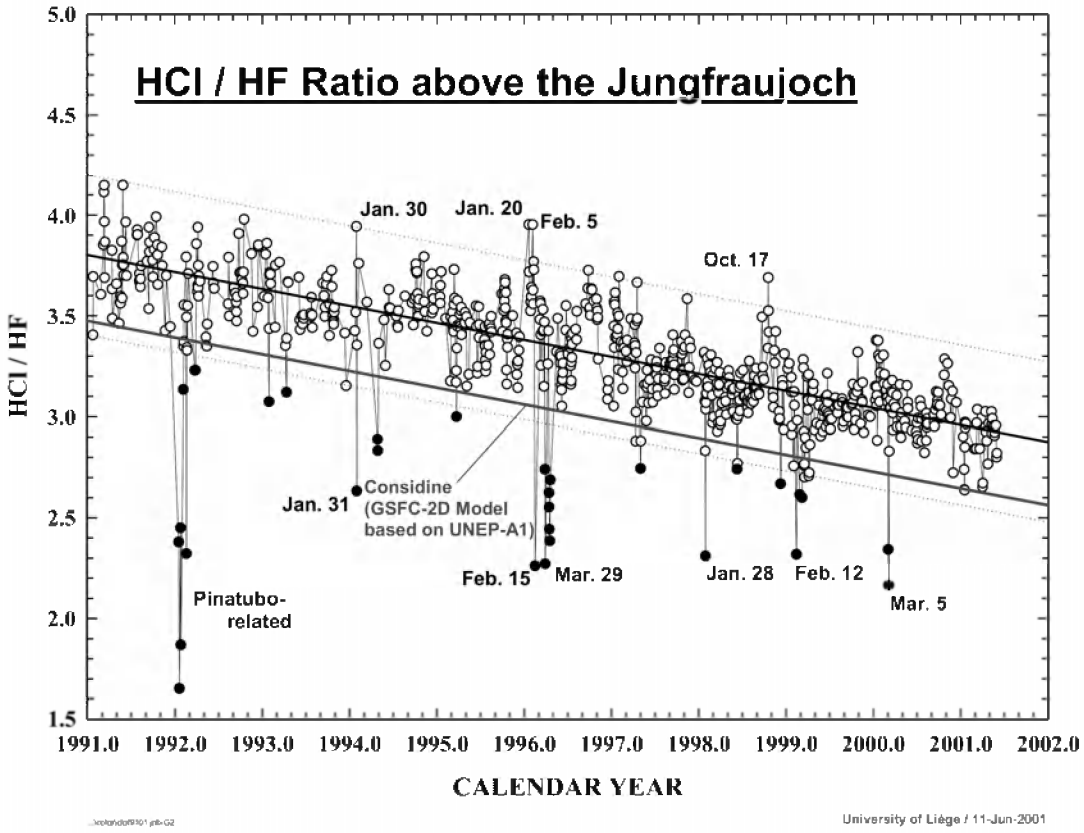

Figure 23: *Timely evolution of the columns ratio HCl/HF above the Jungfraujoch. The overall decrease results from the progressive phase-out by the Montréal Protocol and subsequent Amendments of Chlorine-bearing source gases with large ozone depletion potentials. This evolution is consistent with model predictions. The filled circles indicate days when masses of stratospheric polar air had been transported over central Europe and having eventually undergone heterogeneous chemistry processing in the presence of heavy aerosol loading and polar stratospheric clouds (e.g. low Pinatubo-related values).*

The overall tendency is given by a two-iterations linear fit to the data points; its regular decrease results from the relative background evolution of the HCl and HF loadings, which reflect changes in CFC-, HCFC- and HFC emissions mix; the 99% confidence range is delineated by the thin dotted lines. All HCl/HF ratios falling below this lower range are reproduced by filled circles. These latter, as well as a few ones observed above the high limit of the range are considered to result from unusual atmospheric circulation situations. The extremely low ratios observed during the winter 1991-92 primarily result from polar air transported to mid-latitudes after HCl had undergone heterogeneous conversion in the presence of polar stratospheric clouds at high aerosol loading resulting from the Mt. Pinatubo volcanic eruption in June 1991; this was further confirmed by the record high columns of $ClONO_2$ observed during this period (see Figure 19). Other special pre-1997 features in Figure 23 have been discussed by Mahieu et al. (1998).

During the more recent years, only isolated, less pronounced cases than those of early 1992 and early 1996, have been recorded, but all could be associated with high to low latitudes meridional transport. Confirmation of this latter relation could generally be obtained from the analysis of air circulation back trajectories and potential vorticity maps produced by the ECMWF and made available via NILU.

Worth being mentioned here is that the simultaneous analysis of HCl versus HF (correlation plot) allows to characterise the atmospheric loading of HCl at zero HF loading. The result already reported in 1996 (Zander et al., 1996) was confirmed on the basis of additional measurements performed during this ESAC project, indicating a pre-CFC background loading of HCl above the Jungfraujoch equal to (0.75 ± 0.1) x 10^{15} molec./cm^2. Additionally, series of analyses performed with the retrieval code SFIT2 (which allows to retrieve profile information versus altitude (e.g., Connor et al., 1996) have returned tropospheric columns equal to about (0.3 ± 0.1) x 10^{15} molec./cm^2. From these two estimates one can evaluate the stratospheric background burden of HCl to have been equal to (0.45 ± 0.2) x 10^{15} molec./cm^2 during the pre-CFC time. The weakest point in this evaluation results from the poor knowledge of the *a priori* profile of HCl in the troposphere.

4.1.1.4 *Evolution of the budget of NO_y above ISSJ, and the impact of Mt. Pinatubo on the NO_2 abundance*

The main contributors to the stratospheric budget of reactive nitrogen, NO_y, are NO, NO_2, NO_3, HNO_3, N_2O_5, HNO_4, $ClONO_2$ and $BrONO_2$. This budget is obtained by summing the individual columns of each compound, with N_2O_5 being counted twice. As NO_3, N_2O_5, HNO_4 and $BrONO_2$, which can not be measured from the ground (because, either they are masked by strong water vapour interferences, or their concentrations are too weak to be detected in infrared solar spectra), contribute at most for 5% of the total NO_y under typical daytime background conditions prevailing at mid-latitudes (WMO Report Nr. 44, 1999), the commensurate NO_y daytime column above ISSJ can be defined as:

$$[NO_y] = [NO] + [NO_2] + [HNO_3] + [ClONO_2] \qquad (3)$$

Since last reported (Demoulin et al., 1998; Mahieu et al., 2000) and as shown in Figure 19, the daytime daily mean burdens of these main reactive nitrogen species monitored above ISSJ have continued to show their characteristic seasonal modulation and large short-term and inter-annual variabilities. For reasons evoked before, the upper frames of Figure 24 reproduce the data points of Figure 19 (and their extensions back in time) converted into monthly means for the four contributing species, while the resulting NO_y values calculated as per equation (3) are shown next. It is worth noting the different ordinate scales for the various compounds, with mean contributions to NO_y equal to about 58 % for HNO_3, 20 % for NO, 17 % for NO_2 and 5 % for $ClONO_2$. Consequently, NO_y is heavily "biased" towards the characteristic variations of HNO_3 as well as its variability which is quite large during winter and spring. In this Fig. 6, all data sets have been fitted by a simple sinusoidal function (to visualise the seasonal variations) superimposed on a mean linear background trend. The mean linear rates of change so derived over the displayed time frame are found equal to: (+0.1 ± 0.1)%/yr for NO, (+0.6 ± 0.2)%/yr for NO_2, (-0.2 ± 0.2)%/yr for HNO_3, and (+0.8 ± 0.4)%/yr for $ClONO_2$ (a more detailed rate of change for this latter has been provided in Section 4.1.1.1 with discrete changes in Table 3). The monthly mean NO_y data points return a mean trend equal to (-0.1 ± 0.2)%/yr, which is statistically insignificant, despite the long measurement timeframe. The same remark holds for HNO_3 with its (-0.2 ± 0.2)%/yr rate of change, although this value has significantly improved as compared to the value of (-0.1 ± 0.4)%/yr derived earlier from the 1985-96 time base (Demoulin et al., 1998). It appears that the data bases for the individual species are best behaved as their sum, which likely results from the fact that NO_y data points are fewer than those making up the individual data sets (due to occasional missing monthly mean columns for one or

more of the contributing gases). As a consequence, an approach combining the different best fits to the latter sets (similar to that adopted for the Cl_y evaluation) is being envisaged.

At this time, NO_2 reveals a rate of change that is statistically significant. Its trend of (+0.6 ± 0.2)%/yr observed above the Jungfraujoch has been confirmed recently by Liley et al. (2000) who reported a rate of increase equal to (5 ± 2)% per decade, based on NO_2 UV-Vis measurements at Lauder (New Zealand) from 1984 to 1999. These findings at the two mid-latitude NDSC sites in both hemispheres are important results which modellers need to reproduce and help to understand.

Additionally, the post-Pinatubo HNO_3 column time base from 1992 to present has undergone a statistically significant rate of change equal to (-0.8 ± 0.4)%/yr when including all months of the year, and as high as (-1.4 ± 0.4)%/yr when only considering the more quiet periods from June to November. This negative rate of change for HNO_3 has been confirmed based on observations at Kitt Peak (Arizona, USA) between 1992 to present, with a decrease of nearly 2%/yr during this post Mt. Pinatubo volcanic eruption (C.P. Rinsland, private communication, 2001). As for NO_2, these HNO_3 rates of change will have to be simulated by model calculations and explained (groups at the Universities of Oslo and Leeds are working on this problem); we believe that the stratospheric aerosol loading is a key compound influencing these findings.

The bottom frame of Figure 24 displays the mean trend of N_2O which is the main source gas feeding the NO_y family of compounds in the stratosphere; its long-term rate of increase of (0.30 ± 0.01) %/yr, is quite different from the statistically significant trends observed for NO_2 and HNO_3, but the chemistry and photo-chemistry of the latter is sufficiently complex for a linear source-sink relation not to prevail.

With respect to the growth rates of N_2O volume mixing ratios at the ground derived globally by the *in situ* networks mentioned before (typically 0.25 %/yr), the Jungfraujoch increase in the N_2O vertical column has consistently been higher. We have shown that the difference can be explained by a heightening of the tropopause by some 100 to 150 m over the period 1985 to present, which can result from some warming of the troposphere or/and cooling of the stratosphere. This suggestion is in line with findings in the long-term ozone and temperature data bases gathered at Hohenpeissenberg, Germany (Steinbrecht et al., 1998).

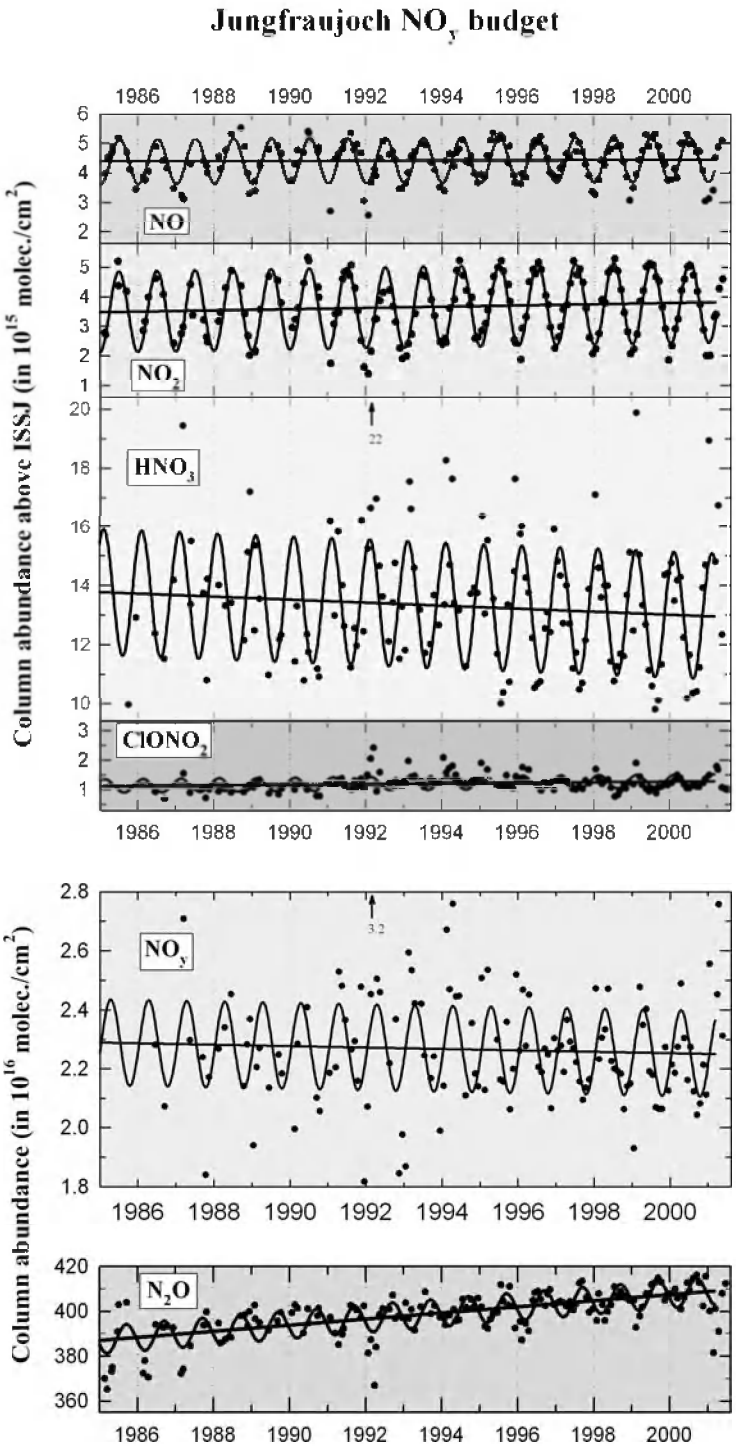

Figure 24: *The 4 upper frames reproduce the evolution of the column abundances of the most important constituents contributing to the stratospheric NO_y loading above the Jungfraujoch, that is shown below. Among all these compounds, only NO_2 shows a long-term statistically significant rate of change equal to (+0.6 ± 0.2) %/yr. The evolution of N_2O, which is the main source of NO_y, is displayed in the bottom frame.*

Due to its long lifetime (120 years), N_2O is an excellent tracer of atmospheric transport and dynamics, and we monitor its variability to identify unusual meridional circulation patterns, primarily polar air intrusions and related "equivalent" subsidence. In Figure 19, the "opposite" variations in the columns of the ground-based long-lived source gas N_2O and the stratospheric long-lived HF are striking and their simultaneous monitoring add confidence in the way latitudinal circulation and subsidence influence the mean atmospheric state at mid-latitude.

Impact of the eruption of Mt. Pinatubo on the NO_2 abundance above the Jungfraujoch

As a consequence of the eruption of Mount Pinatubo in June 1991 in the Philippines (15°N, 120°E) and the corresponding globally enhanced aerosol load in the stratosphere, a reduction of the NO_2 amount was observed at ISSJ. Part of this was attributed to enhanced conversion of N_2O_5 to HNO_3 due to heterogeneous processing on the aerosol particles surfaces (e.g., Hofmann and Solomon, 1989; Brasseur and Granier, 1992; Rinsland et al., 1994). A precise quantification of the reduction required the establishment of a reliable pre-Pinatubo NO_2 climatology. To this end the FTIR time series of NO_2 columns at the Jungfraujoch observatory, which starts as early as 1985, has been combined with the SAOZ series which only starts in mid-1990, but which has the advantage of providing morning and evening twilight data each day. To use the combined data set, they have been corrected first for mutual biases. Still, because of the NO_2 diurnal variation and the different sampling times of the FTIR and SAOZ instruments, a direct intercomparison and/or combination with the SAOZ data is impossible. Therefore, a photochemical model (Nevison et al., 1996) was used for evaluating the morning and evening twilight values corresponding to FTIR measurements which are spread throughout the day. The model uses actual temperature data, locally measured ozone column values and a mean monthly NO_2 vertical profiles at midlatitude derived from SAGE II observations. The resulting combined time series of the NO_2 abundance at Jungfraujoch and its evolution during the last decade, in terms of monthly mean percentage differences relative to the pre-Mount Pinatubo climatology established over the 1988 to mid-1991 period, are displayed in Figure 25.

The figure also shows the reduction of the NO_2 amount: it peaks at the turnover between 1991 and 1992 and amounts to 45% with respect to the pre-Mount Pinatubo 1988 to mid-1991 mean level; no distinct behaviour between morning and evening columns is observed. The recovery can be modeled reasonably well by a sum of two exponentials, an initial fast one with an *e*-folding time of 2.7 months, followed by a slower one with an *e*-folding time of 35 months (solid line in Figure 25). If we limit the

fit to the 24-month period following the maximum impact for comparison with the decay of the aerosol load measured above the closest lidar station of Garmisch-Partenkirchen (Jäger et al., 1995), we find approximately the same 10-month *e*-folding time, as represented by the dashed line in Figure 25. By mid-1994, both the aerosol load and the NO_2 reduction had decreased to about 10% of their maximum value. The NO_2 amount came to complete recovery only by January/February 1995. The NO_2 abundance observed at the end of 1996 appears to be higher by about 7% than the reference level, which might be related to the fact that the actual aerosol load came down approximately to the 1978/1979 background level, at least below the 1988/1991 one (H. Jäger, private communication, 1997), or to the actual rate of increase of NO_2 derived from the FTIR time series as discussed above.

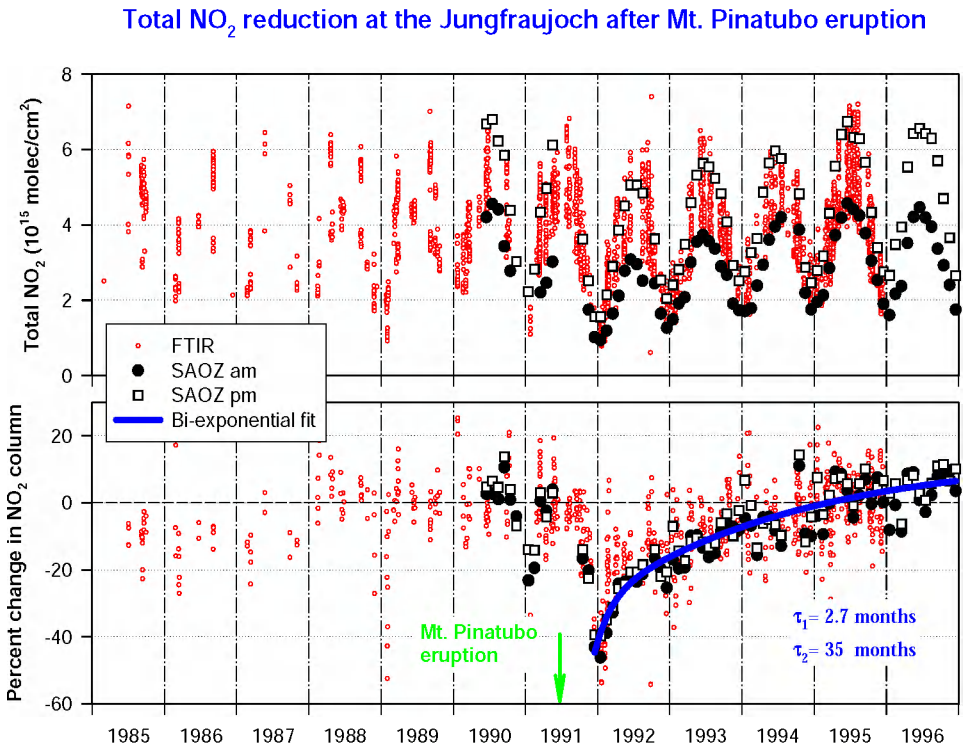

Figure 25: *Top: Superposition of FTIR (small open circles) and SAOZ (solid circles and open squares) time series of NO_2 columns at the Jungfraujoch. Bottom: Percentage monthly mean NO_2 vertical column reductions observed at the Jungfraujoch by the SAOZ and FTIR instruments. Reductions are evaluated relative to the 1988 to mid-1991 monthly mean reference values derived from the FTIR observations. SAOZ data are monthly means for morning and evening vertical column amounts; FTIR data are daily values.*

It is our intention in the near future to re-examine the combined FTIR and SAOZ NO_2 time series at the Jungfraujoch, using the latest homogenised and revised SAOZ data up to present (cf. section 4.1.1); the latter data were not available yet for the analysis discussed here above (De Mazière et al., 1998).

4.1.1.5 Kyoto Protocol-related investigations

The "Kyoto Protocol on Climate Change" (1997) has set initial recommendations and quota to achieve stabilization of the atmospheric loading of strong greenhouse gases at levels acceptable for durable development. These initial measures aim at a first "modest" reduction in emissions referred to 1990 levels, to be reached during the first commitment period ending in 2010. The reduction levels are expressed as "aggregate anthropogenic carbon dioxide equivalent emissions" of the following greenhouse compounds: CO_2, CH_4, N_2O, SF_6, HFCs (hydrofluorocarbons) and PFCs (perfluorocarbons). The amended and adjusted Montreal Protocol is assumed to remain in effect, as ozone depletion and climate change interact through common physical and chemical processes.

While CO_2, CH_4 and N_2O have been recognised for long time as important contributors to the greenhouse characteristics of the atmosphere, SF_6 was included in the Kyoto list, because of being the strongest absorber of infrared radiation on a per-molecule basis (e.g., Rinsland et al., 1990), and once released, it persists in the atmosphere for millennia (Ravishankara et al., 1993; Mahieu et al., 1996). Its presence in the atmosphere is believed to be entirely of anthropogenic origin.

Within that context, the monitoring effort undertaken by GIRPAS since the mid-1980s includes the four gases specifically cited above (see also Zander et al., 2000). Related measurements performed at ISSJ during the recent years are displayed in Figure 26 and confirm the persistence of positive rates of change for all these gases, as already evoked partially in the final SMAC Report (Simon, 1996). However, noteworthy features emerging from the timely extended data bases are briefly pointed out here below.

1. As visualised in the top left frame of Figure 26, the $\underline{CO_2}$ vertical column abundance has continued to increase by a mean 2.16×10^{19} molec./cm^2/yr, which corresponds to a rate of change equal to (0.41 ± 0.01) %/yr, when referenced to year 2000. Its seasonal modulation is primarily the result of CO_2 uptake during the vegetation photosynthesis period. A slight "anomaly" observed in 1997 has also been noticed in the Mauna Loa reference data base accessible at the Carbon Dioxide Information Analysis center (CEDIAC), Oak Ridge, TE, USA; no

explanation has been found for this feature, as additional measurements during a few more years are needed to better quantify it.

2. After H_2O and CO_2, *methane (CH_4)* is the most abundant greenhouse gas in the troposphere and its transformation in the stratosphere leads primarily to water vapour. As can be seen from the top right frame of Figure 26, the rate of growth of the CH_4 column has continued to slow down: during the years 1987, 1992, 1997 and 2000, the rates of increase have been found equal to 1.59×10^{17}, 1.07×10^{17}, 0.55×10^{17}, and 0.23×10^{17} molec./cm^2/yr, or 0.74%, 0.48%, 0.24%, and 0.10%, respectively; this corresponds to a growth rate slowing down by nearly a factor 7 during the past 15 years. The post 1996 rates of change are the slowest observed since the 1940s (Etheridge et al., 1998). Overall, the reported rates of change are consistent with those derived from ground-level *in situ* monitoring networks (WMO Report No.44, 1999).

3. The data set of the *nitrous oxide (N_2O)* column abundances displayed in the bottom left part of Figure 26 also reveals a slight rate of decrease during the recent years, but this remains statistically uncertain, so that we report trends based on a linear rate of increase throughout the 1986 to present period; consequently, the mean rate of increase is found equal to 0.30%/yr, or 1.17×10^{16}, 1.19×10^{16}, 1.22×10^{16} and 1.23×10^{16} molec./cm^2/yr in 1987,1992, 1997 and 2000.

4. The *sulfur hexafluoride (SF_6)* column abundance above ISSJ has reached a value of 7.2×10^{13} molec./cm^2 at the end of year 2000, over 3 times its mean 1986 value (see bottom right frame of Figure 26). The average column increase above ISSJ has been 3.55×10^{12} molec./cm^2/yr, which corresponds to percentage increases equal to 14% in 1987, 8.3% in 1992, 5.86% in 1997, and 4.98% in 2000.

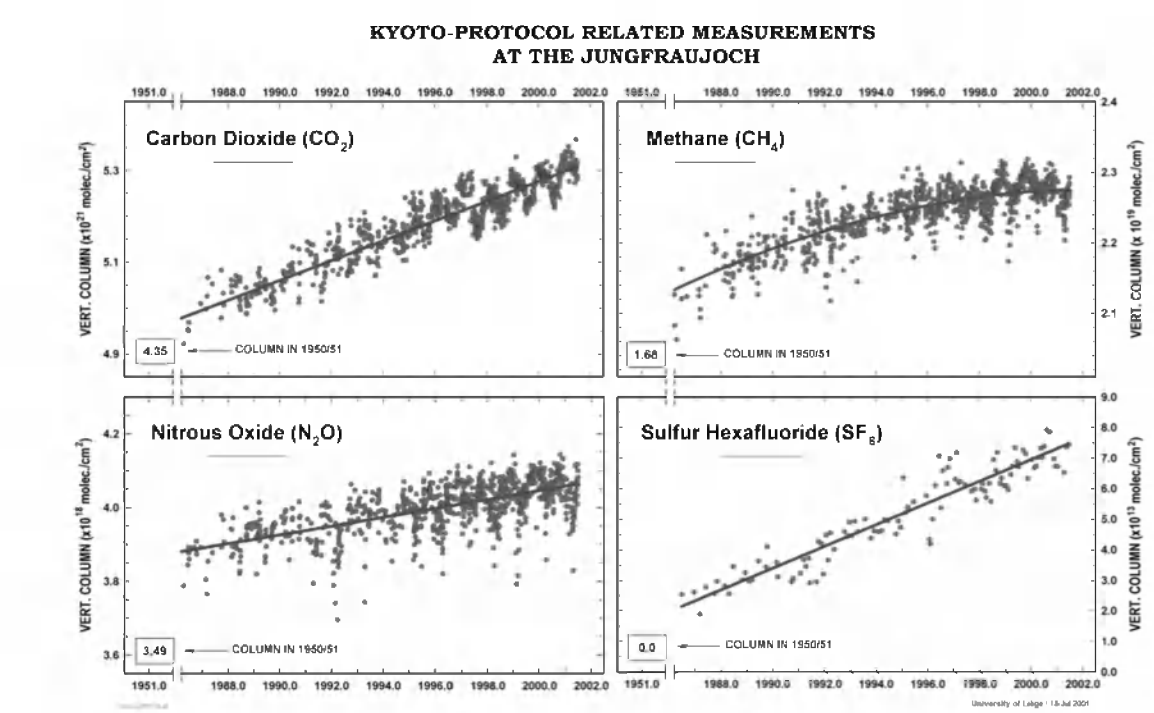

Figure 26: *The timely evolution of the vertical column abundances of 4 important greenhouse gases listed for regulation in the Kyoto Protocol. With the exception of CH_4 whose rate of increase has significantly slowed down during the 1990s, all other species have continued to accumulate in the atmosphere at relatively constant rates. For details, see text.*

4.1.1.6 Findings related to other species

Ozone (O_3)

The entire Jungfraujoch database of O_3 is being re-analyzed using the improved retrieval approach developed by De Mazière et al. (1999), as discussed in section 3.5.1. Advantage will be taken of this reprocessing effort to further implement spectroscopic parameter changes to minimise otherwise systematic residual features in the fittings. Two conclusions which are worth being mentioned here are that (1) the long-term rates of change (trends) in the O_3 columns are not significantly affected by the new approach, and (2) the seasonal differences, otherwise noticeable, disappear in the comparison between the SAOZ and FTIR column retrievals (cf. Figures 12 and 13 and associated discussions). Over the period 1985 to present, the mean rate of change determined for the total O_3 column abundance above ISSJ is equal to (-0.25 ± 0.15)%/yr. Since 1994, the observations indicate that total ozone has started to recover but whether this is a recovery from the minimum observed after the Mt. Pinatubo volcanic eruption or resulting from some change in atmospheric background transport/circulation remains to be assessed through additional

measurements and correlative investigations. It has been shown by De Mazière et al. (1999b) that heightening of the tropopause above the Jungfraujoch in the 80s and early 90s contributes to the observed O_3 decrease. This is in agreement with similar findings by Steinbrecht et al. (1998) at Hohenpeissenberg. Since the mid 90s; the tropopause above ISSJ seems to lower again, which may be correlated with the apparent increase of the ozone abundance, and maybe with the above mentioned decrease of N_2O. This must be confirmed during the next years.

To be noted here are the extreme column abundances observed during the period covered by this project: record high on February 13 (14.1×10^{18} molec./cm^2, or 526 DU), and record low on November 2000 (5.17×10^{18} molec./cm^2, or 192 DU). All high columns are associated with intrusions of unprocessed air masses that originate from higher latitudes, as evidenced from back-trajectories supplied by ECMWF through NILU.

Carbon monoxide (CO), ethane (C_2H_6) and hydrogen cyanide (HCN)

Figure 27 displays the monthly mean vertical column abundances of CO and C_2H_6 observed above the Jungfraujoch between 1984 and present. The mean rates of change over that entire period are equal to (-0.35 ± 0.15)%/yr for CO and (-1.9 ± 0.2)%/yr for C_2H_6; they are the only statistically significant negative rates among all source gases under investigation (see Table I).

Their seasonal modulations are well defined, with mean peak-to-peak modulations of 35% for the former and 45% for the latter. Noticeable in Figure 27 are the high columns observed during 1998 for both species; consequently, a detailed investigation of CO, C_2H_6 and HCN (which was also high in 1998) in the free troposphere above the Jungfraujoch from 1995 to 1999 was undertaken in collaboration with C.P. Rinsland and colleagues from the Swiss federal Laboratories for Materials Testing and Research (EMPA, Dübendorf). Extensive details about that work can be found in Rinsland et al. (2000).

The increased ISSJ 1998 tropospheric columns of all 3 species coincided with the period of widespread wildfires during the strong El Niño warm phase of 1997-1998 which resulted in abnormal emissions of CO, C_2H_6 and HCN, and they peaked after the increases measured above Mauna Loa (Hawaii), suggesting that these south Asia wildfires were responsible for the observed 1998 increases at both Mauna Loa and Jungfraujoch.

Comparisons between the tropospheric columns and local concentrations at the Jungfraujoch by EMPA, confirms that the CO free tropospheric vertical volume mixing ratio profile generally decreases with altitude throughout the year.

Formaldehyde (H_2CO)

Formaldehyde (as well as other aldehydes) is presumed to have a catalyzing effect on the production of chemical smog and of ozone in polluted urban areas, but its background concentrations as well as production sources and destruction processes are poorly known. Column abundance measurements of H_2CO have been derived from investigations of characteristic absorption features showing up very weakly in solar spectra recorded at ISSJ since 1988 (Demoulin et al., 1999). The columns had to be averaged over two-months time intervals to become reasonably reliable.

Beside of the retrieval difficulty, it also appears that the relative quality of the spectroscopic parameters available for various transitions, and missing parameters for weak interfering features need to be further studied in the laboratory. Because of the large variability observed in the columns and the uncertainty in their retrievals, no statistically significant trend emerges from the current 1988-2000 data base and the mean loading above ISSJ is likely to lie between 2 and 4 x 10^{14} molec./cm^2. A seasonal modulation with lower columns in winter is also suggested.

Carbonyl Sulfide (OCS)

OCS (carbonyl sulfide) has maintained an averaged rate of column decrease of –0.35%/yr, with large interannual variability. During the 1998 winter-spring time such variability was abnormally large. OCS is believed to be the main source responsible for the persistence of the sulphur layer in the stratosphere. Its main identified sources are natural, i.e., 30% oceans, 20% microbial processes in soils, 30% conversion of natural CS_2, and 20% anthropogenic.

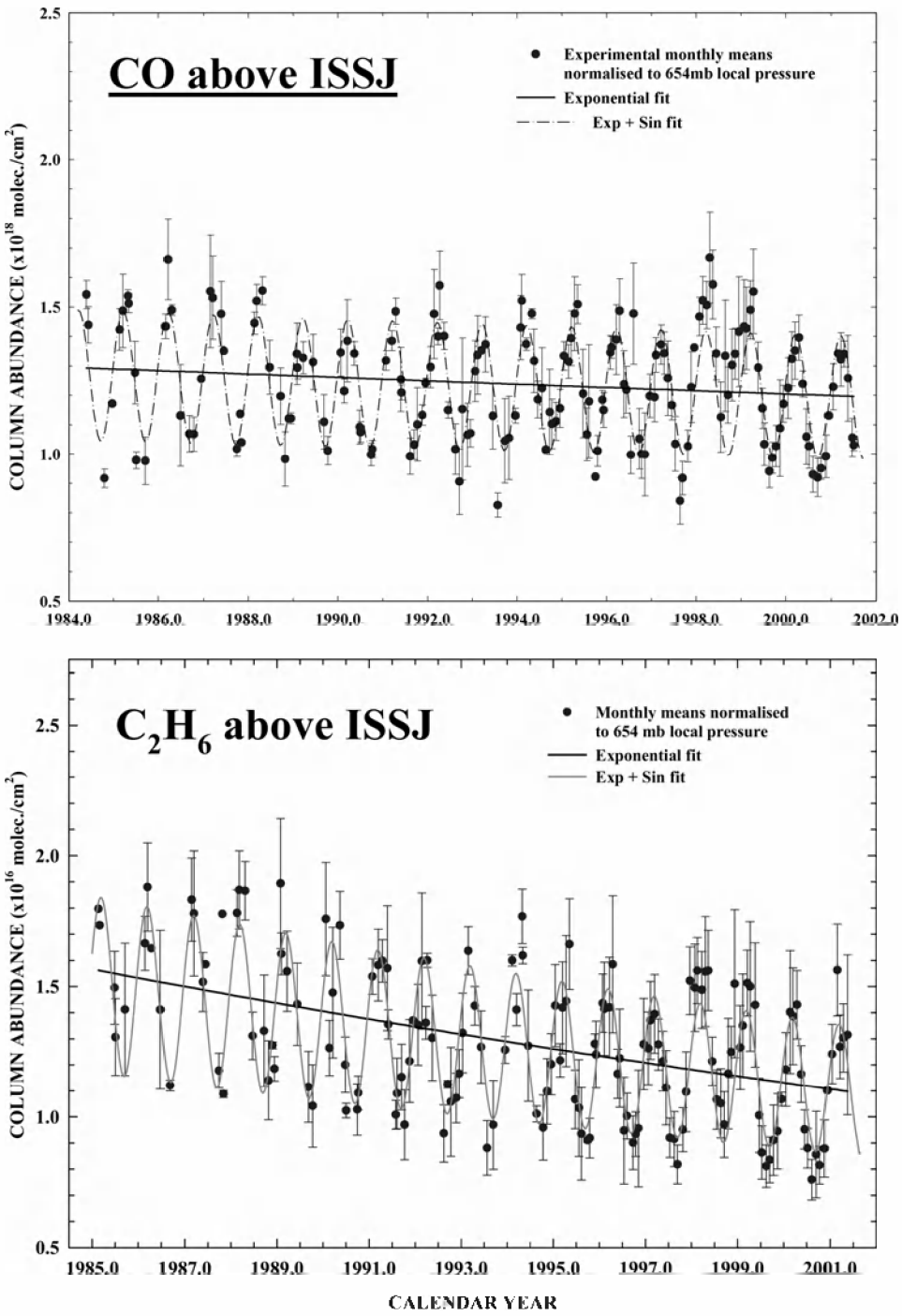

Figure 27: *Graphical representation of the column abundance evolution of CO and C_2H_6, both showing clear seasonal variations as well as rates of decrease, equal to (-0.35 ± 0.15) %/yr for the former and (-1.91 ± 0.18) %/yr for the latter. The monitoring of such species is indirectly of relevance to the Kyoto Protocol, as they affect the oxidizing capacity of the troposphere which influences lifetimes of greenhouse gases, e.g., CH_4.*

4.1.2 Long-term data at Harestua and OHP

4.1.2.1 Introduction

Since 1994, UV-visible zenith-sky observations have been performed by BIRA-IASB at the complementary NDSC site of Harestua (60°N, 10°E). In summer 1998, an additional instrument has been installed in the NDSC Alpine station at the Observatoire de Haute Provence (OHP, 44°N, 6°E). These instruments allow monitoring of O_3, NO_2, BrO and OClO column abundances. Results reported here focus on BrO observations performed in both stations, and on OClO measurements performed in Harestua. As described in section 3.3, a slant column model based on the BIRA-IASB photochemical box-model (PSCBOX) was set up and validated by comparison with similar models developed in other European Institutes. This model was used to interpret the BrO and OClO slant columns simultaneously measured in Harestua, confirming the ability of the model to quantitatively capture the behaviour of both species in conditions of large chlorine activation but also revealing some possible deficiencies of the model in conditions of weak activation.

4.1.2.2 Instrument updates

In early 1998 the UV-visible instrument was modified in order to optimise its performance in the UV region. A new grating and a cooled diode-array detector from Hamamatsu / Princeton Instruments were installed. The BrO spectrometer covers the region from 320 to 390 nm with a spectral resolution of 0.6 nm and a sampling ratio of 8 pixels/FWHM. A depolarising fiber optic bundle is used as entrance slit (200 microns wide).

At OHP a new home-made spectrometer with a design optimised for BrO observation was installed at OHP. This instrument consists of a thermally regulated Czerny-Turner spectrometer (J-Y TRIAX-180) equipped with a 1024 pixels Hammamatsu diode array detector cooled to -40°C. Spectra are recorded over the interval 330-390 nm with a resolution of 0.7 nm and a sampling ratio of 10 pixels/FWHM. In contrast to the instrument operated in Harestua, the OHP spectrometer has a linear polariser mounted at the entrance slit and is attached to a computer-driven rotating plate that follows the direction of polarisation of the zenith-sky. The advantages of this design are (1) to eliminate possible artefacts due to polarisation sensitive parts in the instrument (mainly the diffraction grating) and (2) to reduce the contribution of the Ring effect in twilight observations.

4.1.2.3 Stratospheric BrO

Figure 28 displays the time-series of BrO differential slant columns (DSCDs) measured from January 1998 until July 2000 at the two stations. This analysis uses daily twilight reference spectra taken at 80° of solar zenith angle (SZA), except during the months of December and January where the minimum SZA of the day (larger than 80°) is used instead. Analysis parameters were set according to the recommendations described in Aliwell et al. (2000).

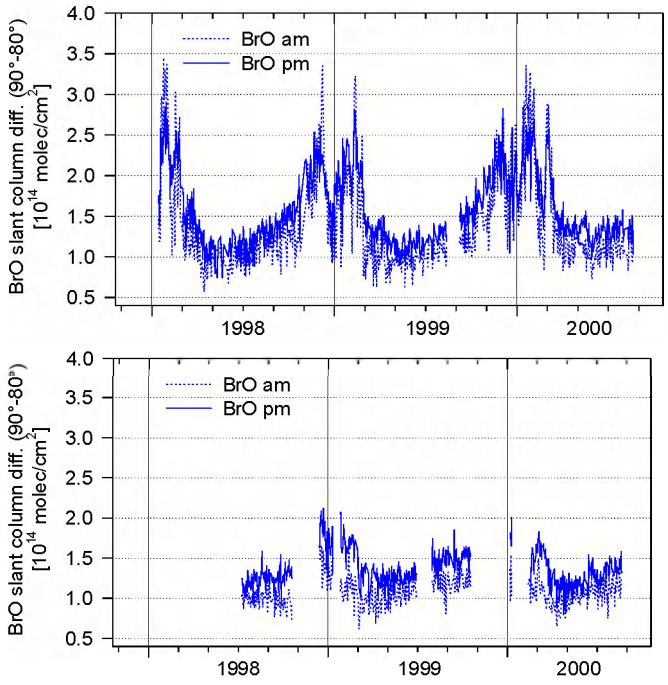

Figure 28: *Daily AM and PM BrO differential slant columns measured in Harestua (upper plot) and in OHP (lower plot) between January 1998 and July 2000.*

BrO differential slant columns are the natural product of the zenith-sky DOAS observations. The choice of the 90-80° SZA range, generally reported in previous studies (e.g., Fish et al., 1995), is done primarily to optimise the signal to noise ratio of the differential BrO absorption. This choice also presents the advantage of maximising the sensitivity of the observation to the stratospheric part of the BrO profile, due to the strong geometrical enhancement of the optical path in the stratosphere at twilight (Solomon et al., 1987) and the comparatively small variation of the tropospheric air mass factor.

A large part of the observed seasonal variation of the BrO DSCD is related to the seasonality of stratospheric NO_2 through the reaction BrO + NO_2 → $BrONO_2$, which

controls the efficiency of conversion of BrO into its nighttime reservoirs. Largest BrO DSCDs are therefore obtained in winter under denoxified conditions. It has been shown that these results are in good quantitative agreement with model simulations (Sinnhuber et al., 2000; Van Roozendael et al., 2000a).

4.1.2.4 Tropospheric BrO

It has been known for some time, that in polar spring episodes of strongly reduced boundary layer ozone occur at many locations. With the ERS-2 Global Ozone Monitoring Experiment (GOME), global BrO measurements have been made possible for the first time, and the extent of the bromine activation in polar spring has become evident. Recent comparisons of GOME BrO columns with 3D model results and with integrated stratospheric BrO profiles measured from balloons also show GOME columns systematically exceeding amounts expected for stratospheric BrO, at all latitudes and seasons. These results suggest the presence of a global background of tropospheric BrO. During this project, ground-based BrO measurements have been used to search for further evidence of BrO in the troposphere and to test for consistency with GOME observations.

One major difference between ground-based and GOME measurements is the time of the measurements: while GOME observes most locations around local noon (10h30 local time), zenith-sky measurements are usually performed during twilight when the sensitivity towards stratospheric absorbers is highest. For this reason, a direct comparison of ground-based DSCDs with GOME measurements is not possible. Two different approaches have been used to allow quantitative comparison with GOME BrO measurements, one using the Langley plot technique and the other one introducing an assumption on the tropospheric BrO column.

For an absorber without diurnal variation, the vertical column can be retrieved from zenith-sky measurements by plotting the measured slant columns as a function of air mass factor, and determining the slope of the resulting straight line. This technique is often called a Langley plot. If, however, the absorber is not constant with time, or if the air mass factor used is not appropriate, then the Langley plot will not be a straight line, but rather have a curvature. By applying the Langley plot to different solar zenith angle ranges, different vertical columns are retrieved as shown in Figure 28. In the case of BrO, the agreement between the GOME measurement and the vertical column from the Langley plot is much improved, if only small solar zenith angles are taken into account. This result can be explained in two ways: either, there is a strong diurnal variation of stratospheric BrO with a maximum at noon, or there is a substantial amount of BrO located in the troposphere. As the first possibility is in

sharp contrast to model results and independent measurements, it is assumed, that the latter explanation is correct.

A second, independent method relies on using a single background spectrum for a complete time series, in contrast to the standard evaluation, where daily background spectra are used. This technique can only be applied if the instrument is very stable. In the analysis, there is one free parameter, namely the amount of BrO in the single background spectrum. By varying this amount, systematic changes can be introduced in the seasonal variation of the BrO time series as an effect of the changing air mass factor. As demonstrated in Figure 29, assuming a tropospheric amount in the background spectrum leads to good agreement between ground-based and GOME BrO columns, whereas the assumption of a purely stratospheric BrO profile leads to unrealistic BrO columns for the ground-based instruments at both stations.

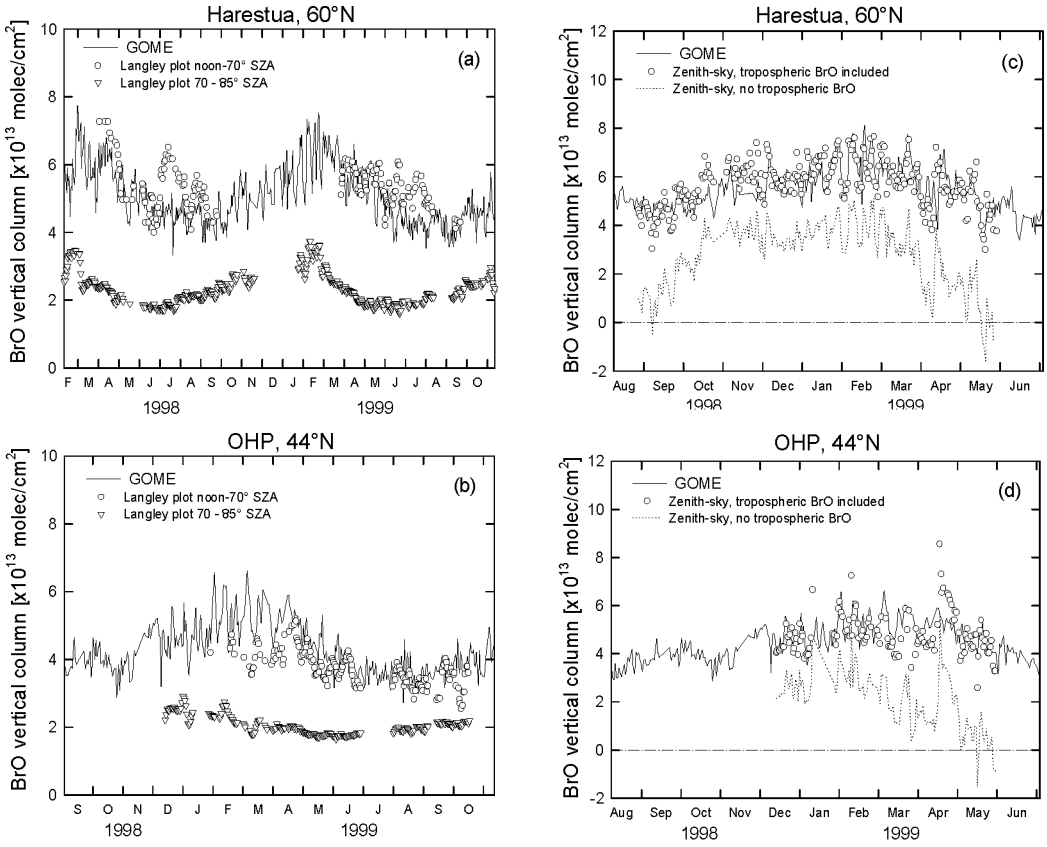

Figure 29: *GOME BrO vertical columns calculated in 500 km radius around indicated ground-based stations, compared to vertical columns derived from zenith-sky data by a Langley plot method (left panel) or from noon "GOME overpass" analyses using a seasonal reference spectrum (right panel).*

Summarising these results, good agreement is found between ground-based and GOME measurements of BrO for both the seasonal and the day to day variation, but only if a tropospheric background is assumed. The sources of this tropospheric BrO are still to be established. Although a significant contribution probably comes from to the transport of BrO plumes produced in the PBL of both polar hemispheres in spring (Wagner and Platt, 1998), it is unlikely that this mechanism can sustain large amounts of BrO over mid-latitudes in all seasons. Alternatively a production mechanism involving the inorganic bromine existing in the free-troposphere could be searched as proposed by Fitzenberger et al. (2000). Further work is needed to address this subject.

4.1.2.5 OClO observations and model simulations

OClO measurements have been performed at Harestua between January 1998 and June 2000. Important efforts have been devoted to the optimisation of the data analysis in order to lower down the detection limit. Figure 30 shows an example of optimised OClO fit obtained in the 358-380.5 nm region. During the project, the OClO (and BrO) observations performed in Harestua have been probed for consistency with current chlorine and bromine chemistry through comparison to calculations from the 3D chemical transport model SLIMCAT (Chipperfield, 1999). OClO DSCDs have been simulated using the model package PSCBOX, daily initialised with noon UT pressure, temperature, and chemical species profiles from SLIMCAT. Validation of the BIRA-IASB slant model was obtained through comparison with two other models, as described in section 3.3.2

Figure 31 shows the time-series of measured and modelled OClO DSCDs between January 1998 and June 2000. DSCDs are calculated between 92 and 80° of SZA (or 92-minimum SZA of the day if 80° is not reached). Note that events of large OClO column enhancements, observed during the winter when activated polar air masses are advected above the station, are generally well captured by the model both in time and amplitude. The comparison suggests an overestimation of modelled OClO during the winter 1998/99, possibly resulting from a dynamical effect. The time-series also clearly show the contrast between the exceptionally cold 1999/2000 winter during which numerous chlorine activation events occurred and the two previous warmer ones.

Although OClO measurements alone do not provide strong constraints on chlorine partitioning, some test on chlorine chemistry can be obtained by investigating the evolution of OClO as a function of the solar zenith angle. Figure 32 shows a comparison between observed and modeled OClO DSCDs as a function of the SZA,

for condition of large chlorine activation. As can be seen, the average agreement between the model and the measurements is excellent up to 92° SZA suggesting that chemical reactions controlling the change in OClO concentration during morning and evening twilight are well understood.

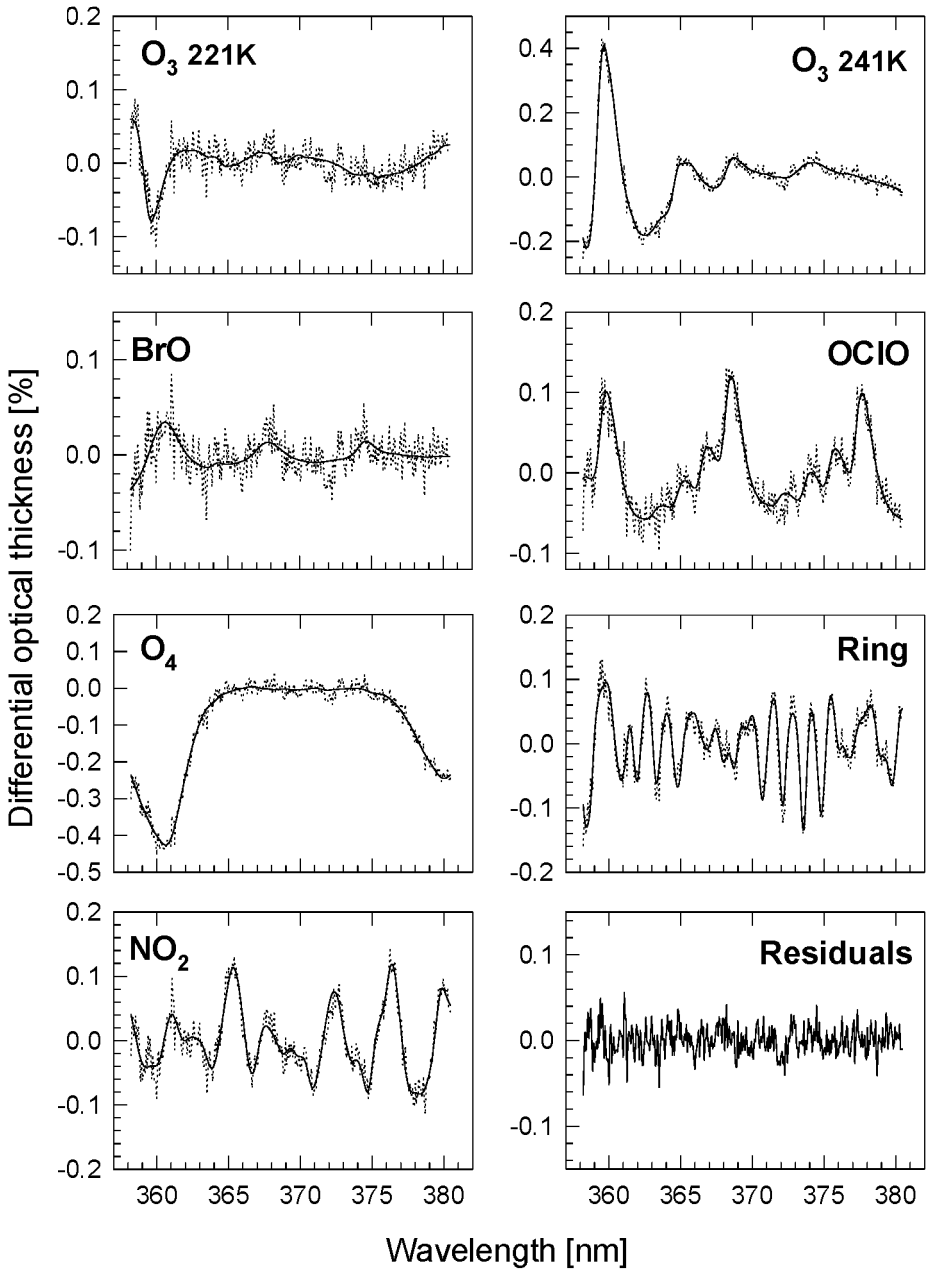

Figure 30: *Example of OClO DOAS spectral fit obtained in Harestua on 27 Jan. 2000, 90.2° SZA, PM. Calculated and measured spectra are represented by solid and dotted lines respectively.*

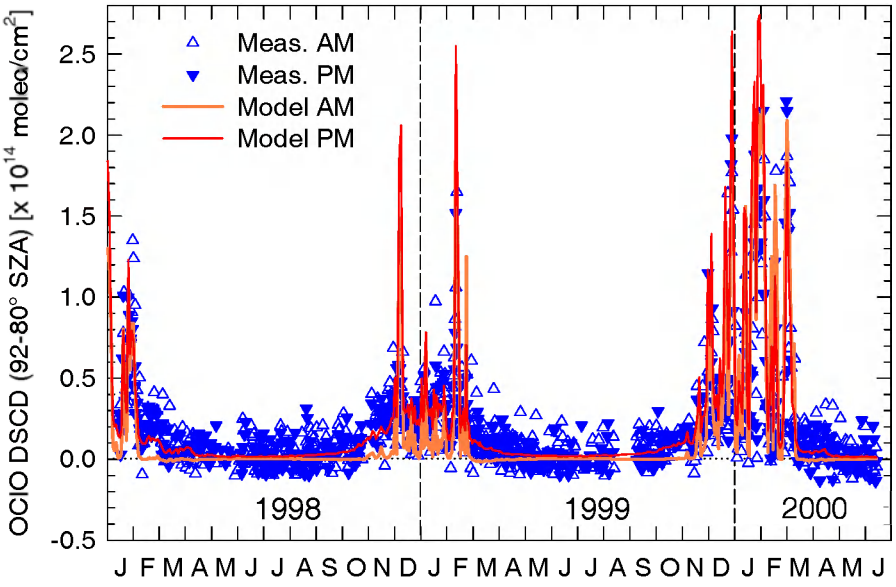

Figure 31: *Time-series of measured and modelled OClO 92-80° SZA DSCDs in Harestua for the period from January 1998 to June 2000.*

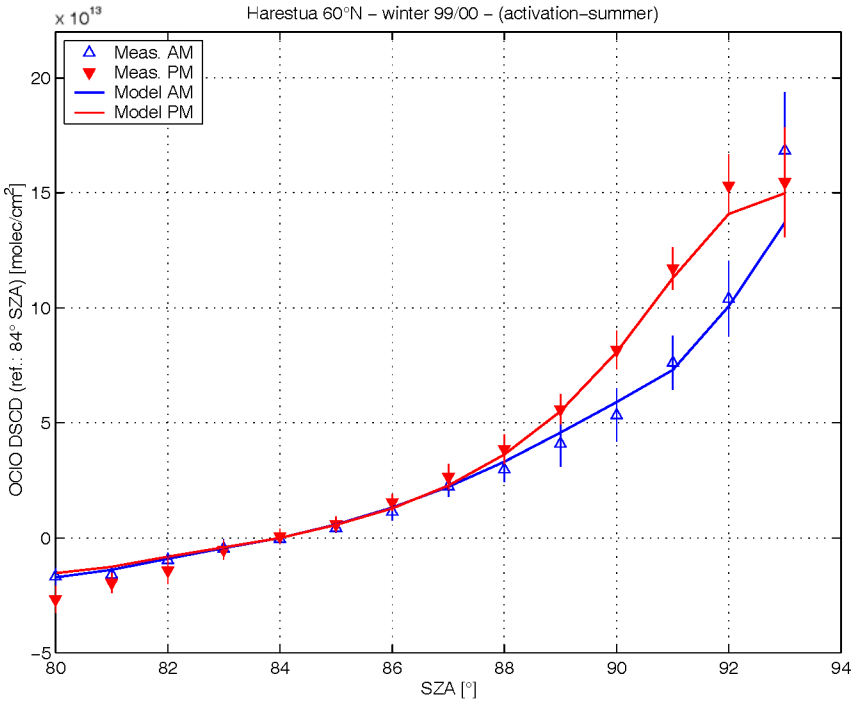

Figure 32: *Measurements and model simulations of the solar zenith angle evolution of the OClO slant columns, for conditions of large chlorine activation above Harestua (60°N).*

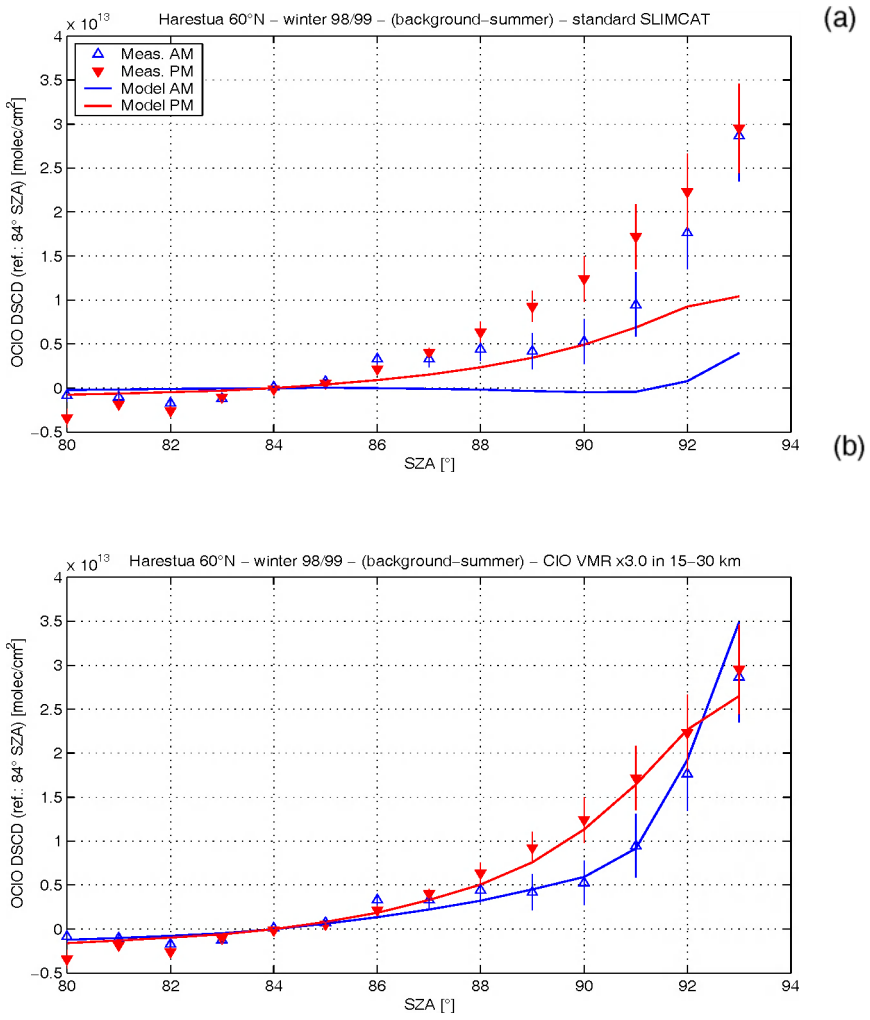

Figure 33: *Measurements and model simulations of the solar zenith angle evolution of the OClO slant columns, for conditions of weak chlorine activation above Harestua. In the upper plot, the PSC-BOX model is initialised with concentration profiles from the SLIMCAT 3D CTM model. In the lower plot, the concentration of ClO used to initialise PSC-BOX has been increased by a factor 3.*

Figure 33(a) displays a similar comparison obtained in conditions of weak activation outside of the vortex. In these conditions, the model definitely tends to underestimate the observations. Increasing the amount of ClO available to react with BrO allows to reconcile model results and measurements as shown in Figure 33(b). Work is in progress to test whether the needed ClO amounts would be consistent with in-situ measurements of ClO performed in comparable conditions during the SOLVE/THESEO 2000 campaign.

4.1.2.6 Simulations of NO_2 DSCDs at Harestua and OHP with PSCBOX

Ground-based UV-visible zenith-sky observations of NO_2 slant column densities have been performed from January 1998 through June 2000 at Harestua (60°N) and OHP (44°N). The observed time-series of 90-80° SZA NO_2 differential slant column densities (DSCDs) - which are the direct product of the DOAS analysis – have been compared to time-series calculated using the model package PSCBOX. The RT model S-DISORT in multiple scattering mode and including Mie scattering (stratospheric background conditions) has been used for these calculations. The results of this comparison are shown in Figure 34.

A good agreement between measured and calculated NO_2 DSCDs is obtained at both stations until August 1998. However, comparisons at other SZAs – which are currently under progress - are needed to conclude on the ability of the model to well reproduce the observations for this period. From September 1998 onwards, the model underestimates the observations by 20% in average. This behaviour results from a decrease of NO_2 concentrations in the SLIMCAT 12h UT profiles in this period, especially between 12 and 30 km of altitude. This feature – which is currently being investigated – seems to be related to the UKMO meteorological analyses (B.-M. Sinnhuber and M. P. Chipperfield, personal communication).

4.1.3 Long-term ozone data at Ukkel

The routine ozone measurements at KMI-IRM were continued as planned during the whole period of ESAC. These measurements comprised:

- daily measurements of the total ozone amounts with a Dobson and a Brewer spectrophotometer;
- ozone soundings three times per week (on Monday, Wednesday and Friday) by means of Vaisala radiosondes and ECC ozonesondes.

Figure 35 shows the daily variation of the total ozone amount at Uccle in 2000.

The 2000 annual mean total ozone amount was slightly higher than the long term mean.

Very low values were measured during a 2-days period, on 28 November and 29 November. These low values were mainly caused by the fact that in the altitude region between 11 and 17 km there was an intermediate layer comprising air masses with low ozone concentrations that originated from the subtropical tropopause.

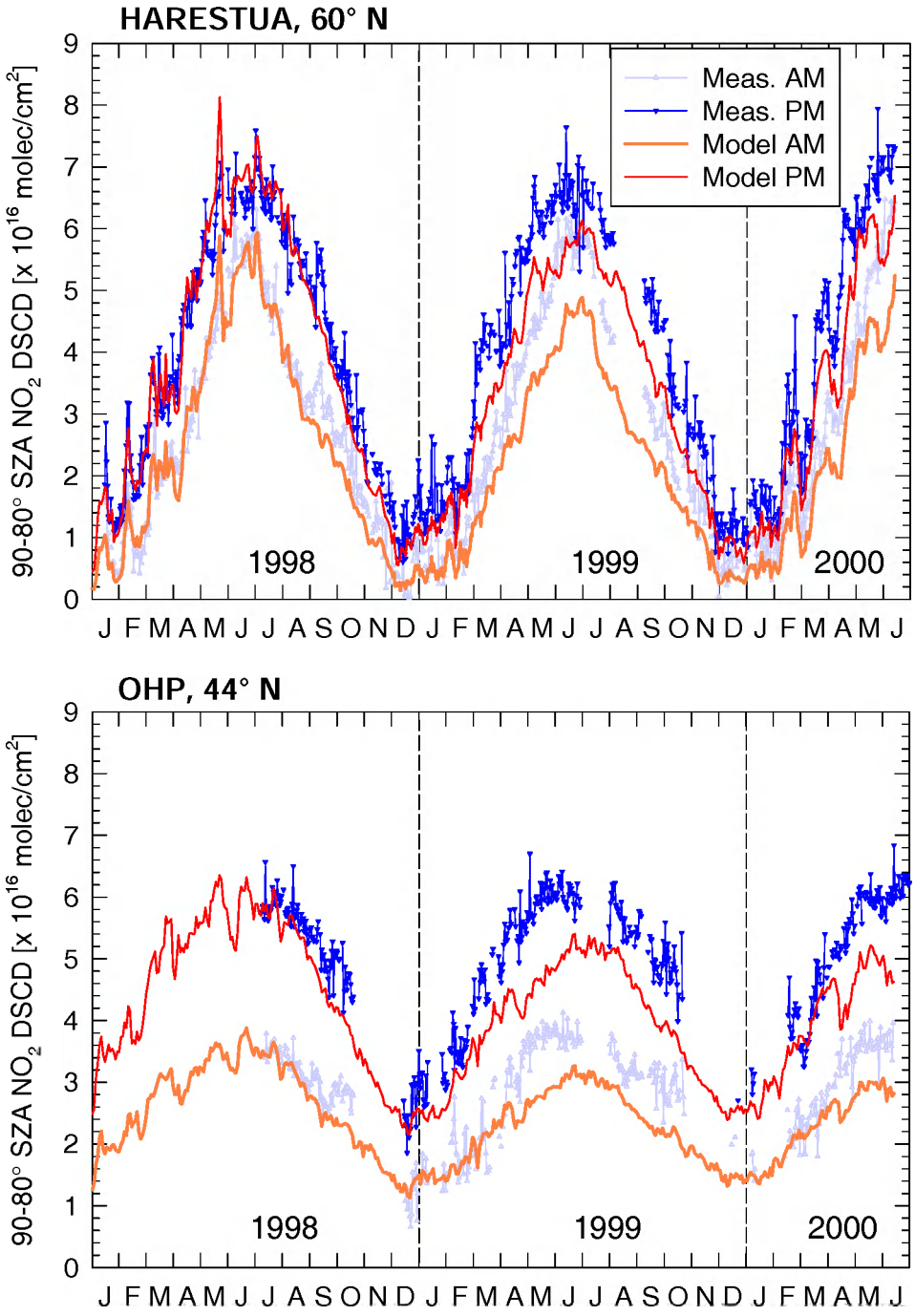

Figure 34: *Time-series of measured and calculated 90-80° SZA NO_2 DSCDs at Harestua (60°N) and OHP (44°N) for the period from January 1998 through June 2000.*

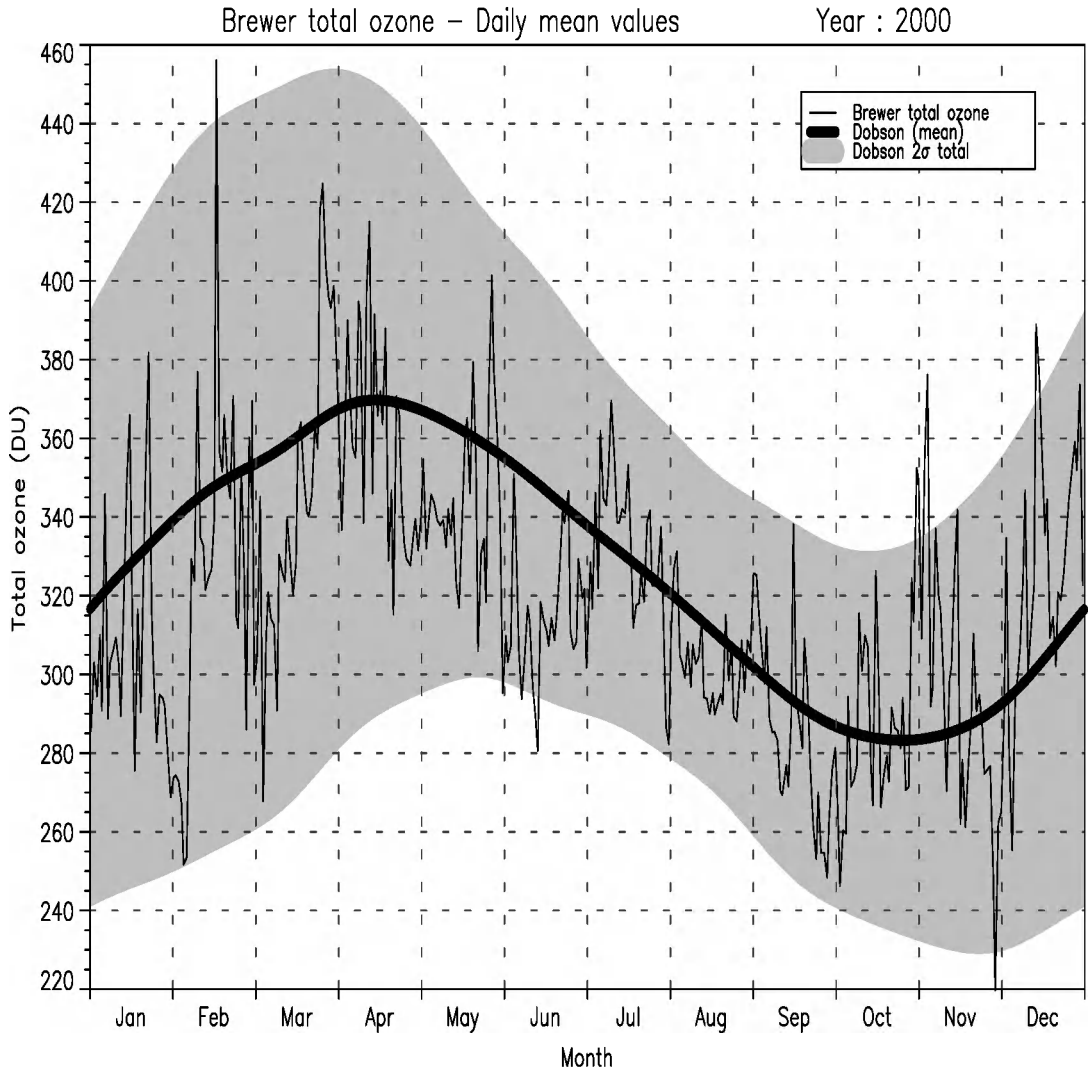

Figure 35: *Daily means of total ozone amounts measured at KMI-IRM with a Brewer spectrophotometer in 2000. The thick line shows the mean seasonal variation since the start of the total ozone observations (in 1971); the shaded area shows the 2-sigma variability over the same period.*

4.1.3.1 Data homogenisation

The homogenisation of the Uccle ozone sounding data set was finished in 1999. The corrections worked out in this study are all based on physical evidences such as changes in the equipment and changes in the operational procedures. The results were published by De Backer (1999).

In a continuous effort to improve the accuracy of the ozone measurements with the ozone sondes, the homogeneity of the time series may be lost. Post-flight processing

of the data is introduced to correct as much as possible the deficiencies of the historic observations. The main corrections applied are described below.

1. Box temperature. To convert the electronic signal of the sensor to ozone partial pressure, the temperature of the air passing through the pump is needed. This is only measured since 1990. Before that time a fixed temperature of 300K was assumed. Now the mean temperature of one year of observations is used, which reduces the ozone by about 8% at the top of the sounding (10hPa).
2. Altitude measurement. Changes in the errors in the altitude measurements cause a corresponding error in the ozone profile by shifting it up- or downward. The known altitude errors are now corrected.
3. SO_2 correction. If SO_2 is present in the air this causes an opposite signal in the ozone sensor. With the aid of measurements of a ground-based network an estimate is made of the profile of SO_2 on days of ozone soundings. This is especially important for the profiles obtained at the beginning of the time series, since at that time the concentration of SO_2 was high, and the corrections may amount to 50% and more in the lower troposphere. Since there was a spectacular downward trend in SO_2, not correcting for this effect would yield erroneous trend analyses.
4. Background current. A better preconditioning of the sondes caused a change in the background current. Again a post-flight procedure was introduced to remove this effect from the time series.
5. Pump efficiency. The standard procedure provides a mean pump efficiency profile to be used. De Backer et al. (1998) found that this procedure is not adequate for Brewer-Mast sondes and proposed a new correction profile (see chapter 3.7). This algorithm is now applied to all the ozone profiles. Also some changes in the performance of the pumps during the years have been taken into account.

A comparative study of the re-evaluated ozone sounding data with co-located ozone profiles obtained from space by the SAGE II instrument was initiated. Initial results confirm the homogeneity of the post-processed Uccle ozone sonde data. An example of results is shown in Figure 36.

The calibration level of the Brewer instrument for UV measurements was adjusted to the results obtained with new certified 50W lamps. This calibration level turned out to be consistent with a re-calibration of some of the old UV lamps during a Brewer workshop in Halkidiki in September 1998.

In May-June 2000 the calibration of the Dobson instrument nr 40 was verified during an intercomparison campaign in Hohenpeißenberg (Germany). It turned out that there was only a slight shift in the calibration level of 0.5%. This was taken into

account and this resulted in a very good agreement between the time series of total ozone obtained with the Dobson and the Brewer spectrophotometers at Uccle (Figure 37).

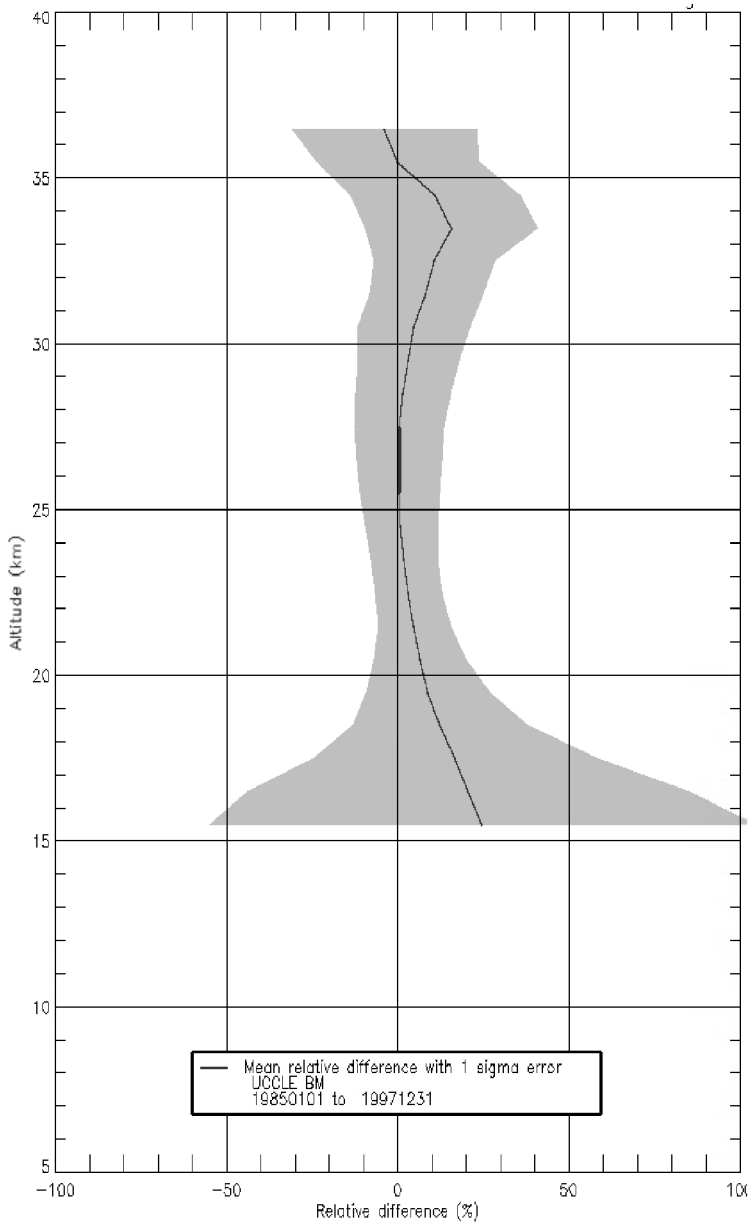

Figure 36: *Mean relative difference between colocated ozone profiles from SAGE II and from Brewer-Mast ozone sonde launches at Uccle.*

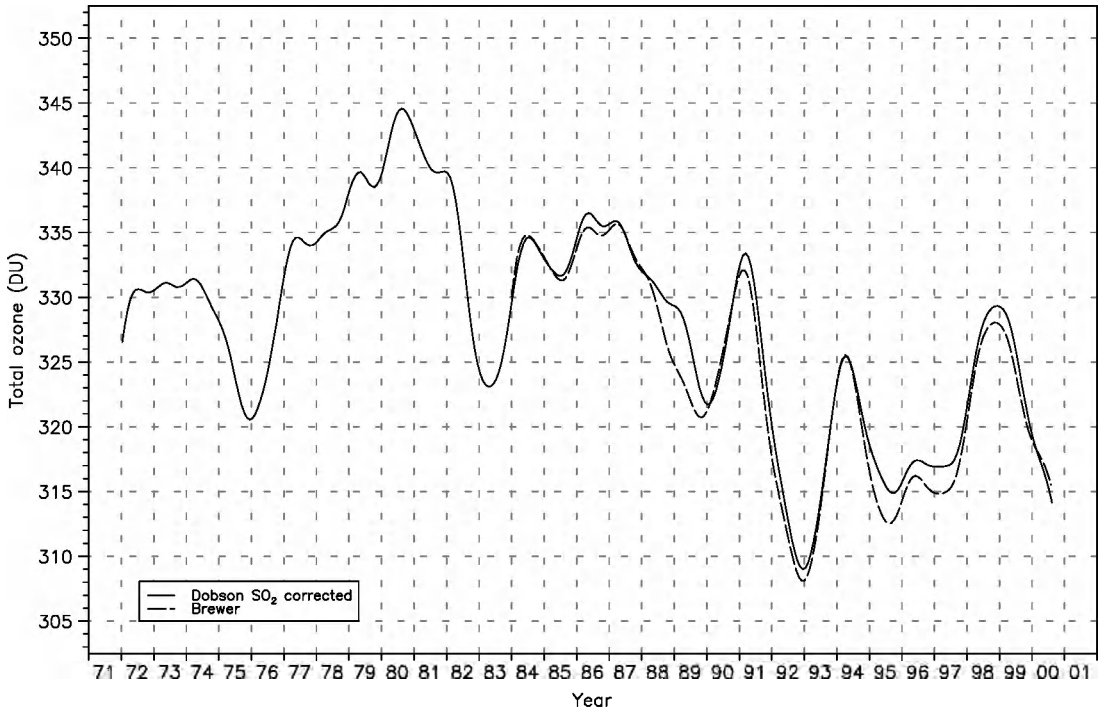

Figure 37: *Smoothed total ozone time series measured with Dobson nr 40 (full line) since 1971 and with Brewer nr 16 (dashed line) since 1983.*

4.1.3.2 Ozone trends

The re-evaluated data set of ozone soundings at Uccle from 1969 to 1996 was used for a sensitivity study of instrumental effects on calculated ozone trends. The results are shown in Figure 38. All the calculated trends are based on a least squares analysis of deseasonalized data. Results of this analysis have been presented at the EUROTRAC symposium (De Backer, 2001)

With the standard algorithm and corrections for calculation of ozone profiles from soundings with sondes of the Brewer type, the ozone trends in the middle troposphere amount to 1.2 to 1.4 %/yr; in the boundary layer the calculated trends are even larger than 2.5 %/yr (dashed line in Figure 38). In the middle stratosphere the magnitude of the negative trends shows a pronounced increase with altitude, to values of about -1.4% near mean burst level.

The SO_2 levels in the lower troposphere above the urban area of Brussels decreased rapidly in the 1970s and to a lesser extend in the 1980s. After applying a correction for the SO_2 interference on the ozone soundings at Uccle, as described by De Muer et al. (1995), the calculated ozone trends in the boundary layer are reduced by about half of the value without SO_2 correction; in the lower free troposphere trends of about

1%/yr are found (see curve with solid triangles in Figure 38). Upper tropospheric and stratospheric trends are hardly affected by this additional correction.

Before re-evaluation of the Uccle time series of ozone soundings, a jump was observed in 1989, resulting in too high ozone values in the troposphere and too low values above the ozone maximum. After application of the pump efficiency profile that was measured in the lab (and that shows much higher pump corrections than adopted in the standard profile), this jump was largely removed. This new pump correction had also a pronounced effect on the calculated ozone trends, the magnitude of the calculated negative trends in the middle stratosphere being considerably reduced. As a consequence of the normalization of the ozone profiles, the calculated ozone trends below the ozone maximum are also affected: the ozone trend profile below the ozone maximum (which is at about 22 km) is lowered, resulting in more pronounced year-round negative trends up to about -0.5%/yr in the lower stratosphere. With all corrections applied, the positive trend in the troposphere is considerably reduced and varies between 0.35 and 0.85%/yr (see solid line in Figure 38).

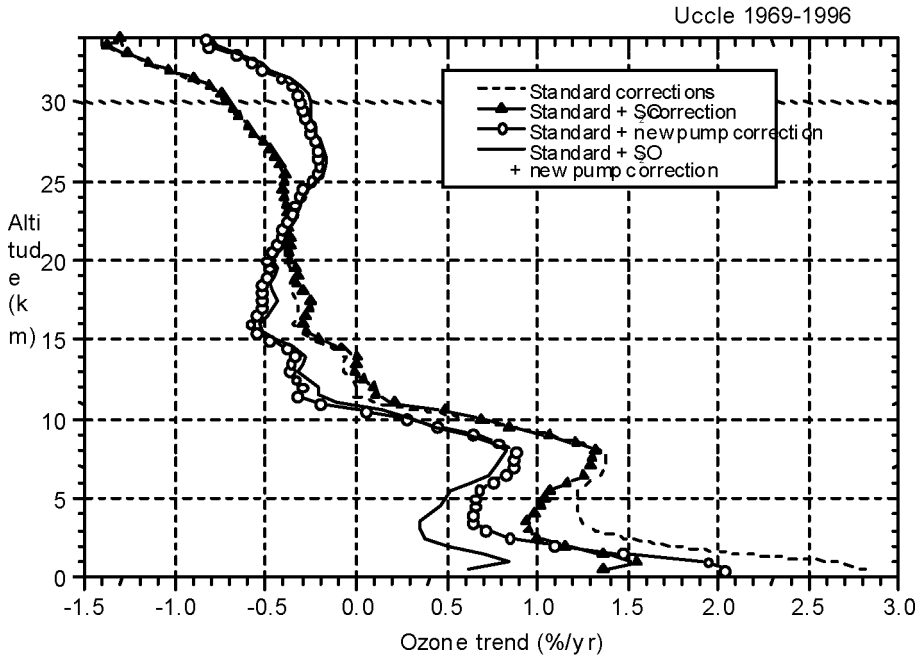

Figure 38: *Profiles of calculated ozone trends at Uccle for the period 1969-1996. The different curves are obtained with different combinations of corrections applied to the sounding data.*

The homogenised data set of ozone soundings at Uccle was subjected to a trend analysis (a least squares analysis of deseasonalized monthly means). The result is shown in Figure 39.

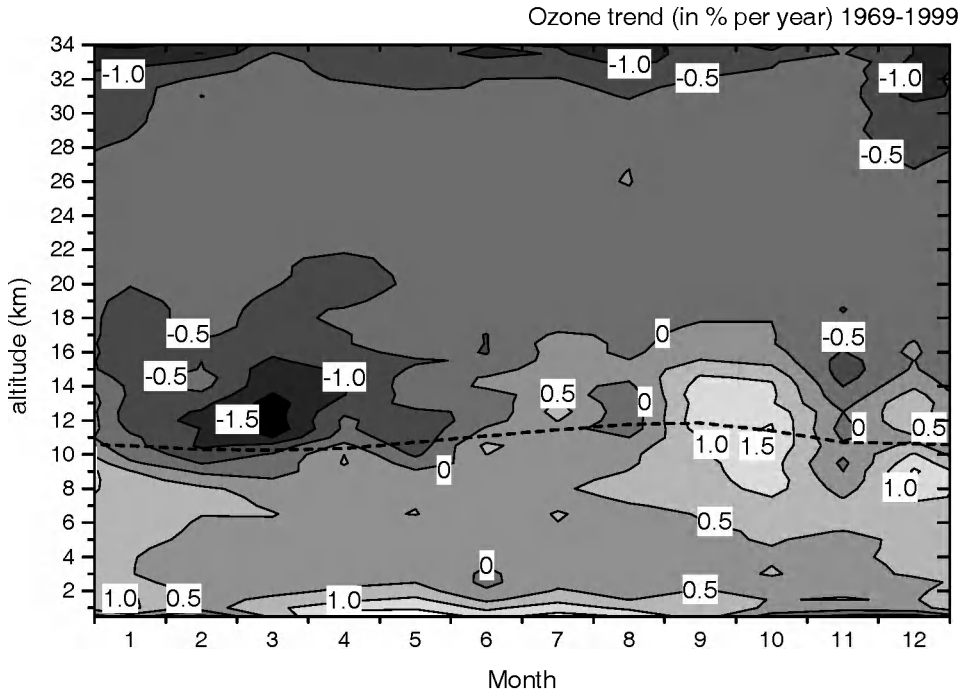

Figure 39: *Season – altitude cross section of ozone trends (in % per year) at Uccle over the period 1969-1999. Dashed line: mean tropopause level.*

The main feature is a pronounced long-term decrease of ozone in winter and spring at lower stratospheric levels.

The ozone in the free troposphere increases at nearly all levels and seasons. The ozone in the boundary layer shows a strong seasonal variation: a strong increase from March to September and a decrease during the other months.

From Figure 40 we see that at the 5 km altitude level, which is in the free troposphere, the highest ozone increases occurred in the 70s and the early 80s. Over the last 15 years there is no noticeable trend at that level.

At an altitude of 1 km, which is in the boundary layer, the situation is completely different: at that level the ozone increase is discernible at any sub-period, with the highest trends in recent years. There is no doubt that this trend (that is mainly imposed by an ozone increase in the summer months as is shown in Figure 40) is

induced by an increase of photochemical ozone production in the boundary layer. Therefore it may be a local effect that is not necessarily representative for other areas.

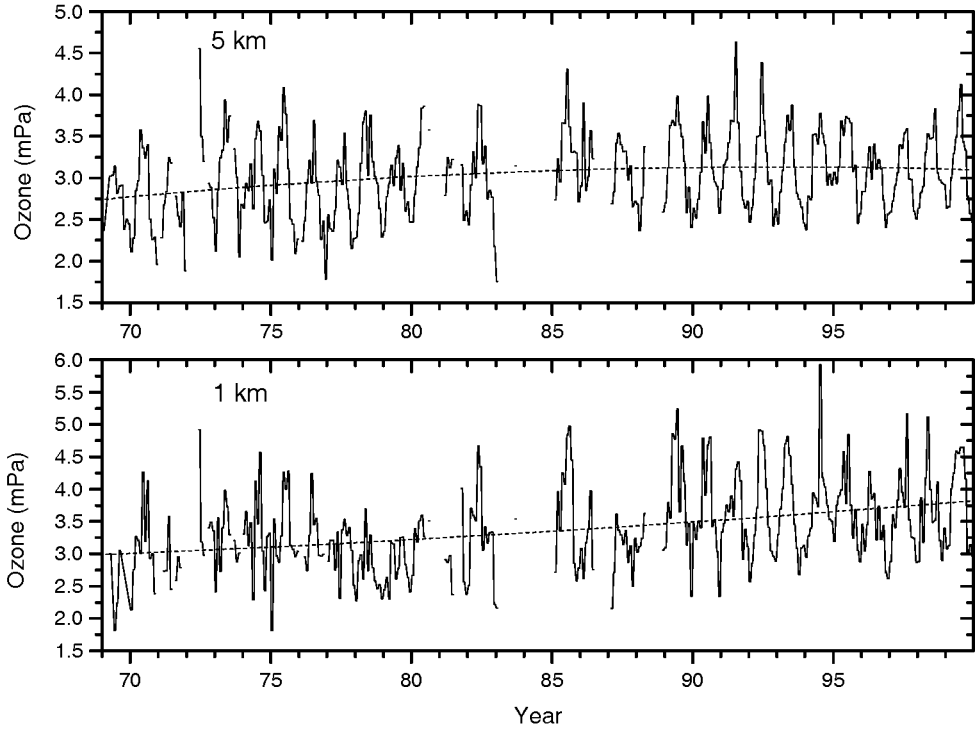

Figure 40: *Monthly means of ozone partial pressures at two tropospheric levels over Uccle. Dashed lines: 2nd order polynomial fit.*

The aim of ozone trend analyses is to examine whether there exists a systematic change in the ozone concentration throughout the atmosphere. However, these trends, if present, are small compared to the short-term weather-related fluctuations and the seasonal variation caused by the sun. Therefore, the key issue in trend analysis is to find a suitable technique to disentangle the potential long-term trend from the data. A literature study of existing techniques revealed the high effectiveness of the Kolmogorov-Zurbenko (adaptive) filter technique. We therefore started programming this filter technique which will enable us in the future to carry out a more in-depth trend analysis of the Uccle ozone sounding time series. First results are shown in Figure 41. This picture shows some anomalies around 1984.

This is probably caused by the lack of data in this period and it must be further investigated how to handle this period with missing data.

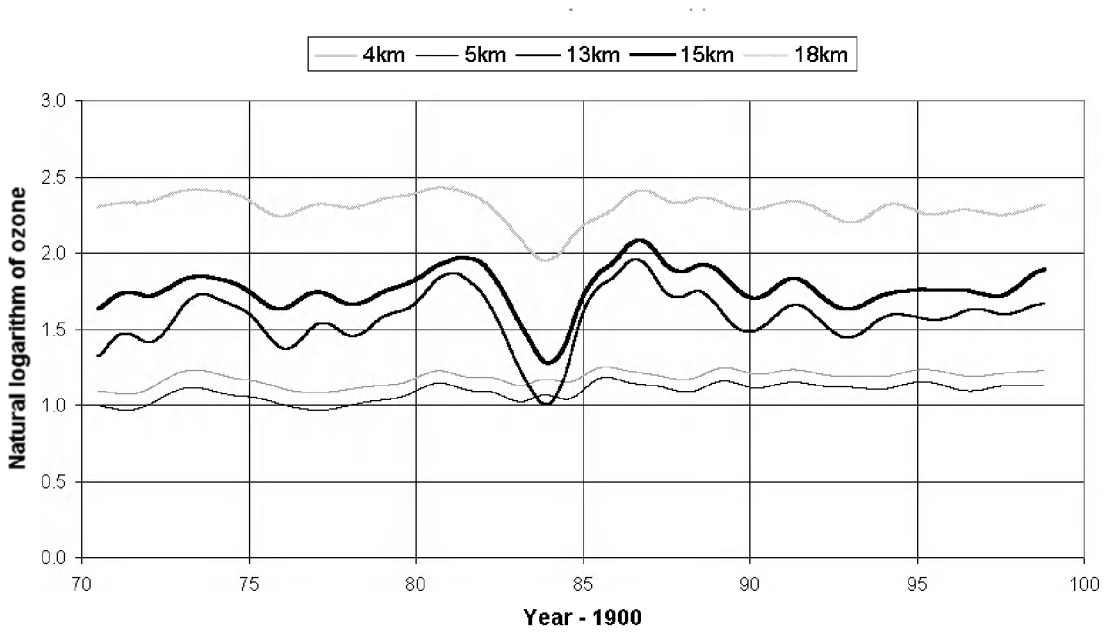

Figure 41: *Low frequency signal of the logaritm of ozone concentrations (in mPa) at Uccle, obtained with a Kolmogorov-Zurbenko filter.*

4.1.4 Synergy with satellite data

4.1.4.1 Satellite validation

TOMS and ADEOS O_3 data

Several years of total ozone measured from space by the Earth Probe TOMS (since July 1996), the ADEOS TOMS (September 1996-June 1997), and the ERS-2 GOME (since June 1995), have been compared with high-quality ground-based observations associated with the NDSC, over an extended latitude range and a variety of geophysical conditions. The comparisons with each spaceborne sensor have been combined altogether for investigating their respective solar zenith angle (SZA) dependence, dispersion, and difference of sensitivity. From the qualitative analysis of global ozone maps derived from TOMS-EP, TOMS-AD and ERS-2 GOME data, one concludes that the three spaceborne sensors capture similarly the spatial structure of the total ozone field. The comparison of the space- and ground-based time-series leads to similar conclusions for the day-to-day variability of the ozone column, under normal conditions as well as during springtime polar ozone depletion. The

quantitative comparison of time-series does not reveal any significant long-term drift. Although mutually consistent within a few percent, systematic differences are observed between TOMS-AD and TOMS-EP total ozone. They might be attributed partly to air mass differences in time (the orbits of ADEOS and Earth Probe are different) and in space (the lines of sight and resulting ground pixels are different), and partly to calibration uncertainties. No significant difference is observed between TOMS-AD data prior to and after the recent re-calibration performed at NASA/GSFC.

After properly taking into account the known biases of the ground-based total ozone time-series (e.g., seasonal/latitudinal variation in real-time SAOZ data, or temperature dependence of the ozone absorption coefficients for the Dobson and Brewer instruments), comparisons between satellite and different ground-based observations generally are consistent within the accuracy level of the ground-based data. A consistency by latitude belt is also noticed. The average agreement between the TOMS and ground-based total ozone is better than ±2-3% at northern middle latitudes. The agreement at higher latitudes depends on the SZA. At low and moderate SZA, the TOMS instruments report in the Arctic larger total ozone values by 3-5% on average in summer-fall, while the agreement is better in wintertime. Beyond 80° SZA, the TOMS columns are smaller by 5-10% on average. A SZA dependence similar in shape and amplitude is observed in Antarctica, but there the mean relative difference is dominated by the systematic bias described in the next paragraph. The shape of the SZA dependence does not vary with the season. The most striking feature of both TOMS-EP and TOMS-AD total ozone data is the pseudo interhemispheric difference of their agreement with ground-based observations as well as with ERS-2 GOME data. At the southern Tropics, a small difference of sensitivity appears compared to the SAOZ.

The pole-to-pole comparison confirms the clear north/south difference already reported in the agreement between the TOMS and ground-based data. While the agreement is reasonable in the northern hemisphere, both TOMS-EP and TOMS-AD are reporting larger ozone columns in the southern hemisphere. At low and middle latitudes, the overestimation of ground-based data by TOMS is about 4-8% on average. At the three stations around the Antarctic polar circle, the agreement is better in winter likely because of the SZA dependence as observed in the Arctic, however, a systematic bias of 6-10% appears after September as the SZA decreases. The bias does not vanish in summer, that is, when both Dobson and SAOZ data are expected to be the most accurate. At the high Antarctic site of Halley, a permanent offset of 8-12% is observed from early spring through late fall. The recent re-calibration and subsequent reprocessing of the entire TOMS-AD data record does not yield much improvement. GOME data exhibit cyclic signatures

compared to ground-based data, but show no evidence of a year-round systematic offset as that reported with TOMS data. It must be pointed out that, although representative of a variety of relevant geophysical conditions, the distribution of ground-based stations used in the present study does not allow to determine whether the difference is really interhemispheric, or changing with the latitude in a more complex way, e.g., with the latitude belts defined in the TOMS V7 algorithm.

Possible causes have already been proposed, but further research is still required. An interhemispheric difference might arise from the climatology of ozone and temperature profiles used in the TOMS V7 algorithm, possibly biased towards the northern hemisphere, and poorly represented at polar latitudes. The interhemispheric consistency of the comparison with GOME seems to indicate a separate treatment of each hemisphere. At Antarctic stations, both the cloud cover fraction derived from GOME and the reflectivity derived from TOMS indicate an almost permanent overcast. The tropospheric contribution to the satellite measurement is partly masked and a climatological ozone profile below clouds must be used, which can also introduce an offset in the satellite data. Errors of the TOMS calibration in the southern hemisphere can not be excluded, however, as already mentioned, the recent re-calibration of TOMS-AD data does not modify the results.

To conclude, the global picture of total ozone provided by the three spaceborne sensors studied in this work is globally consistent with high-quality ground-based observations associated with the NDSC. No long-term drift can be detected after several years of operation. However, various discrepancies are identified or confirmed, that could impact the scientific interpretation of satellite data: (i) a SZA dependence with TOMS beyond 80° SZA; (ii) a north/south difference of TOMS with the ground-based observations; (iii) and a difference of sensitivity to low total ozone values between satellite and SAOZ sensors around the southern tropics. The recent re-calibration of the whole TOMS-AD data record does not attenuate its interhemispheric bias. Further investigations are required to understand the discrepancies.

Geophysical consistency of stratospheric NO_2 measurements

Several sensors operating from space, balloon and the ground monitor the column abundance and vertical distribution of stratospheric NO_2. Within the framework of the international Network for the Detection of Stratospheric Change (NDSC), the vertical column abundance of sunrise and sunset NO_2 is monitored from pole to pole by a network of ground-based UV-visible spectrometers, including several BIRA-IASB instruments. The HALogen Occultation Experiment (HALOE) aboard NASA's UARS

satellite measures stratospheric NO_2 profiles at sunrise and sunset, extending ground-based results to the global domain. The nadir-viewing ESA's ERS-2 Global Ozone Monitoring Experiment (GOME) monitors the vertical column amount of mid-morning NO_2.

In the present study, the geophysical consistency of those three complementary components of the multi-platform observing system for atmospheric NO_2 have been examined at a number of NDSC stations, including Jungfraujoch and Harestua as illustrated in Figure 42 as well as stations at other latitudes (see e.g. Figure 43). The investigation relies on correlative studies of measurement data records under a variety of geophysical conditions. Results have been interpreted in the light of information provided by the chemical transport model of the troposphere IMAGES. In particular, to derive HALOE vertical columns, HALOE profiles have been integrated over the stratosphere and extended towards the ground using a tropospheric content estimated by IMAGES, also depicted in Figure 42.

The study concludes to a reasonable geophysical consistency of stratospheric measurements. All instruments capture similarly major features such as post-Pinatubo recovery of stratospheric NO_2, annual variation, other low-frequency periodic signals (e.g., Southern Atlantic Oscillation and Quasi-Biennial Oscillation), wintertime polar denoxification, and dawn-to-dusk diurnal variation. In general, ground-based UV-visible spectrometers and HALOE report a similar day-to-day scatter. GOME data are somewhat more scattered. Most of outlying GOME data observed at the Jungfraujoch – where ground-based UV-visible data have been filtered out – are indicative of enhanced tropospheric NO_2 to which the GOME measurement is highly sensitive. Despite the reasonable general agreement, the study also highlights some discrepancies such as those observed between sunset measurements in the subtropics. It also raises some issues such as the possible enhanced NO_2 observed by HALOE under midnight sun.

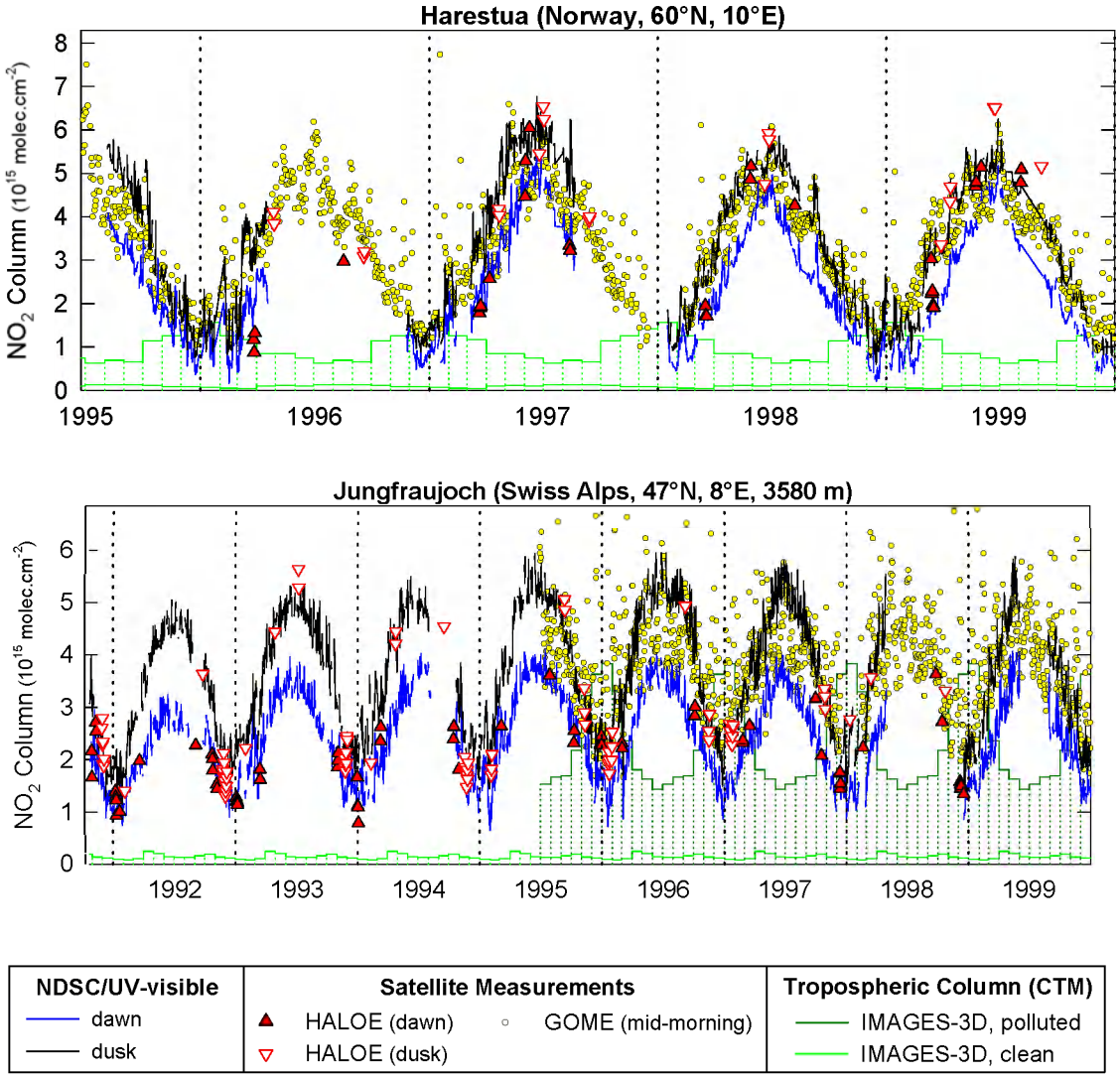

Figure 42: *NO_2 column time-series at Harestua (1995-1999) and Jungfraujoch (1991-1999) as derived from measurements acquired by BIRA-IASB and SAOZ UV-visible spectrometers, HALOE v19, and GOME GDP2.7. Bar plots show modelled tropospheric contents representative of clean and polluted conditions, respectively.*

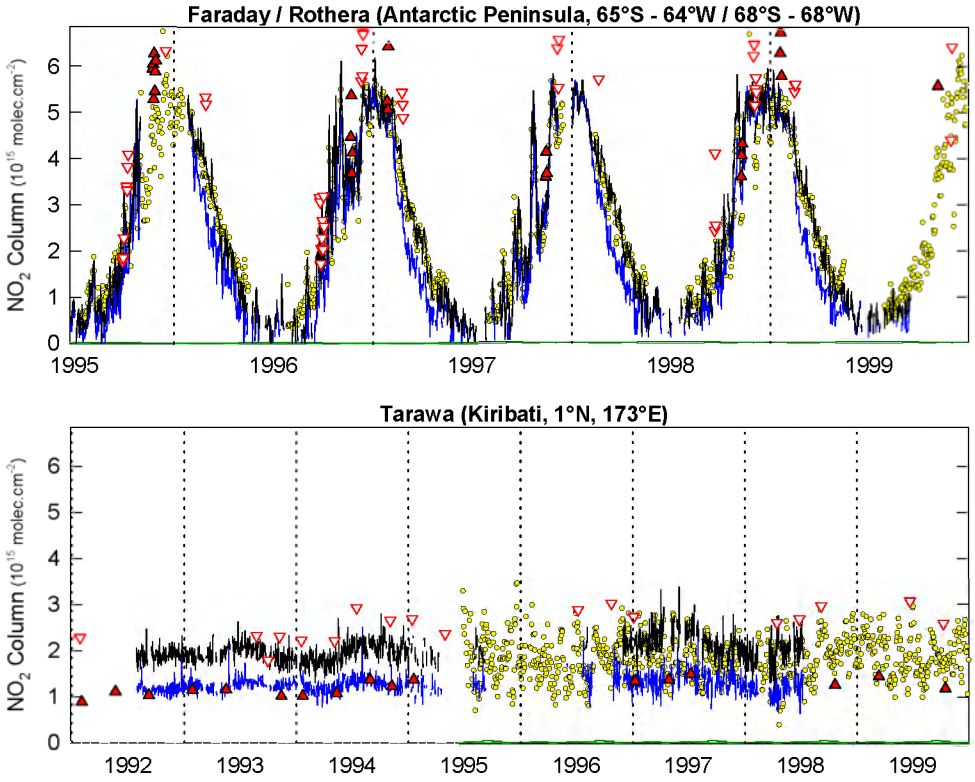

Figure 43: *Same as in Figure 42, but at Rothera in Antarctica (1995-1999) and at Tarawa on the Equator (1992-1999).*

4.1.4.2 Development of an NO_2 vertical profile climatology

Within the framework of the NDSC, the vertical column abundance of sunrise and sunset NO_2 is monitored from pole to pole by a network of ground-based UV-visible spectrometers. Slant column amounts derived from the measurement of the zenith-scattered sunlight at twilight are converted into vertical columns using an optical enhancement factor, or air mass factor (AMF). AMFs are calculated with a radiative transfer model assuming the vertical distributions of NO_2 and of radiatively active atmospheric parameters. Current NO_2 AMFs are based on a basic reference atmosphere. Previous studies have raised the issue of the AMF sensitivity to the profile shape of NO_2 and of other atmospheric parameters. In this study, the sensitivity of NO_2 AMF towards a variety of inputs has been studied in order to identify the critical parameters that have to be improved for better accuracy of the data products.

As a first step, AMF from 4 different radiative transfer models (see Table III) were compared for the case of a pure Rayleigh atmosphere. Carried out in collaboration with three other research institutes involved in UV-visible spectrometry (CNRS, NILU, and U. Bremen), the purpose of this test is to detect discrepancies between the models and problems with synchronising the input. The four NO_2 AMFs are plotted in Figure 44, arbitrarily normalised to the SAOZ standard AMF. The differences between the models are in the order of 1% and even smaller below 90° SZA, showing that no further model tests are necessary at this point.

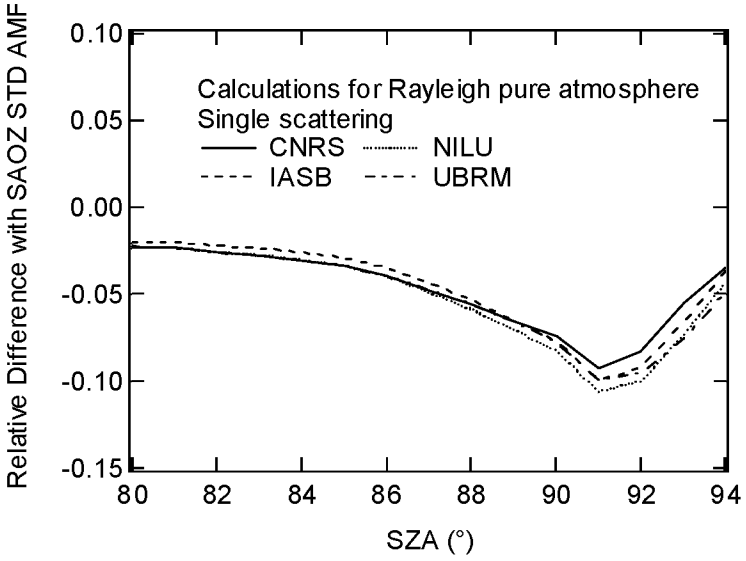

Figure 44: *Normalised NO_2 Air Mass Factors from 4 different radiative transfer models for a pure Rayleigh atmosphere. The differences are small for all SZA and negligible below 90° SZA.*

Table III*: Legend to the plots in Figure 45. The AMF for Haute Provence (OHP) have been added as they have been used for the SCUVS intercomparison campaign at OHP in June 1996 and have to be compared to the improved AMFs computed in this study using vertical profiles appropriate for this time and location.*

SSC	SSA	MSC	MSA	OHP	STD
Single Scattering Calculations	Single Scattering with Aerosol	Multiple Scattering Calculations	Multiple Scattering with Aerosol	AMF used in June 1996 at OHP (SCUVS)	AMF used in the instrument in real time

The sensitivity of the NO_2 AMF has been investigated further towards changes in the assumptions of the radiative transfer. Six different scenarios, of which details are described in Table III, have been analysed with all models. The resulting AMFs are depicted in Figure 45. All models agree very well for all scenarios. Inclusion of multiple scattering increases the AMF at all solar zenith angles (SZA), while accounting for aerosol scattering leads to increases at large SZA only. Changes in surface albedo were found to be negligible for twilight conditions but induce changes of up to 1.5% at high sun. All scenarios are significantly different from the SAOZ standard AMF at 90° SZA, emphasising the need for improvements in NO_2 AMF.

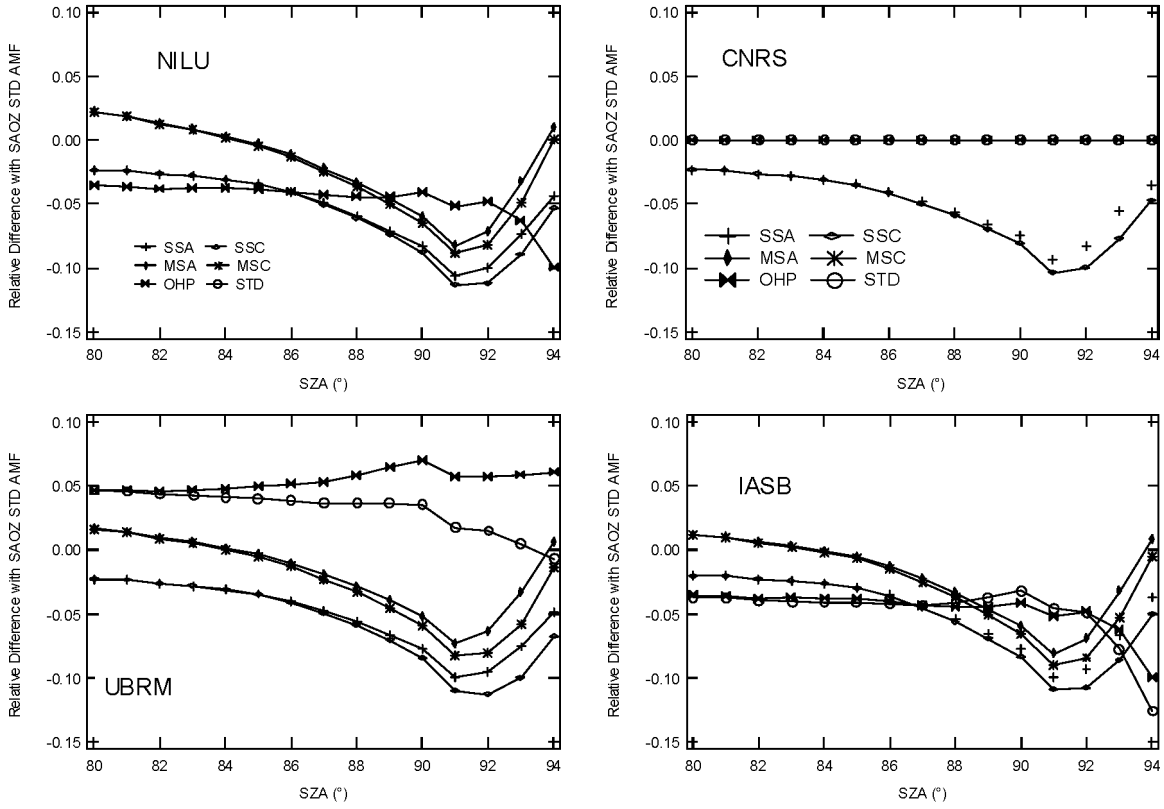

Figure 45: *Influence of multiple scattering, stratospheric aerosols, and profile assumptions on arbitrarily normalised AMF to the SAOZ standard AMF. See Table III for details on the scenarios.*

As a second step, an improved NO_2 reference atmosphere has built up. A perturbation study has revealed that the AMF sensitivity is highest for NO_2 changes in the stratosphere between 20 and 35 km and in the troposphere below 5 km. Accordingly, a climatological model of NO_2 profiles has been derived from measurements from space (UARS HALOE), balloon (SAOZ-balloon) and the ground (NDSC/UV-visible network), and complemented by modelling results (IMAGES). The resulting NO_2 profile climatology covers altitudes from the ground up to 70 km. The

principle of this composite database is illustrated in Figure 46 The mutual consistency of the various databases has been investigated carefully and has led to the validation of NO_2 stratospheric columns as derived from the integration of HALOE profile measurements.

As a third step, the new NO_2 reference atmosphere has been combined with pressure, temperature and ozone climatological databases in order to investigate possible periodic signatures in the AMF related to seasonal, latitudinal, and sunrise/sunset change of the vertical distribution of NO_2, pressure, temperature, and ozone. The study highlights periodic signatures in the AMF which need to be taken into account when retrieving NO_2 vertical columns from ground-based observations of zenith-scattered sunlight. Figure 47 shows that, in general, the AMF based on the US Standard Atmosphere would yield an underestimation of the retrieved vertical columns in the northern hemisphere and an overestimation at southern middle and high latitudes. The bias would exceed 10% in denoxification conditions in polar winter. The US Standard AMF exhibits a seasonal variation, which grows from a few percent in the tropics, up to about 5-6% at middle latitudes and 8-10% at high latitudes. The dawn-to- dusk photochemical variation of stratospheric NO_2 affects the AMF by a few percent, sunset AMFs being generally larger than sunrise AMFs.

In conclusion, sensitivity studies have been performed to identify critical parameters in the NO_2 AMF calculation. A model intercomparison showed excellent agreement between 4 models used in the international NDSC/UV-visible community. Multiple scattering and to a lesser degree aerosol loading increase NO_2 AMFs, tropospheric contributions on the other haFnd decrease it. Changes in the vertical profiles of temperature, pressure, ozone, and NO_2 mixing ratio lead to a seasonal variation of NO_2 AMF, but the magnitude depends on the NO_2 profile shape. All tests show, that the use of current standard AMF for NO_2 is not acceptable, and that more sophisticated approaches have to be used to improve the accuracy of NO_2 columns from zenith-sky measurements.

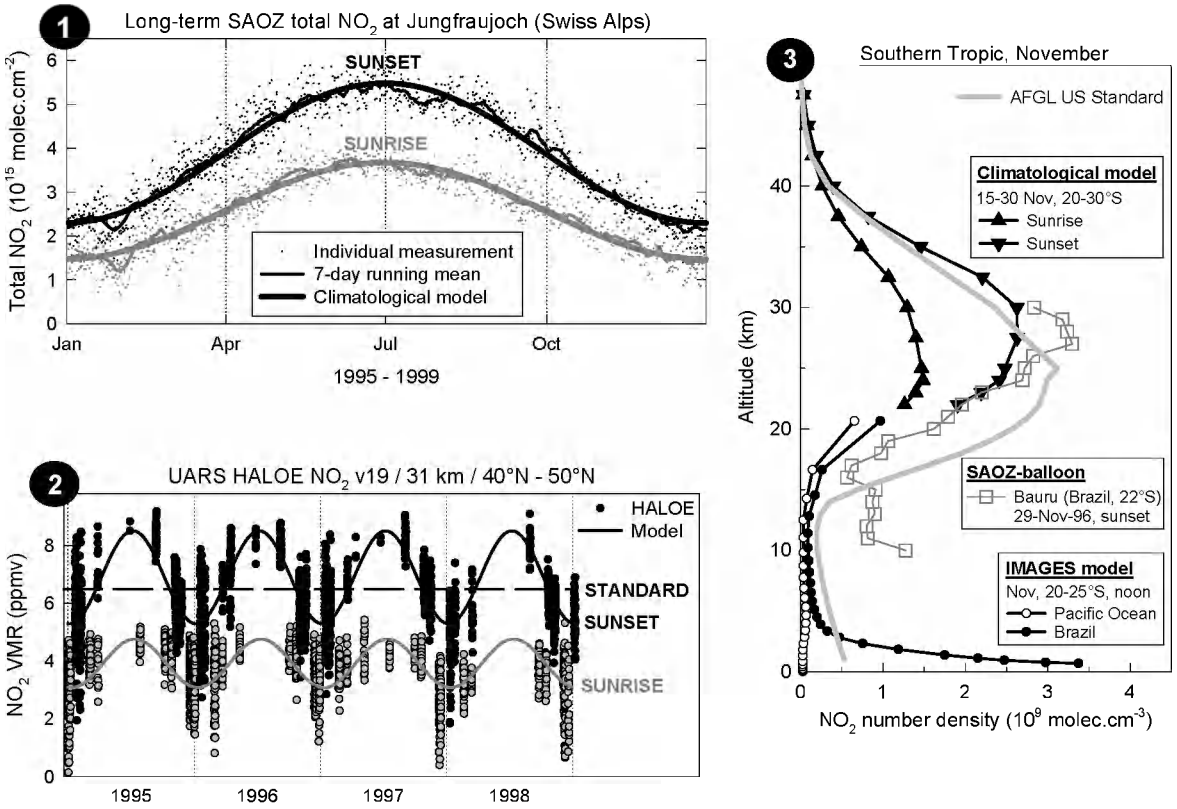

Figure 46: *Construction of the composite NO_2 profile database: (1) ground-based determination of climatological characteristics of stratospheric NO_2; (2) at each altitude, fitting of HALOE data with functions inspired from the ground-based characteristics; (3) use of IMAGES model results and SAOZ-balloon observations to complete the profile down to the ground. US Standard Atmosphere values are depicted for comparison.*

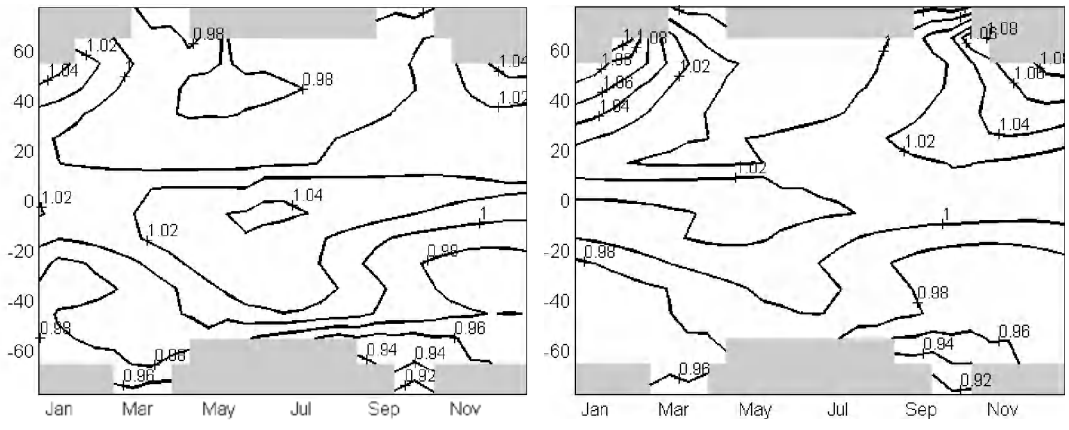

Figure 47: *Seasonal, latitudinal, and sunrise/sunset variation of NO_2 air mass factors: ratio of NO_2 AMFs at 90°SZA calculated with the US Standard and the climatological NO_2 profiles for a sunrise (left) and a sunset (right) stratosphere and a clean troposphere.*

4.1.4.3 ATMOS-related research

The ATMOS (Atmospheric Trace Molecule Spectroscopy) instrument is a fast-scanning, fast-response and high-resolution FTIR spectrometer that operates from space in the solar occultation mode over the 2.1 to 15 □m (4800 to 650 cm^{-1}) infrared domain. As a core experiment of the NASA-Spacelab and ATLAS (ATmospheric Laboratory for Applications and Science) programmes, the ATMOS instrument took part in the Spacelab-3 (SL-3; Challenger shuttle; 29 April- 7 May 1985), ATLAS-1 (AT-1; Atlantis; 24 March-3 April 1992), ATLAS-2 (AT-2; Discovery; 8-16 April 1993) and ATLAS-3 (AT-3; Atlantis; 3-14 November 1994) missions. During these missions, it performed altogether measurements over 480 complete occultations, about half of which were sunrises and the others sunsets, spanning latitudes from about 65°N to 73°S. Until about 1995, the data processing and analysis method adopted for the inversion of the ATMOS solar occultation measurements into geophysical parameters followed the procedure described by Norton and Rinsland (1991), making use of the "ODS" (for Occultation Display Spectra) retrieval code specifically developed for ATMOS and based on the "onion peeling" approach, with the individual spectra being investigated successively for each target gas and each chosen characteristic absorption feature (microwindow), in a top-to-bottom retrieval sequence. The data base resulting from the consistent analysis of all four ATMOS missions with ODS was called "Version 2" (abbreviated hereafter as V2). An important aspect of spectroscopic remote sensing of the atmosphere by the solar occultation method from space is the precision and accuracy with which related measurements can be made (Abrams et al., 1996a). Considering the methodology and input parameters adopted along the data processing and inversion, these have been determined for all individual VMR profiles of the V2 data base (Abrams et al., 1996b) which is publicly available at ftp://remus.jpl.nasa.gov/pub/atmos/version2.

The "ODS" procedure was slow and did not take advantage of simultaneous, multiple microwindows fittings, and its automatic operation in the "spectra after spectra" onion-peeling mode generally failed in the inversion of observation into geophysical parameters below about 16 km (~ 100 mb pressure level; e.g., Zander et al., 1996), although many occultations showed high quality spectra recorded by ATMOS well below that altitude.

The ATMOS "Version 3" geophysical data

Within the ESAC research context reported about here, our main task was to contribute, as ATMOS Science Team partner, to the production of an "ATMOS-Version-3" set of volume mixing ratio profiles that would extend reliably to lower altitudes, down into the free troposphere, and to inter-compare such profiles with

independent measurements from other space- and ground-based instruments. Here below, Version-2 and Version-3 will be abbreviated by V2 and V3, respectively.

Following a Science Team meeting and numerous teleconferences, it was decided to implement the GFIT retrieval code which itself was an adaptation of "ODS" but specifically developed at the Jet Propulsion Laboratory (Pasadena, CA, USA) for the analysis of MkIV-balloon observations (Toon et al., 1999). This batch-automated code allows to fit numerous (target- and interfering-) species simultaneously, using various sets of microwindows, and treating all spectra of an occultation at once. The main benefits resulting from this adaptation include (i) the extension of retrieved concentration profiles to lower altitudes, well into the free troposphere, (ii) the retrieval of a couple of additional species such as CH_2O and HOCl, and (iii) a more reliable evaluation of the statistical uncertainties (precision) affecting the VMR profiles at all altitudes. During 1998-99, the V3 data base has undergone quantitative evaluations with respect to V2 (at least over overlapping altitude ranges) and versus data produced by other space-based instruments such as MAS (Millimeter-wave Atmospheric Sounder), HALOE (Halogen Occultation Experiment) and MLS (Microwave Limb Sounder), also with measurements performed by experiments aboard the NASA ER-2 airplane and the MkIV-balloon FTIR spectrometer (e.g., Toon et al., 1999). The V3 database includes profiles regarding all four ATMOS missions performed between 1985 and 1994.

Typical examples of the V3 profile retrievals with GFIT, to which ULg has contributed significantly are reported hereafter. Figure 48 displays the profiles of the various constituents intervening in the evaluation of the total chlorine loading versus altitude at the time of the ATMOS/ATLAS-3 mission of November 1994, for the northern mid-latitude zone spanning 35 to 49ºN. With the exception of $C_2Cl_3F_3$, CH_3CCl_3, COClF and ClO, all other contributing species are derived from the ATMOS-FTIR solar occultation observations. The important contributors to the organic Cl inventory in the upper troposphere (e.g., CCl_2F_2, CH_3Cl, CCl_3F, $CHClF_2$, CCl_4) appear to be properly retrieved with the GFIT algorithm; these free tropospheric concentrations are in good agreement with related concentrations made independently at the ground by *in situ* networks (see the square symbols on the lower frame of Figure 48) at the time of the AT-3 mission. The horizontal arrow indicates the altitude above which the chlorine budget was evaluated and reported on the basis of the V2 retrieval data (Zander et al., 1996).

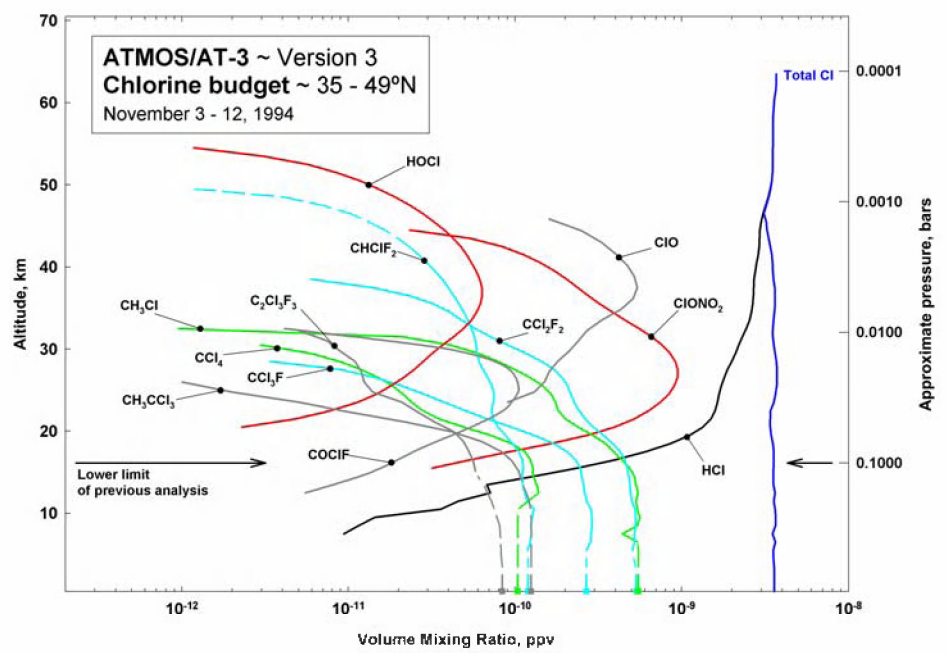

Figure 48: *The chlorine budget of the upper troposphere and stratosphere as derived for northern mid-latitudes in November 1994. It includes all important chlorinated gases (sources, sinks and reservoirs combined) observed by ATMOS during the ATLAS 3 shuttle mission, as well as a few complementary species (grey traces) measured by other techniques. The horizontal arrows indicate the level down to which the Version 2 data were retrieved automatically with the ODS code; the new Version 3 allows to extend the profiles further down, well into the free troposphere. Notice the good agreement (except for CCl_4; see text) between lowermost volume mixing ratios derived from ATMOS spectra and corresponding in situ concentrations measured at the ground (square symbols).*

In a way similar to the confection of total Cl in Figure 48 Figure 49 displays the elements intervening in the production of total fluorine budget throughout the troposphere and stratosphere.

The comparison between the latter 1994 budgets of Cl and F and similar ones produced from the ATMOS SL-3 mission of 1985 (Zander et al., 1992), indicates increases in the stratospheric loading of Cl and F equal to nearly 40% and 70%, respectively. When taking into account the time delay necessary for long-lived source gases to mix into the mid-latitude stratosphere (4 to 6 years), the above increases are consistent with the trends measured in the tropospheric Cl and F loading resulting from increased ground-level emissions, during the 1980s, of anthropogenic Cl- and F-bearing source gases, in particular the CFCs -11 and -12, and the HCFC-22. No volcanic contribution needs to be invoked to explain both the loadings and trends of inorganic Cl and F throughout the stratosphere as observed by ATMOS over the 1985 to 1994 time period. These results and conclusions have been

extremely important in justifying and assessing the merits of international policy decisions such as those defined in the Montreal Protocol (1987) and its successive Amendments and Adjustments (1990, 1992, 1995 and 1997).

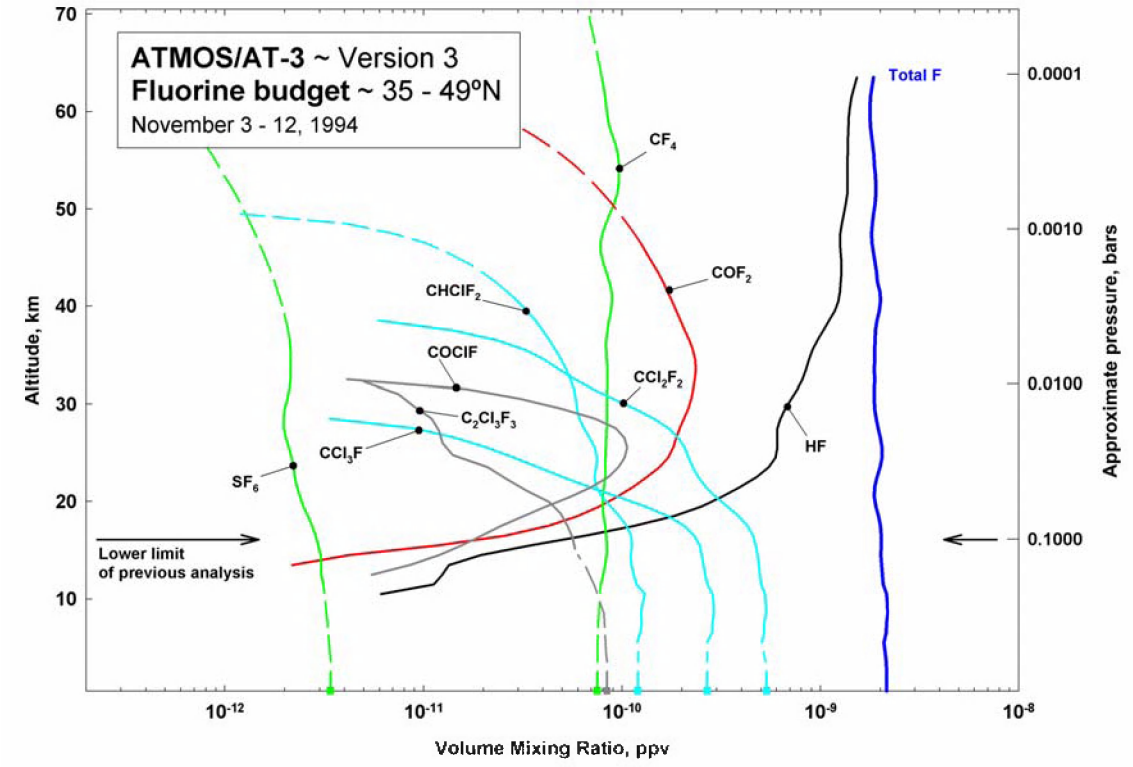

Figure 49: *The fluorine budget of the upper troposphere and stratosphere as derived for northern mid-latitudes in November 1994. It includes all important fluorinated gases (sources, sinks and reservoirs combined) observed by ATMOS during the ATLAS 3 shuttle mission, as well as a few complementary species (grey traces) measured by other techniques. The horizontal arrows indicate the level down to which the Version 2 data were retrieved automatically with the ODS code; the new Version 3 allows to extend the profiles further down, well into the free troposphere. Notice the good agreement between lowermost volume mixing ratios derived from ATMOS spectra and corresponding in situ concentrations measured at the ground (square symbols).*

A concerted activity has also been maintained (via teleconferences) among the ATMOS Science Team regarding the precision and accuracy with which water vapor volume mixing ratio profiles can be derived from the V3 data analysis, especially in the lower stratosphere and upper troposphere (Michelsen et al., 2001). Important conclusions from that investigation indicate that (i) the consistency between V2 and V3 averaged H_2O profiles is very good in the lower and middle stratosphere; (2) in the upper stratosphere and mesosphere, the retrievals are dryer for V3 than for V2; (3) compared to V2, the V3 profiles of H_2O reveal more small-scale variability in the

stratosphere and capture more reliably sharp features such as the hygropause. Improvements have resulted, not only from adopting the "global fit" approach evoked before, but also by adding a number of new microwindows (which can be partly corrupted by interfering gases, because of the multiple-species retrieval possibility of the GFIT algorithm). H_2O-related intercomparisons with measurements by airborne Lyman-α hygrometers from NOAA and from Harvard (Hintsa et al., 1999), by the MkIV balloon FTIR (Toon et al., 1999), by the shuttle-based MAS microwave instrument (Bevilacqua et al., 1996), by the UARS-HALOE (Harries et al., 1996) and –MLS (Pumphrey, 1999) indicate differences ranging from 4 to 30 % in the lower stratosphere, 3 to 15 % in the middle stratosphere, 5 to 15 % in the upper stratosphere, and 0 to 30 % in the mesosphere. The best agreement is with the MkIV balloon FTIR (3 to 5 %) throughout the lower and middle stratosphere.

Another research to be briefly evoked here deals with ATMOS observations inside the November 1994 Antarctic stratospheric vortex and inside the April 1993 remnant Arctic stratospheric vortex. In both regions, a pocket of elevated CO was observed in the midstratospheric vortex, a feature resulting from downward transport of air originating at mesospheric altitudes. In the Antarctic, the CO peak was located about 1 km below a region of elevated NO_y, whereas there was no evidence of such an enhancement in the Arctic observations. The interpretation of these new findings has been reported in Rinsland et al. (1999).

Auxiliary data

During the past year, we have further investigated UARS/HALOE measurements regarding HCl, HF and CH_4, the ultimate aim being to produce series of "most realistic" profiles to be used in the retrieval of vertical column abundances from ISSJ observations. HALOE data have been taken since October 1991, with on average 15 occultations being registered per day. The latest "Version 19" (abbreviation V19) is publicly accessible via Internet. The procedure adopted to derive most realistic profiles for ISSJ from the HALOE archive includes calculations of daily and monthly zonal averaged profiles in the 41.5 to 51.5ºN latitudinal band, i.e ±5º centered on the Jungfraujoch. In this 10º latitude zone, the HALOE occultations are not distributed homogeneously versus time, the April to August months being poorly covered (1 to 3 occultations per month and per year). However, a recurrent seasonal behaviour of the vertical distributions has been derived from the entire 9-year HALOE database and typical monthly profiles have been produced. The latter, regrouped per season, are currently being used as "reference" profiles in conjunction with an approach to derive partial column abundances throughout the year.

On the basis of the most recent ATMOS-V3 and HALOE-V19 data bases, we have compared average HCl profiles derived from spatial and temporal coincidences over the latitudinal zones 63-69ºN and 44-50ºS during the ATMOS-AT2 mission, as well as the 20-35ºN and 35-49ºN zones during AT3. The intercomparisons show that HALOE measurements are systematically lower by about 11% throughout the stratosphere; this value has lowered somewhat with respect to corresponding values (10 to 20%) reported by Russell et al. (1996) on the basis of earlier data versions.

4.2 Evaluation of long-term spectral UV irradiance and UV Index data at Ukkel. Variability, global changes, and UV Index forecasting

4.2.1 Introduction

The penetration of solar UV radiation through the atmosphere depends on the solar zenithal angle (SZA), the ozone overhead column and other atmospheric absorbers and scatters such as clouds and aerosols. In particular, clouds are responsible for a great deal of the observed irradiance variability. The interpretation of observed UV-B time series, and, e.g., the detection of possible trends due to human activity, requires the correct understanding of the effects of these different 'factor of influence' and a detailed study of their evolution with time.

The automated station for UV monitoring at BIRA-IASB is operational since mid-March 1993. At KMI-IRM, spectral UV measurements (280 – 325 nm) are available since 1989; initially, from April 1989 to December 1990, data were taken at noon; since January 1991, they are taken on an hourly base. Auxiliary data (total ozone, ozone, temperature and relative humidity profiles as well as cloud fraction, cloud type and ground meteorological parameters (pressure, temperature, horizontal visibility…) are provided routinely by KMI-IRM. Periodical absolute calibrations of the instruments and instrument intercomparisons are performed: calibration uncertainties can be estimated to be less than ±5% over the whole wavelength range. This estimation was confirmed during the previous European Inter-comparison Campaign (Gardiner et al., 1993).

From the available 11-years period of continuous measurements, it is possible to define the major characteristics of the UV climatology in Belgium and by extension in the 50° - latitude band. Hereinafter, The major results are presented and discussed in terms of correlation between the UV-B irradiance and the main atmospheric parameters like ozone, SO_2, clouds cover, aerosols… Some preliminary results on potential trends are also presented and discussed. The development of a UV Index forecasting model is also discussed.

4.2.2 Time series of effective UV irradiances

Erythemal doses (or effective UV irradiances) at noon in Uccle are evaluated from both sets of spectral UV-Visible measurements, by weighting each spectrum by the CIE action spectrum (McKinlay and Diffey, 1987). The KMI-IRM data set is corrected to take into account the lack of spectral measurements between 325 and 400 nm. The comparison of the two data sets gives a good agreement (within 5%) for most of the cases over the overlap period (1993-1999). Nevertheless, in some occasions, the discrepancy can reach 20-25%. This is probably due to 1) the unperfected synchronism between the measurements and 2) the correction of the Brewer measurements which does not take into account the modification of the cloud cover during one scan duration. Figure 4.33 illustrates the available time series and shows their seasonal variation. The peak values are achieved in June, corresponding to the smallest SZA of the year and relatively low ozone columns. The scatter within the seasonal fluctuation can be ascribed to changes in cloud coverage.

From the daily observations of UV spectra, a climatology of effective UV-irradiance at local noon was extracted. It was checked how this effective irradiance depends on the degree of cloudiness (see Figure 51). From this figure the influence of the mean annual variation of the thickness of the ozone layer may also be noted: at mid April (when the mean total ozone amount is largest) the intensity of the effective UV irradiance is about 20 % smaller than at the end of August (when the elevation of the sun at solar noon is the same as at mid April).

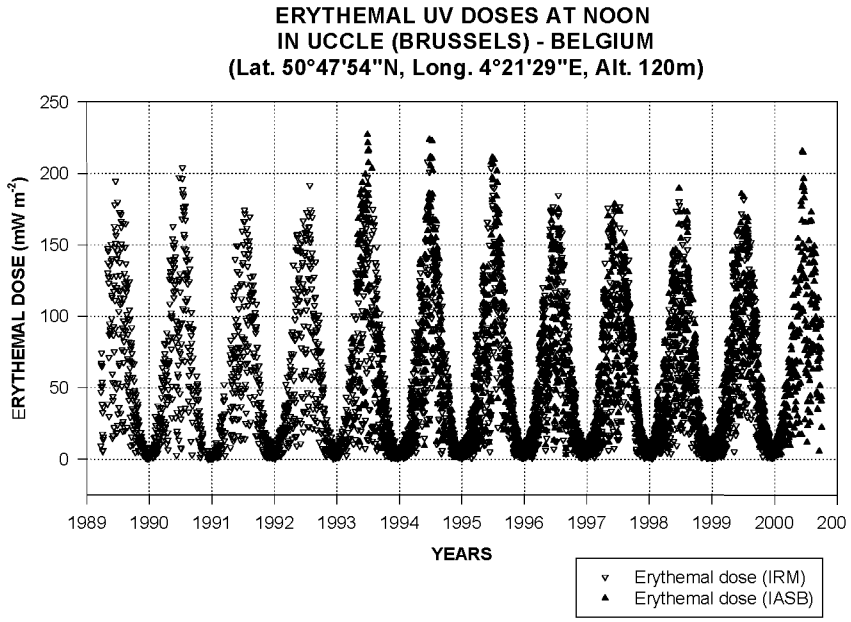

Figure 50: *Time series of the erythemal doses at Uccle*

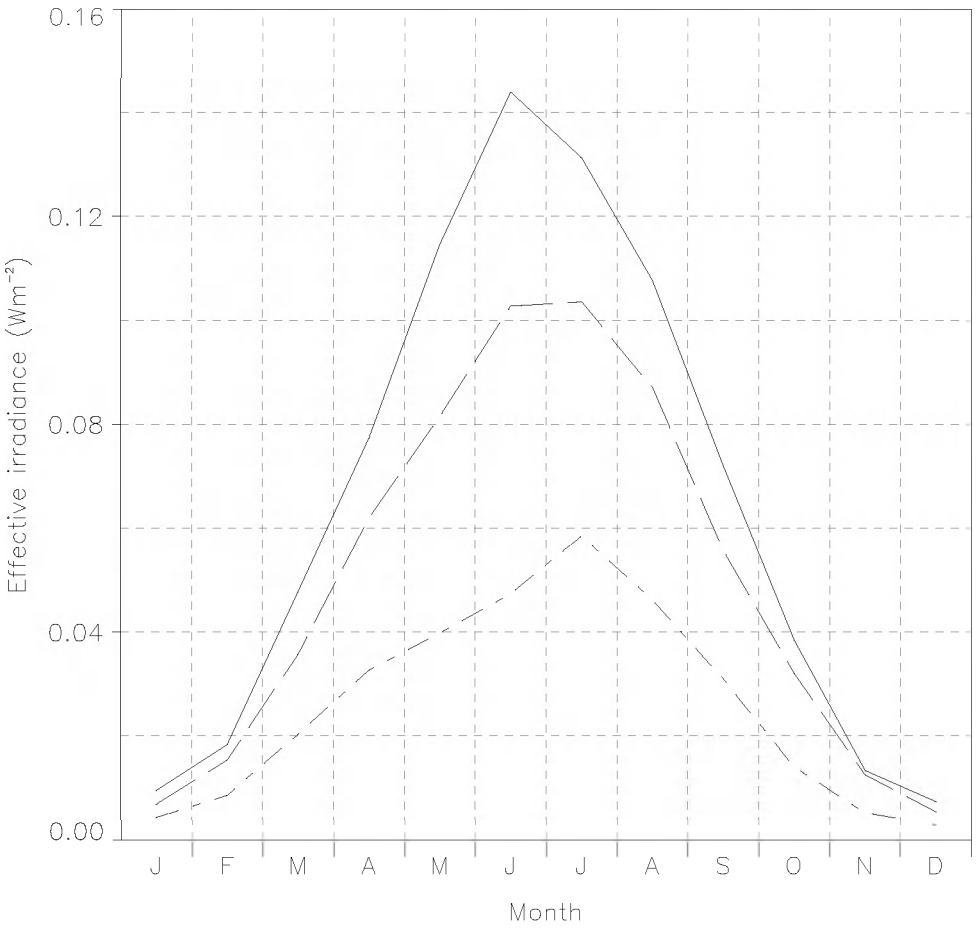

Figure 51: *Influence of cloud cover on effective UV irradiance at solar noon (Uccle, 1989-1997): cloudless sky (solid line), cloud cover between 1/8 and 6/8 (dashed line) and cloud cover > 6/8 (dash-dot line).*

4.2.3 Factors of influence

The two most important factors limiting the penetration and explaining the day to day variations of the UV-B radiation to the Earth's surface are the ozone and the cloud coverage. These two 'factors of influence' will be detailed in the next sections. Other factors like aerosols, which are relatively constant in Brussels, will be neglected.

4.2.3.1 Ozone

Figure 52 illustrates the anti-correlation between ozone total column and UV-B integrated irradiance corrected for the effect of cloud cover. The applied correction is simply the ratio UV-B/UV-A that takes into account, as a first approximation, the effect of clouds as a neutral filter.

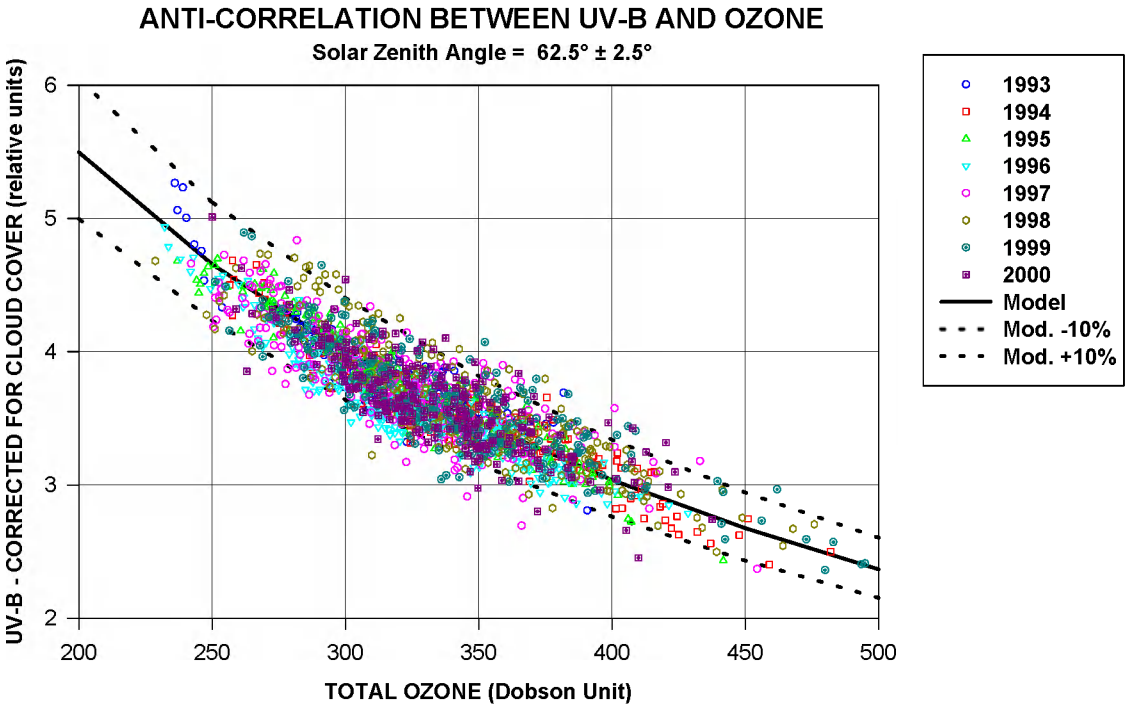

Figure 52: *Anti-correlation between ozone and UV-B.*

A discrete ordinates radiative model (Stamnes et al., 1988) has been used to simulate the experimental data and verify the anti-correlation between ozone and UV-B. The extraterrestrial flux is a combination of the SUSIM spectrum below 350 nm (Van Hoosier et al., 1984) and the Neckel and Labs spectrum (Neckel and Labs, 1984) up to 600 nm. The wavelength dependence of the aerosol optical properties follows the parameterisation of WCP (WCP, 1986) for typical continental mixtures. This choice is motivated by air pollution lower in Uccle than in typical urban centres. The weak dependence of cloud extinction and asymmetry factor is parameterised following (Slingo, 1989, private communication).

A good agreement (better then 5%) between experimental data and the simulation has been established for SZA between 30° and 70° in clear sky condition. The discrepancies between modelled and experimental data increase generally with the SZA and can exceed 10% at high SZA in the visible range. Figure 52 shows clearly that the anti-correlation observed experimentally is well reproduced by modelling and that practically all the experimental conditions are included in ± 10% limit compared to the predicted anti-correlation. This 10 % variation can easily be explained by considering the error in the ozone measurements (5%) and the unsophisticated correction of the cloud layer effects.

4.2.3.2 Clouds

In order to investigate the role of clouds as a function of wavelength, average spectra for well-defined conditions (complete overcast, similar zenith angles) have been derived from the observations, and compared with a corresponding clear sky spectrum. The average cloud transmission ratios for SZA=30 ° are displayed on Figure 53, and compared to a modelled transmission ratio. A 1-km low cloud with an optical depth equal to 50 has been assumed.

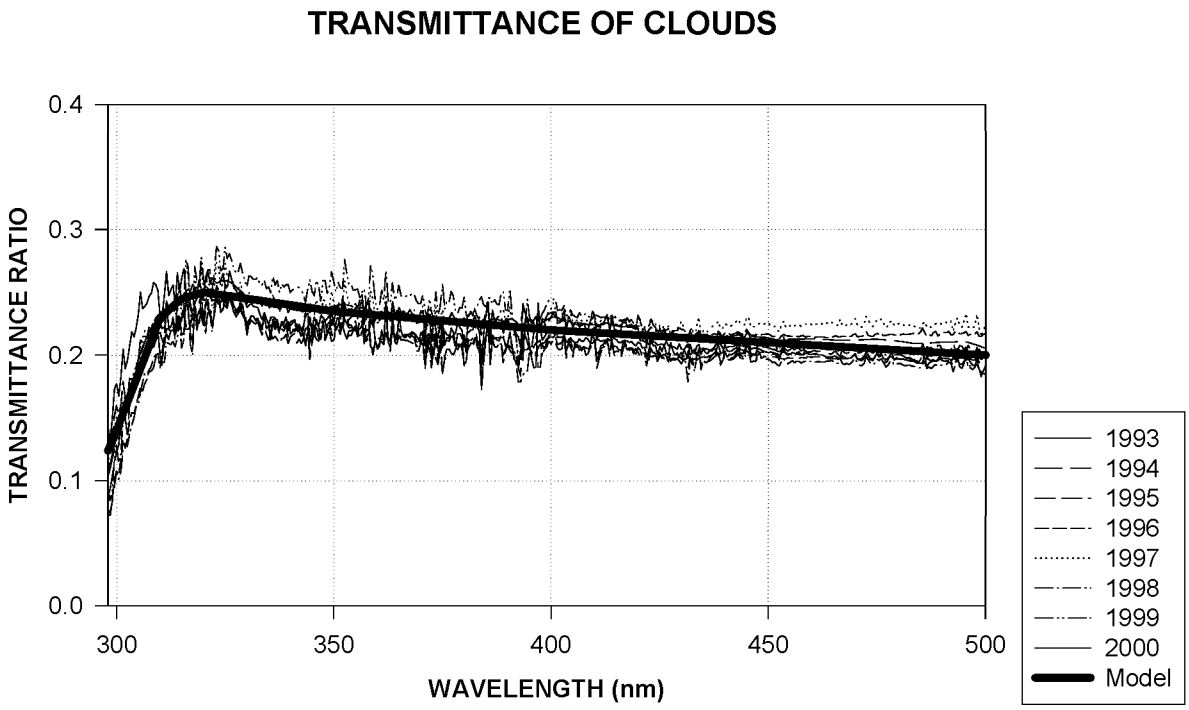

Figure 53: *Ratio of cloudy (8 Octas) to clear sky irradiance.*

Despite the large variability of the cloud impact, a consistent picture is found. The attenuation is lowest in the UV-A, and highest in the ozone absorption bands (UV-B) because of the increased multiple scattering and tropospheric ozone absorption caused by cloud. The attenuation increases to a lesser extent in the visible range, reflecting the smaller importance of Rayleigh diffusion at higher wavelengths. Finally, the average attenuation of sunlight by different type of clouds can also be directly estimated from the pyranometers data. As expected, the attenuation by cirrus clouds (high altitude) is found to be very small. In contrast, low clouds (mainly stratocumulus) reduce solar irradiance by about a factor 5 on average.

This attenuation is found to increase monotonously with the solar zenith angle in the UV-A and UV-B ranges, but not for the total integrated irradiances (300-3000 nm). These last results have to be examined in the more detailed future modelling studies.

4.2.4 Trends in UV effective irradiance

Possible trends of UV-B radiation at the Earth's surface due to human activity is of high interest for the public health medical community as well as for all the scientists interested in the effects of UV-B on biology and material sciences.

The aim of this chapter is just to illustrate what can be deduced from an 11-years period of UV-B monitoring. Figure 54 illustrates the high variability of UV-B effective doses on a monthly base mainly due to the variability of meteorological conditions.

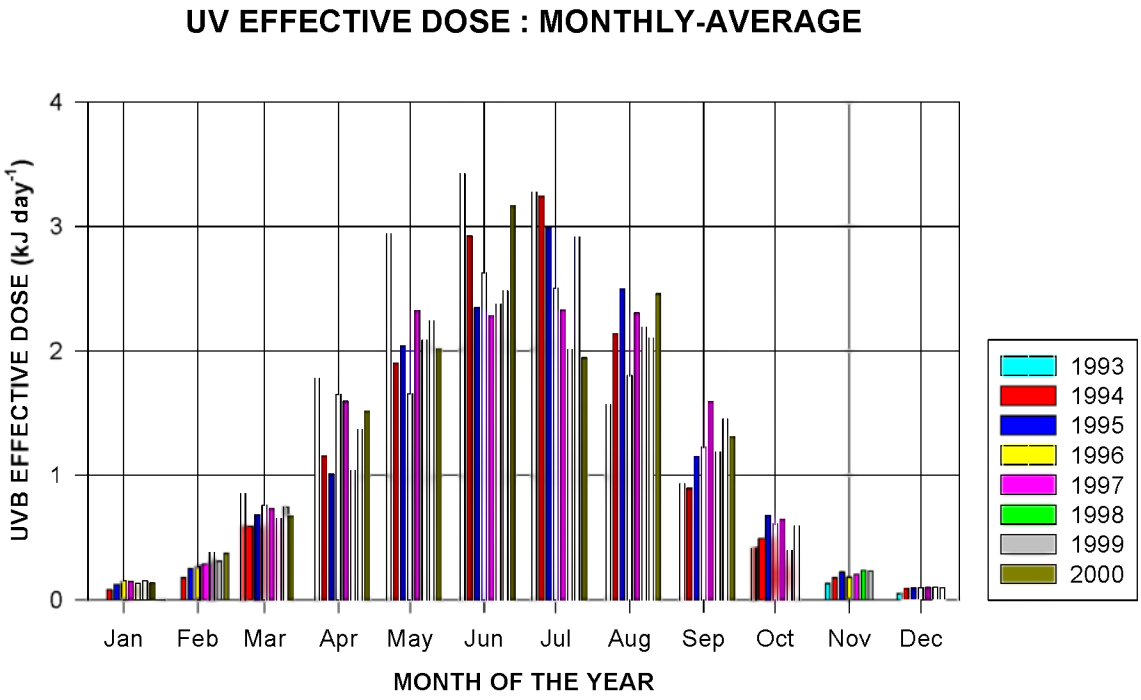

Figure 54: *UV-B effective monthly averaged doses in Uccle (Brussels) Belgium.*

Figure 55 gives a first idea of the potential trend of UV-B in Brussels. UV-B shows an increase of 0.6% per year that looks coherent with observed ozone trends of order -0.3%/year.

4.2.5 UV Index forecasting

4.2.5.1 Development of an operational UV Index forecasting procedure

The UV erythemally weighted irradiances can be converted to the international standardized UV Index, which is an indication for the sunburn risk. A UV Index forecasting algorithm was developed at KMI-IRM, in several steps.
In a first step, the Tropospheric Ultraviolet Visible (TUV) model developed by Madronich (1993) was installed and adapted to the local situation. TUV is a freely distributed FORTRAN coded multiple scattering radiative transfer model. Based on some input parameters, such as solar zenith angle and total ozone column, it calculates the corresponding spectrum. A good agreement with the observed spectra was obtained. Therefore, TUV is a valuable tool for making clear-sky UV Index forecasts, the quality of the forecasts mainly depending on the accuracy of the total ozone forecast.

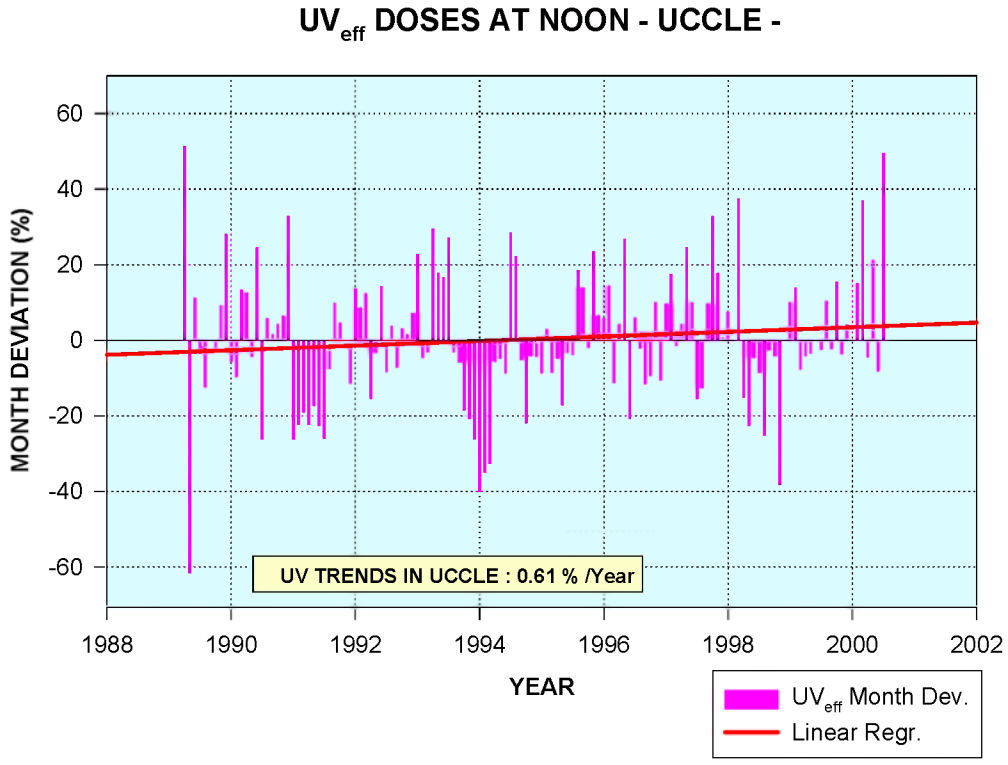

Figure 55: *UV-B trends in Brussels 1989-2000.*

4.2.6 UV Index forecasting

4.2.6.1 Development of an operational UV Index forecasting procedure

The UV erythemally weighted irradiances can be converted to the international standardized UV Index, which is an indication for the sunburn risk. A UV Index forecasting algorithm was developed at KMI-IRM, in several steps.

In a first step, the Tropospheric Ultraviolet Visible (TUV) model developed by Madronich (1993) was installed and adapted to the local situation. TUV is a freely distributed FORTRAN coded multiple scattering radiative transfer model. Based on some input parameters, such as solar zenith angle and total ozone column, it calculates the corresponding spectrum. A good agreement with the observed spectra was obtained. Therefore, TUV is a valuable tool for making clear-sky UV Index forecasts, the quality of the forecasts mainly depending on the accuracy of the total ozone forecast.

Initially, a stepwise multilinear regression of both analyzed and forecasted meteorological parameters together with the last observed total ozone value appeared to be the most adequate ozone forecast method. It resulted in a standard deviation of the difference between forecasted and observed values of the clear-sky UV index in July of the order of 0.5.
In a second step (end of 1997 - early 1998) the UV Index forecasting procedure was further developed. It became operational on April 10, 1998. Since then, each year from April to September, next day's UV Index for Belgium has been disseminated to the press on a daily base. It is broadcasted on TV at noon and in the evening and published in a few newspapers. Twice a week a color map displaying the distribution of the UV Index over Europe is also shown on TV. The meaning of the UV Index has been explained via an Internet site and a leaflet, which was written in collaboration with the 'Belgische Vereniging voor Dermatologie en Venerologie'. A renewed version of an explanatory leaflet for the general public was made in 1999, now in co-operation with Laboratoires Vichy and distributed on a much larger scale. Within the COST action 713 we participated in the edition of a booklet on the UV-index problems which was distributed by the COST secretariat into the participating countries.

Details of the UV Index forecasting procedure can be found in Plets (2000).

As said before, the quality of the UV Index forecast mainly depends on the accuracy of the prediction of the total ozone column. An inventory of existing ozone prediction

models has been made. The best models currently in use are statistical regression models that explain tomorrow's ozone in terms of today's ozone and a set of meteorological parameters. The dynamics of changing weather systems affects the total ozone amount above a given area. This is quantified by correlating the time series of total ozone with the time series of a set of meteorological variables and selecting the ones with the highest correlation. One then usually constructs a multiple linear regression model with this set of meteorological variables. We considered this model as our benchmark model. However, the method of least squares, which is used in linear regression models, requires that there is no serial correlation between the values of the dependent variable and that its variance remains constant. In the case of total ozone column data, both conditions are violated. The serial correlation is high (today's ozone being a better predictor for tomorrow's ozone than the available meteorological variables). The variance changes from relative low values from mid-summer to the beginning of fall to rather elevated values during winter and the beginning of spring. Also the mean ozone value changes with time. The first problem (serial correlation) is usually coped with by adding today's ozone to the pool of predictors. To avoid the second problem (non-stationary mean and variance), all known ozone forecasting regression models use stratified data sets. This means that separate analyses of subsets of the data record which are short enough to be regarded as stationary (usually monthly data sets) are conducted, i.e., an independent regression model is constructed for each month.

However, we felt that this approach was not fully satisfactory. Instead of cutting the time series in monthly subsets, we looked for a transformation on the whole time series to remove the nonstationarity. We developed one global model instead of 12 separate models. We obtained one single regression equation for the whole time series, which yields slightly better results than the common approach. This method was developed in collaboration with Prof. J. Beirlant of the Department of Statistics of the University of Leuven. This approach to deal with the non-stationarity problem allowed us to handle the first problem (serial correlation) by adding a term that deals with the autocorrelative structure of the error term, resulting in a so-called autoregressive (AR) model. We then still had to find a way to correct for the changing variability of the data. This was achieved by incorporating an autoregressive conditional heteroskedasticity (ARCH) model. The ARCH models, widely used in econometric problems, provide a means of estimating the next day's variance of the dependent variable by looking at the previous days' variances. The resulting AR-ARCH model is not only preferable from a theoretical point of view. It reduces the variance of the difference between observed and forecasted values with 8% with respect to the benchmark model. In the period April-September, i.e., the UV forecasting period, the variance was even reduced by 12%.

It can thus be concluded that the effort we took in examining the validity of the regression assumptions exceeds the purely academic interest and can be applied operationally to obtain more accurate UV Index forecasts. The results are published in an international journal (Plets and Vynckier, 2000).

An overview of the UV Index forecasting procedure together with an evaluation of the operational forecasts made so far has been published by Plets (2000).
The UV Index is defined for clear-sky conditions. As can be seen from Figure 56 below, the quality of the predictions is mostly very good for cloudiness less than 4 octas.

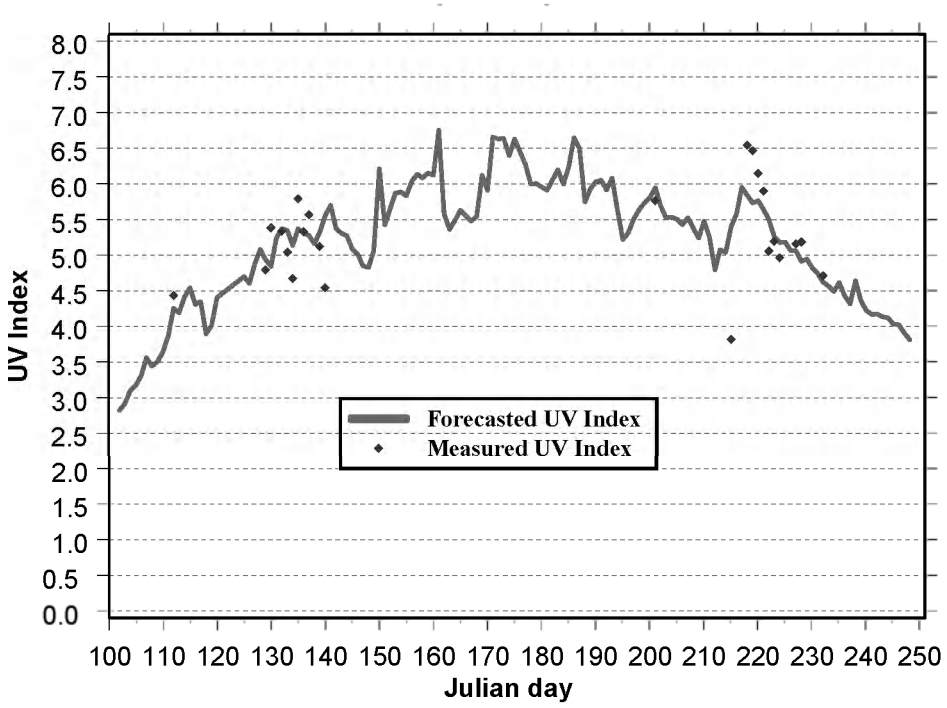

Figure 56: *Evaluation of the UV index forecasts on days with cloudiness < 4/8 at Uccle during April 10 until September 5, 1998.*

Figure 57 shows the difference between the measured and the forecasted UV Index at local noon as a function of cloudiness for the 1998 and 1999 forecasting season. As the UV Index by definition refers to clear-sky conditions, the discrepancy between forecast and measurement will increase with cloudiness. Except for broken clouds, cloudiness always yields a reduction of the intensity of incoming UV radiation. This explains why the differences in Figure 57 are negative in most cases. Typical noontime UV Index values in the forecasting season range from 3.5 in April to 6.5 in the beginning of July, subsequently decreasing again to 3 in September.

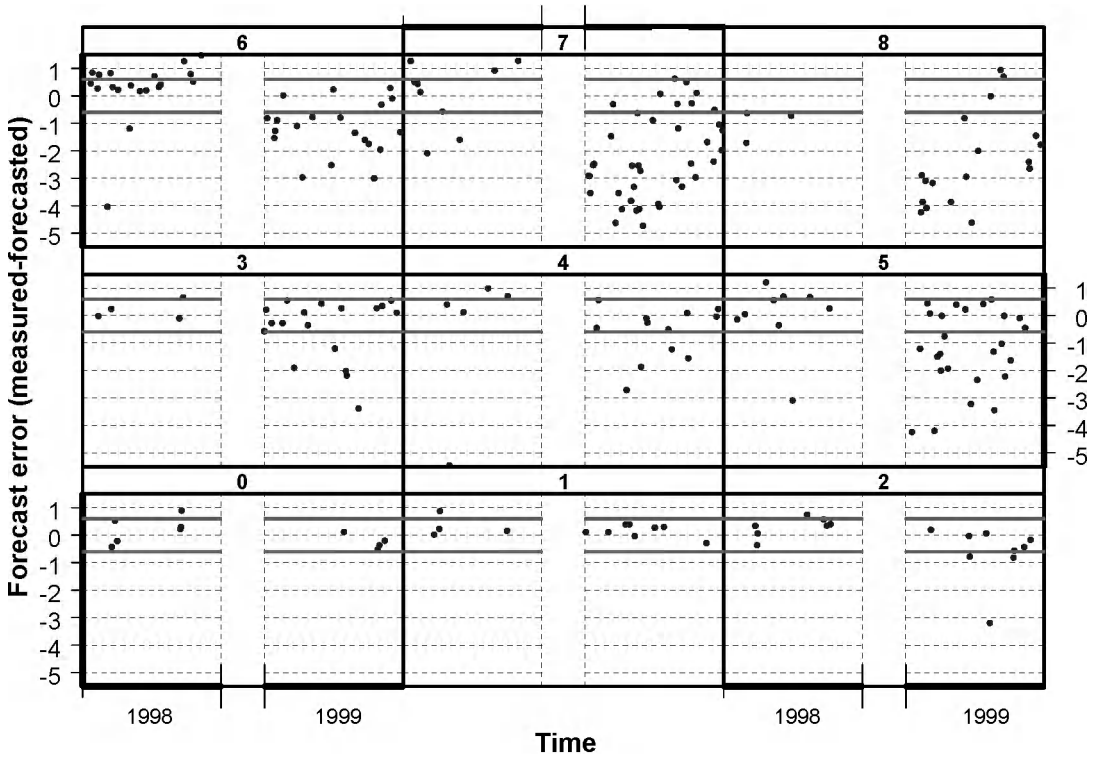

Figure 57: *Evaluation of the UV forecasts (expressed in units of UV Index) as a function of cloudiness (expressed in octas).*

4.2.6.2 Comparison of UV models and UV Index forecasts

Within the framework of the COST action 713 on UVB first a study was performed on the comparison of UV models. The results (Köpke et al, 1998), showed that all radiative transfer models agreed well when the same input parameters are used. Afterwards, a study was initiated to compare UV indices calculated with different models used for UV-Index forecasting and observations at different sites with different instruments. This required the exchange of data between a large number of different UV groups, mainly located in Europe. Finally 13 models were compared with measurements of 5 instruments at 4 locations at very different environments. As an example Figure 58 shows the differences between the measurements and the calculations with three different versions of the Tropospheric Ultraviolet and Visible model (TUV), one of which is in use at RMI. A manuscript on this subject is in press (De Backer et al., 2001). The intermediate results were presented at the EGS assembly in Den Haag (De Backer et al., 1999b). The results were also thoroughly discussed at the Management committee meeting of COST713, held in Antwerp in 1999, and organised by KMI-IRM. UV-Index measurements and forecasts, together with synoptic observations of the summer season of 1999, were transmitted to another COST713 member, for the study of the impact of clouds on the UV-Index.

Also the total ozone forecasts at Uccle were exchanged within the COST713 members. Preliminary results reported during one of the COST713 management committee meetings showed that the total ozone forecasts at Uccle are of good quality.

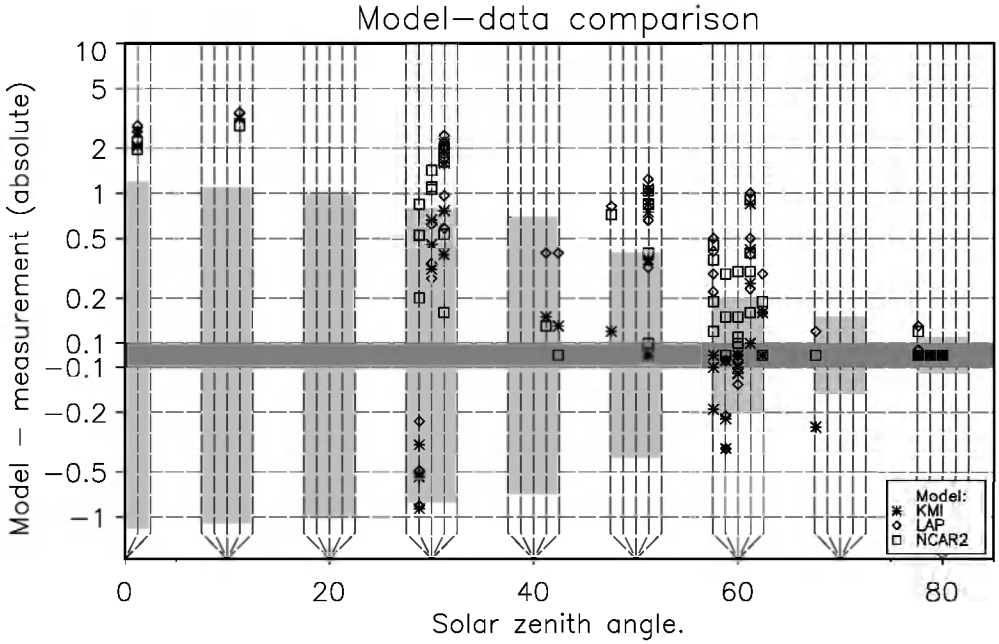

Figure 58: *Absolute differences in UVI units between model and measurement results as a function of solar zenith angle. The different symbols refer to different versions of the TUV model run at different institutes (KMI: Royal Meteorological Institute of Belgium, LAP: Laboratory of Atmospheric Physics of the University of Thessaloniki, NCAR2: National Centre of Atmospheric Research in Boulder). The results are shown for ten degree solar zenith angle intervals, each time from left to right for the stations Sodankylä, Uccle, Thessaloniki, Izaña (Spanish instrument) and Izaña (Finnish instrument). The light grey bars show the estimated uncertainty of the measurements.*

4.3 Atmospheric process studies

4.3.1 Tropospheric O_3 in Ukkel

The Riftoz (Regional Differences in Tropospheric Ozone) project aims at explaining the differences observed in the tropospheric ozone behavior in different European regions. Taking part in this project, the KMI-IRM had to carry out ozone soundings each day during June, July and August 1997 by means of ECC ozonesondes. This resulted in a very valuable time series of ozone soundings that will be used in creating a coherent and complete 3-D tropospheric ozone data set over Europe for the summer of 1997. Additional information such as general meteorological situation,

vertical air mass stability and horizontal extent to which the ozone soundings can be extrapolated, has also been provided.

Figure 59 shows time series of various relevant parameters during June to August 1997. In the time series of the integrated ozone amount in the troposphere we see a very high value on the 1st of June, which is due to a difference between the thermal tropopause (WMO definition) and the ozone tropopause. During the periods from 12 to 13 July and from 6 to 13 August (delimited by dashed lines in Figure 59) there is a clear signature of photochemical ozone production in the boundary layer (sunny weather, high temperatures, and high integrated ozone amounts in the boundary layer).

It is interesting that during the latter period the integrated ozone amount in the free troposphere also shows a cumulative effect, which points to an overflow of ozone from the boundary layer to the free troposphere during ozone episodes. On August 14 the ozone amount in the boundary layer and in the free troposphere dropped by about 60 and 40 percent respectively, due to a change of air mass from a continental to a marine one.

Several cases of stratospheric intrusions were found from the soundings, which could sometimes be followed during some days. A very pronounced intrusion was seen from 14 to 16 July, with signatures of stratospheric air to levels as low as the 700 hPa pressure level.

The first objective of the RIFTOZ (Regional differences in Tropospheric Ozone in Europe) project was to create a coherent hourly averaged tropospheric ozone field covering Europe, through a combination of observations, photochemical dispersion models and data assimilation. The database of daily ozone soundings from KMI-IRM was used to study the ozone budget of the planetary boundary layer (PBL) during ozone episodes. This ozone budget has the following components:

- accumulation in the PBL,
- transfer from the PBL to the free troposphere (FT),
- deposition at the surface,
- horizontal advection.

The ozone accumulation between day [i) and day [i+1) in the layer between z1 and z2 is calculated as follows:

$$A(i)_{z1,z2} = \int_{z1}^{z2} \rho(z, day[i+1])\,dz - \int_{z1}^{z2} \rho(z, day[i])\,dz \qquad (1)$$

where ρ is the ozone density

The terms contributing to the ozone budget in the PBL were calculated as follows:

Accumulation in the PBL: $A(i)_{ground,\ 2km}$ (2)

Transfer: $A(i)_{2km,4km}$ (3)

Deposition:

$$D(i) = \int_{t=noon}^{t=sunset} \rho_g(t, day[i]).q_{day}\ dt + \int_{t=sunset}^{t=midnight} \rho_g(t, day[i]).q_{night}\ dt + \int_{t=midnight}^{t=sunrise} \rho_g(t, day[i+1]).q_{night}\ dt + \int_{t=sunrise}^{t=noon} \rho_g(t, day[i+1]).q_{day}\ dt \quad (4)$$

where ρ_g is the ozone density at the surface;
q is the surface ozone deposition velocity;
z is the altitude.

The top of the PBL of each individual sounding during ozone episodes was determined as the level where the ozone concentration and specific humidity show a sharp decrease with altitude and where the potential temperature steeply increases. In this way a mean PBL height of about 2 km was found.

The mean day-to-day ozone accumulation during ozone episodes with stable air masses above Ukkel was calculated in different layers. In the layers 0 to 2 km, 2 to 3 km, 3 to 4 km and 4 to 5 km, the mean accumulation (in mg m^{-2} day^{-1}) was 45, 10, 5 and –2 respectively. It appears that the accumulation is limited to the lowest 4 km of the troposphere. Therefore, we only take into account the lowest 2 km of the FT for calculation of the transfer of ozone from the PBL to the FT.

The deposition at the ground is calculated assuming a deposition velocity of 1.4 cm s^{-1} at daytime and 0.64 cm s^{-1} at night (De Muer et al., 1997). Hourly mean values of ozone concentration near the ground were kindly provided by the Belgian Interregional Cell for the Environment (IRCEL).

We studied the meteorological synoptic situation and retained only the ozone episodes during which our station was in the same type of air mass. In these cases, the assumption of no horizontal advection is adequate. So the ozone production in the PBL is essentially the sum of the ozone amount deposited at the ground, accumulated in the PBL and transferred to the FT:

$$P(i) = A(i)_{ground,2km} + D(i) + A(i)_{2km,4km} \quad (5)$$

From these calculations the following mean values of the ozone budget during ozone episodes were obtained:

- ozone production in the convective mixed layer: 111 mg m^{-2} day^{-1};
- ozone deposition at the surface: 51 mg m^{-2} day^{-1} (46%);
- accumulation of ozone in the boundary layer: 45 mg m^{-2} day^{-1} (40%);
- overflow of ozone to the free troposphere: 15 mg m^{-2} day^{-1} (14%).

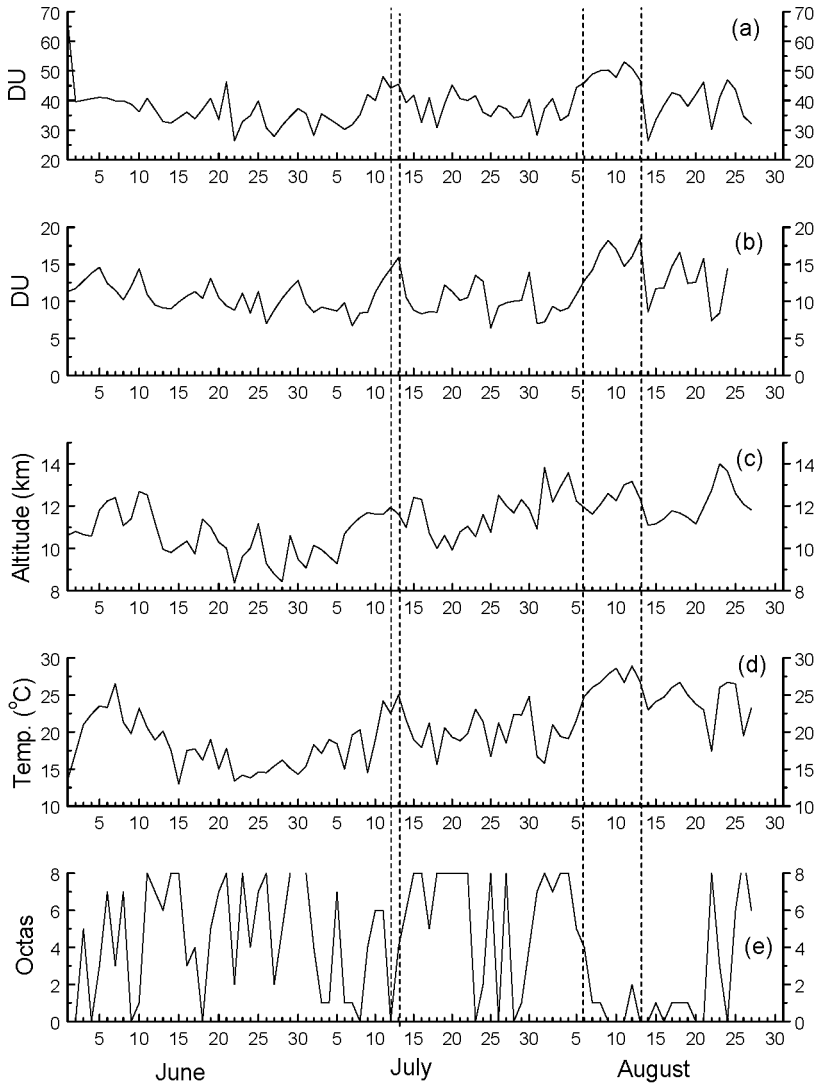

Figure 59: *Day-to-day variation during the period June to August 1997, of the following parameters: integrated ozone amount (expressed in Dobson units (DU)) in (a) the troposphere and in (b) the boundary layer, (c) altitude of the tropopause, (d) surface temperature and (e) cloud cover. integrated ozone amounts in the boundary layer).*

4.3.2 Urban pollution in Brussels

4.3.2.1 Methodology

A 4-months measurement campaign was held at the ULB Campus during 1997. Spectra were obtained with the BRUKER IFS120M Fourier Transform spectrometer in the UV-visible region. Concentrations of O_3, NO_2, SO_2, benzene, toluene, H_2CO, and HONO were routinely measured. Night-time measurements of NO_3 were also performed. O_3 and NO_2 concentrations were also monitored by the Institut Bruxellois pour la Gestion de l'Environnement (IBGE) at the IASB-BIRA location.

The influence of several meteorological parameters on the evolution of the O_3 concentration was investigated. The meteorological parameters were measured by KMI-IRM and by the IBGE. They comprised the wind speed and direction, the irradiance, the temperature, the nebulosity, the thermal inversion height, and the relative humidity. Parameters that were found to be highly correlated with the O_3 values were the wind speed (WS) and direction (WD), the temperature (T), the relative humidity (H), and the irradiance (Ir).

Based on these results two regression models of the O_3 concentration in the city of Brussels have been developed using atmospheric and meteorological measurements: The first one considers only meteorological parameters to explain the O_3 concentrations; the second one makes also use of the NO and NO_2 concentrations. The models are based on the ordinary least square method (OLS). The concentration of ozone $C(O_3)$ is expressed as a function of k chosen explanatory variables X_i (i=1..k), using an exponential relation:

$$C(O_3) = e^{B_0} X_1^{B_1} \cdots X_k^{B_k} \qquad (1)$$

where B_i are the partial regression coefficients which need to be determined. Using natural logarithms, expression (1) can also be written for the j^{th} values of the variables, as:

$$\mathrm{Ln}\left(C(O_3)\right)_j = B_0 + \sum_{i=1}^{k} B_i \mathrm{Ln}\left(X_{ij}\right) + u_j \qquad (2)$$

where u_j are the residuals. Such an exponential relation is believed to be adequate since many of the meteorological parameters have multiplicative effects on the analysed concentration. In the case of the temperature, the adopted form (Table IV) was chosen based on the analysis of several types of relations between O_3 and the

temperature (linear, polynomial, or logarithmic). The function ln([O_3))÷1/T was found to give the best correlation coefficient. The use of the NO and NO_2 concentrations supposes that these values are known in advance. Estimate values, determined either by regression analysis or by photochemical models can be used. In our study we used measured concentrations of the two constituents: NO measured by the IBGE and NO_2 measured with our instrument. The models are summarised in Table IV.

Table IV: *Definition of the regression models.*

Model	Ln($C(O_3)$) =
M1	B_0 + B_1*1400/T + B_2*Ln(WS) + B_3*Ln(WD) + B_4*Ln(H) + B_5*Ln(Ir)
M2	B_0 + B_1*1400/T + B_2*Ln(WS) + B_3*Ln(WD) + B_4*Ln(H) + B_5*Ln(Ir) + B_6*Ln([NO_2)) + B_7*Ln([NO))

The Durbin-Watson test (Draper and Smith, 1980) has been applied to identify the independent variables, which predominate in the model in order to eliminate the ones that are not significant. Moreover a thorough residuals analysis is required to certify the quality of the estimates of the coefficients. Residuals might indeed be highly auto-correlated, in violation with the hypothesis concerning the residual independence (Draper and Smith, 1980). In the case of the presence of a Lag1 correlation, a new model (M1AC) was defined:

$$\mathrm{Ln}\left(C_j\right) = \beta_0 + \sum_{i=1}^{k} \beta_i \mathrm{Ln}\left(X_{ij}\right) + \beta_{k+1} \mathrm{Lag1}_j + e_j \qquad \text{with} \quad j=1..N \qquad (3)$$

where C_j represents the j^{th} value of the independent variable, X_{ij} the j^{th} value of the i^{th} dependent one, and e_j are the residuals (normal distribution with 0 mean value and Σ^2 variance). $Lag1_j$ is a new variable that determines the auto-correlation of the first order of the residuals. It is defined by the following expression:

$$\mathrm{Lag1}_j = \mathrm{Ln}\left(C_{j-1}\right) - B_0 - \sum_{i=1}^{k} B_i \mathrm{Ln}\left(X_{ij-1}\right) \qquad (4)$$

With this formulation, the analytical form of the model M1AC can be rewritten as:

$$\begin{aligned}\mathrm{Ln}[O_3]_j = \; & \beta_0 + \beta_1\left(\frac{1400}{T}\right)_j + \beta_2 \mathrm{Ln}(WD)_j + \beta_3 \mathrm{Ln}(H)_j + \beta_4 \mathrm{Ln}(Ir)_j \\ & + \beta_5\left[\mathrm{Ln}(O_3)_{j-1} - B_0 - B_1\left(\frac{1400}{T}\right)_{j-1} - B_2 \mathrm{Ln}(WD)_{j-1} - B_3 \mathrm{Ln}(H)_{j-1} - B_4 \mathrm{Ln}(Ir)_{j-1}\right] \\ & + e_j \end{aligned} \qquad (5)$$

A similar expression is obtained for the M2AC model, based on the M2 definition.

4.3.2.2 Discussion of the results

ULB97 campaign

The analysis provided almost continuous time series for the three molecules O_3, SO_2, and NO_2. They have been compared to the measurements made by the IBGE during the same period, showing a very good agreement between the two sets of data, as can be seen in Figure 60.

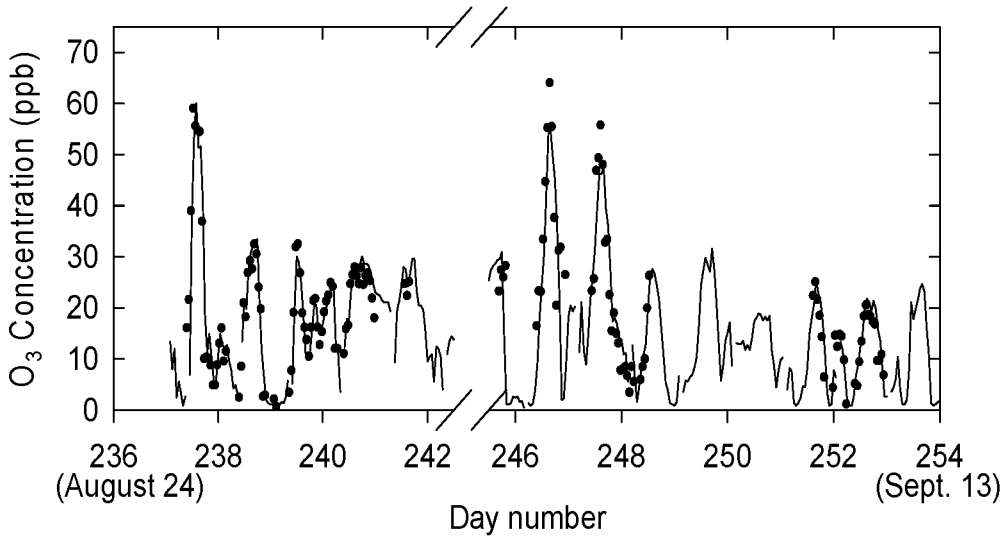

Figure 60: *Comparison of the O_3 concentrations of this work and those of IBGE.*

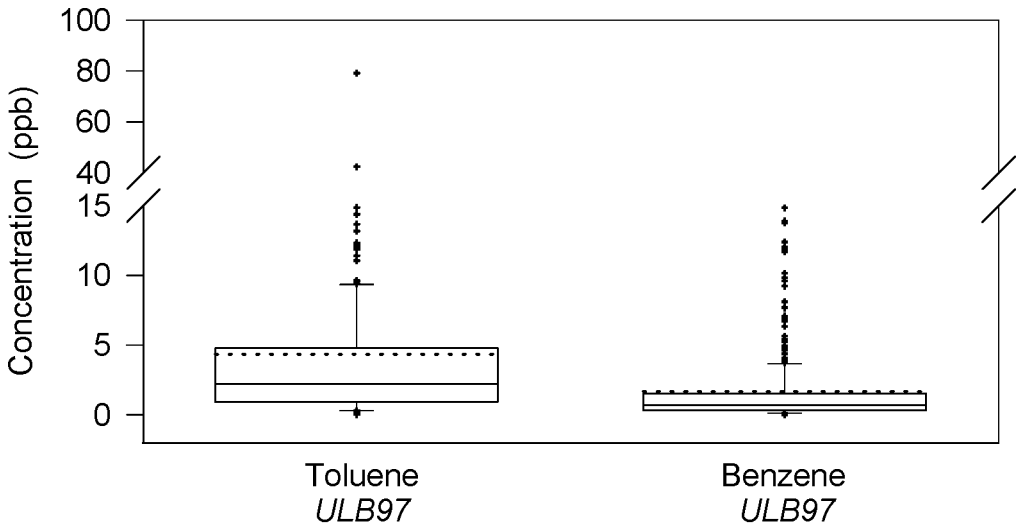

Figure 61: *Distribution of the concentrations of toluene and benzene during the campaign (see text for the description of the symbols).*

Benzene and toluene concentrations up to respectively 19.0 and 80.0 ppb were observed. The mean values are indicated by the broken lines in Figure 61, which gives also some other statistical quantities describing the toluene and benzene fluctuations during the campaign: the median value (plane line), the 25 and 75 percentiles (box limits), and the 10 and 90 percentiles (low and high external lines). The diurnal variation of the toluene concentration reflects the combined effects of the emissions, the transport, the dilution, and the chemical removal. The analysis of the diurnal evolution shows the presence of two peaks centred respectively around 8 am and 6 pm. They correspond to rush hours of the car traffic. This is not surprising as toluene is mainly emitted by car traffic. The first peak is higher than the second one, due to the higher photochemical activity of the atmosphere during the afternoon.

The comparison between the toluene and benzene concentrations shows in general no clear correlation between these two constituents. The toluene concentrations are however always higher than those of benzene by a factor varying between 1.5 and 4. This is not surprising as the toluene content is higher by a factor 3 to 4 in the gasoline and the exhaust gases.

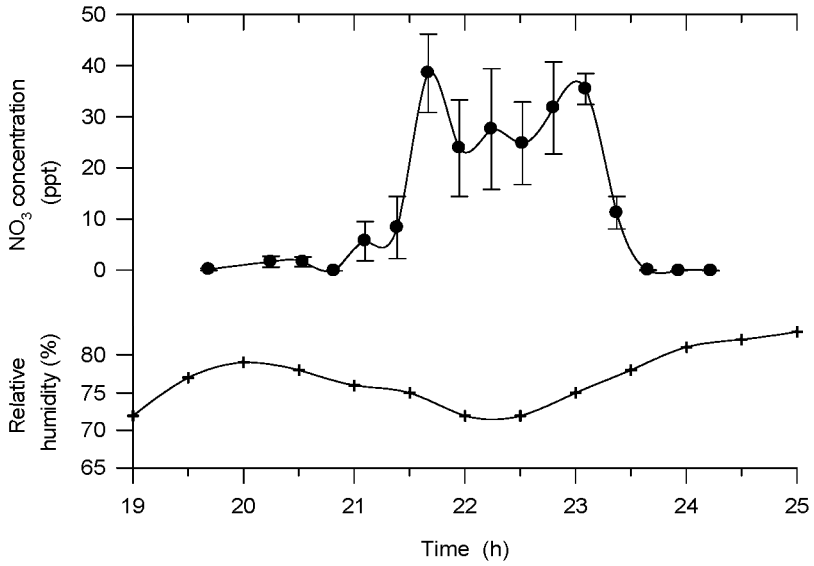

Figure 62: *NO_3 concentration during the night from the 3rd to the 4th of September 1997.*

NO_3 measurements have been performed during the *ULB97* campaign. Concentrations were detected during three nights (3/4, 8/9, and 11/12 September). Figure 62 shows the variation of the NO_3 concentrations during the night from the 3rd to the 4th of September 1997; the evolution of the relative humidity is also shown. The interpretation of these measurements is still under progress.

Models results

The models have been applied to the measurements performed during three measurement campaigns, which were organised by the Laboratoire de Chimie Physique Moléculaire (LCPM) of the ULB and BIRA-IASB. These campaigns have been denoted *ULB95* (May, June and July 1995), *IASB96* (December 6, 1996 – February 2, 1997), and *ULB97* (August - November 1997).

Figure 63 shows the comparison between the measured O_3 values and the predicted ones. The results of the three models M1, M1AC, and M2AC are plotted. The prediction coefficient of the M1AC model is 0.735 for the period from 1st to 18th July, and 0.86 for the 4th to 9th July. The regression coefficient of the M2AC model is 0.938, which is an improvement compared to the M2 value (R=0.85). The prediction coefficient for the 1st to the 18th of July is 0.836, which is quite better than what the M1AC model provided.

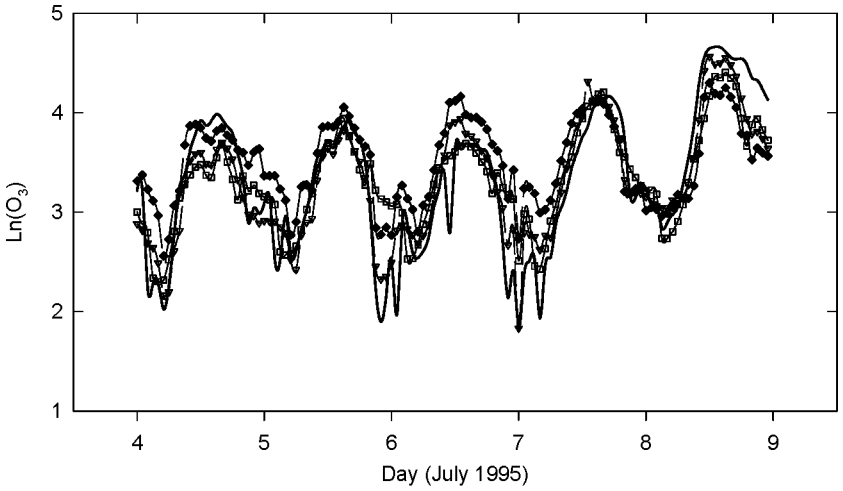

Figure 63: *Comparison of the predicted O_3 concentrations with the IBGE measured ones (—). The predictions of the three models M1 (□), M1AC (♦), and M2AC (▽) are indicated.*

Conclusions

Measurements of several tropospheric species, such as O_3, NO_2, SO_2, benzene, toluene, H_2CO, and HONO, have been performed using a Fourier transform spectrometer operated in the UV-visible region. The feasibility of night-time NO_3 measurements has been demonstrated.

Considering the analysis of the influence of some meteorological parameters, regression models of the O_3 concentration have been developed for the urban area of Brussels. Different meteorological parameters such as the temperature, the wind speed and direction, the relative humidity, and the irradiance have been considered. The models have been tested using the data of three distinct measurement campaigns with different meteorological conditions and with different O_3 levels. They have shown that good estimations of the O_3 concentrations can be performed using only the meteorological parameters ($R_{prediction}$ ~ 0.7), and have pointed out that the use of estimates of the NO and NO_2 concentrations improve the results ($R_{prediction}$ ~ 0.8).

This work contributed to tropospheric process studies by ground-based measurements of several gaseous species, and was part of the PhD thesis of A. Tsouli, presented on the 22 September 2000 (Tsouli, 2000).

4.3.3 Planetary boundary layer investigations in the Jungfraujoch area

To test the method of altitude-differential column measurements presented in section 3.4, a measurement campaign has been organized during the months of May and June 1998 in the Jungfraujoch area. After an initial period of instrument intercomparison at ISSJ, the mobile instrument (Bruker 120M) was moved down in the valley and installed for one month in Grindelwald.

When operated side by side at the Jungfraujoch, measurements made by both instruments showed a very good agreement (maximum bias of 1.5%). Analysis of spectra recorded synchronously at the Jungfraujoch (Bruker 120 HR) and at Grindelwald (mobile Bruker 120 M) gave average boundary layer concentrations for a selected set of tropospheric molecules, i.e., methane, nitrous oxide, carbon monoxide and ethane. We made the assumption of constant volume mixing ratio in the layer between 1070 m and 3580 m asl. Results are shown in Table V. The concentrations presented are the average of all daily means available through the month of June and RSD is the relative standard deviation between all the daily means. With relative standard deviation of less than 3% CH_4 and N_2O are quite constant in the tropospheric boundary layer (TBL) during the month of June while CO and C_2H_6 with RSD of 13 and 18%, respectively, exhibit a strong day to day variability.

Table V: *Average tropospheric boundary layer VMR for CH_4, N_2O, CO and C_2H_6 at Grindelwald (Jungfraujoch area) for the month of June 1998. RSD represents the 1σ standard deviation over all days with observations.*

Molecule	VMR (ppmv)	RSD %
CH_4	1.647	2.03
N_2O	0.298	2.6
CO	0.124	13
C_2H_6	0.001196	18.3

Comparison with other results and with carbon monoxide in-situ measurements made at ISSJ showed a good agreement. In particular, CO is difficult to compare to other data due to its high spatial and temporal variability. The observed CO variations have been compared with in-situ measurements of CO made by EMPA at ISSJ. Hourly means of the FTIR results have been compared with four hour means of the EMPA results: they are shown in Figure 64. A good agreement is observed.

More details about the retrieval technique and results are found in Barret et al. (1999).

It has been verified (for C_2H_6) that the results obtained with the altitude-differential measurements technique agree with the results obtained with SFIT2, the vertical inversion algorithm (taking into account the assumptions made and the limits of uncertainty of both methods).

The results prove that the technique is valuable for making measurements in the free troposphere and tropospheric boundary layer. The probed vertical layer is set by the choice of the (altitudes of) the observation sites, so one can obtain a higher vertical resolution than the one achieved with vertical inversion algorithms like SFIT2 and SFSP2. But the experimental requirements are very stringent, making the technique suitable almost only for campaign measurements, e.g., for satellite validation. Long-term data in the troposphere should be derived better from vertical inversion techniques.

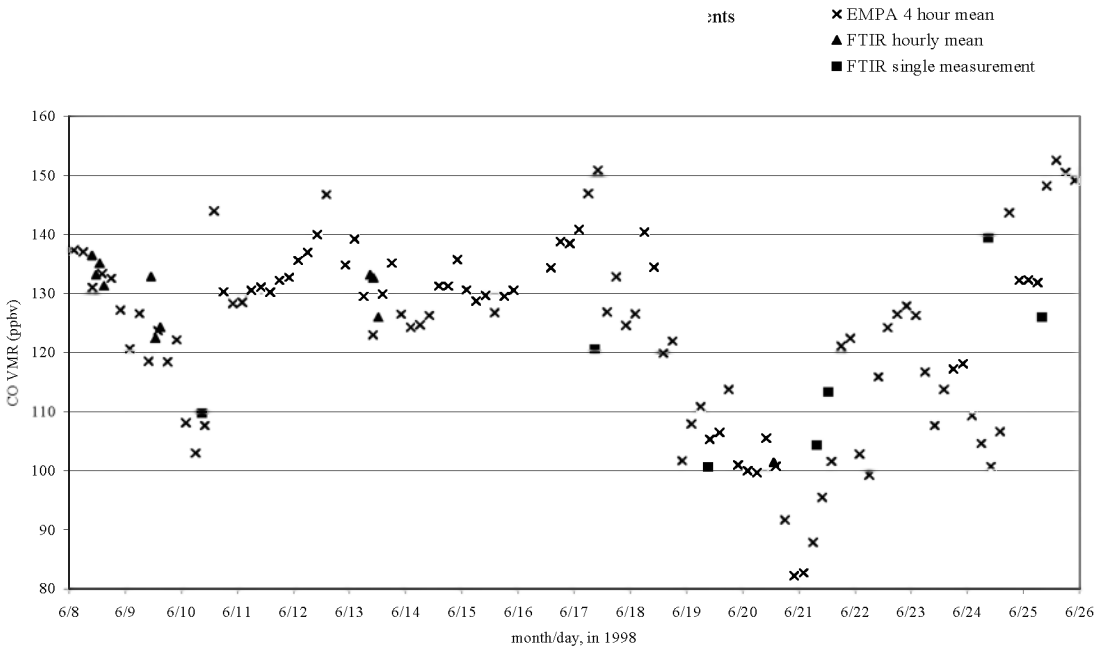

Figure 64: *Comparison between CO VMR values from differential FTIR and in situ measurements at the Jungfraujoch, during the June 1998 campaign. See the legend for the different symbols.*

4.4 Laboratory measurements of spectroscopic parameters of atmospheric relevance

The main objective of this work was to obtain high quality spectroscopic data - essentially absorption cross-sections and line positions and intensities- for atmospherically important molecules in order to improve the existing databases, to lower uncertainties and to resolve discrepancies between data sets. The molecules studied during this work were: O_2 and its collision complex O_2-X (where X can be O_2 itself, N_2 or Ar), NO_2 and its dimer N_2O_4, H_2O and their isotopomers HOD and D_2O, C_2H_2, OCS, HOCl and CFC replacements (HCFC-22 and HFC-152a). They were measured under different conditions of temperature and pressure in the infrared (IR), near infrared (NIR), visible (VIS) and ultraviolet (UV) ranges using Fourier transform spectroscopy. It should be noted that the laboratory work on thirteen CFC's, HCFC's and HFC's performed during the previous Global Change and EUROTRAC programs (1990-1996), has led to new values of the Global Warming Potential (GWP) for these compounds (Clerbaux et al., 1993; Clerbaux and Colin, 1994). Part of this work was published during the period of the present contract (Barry et al., 1997), and these data were incorporated in the GEISA spectroscopic database (Jacquinet-Husson et al., 1999).

4.4.1 Experimental conditions

The species that we have studied in the frame of the ESAC 1996-2000 project are listed in Table VI. Their absorption spectra were recorded using two commercial high-resolution Fourier transform spectrometers (FTS): a portable Bruker IFS120M, having a programmable resolution up to 0.008 cm^{-1} and operating from the IR to the UV and a Bruker IFS120HR, having a programmable resolution up to 0.0018 cm^{-1} and operating from the far infrared (FIR) to the UV. Both instruments are equipped with a variety of absorption sources, beamsplitters, optical filters and detectors, to cover the above-mentioned spectral ranges.

Table VI: *Measurements performed during the 1996-2000 ESAC project.*

	Place Date	Molecules	Resolution (cm^{-1})	Spectral Range	T (K)	P_{tot} (torr)	Ref.
1	Reims 09/95	O_2, O_2+N_2	16, 0.12	10000-42000	290	≤ 760	(a) (c)
2	Reims	NO_2	2	10000-42000	290, 220	0.01-2	(b)
	05-06/96	O_2+N_2	2	25000-42000	290	≤ 760	(a) (c)
3	Reims 04-06/97	O_2,O_2+X#	2, 0.12	25000-42000	290	≤ 760	(a) (c)
		O_2, O_2+N_2	0.02-0.2	7000-18000	290, 220	≤ 760	(c) (d)
4	Reims 03-05/98	H_2O, H_2O+N_2, H_2O+D_2O	0.03, 0.06	10000-26000	290	≤ 760	(e)
5	Reims 11-12/98	NO_2, NO_2+air	0.05-0.1	10000-25000	290, 220, 240	≤ 760	(b)
6	Reims 05-06/99	H_2O, H_2O+HDO	0.03, 0.06	10000-26000	290, 273, 261	≤ 15	(e)
7	ULB	OCS	0.005-0.015	4800 – 8000	294	2 – 76	(f)
8	ULB	C_2H_2	0.003	550 – 1970	296	2 – 8	(g)
9	ULB	HCFC-22 HFC-152a	0.03	600 – 1700	203 – 293	1 – 600	(h)
10	ULB	HOCl	0.007	550 – 1970	295	22	(i)

X= N_2 or Ar. (a) (Bernath et al., 1998) (b) (Vandaele et al., 1998) (c) (Jenouvrier et al., 1999; Fally et al., 2000; Mérienne et al., 2000) (d) (Hermans et al., 1999) (e) (Carleer et al., 1999; Zobov et al., 2000) (f) (Rbaihi et al., 1998); (g) (Vander Auwera, 2000a); (h) (Vander Auwera, 2000b; Ballard et al., 2000); (i) (Vander Auwera et al., 2000).

The measurements performed with the first instrument were carried out at the Université de Reims Champagne-Ardennes (France), in collaboration with the Laboratoire de Spectrométrie Moléculaire et Atmosphérique (GSMA). They involved the coupling of the portable IFS120M with two long path absorption cells, developed by the GSMA. The first one is 50 m long and can cover optical lengths up to 2 km. The second cell, which is 5 m long and can reach paths up to 300 m, is temperature controlled. Experiments no. 1 to 6 in Table VI were carried out in Reims using this

set-up. Experiments no. 7 to 10 were carried out at ULB, using the IFS120HR. This instrument is equipped with two commercial multiple-reflections absorption cells, providing total absorption paths ranging from 60 cm to about 50 m. Home-made thermostatic absorption cells are also available, with nominal path lengths ranging from 1.5 to 25 cm and designed to operate at any temperature between 200 and 300 K. Table VI provides a brief description of the experiments performed for the various target species. Further details can be found in the references mentioned. The treatment of the spectra was performed using a number of programs, most of them home-made and running on personal computers, in particular Wspectra and bFit – see section 3.6.

4.4.2 Results

4.4.2.1 Line parameters and absorption cross-sections in the UV-VIS-NIR

Compared to previous studies, our aim was to work under lower pressures and lower temperatures (when possible) in order to simulate more "atmospheric-like conditions". Another objective was to obtain data at higher resolution, i.e. sufficient for the spectra to be fully resolved.

NO_2

NO_2 plays an important role in the photochemistry of the Earth's atmosphere. It acts as the main ozone source and as a nitric acid precursor in the troposphere. In the stratosphere, it is well known that NO_2 is closely linked to the ozone cycle as well as to the ClO cycle and plays a major role in the coupling of the NO_x and ClO_x families. Atmospheric NO_2 concentrations and their variations, partially due to man-made gaseous emissions, need to be known accurately to help in political decisions concerning the preservation of the stratospheric ozone layer.

The DOAS (Differential Optical Absorption Spectroscopy) technique, widely used for the determination of the NO_2 atmospheric concentrations, often led to inconsistent results (Camy-Peyret et al., 1996). It was first suspected that residual structures appearing in atmospheric spectra after the removal of the NO_2 signature could be due to the temperature dependence of the NO_2 absorption cross-section. Later, discrepancies of the order of 10-20% were found between laboratory absorption cross-sections measured at room temperature (Mérienne et al., 1995; Vandaele et al., 1996). It was therefore urgent to produce accurate absorption cross-sections at (low) temperatures representative of the stratosphere, and to resolve the discrepancies between literature data. The precise knowledge of the temperature

dependence allows moreover the simulation of a spectrum at any temperature, which can be very useful in the determination of the vertical distributions of the concentrations.

Laboratory measurements of NO_2 are very difficult because:

- absorption cross-sections are temperature dependent;
- the NO_2 photodissociation imposes a short time for recording spectra;
- an absorption/desorption phenomena of NO_2 on the cells walls is present;
- the dimer N_2O_4 is present through the reaction $2NO_2 \leftrightarrow N_2O_4$. The equilibrium constant of this reaction is not well defined, particularly at low temperature, and in addition N_2O_4 absorbs light in a region where NO_2 has to be measured (>25000 cm^{-1}).

The first laboratory campaign allowed the determination of NO_2 absorption cross-sections at medium resolution (2 cm^{-1}) in the UV to NIR region (42000-10000 cm^{-1}) and at 2 temperatures (290 and 220 K).

Figure 65 shows as an example the absorption cross-section obtained at 294 K. The temperature effect is confirmed. Its impact on the stratospheric NO_2 calculation was assessed, and the absolute necessity to use cross-sections measured at a temperature as close as possible to that prevailing in the atmospheric layer investigated was emphasized. For the first time, a significant pressure effect was observed in the visible region of the spectrum at both temperatures (Vandaele et al., 1998).

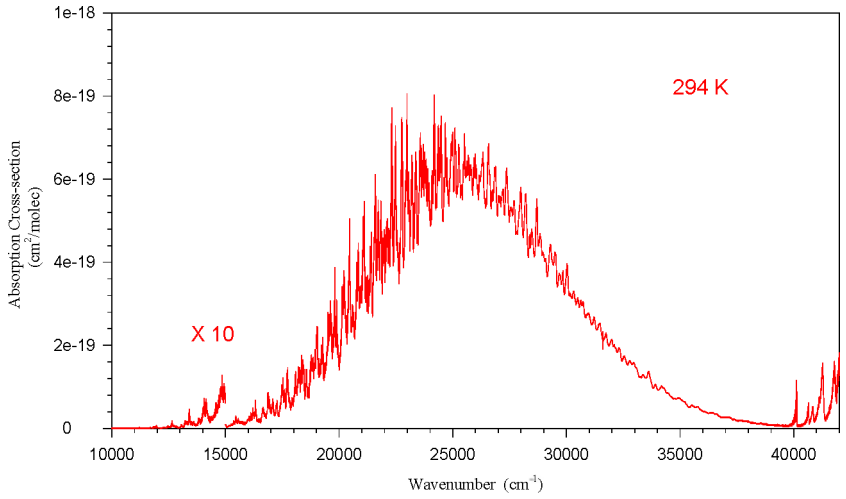

Figure 65: *NO_2 absorption cross-section at 294 K and at a resolution of 2 cm^{-1}.*

During the second laboratory campaign, the pressure effect was investigated through measurements at various pressures (pure NO_2 and NO_2 mixtures with different dilutions) and at 3 different temperatures in the visible to NIR region (25000-10000 cm^{-1}). This campaign has allowed the determination of new absorption cross-sections at higher resolution (0.1 cm^{-1} in the visible and 0.05 cm^{-1} in the NIR instead of 2 cm^{-1}) at 3 temperatures (220, 240, and 290 K). The necessity to work at higher resolution was demonstrated by the fact that the spectra recorded at a resolution of 2 cm^{-1} still showed unresolved absorption features. A linear regression expression was used to quantify the temperature dependence. This expression:δ_{NO2} = :δ_0 + a.T is able to reproduce cross-sections at any temperature with an accuracy better or equal to 10% (Figure 66). The pressure effect has also been investigated by analysing the spectra recorded at different total pressures and at 294 K (Figure 67). The method, which consists of broadening the pure NO_2 spectra with a gaussian function whose width is linearly dependent on the total pressure, is quite satisfactory at room temperature. However, at lower temperature the assumption of a constant width for the gaussian function is not adequate and a more sophisticated model should be developed in the future.

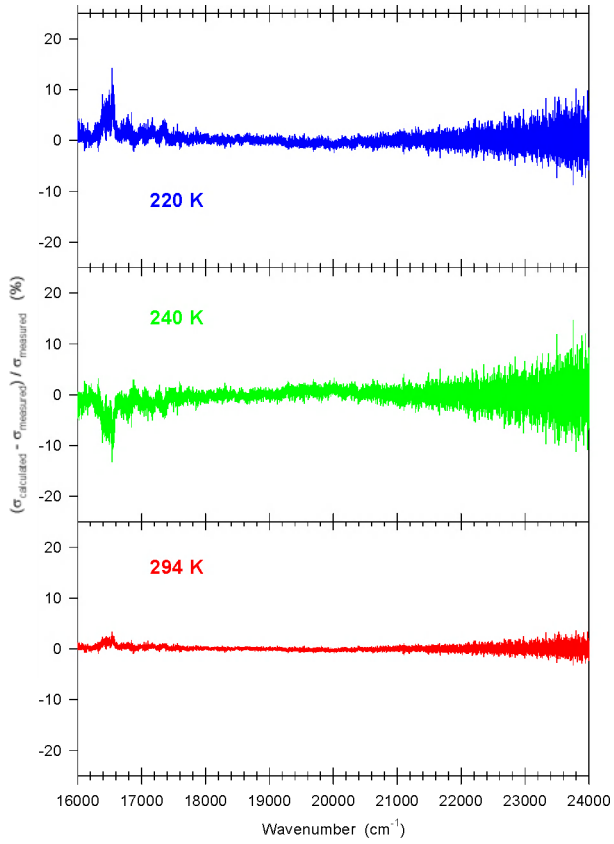

Figure 66: *Temperature effect: Comparison between observed and calculated cross sections using the linear regression parameters.*

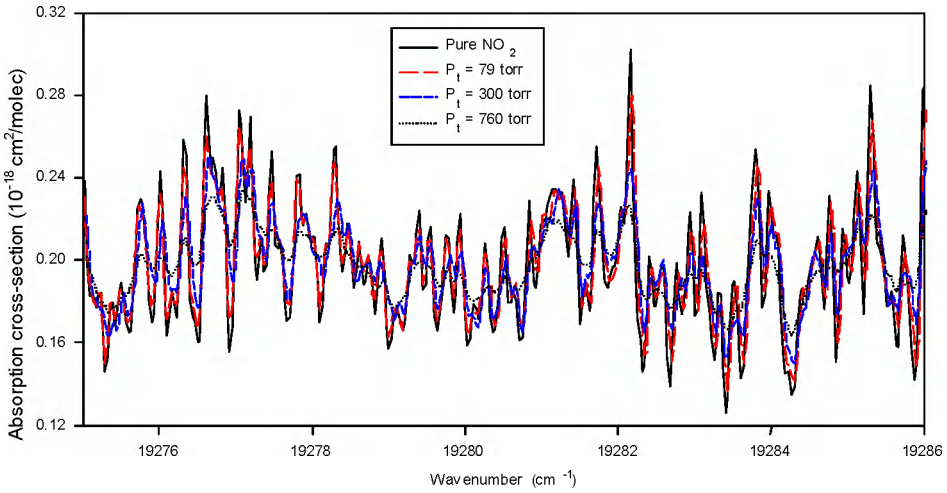

Figure 67: *Pressure effect on a small portion of the NO_2 absorption cross-section obtained at 294 K.*

O_2

In the UV region, the strong ozone Hartley band, which is used to retrieve tropospheric ozone concentrations, overlaps with oxygen bands. Improvements in the spectroscopic analysis of the discrete forbidden Herzberg band systems of oxygen are therefore essential for atmospheric applications. Moreover, the O_2-O_2 diffuse bands, which overlap the discrete forbidden Herzberg bands in this region show similar absorption structures as ozone, as shown in Figure 68.

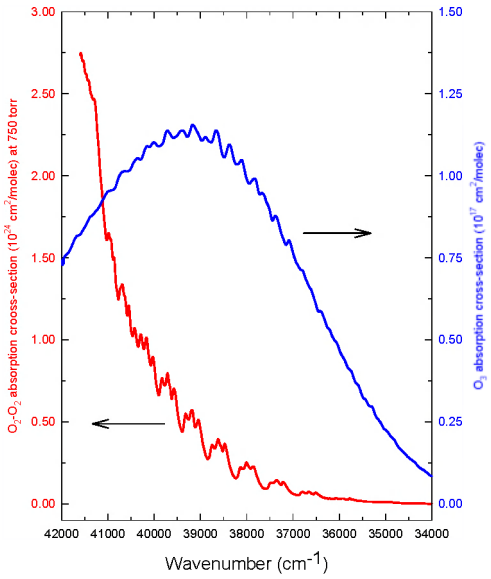

Figure 68: *Overlapping between the ozone Hartley band and the O_2-O_2 absorption bands (=Wulf bands).*

In the visible and NIR regions, the discrete and the diffuse bands of oxygen contribute to the solar absorption and therefore play an important role in the Earth's radiative budget. Up to now, the diffuse bands are not mentioned in the widely used HITRAN and GEISA databases (Rothman et al., 1996; Jaquinet-Husson et al., 1999). The absorption bands of O_2 in this region can also be used to derive various atmospheric properties such as cloud height and coverage parameters, owing to the constant mixing ratio of oxygen in the middle and lower atmosphere. For all these reasons, a complete reinvestigation of the oxygen spectrum from the UV to the NIR (42000-7500 cm^{-1}) was undertaken.

In the UV, a complete spectroscopic high-resolution reinvestigation of the Herzberg I, II and III band systems was carried out (Figure 69). The important parameters deduced from these laboratory measurements are: the line positions, the line intensities, the integrated cross-section values, the band oscillator strengths and the effective transitions moments. The spectroscopic knowledge of the three Herzberg systems was greatly improved: Rotational assignments were extended, molecular constants were improved significantly, interaction between states were better described, and local perturbations near the dissociation limit were reinterpreted. All these parameters constitute an accurate and extensive dataset. Two papers on this subject are published (Jenouvrier et al., 1999; Mérienne et al., 2000), and a complementary note is submitted (Mérienne et al., b). A complete linelist is available on the IASB website (http://www.oma.be/BIRA-ASB/Scientific/Topics/Lower/LaboBase/laboratory. html).

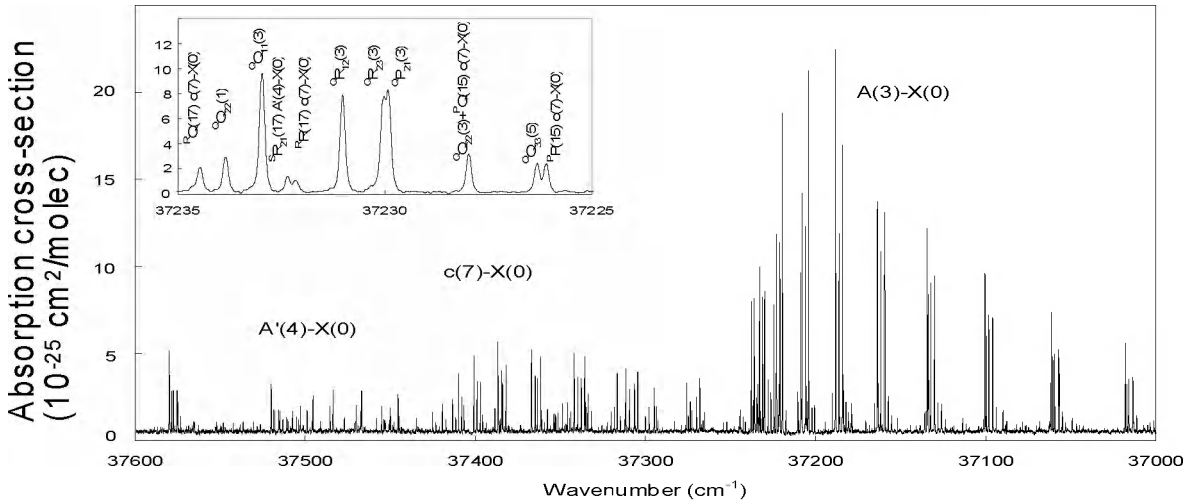

Figure 69: *Portion of a high-resolution O_2 spectrum showing the quality of the data and some rotational assignments.*

In the UV, the medium resolution study of the non-structured absorption, namely the O_2 Herzberg continuum, and the O_2-X collision-induced bands (or Wulf bands) was also completed.

The experimental spectrum (Figure 70a) is composed of the Herzberg I, II, and III systems, the Herzberg continuum, and the broad O_2-O_2 Wulf bands. The Herzberg lines are eliminated by subtracting from an experimental spectrum (Figure 70a) a simulated spectrum at the same pressure and resolution (Figure 70b). The result of the subtraction is shown in Figure 70c, where the three absorption cross-sections are calculated from spectra recorded at several pressures. The separation between the Wulf bands –which are pressure dependent- and the Herzberg continuum –which is pressure independent- is achieved by linear regression. Figure 70a and b show the separated components with their error bars.

The Herzberg continuum absorption cross-section and the collision-induced absorption cross-section have thus been determined, and the Wulf bands characteristics (rotational analysis, pressure effect, foreign gas effect) have been investigated in details. These results are published (Bernath et al., 1998; Fally et al., 2000) and the absorption cross-sections are accessible on the BIRA-IASB website. The originality of these results lies in the removal of the Herzberg bands prior to the determination of the intensity of the Wulf bands.

This enables us to measure the Wulf bands at atmospheric pressures, as opposed to previous studies, which were generally conducted at pressures sufficiently high that the contribution of the Herzberg bands could be neglected.

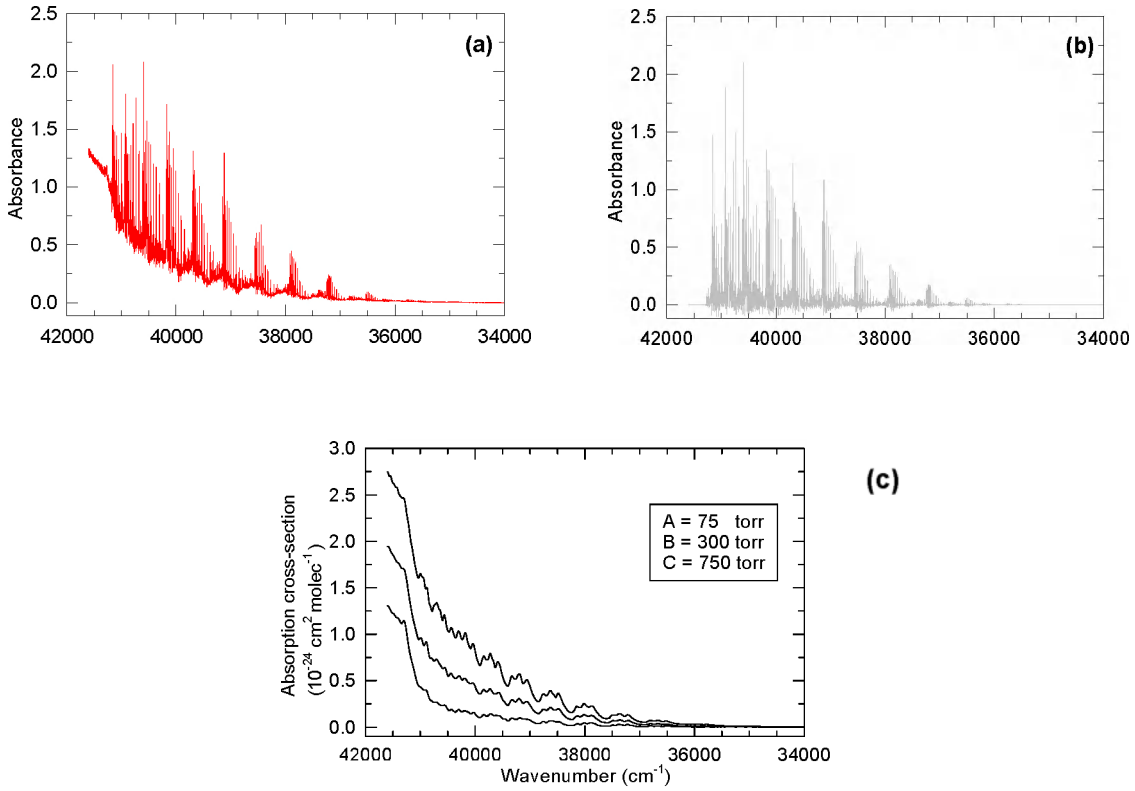

Figure 70: ***(a)*** *Experimental spectrum of pure O_2 at 450 torr.* ***(b)*** *Simulated spectrum at the same pressure and resolution.* ***(c)*** *Absorption cross-sections resulting from the subtraction (a)-(b) at 3 pressures*

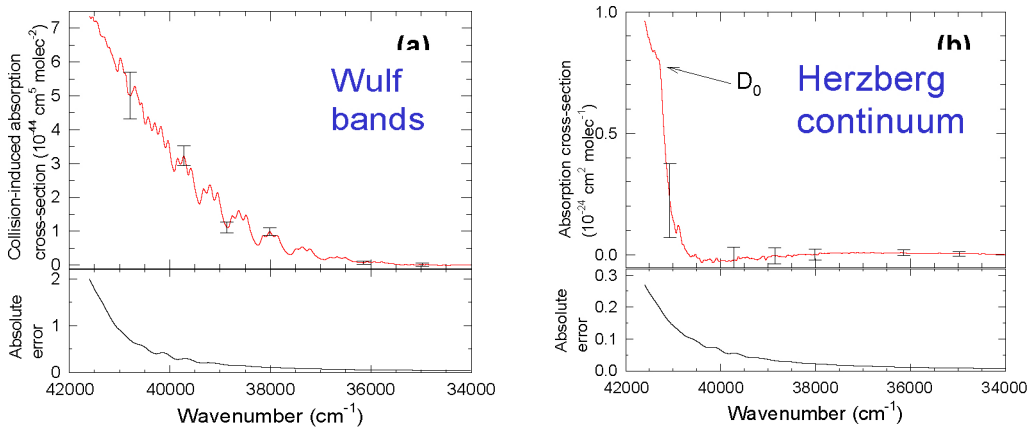

Figure 71: ***(a)*** *O_2-O_2 Collision-induced absorption cross-section.* ***(b)*** *Herzberg continuum absorption cross-section.*

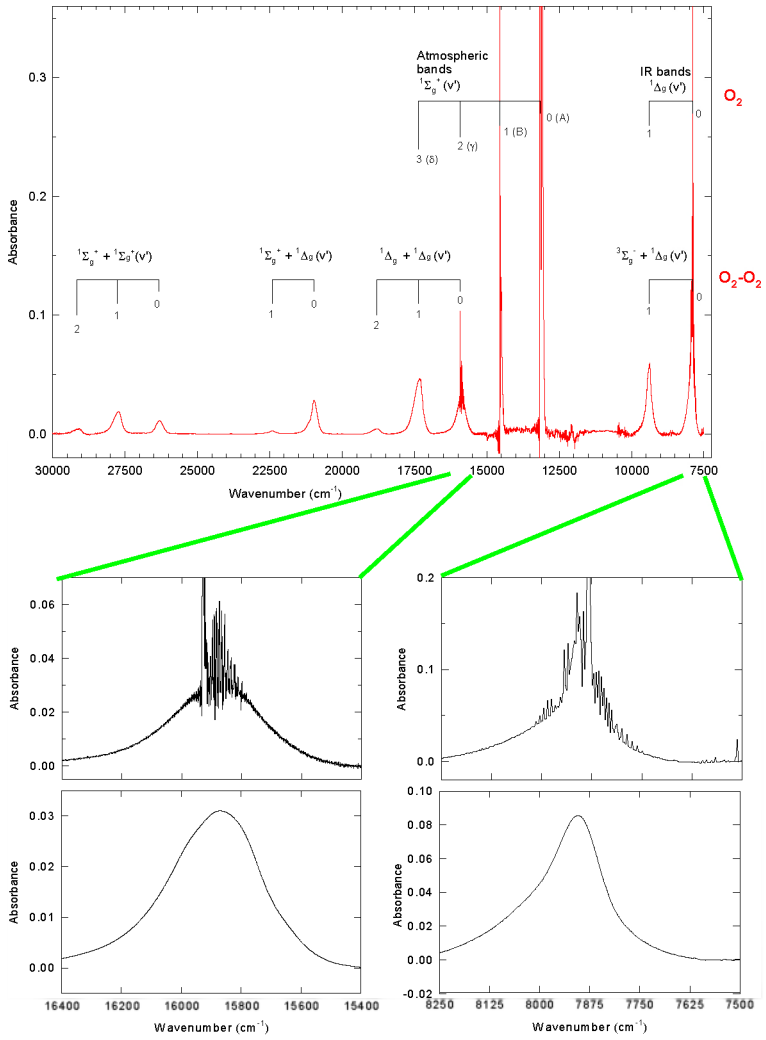

Figure 72: *Visible and NIR experimental spectrum of pure O_2 at 600 torr. Expanded portions show the separation of the O_2 and of the O_2-O_2 contributions.*

In the visible-near infrared region, the oxygen spectrum is composed of the O_2 discrete bands and the overlapping broad O_2-O_2 bands, as shown in the upper part of Figure 72. The spectroscopic study of the A, B, and У atmospheric bands and of the infrared bands allows to determine line positions and intensities. By applying the same procedure as in the UV region, the discrete and diffuse components of the spectrum have been separated. The result of this separation is shown in the bottom part of Figure 72 for two bands. This procedure allows the determination of a new set of O_2-O_2 absorption cross-sections, band centre positions, and bandwidths (Hermans et al., 1999). Pressure and temperature effects have also been described and will appear in a forthcoming paper (Hermans et al.).

H_2O

As the most abundant minor constituent and greenhouse gas of the Earth's troposphere, the water molecule plays a key role in atmospheric studies. The water molecule absorbs strongly in the infrared region, but recently greater interest has been put on the visible and ultraviolet weak absorption lines. The major importance of these weak water vapor lines is their possible contribution to the earth's radiation balance. Up to now, the atmospheric models of the Earth's radiation budget underestimate the observed values (Ramanathan and Vogelman, 1997), and water vapor forms a possible candidate for what is sometimes called the "missing absorber" (Learner et al., 1999). Considering this, it appears essential to improve and extend the spectroscopic data of H_2O by new laboratory measurements, especially in the UV-visible region where the existing data are scarce and mostly inaccurate. However, due to the weakness of the lines in the near-UV and visible regions, this requires very long optical pathlength and very sensitive laboratory techniques. Camy-Peyret et al. (1985) were the first to obtain high-quality laboratory spectra of water vapor between 25000 and 16000 cm^{-1}. They identified 1947 water lines in the 25000 - 16000 cm^{-1} spectral range, measured absolute line intensities for about 35% of them, and assigned about 60 % of them. The spectroscopic measurements and theoretical attributions made by Camy-Peyret et al. (1985) were included in the widely used HITRAN and GEISA databases (Rothman et al., 1996; Jaquinet-Husson et al., 1999). More recently, using a FT solar spectrum, Harder and Brault (1997) identified about 60 % more lines than listed by Camy-Peyret et al. (1985) in the narrow 22721-22230 cm^{-1} spectral range.

By combining the Fourier Transform Spectrometer with the very long multipass cell of the Université de Reims, we have undertaken to improve and extend the existing spectroscopic data. The two measurement campaigns (Table VII) have allowed us to record numerous high resolution spectra at different pressures and temperatures from the near-UV to the NIR (26000-10000 cm^{-1}). Figure 73 presents a raw spectrum of pure H_2O at 16 torr, and expanded portions in the visible and in the UV regions. The line identification by itself is a very time consuming task, because many weak lines are difficult to discriminate from the noise, and also because the high density of lines in most regions causes the overlapping of numerous lines. As the objective is to obtain the best possible line parameters, the fitting procedure is also a long and difficult task. Compared to the HITRAN database, a large number of new lines were identified and assigned in the 26000-13000 cm^{-1} spectral range. The spectral analysis performed in collaboration with the theoretical group at the University College London led to the assignment of about 2500 new lines corresponding to different rovibrational transitions, including transitions to 20 new overtone and

combination bands. Energy levels were successfully calculated (Carleer et al., 1999; Zobov et al., 2000). At present, cross sections and self broadening parameters of about 10000 lines have also been determined. This represents three times more lines than those reported in HITRAN (Table VII). The comparison of our line cross-sections with those listed in HITRAN shows an average discrepancy of about 10% although slight differences appear from band to band, as shown in Figure 74. These smaller values are such that, despite a much larger number of lines, our integrated absorption cross-section over the spectral range investigated is nearly equal to that obtained with the HITRAN data (Table VII).

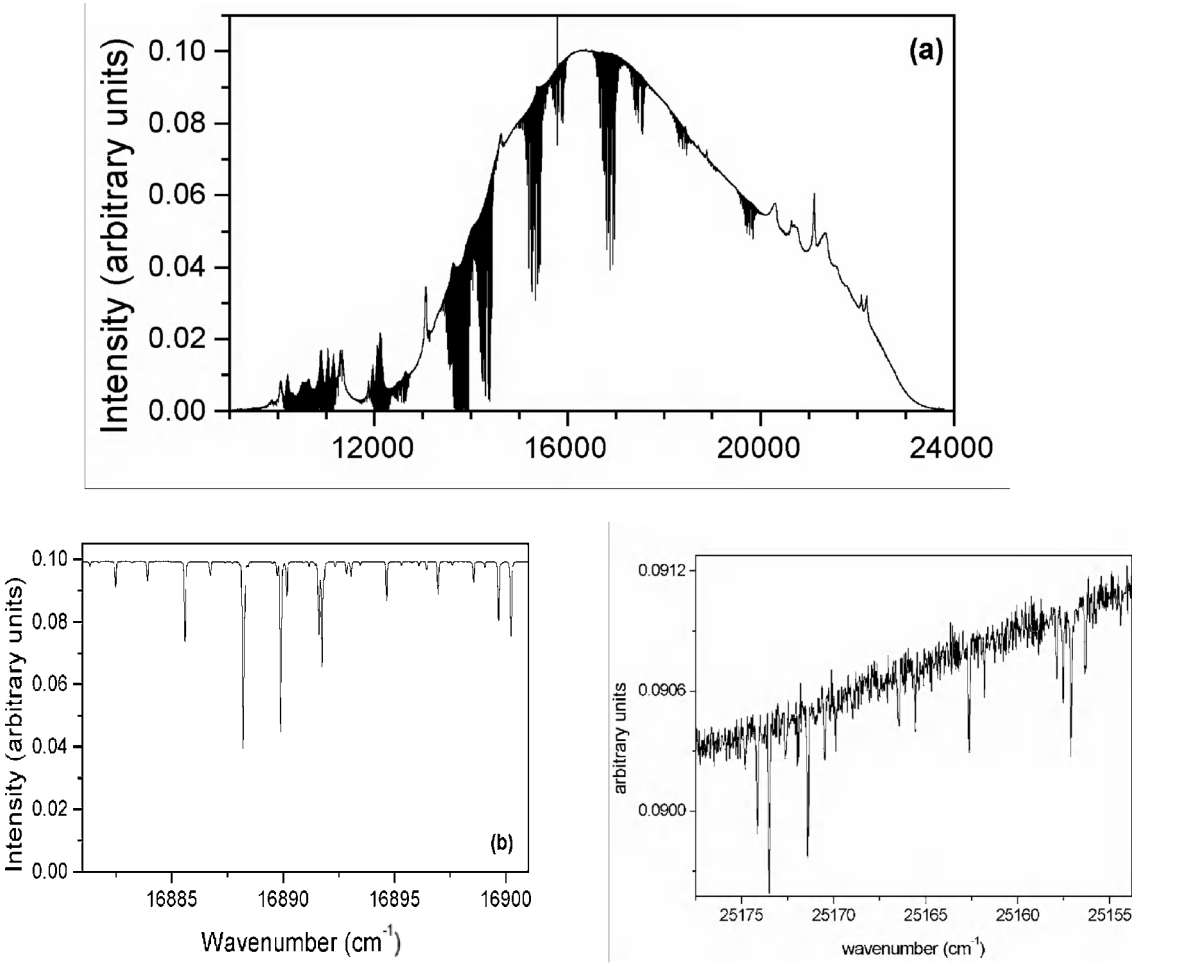

Figure 72: ***(a)*** *Raw water vapor spectrum from the NIR (10000 cm^{-1}) to the near-UV (24000 cm^{-1}). Expanded portions of the spectrum in the visible* ***(b)*** *and in the UV region* ***(c)****.*

By combining the Fourier Transform Spectrometer with the very long multipass cell of the Université de Reims, we have undertaken to improve and extend the existing spectroscopic data. The two measurement campaigns (Table VII) have allowed us to

record numerous high resolution spectra at different pressures and temperatures from the near-UV to the NIR (26000-10000 cm^{-1}). Figure 73 presents a raw spectrum of pure H_2O at 16 torr, and expanded portions in the visible and in the UV regions. The line identification by itself is a very time consuming task, because many weak lines are difficult to discriminate from the noise, and also because the high density of lines in most regions causes the overlapping of numerous lines. As the objective is to obtain the best possible line parameters, the fitting procedure is also a long and difficult task. Compared to the HITRAN database, a large number of new lines were identified and assigned in the 26000-13000 cm^{-1} spectral range. The spectral analysis performed in collaboration with the theoretical group at the University College London led to the assignment of about 2500 new lines corresponding to different rovibrational transitions, including transitions to 20 new overtone and combination bands. Energy levels were successfully calculated (Carleer et al., 1999; Zobov et al., 2000). At present, cross sections and self broadening parameters of about 10000 lines have also been determined. This represents three times more lines than those reported in HITRAN (Table VII). The comparison of our line cross-sections with those listed in HITRAN shows an average discrepancy of about 10% although slight differences appear from band to band, as shown in Figure 74. These smaller values are such that, despite a much larger number of lines, our integrated absorption cross-section over the spectral range investigated is nearly equal to that obtained with the HITRAN data (Table VII).

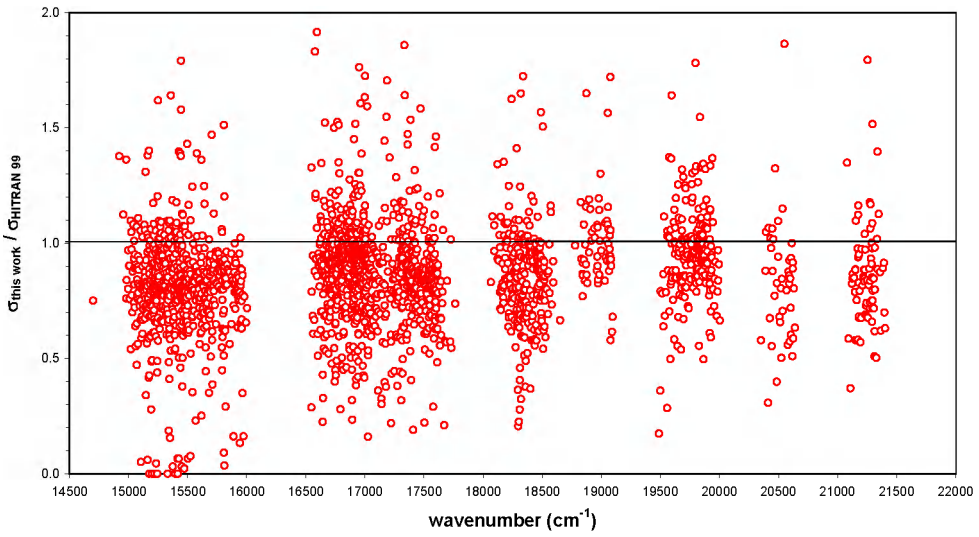

Figure 74: *Comparison of absorption cross-sections obtained in this work ($\sigma_{this\ work}$) and reported in the HITRAN database (σ_{HITRAN}) as a function of wavenumber.*

In the visible-near UV spectral range (26000-20000 cm^{-1}), the number of lines is five times greater than reported in HITRAN and the integrated absorption cross section is twice that reported in HITRAN, as shown in Table VII (sub-total). These results demonstrate the importance of the weak absorption lines of water vapor in the total attenuation of UV light by the atmosphere. This effect can be seen on Figure 75 were preliminary atmospheric simulations performed with a 1D high-resolution radiative transfer model (Clough et al., 1992; Mlawer et al., 1998) using our line list (Figure 4.58a) and the HITRAN line list (Figure 4.58b) as input data are shown. Significant differences between both simulations appear, but the impact of these results on the atmospheric radiative budget has not yet been quantified.

Table VII: *Comparison between the line parameters measured in this work and those reported in the HITRAN database. n refers to the number of lines; σ to the absorption cross-section; and γ_{self} to the self-broadening parameter.*

Spectral Range [cm^{-1}]	**This work**			**HITRAN99**		
	n	σ [cm $molec^{-1}$]	γ_{self} [cm^{-1} atm^{-1}]	n	σ [cm $molec^{-1}$]	γ_{self} [cm^{-1} atm^{-1}]
26000-24000	75	$9.05\ 10^{-25}$	0.68	0		
24000-22000	398	$5.17\ 10^{-24}$	0.52	72	$3.50\ 10^{-24}$	0.45
22000-20000	510	$3.78\ 10^{-24}$	0.45	124	$1.07\ 10^{-24}$	0.46
20000-19300	641	$2.42\ 10^{-23}$	0.59	229	$2.18\ 10^{-23}$	0.45
19300-18700	175	$1.51\ 10^{-24}$	0.53	61	$1.07\ 10^{-24}$	0.46
18700-18000	605	$1.28\ 10^{-23}$	0.55	293	$1.28\ 10^{-23}$	0.45
18000-17200	737	$2.16\ 10^{-23}$	0.54	341	$2.30\ 10^{-23}$	0.44
17200-16400	1295	$1.58\ 10^{-22}$	0.50	678	$1.60\ 10^{-22}$	0.43
16400-15600	810	$1.72\ 10^{-23}$	0.58	197	$1.85\ 10^{-23}$	0.44
15600-14700	1754	$1.07\ 10^{-22}$	0.60	499	$1.07\ 10^{-22}$	0.42
14700-13000	3242	$1.65\ 10^{-21}$	0.44	2052	$1.59\ 10^{-21}$	0.43
Sub-total 26000-20000	983	$9.86\ 10^{-24}$		196	$4.57\ 10^{-24}$	
Total	10242	$2.00\ 10^{-21}$		4546	$1.94\ 10^{-21}$	

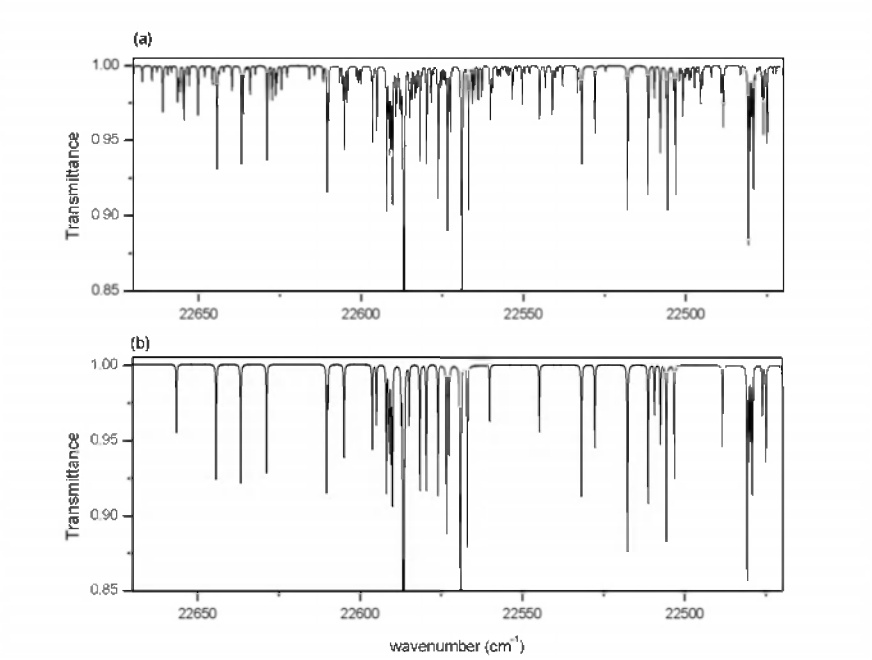

Figure75: *Atmospheric water vapour absorption spectrum, as obtained by a 1D high-resolution radiative transfer simulation in the solar regime using as source data (a) the present line list and (b) the HITRAN line list.*

The analysis of the water vapor spectra recorded under various pressures of nitrogen, which allows the determination of the line broadening and line shifting parameters is in progress. Also, the temperature dependency of all spectral parameters is under investigation. A paper reporting the spectroscopic analysis of the HOD spectrum has been submitted (Mérienne et al, b).

4.4.2.2 Line parameters and absorption cross-sections in the IR-NIR

Stable species (OCS, $^{12}C_2H_2$, HCFC-22 and HFC-152a)

We have studied the absorption spectra of several isotopomers of OCS, of $^{12}C_2H_2$ and two CFC replacements, HCFC-22 and HFC-152a:

- **OCS**: We have recorded the FT spectrum of natural OCS from 4800 to 8000 cm^{-1} with a near Doppler resolution. Vibration-rotation line positions have been measured for a total of 52 absorption bands of 4 isotopomers of the species, with accuracy between 2 and 8×10^{-4} cm^{-1}. Line intensities have also been determined. A global rovibrational analysis of the main isotopomer has been done, leading to a complete description and prediction of its vibration-rotation absorption spectrum (Rbaihi et al., 1998).

- **$^{12}C_2H_2$**: We have measured absolute line intensities in the $\nu_4+\nu_5$ band observed near 7.5 μm (Vander Auwera, 2000a). These measurements have put forward a significant Herman-Wallis dependence, involving an increase of the individual line intensities by as much as 20% from the *P*- to the *R*-branch. The accuracy of the line intensities is estimated to be better than 2%. These intensity data are included in the latest version of the HITRAN database (HITRAN 2000) and will be in the forthcoming version of the GEISA databank.
- **HCFC-22 and HFC-152a**: We have measured absorption cross-sections between 600 and 1700 cm^{-1} for these two species, either as pure gases or in mixtures with dry air at total pressures of 150 torr and 600 torr. Cross-sections have been obtained at several temperatures between 293 and 203K (Vander Auwera, 2000b; Ballard et al., 2000). These experimental conditions aim at reproducing at best the physical conditions encountered in the troposphere and lower stratosphere. Figure 4.59 presents examples of the cross-sections obtained for HFC-152a. These data will also be included in the forthcoming version of the GEISA databank.

Unstable species: HOCl

We have recently extended absolute line intensities measurements to chemically unstable and reactive species, such as acidic compounds found in the troposphere and stratosphere. Such measurements are most challenging because the required concentration of the species is not directly accessible, for instance through the measurement of the total gas pressure. These unstable compounds indeed usually exist only in equilibrium mixtures. Furthermore, their concentration may evolve while their spectra are being recorded, as a result of their reactivity.

In the visible-near UV spectral range (26000-20000 cm^{-1}), the number of lines is five times greater than reported in HITRAN and the integrated absorption cross section is twice that reported in HITRAN, as shown in Table VII (sub-total). These results demonstrate the importance of the weak absorption lines of water vapor in the total attenuation of UV light by the atmosphere. This effect can be seen on Figure 75 were preliminary atmospheric simulations performed with a 1D high-resolution radiative transfer model (Clough et al., 1992; Mlawer et al., 1998) using our line list (Figure 4.58a) and the HITRAN line list (Figure 4.58b) as input data are shown. Significant differences between both simulations appear, but the impact of these results on the atmospheric radiative budget has not yet been quantified.

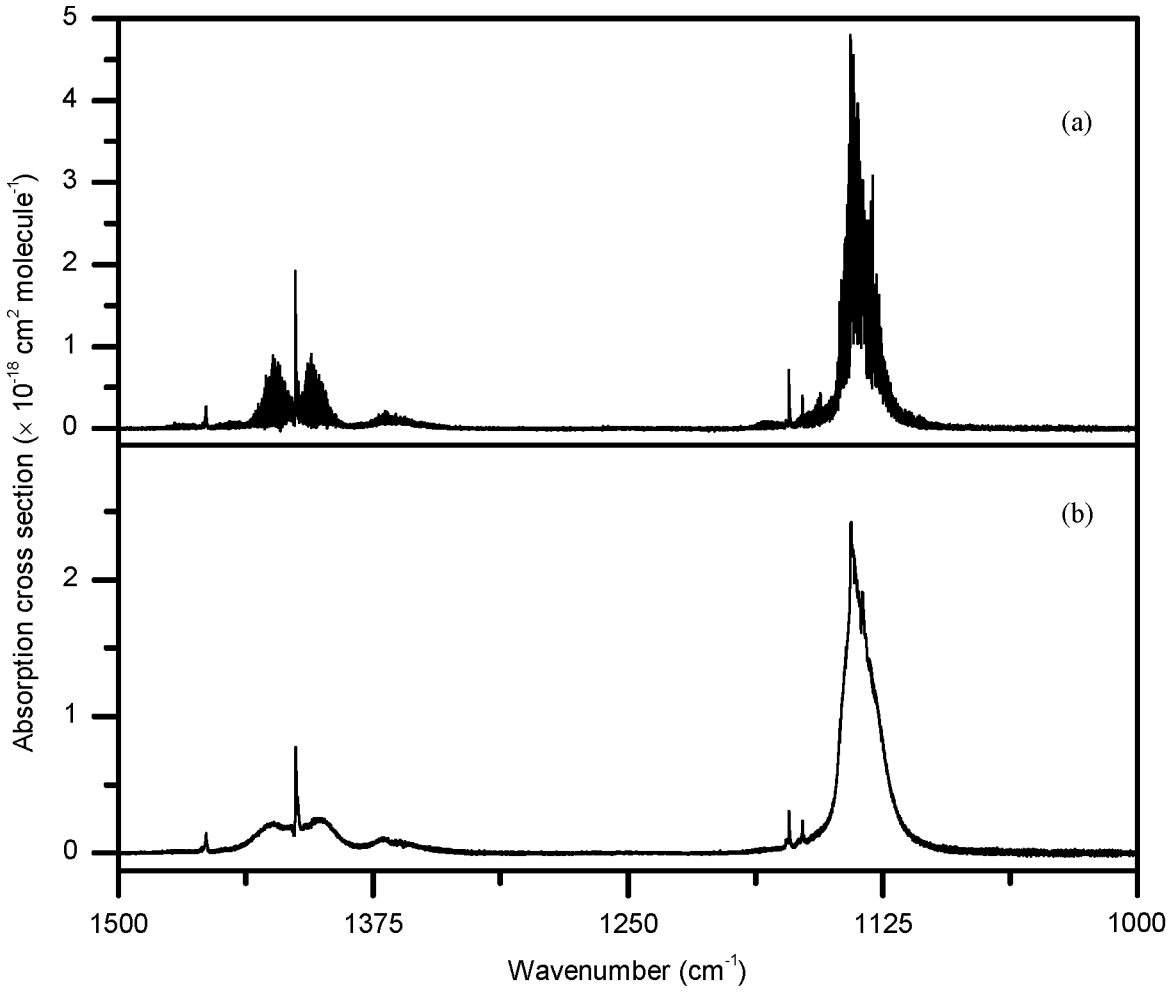

Figure 76: *Absorption cross-sections of HFC-152a: pure sample at 203 K (a) and mixture with dry air at a total pressure of 800 mbar at 293 K (b) (adapted from (Vander Auwera, 2000b).*

ACRONYMS

AMF	Air Mass Factor
BIRA-IASB	Belgisch Instituut voor Ruimte Aeronomie - Institut d'Aéronomie Spatiale de Belgique
CIE	Commission Internationale de l'Eclairage.
CTM	Chemistry Transport Model
DOAS	Differential Optical Absorption Spectroscopy
DSCD	Differential Slant Column Density
EAP	Effective Apodisation Parameter
ECMWF	European Centre for Meteorology and Weather Forecasting
EMPA	Swiss federal Laboratories for Materials Testing and Research
FT	Fourier Transform
FTS	Fourier Transform Spectrometer
FTIR	Fourier Transform Infrared
FWHM	Full width half maximum
GIRPAS	Groupe Infra-Rouge de Physique Atmosphérique et Solaire
GAW	Global Atmosphere Watch
IBGE	Institut Bruxellois pour la Gestion de l'Environnement
IRCEL	Belgian Interregional Cell for the Environment
ISSJ	International Scientific Station of the Jungfraujoch
KMI-IRM	Koninklijk Meteorologisch Instituut van België – Institut Royal Météorologique de Belgique
LCPM	Laboratoire de Chimie Physique Moléculaire
NDSC	Network for the Detection of Stratospheric Change
OEM	Optimal Estimation Method
OHP	Observatoire de Haute Provence
PBL	planetary boundary layer
PSC	Polar Stratospheric Cloud
RT	Radiative Transfer
SAOZ	Système d'Analyse par Observations Zénithales
SCD	Slant Column Density
SPARC	Stratospheric Processes and Their Role in Climate
SZA	Solar Zenith Angle
TBL	Tropospheric Boundary Layer
UKMO	United Kingdom Meteorological Office
ULB	Université Libre de Bruxelles
Ulg	Université de Liège
UV	Ultraviolet
UVI	UV Index
Vis	visible
VMR	volume mixing ratio
WCRP	World Climate Research Programme
WMO	World Meteorological Office

REFERENCES

We use the term greenhouse gases because of its widespread use. However it must be noticed that the term is badly chosen, because the atmospheric warming effect is a different physical process than the one that controls the real greenhouse: the latter is based on the reduction of convective transport, the atmospheric warming is caused by absorption of thermal infrared radiation (Kockarts, 2000).

Abrams, M. C., Gunson, M. R., Lowes, L. L., Rinsland, C. P. and Zander, R. 1996a. Pressure sounding of the middle atmosphere from ATMOS solar occultation measurements of atmospheric CO_2 absorption lines. Appl. Opt. 35: 2,810-2,820.

Abrams, M. C., Chang, A. Y., Gunson, M. R., Abbas, M. M., Goldman, A. G., Irion, F. W., Michelsen, H. A., Newchurch, M. J., Rinsland, C. P., Stiller, G. P. and Zander, R. 1996b. On the assessment and uncertainty of atmospheric trace gas burden measurements with high-resolution infrared solar occultation spectra from space by the ATMOS experiment. Geophys. Res. Lett. 23: 2,337-2,340.

Aliwell, S.R., Van Roozendael, M., Johnston, P.V., Richter, A., Wagner, T., Arlander, D.W., Burrows, J.P., Fish, D.J., Jones, R.L., Tørnkvist, K.K., Lambert, J.-C., Pfeilsticker K. and Pundt, I. (In press 2001). Analysis for BrO in Zenith-Sky Spectra: An Intercomparison Exercise for Analysis Improvement. J. Geophys. Res.

Anderson, J., Russell III, J.M., Solomon, S. and Deaver, L.E. 2000. Halogen Occultation Experiment confirmation of stratospheric chlorine decrease in accordance with the Montreal protocol. J. Geophys. Res. 105: 4,483-4,490.

Ballard, J., Knight, R. J., Vander Auwera, J., Herman, M., Di Leonardo, G., Masciarelli, G., Nicolaisen, F. M., Beukes, J. A., Christensen, L. K., McPheat, R., Duxbury, G., Freckleton, R. and Shine, K. P. 2000. An intercomparison of laboratory measurements of absorption cross-sections and integrated absorption intensities for HCFC-22. J. Quant. Spectrosc. Radiat. Transfer 66: 109-128.

Barret, B., Mahieu, E., Carleer, M., De Mazière, M., Colin, R. and Zander, R. 1999. Tropospheric boundary layer investigations by differential ground-based solar FTIR spectrometry. In: Environmental Sensing and Applications. SPIE Proceedings 3821: 116-123.

Barry J., Locke, G., Scollard, D., Sidebottom, H., Treacy, J., Clerbaux, C., Colin, R. and Franklin, J. 1997. 1,1,1,3,3-pentafluorobutane (HFC-365mfc): atmospheric degradation and contribution to radiative forcing. Int. J. Chem. Kinet. 29: 607-617.

Bell, W., Duxbury, G. and Stuart, D.D. 1992. High-resolution spectra of the v_4 band of chlorine nitrate. J. Mol. Spectrosc. 152: 283-297.

Bernath, P., Carleer, M., Fally, S., Jenouvrier, A., Vandaele, A. C., Hermans, C., Mérienne, M.-F. and Colin, R. 1998. The Wulf bands of oxygen. Chem. Phys. Letters 297: 293-299.

Bevilacqua, R.M., Kriebel, D.L., Pauls, T.A., Aellig, C.P., Siskind, D.E., Daehler, M., Olivero, J.J., Puliafito, S.E., Hartmann, G.K., Kampfer, N., Berg, A. and Croskey, C.L. 1996. MAS measurements of the latitudinal distribution of water vapor and ozone in the mesosphere and lower thermosphere. Geophys. Res. Lett. 23: 2,317-2,320.

Birk, M., Hausamann, D., Wagner, G. and Johns, J. W. C. 1996. Determination of line strenghts by Fourier transform spectroscopy. Appl. Opt. 35: 2,971-2,985.

Birk, M., and Wagner, G. 2000. A new spectroscopic database for chlorine nitrate. In: Poster session 2, Sixth Biennial Hitran Database Conference, Harvard-Smithsonian Center for Astrophysics, Cambridge, MA, 19-21 June 2000.

Brasseur, G., and Granier, C. 1992. Mount Pinatubo aerosols, chlorofluorocarbons, and ozone depletion. Science 257: 1,239-1,242.

Camy-Peyret, C., Flaud, J.-M., Mandin, J.-Y., Chevillard, J.-P., Brault, J., Ramsay, D. A., Vervloet, M. and Chauville, J. 1985. The high-resolution spectrum of water vapor between 16500 and 25250 cm^{-1}. J. Mol. Spec. 113: 208-228.

Camy-Peyret, C., Bergqvist, B., Galle, B., Carleer, M., Clerbaux, C., Colin, R., Fayt, C., Goutail, F., Nunes-Pinharanda, M., Pommereau, J. P., Hausmann, M., Plat,t U., Pundt, I., Rudolph, T., Hermans, C., Simon, P. C., Vandaele, A. C., Plane, J. M. and Smith, N. 1996. Intercomparison of instruments for tropospheric measurements using Differential Optical Absorption Spectroscopy. J. Atm. Chem. 23: 51-80.

Carleer, M., Jenouvrier, A., Vandaele, A. C., Bernath, P. F., Mérienne, M.-F., Colin R., Zobov, N. F., Polyansky, O. L., Tennyson, J. and Savin, S. A. 1999. The near

infrared, visible, and near ultraviolet overtone spectrum of water. J. Chem. Phys. 111 (6): 2,444-2,450.

Chipperfield, M. 1999. Multiannual simulations with a three-dimensional chemical transport. Model. J. Geophys. Res. 104: 1,781-1,805.

Clerbaux, C., Colin, R., Simon, P. C. and Granier, C. 1993. Infrared cross sections and Global Warming Potentials of 10 alternative hydrohalocarbons. J. Geophys. Res. 98 (D6): 10,491-10,497.

Clerbaux, C. and Colin, R. 1994. Determination of the infrared cross sections and Global Warming potentials of 1,1,2-Trifluoroethane (HFC-143). Geophys. Res. Letters 21 (22): 2,377-2,380.

Clough, S. A., Iacono, M. J. and Moncet, J.-L. 1992. Line-by-line calculation of atmospheric fluxes and cooling rates- 1. Application to water vapor. J. Geophys. Res. 97 (D14): 15,761-15,785.

Connor, B.J., Jones, N.B., Wood, S.W., Keys, J.G., Rinsland, C.P. and Murcray F.J. 1996. Retrieval of HCl and HNO_3 profiles from ground-based FTIR data using SFIT2. In: Proceedings of XVIII Quadrennial Ozone Symposium. Bojkov R.J. and Visconti G. (Ed). Parco Sci. e Technol. d'Abruzzo, L'Aquila, Italy : 485-488.

Considine, D.G., Deaver, L.E., Remsberg, E.E. and Russell III, J.M. 1997. HALOE observations of a slowdown in the rate of increase of HF in the lower mesosphere. Geophys. Res. Lett. 24: 3,217-3,220.

De Backer, H., De Muer D. and De Sadelaer, G. 1998. Comparison of ozone profiles obtained with Brewer-Mast and Z-ECC sensors during simultaneous ascents. J. Geophys. Res. 103: 19,641-19,648.

De Backer, H. 1999. Homogenisation of ozone vertical profile measurements at Uccle. Wetenschappelijke en technische publicaties van het K.M.I. 7, ISSN D1999/0224/007, KMI, Ukkel: 26.
(ftp://ftp.kmi-irm.be/dist/meteo/hugo/publ/1999/o3prof.ps)

De Backer, H., Köpke, P., Bais, A., Cuevas, E., Gillotay, D., Haite, C., Heikkilä, A., Koskela, T., Kyrö, E., Lapeta, B., Lorente, J., Mayer, B., Plets, H., Renaud, A., Schmalwieser A.W. and Vanicek, K. 1999. Comparison of measured and modelled UV Indices. 24th General assembly of EGS, Geophysical Research Abstracts. Vol. 1, number 2: 477.

De Backer, H., Koepke, P., Bais, A., de Cabo, X., Frei, T., Gillotay, D., Haite, C., Heikkila, A., Kanzantzidis, A., Koskela, T., Kyrö, E., Lapeta, B., Lorente, J., Masson, K., Mayer, B., Plets, H., Redondas, A., Renaud, A., Schauberger, G., Schmawieser, A., Schwander, H. and Vanicek, K. In press, 2001. Comparison of Measured and Modelled UV Indices. Meteorological Applications.

De Backer, H. In Press. Tropospheric ozone trends in Uccle 1969-1999 after homogenisation of the dataset. In: Proceedings from the EUROTRAC symposium 2000. Midgley, P.M., Reuther, M., Williams M. (Ed). Springer Verlag Berlin, Heidelberg 2001.

De Mazière, M., Van Roozendael, M., Hermans, C., Simon, P.C., Demoulin P. and Roland, G. 1998. Quantitative evaluation of the post-Pinatubo NO_2 reduction and recovery, based on 10 years of FTIR and UV-visible spectroscopic measurements at the Jungfraujoch. J. Geophys. Res. 103: 10,849-10,858.

De Mazière, M., Hennen, O., Van Roozendael, M., Demoulin P. and De Backer, H. 1999. Daily ozone vertical profile model built on geophysical grounds, for column retrieval from atmospheric high-resolution spectra. J. Geophys. Res. 104: 23,855-23,869.

De Mazière, M., Van Roozendael, M., Hennen, O., Demoulin, P. and Mahieu, E. 1999b. Revision of the O3 trend analysis at the Jungfraujoch station. Poster presentation at the Sixth Scientific Conference of the International Global Atmospheric Chemistry Project (IGAC), Bologna, Sept. 13-17, 1999.

De Muer, D., and De Backer, H. 1992. Revision of 20 years of Dobson total ozone data at Uccle (Belgium): Fictitious Dobson total ozone trends induced by sulfur dioxide trends. J. Geophys. Res. 97: 5,921-5,937.

De Muer, D., De Backer, H. and Van Haver, Ph. 1995. Analysis of 25 years of regular ozone soundings at Uccle (Belgium). Atmospheric ozone as a Climate gas. Wang, W. and Isaksen, I. (Ed). Springer-Verlag Berlin: 113-129.

De Muer, D., Heylen, R., Van Loey, M. and De Sadelaer, G. 1997. Photochemical ozone production in the convective mixed layer, studied with a tethered balloon sounding system. J. Geophys. Res. 102: 15,933-15,947.

DeMore, W. B., Sander, S. P., Golden D. M., Hampson, R. F., Kurylo, M. J., Howard, C. J., Ravishankara, A. R., Kolb, C. E., and Molina, M. J. 1997. Chemical Kinetics and Photochemical Data for Use in Stratospheric Modelling. JPL Publication 97-4.

Demoulin, P., Mahieu, E., Zander, R., Roland, G., Delbouille, L., Servais, C., De Mazière, M. and Van Roozendael, M. 1998. The Current Budget of NO_y above the Jungfraujoch as derived from IR Solar Observations. In: Proceedings of the Fourth European Symposium on Polar Stratospheric Ozone Research, Schliersee, Germany, September 22-26, 1997. European Commission, Air pollution research report 66: 427-430.

Demoulin, P., Zander, R., Mélen, F., Mahieu, E. and Servais, C. 1999. Column abundance measurements of formaldehyde above the Jungfraujoch. In: Proceedings of Atmospheric Spectroscopy Applications 1999, Reims, France, September 1-3, 1999: 59-62.

Draper, N. and Smith, H. 1980. Applied regression analysis. J. Wiley & Sons (Ed). New York.

Etheridge, D.M., Steele, L.P., Francey, R.J. and Langenfelds, R.L. 1998. Atmospheric methane between 1000 A.D. and present: Evidence of anthropogenic emissions and climate variability. J. Geophys. Res. 103: 15,979-15,993.

Etheridge, D.M., et al. 2001 (in press). Atmospheric methane between 1000 AD and present: evidence of anthropogenic emissions and climate variability. J. Geophys. Res.

Fally, S., Vandaele, A. C., Carleer, M., Hermans, C., Jenouvrier, A., Mérienne, M.-F., Coquart, B. and Colin, R. 2000. Fourier transform spectroscopy of the O_2 Herzberg bands. III. Absorption cross-sections of the collision-induced bands and of the Herzberg continuum. J. Mol. Spectrosc. 204: 10-20.

Fish, D.J., Jones, R.L. and Strong, E.K. 1995. Midlatitude observations of the diurnal variation of stratospheric BrO. J. Geophys. Res. 100: 18,863-18,871.

Fitzenberger, R., Bösch, H., Camy-Peyret, C., Chipperfield, M.P., Harder, H., Platt, U., Sinnhuber, B.-M., Wagner,T. and Pfeilsticker, K. 2000. First Profile Measurements of Tropospheric BrO. Geophys. Res. Lett. 27: 2921-2924.

Fonteyn, D., Larsen, N. and Remedios, J. J. 2000. Interactive PSC-Chemical Modelling: Lagrangian and Eulerian model case studies. In: Proceedings of the Quadriennial Ozone Symposium, Hokkaido University, Sapporo, Japan, 3-8 July 2000.

Gardiner, B.G., Webb, A.R., Bais, A. F., Blumthaler, M., Dirmhirn, I., Forster, P., Gillotay, D., Henriksen, K., Huber, M., Kirsch, P.J., Simon, P.C., Svenoe, T., Weihs, P. and Zerefos, C.S. 1993. European Intercomparison of ultraviolet spectroradiometers. Environ. Technol. 14: 25-43.

Gillotay D. 1996. UV monitoring in Belgium: Past, present and future. In Measurements and Trends of Terrestrial UVB Radiation in Europe. B. L. Diffey (Ed): 41-53.

Harder, J. W. and Brault, J. W. 1997. Atmospheric measurements of water vapor in the 442-nm region. J. Geophys. Res. 102 (D5): 6,245-6,252.

Harries, J.E., Russell, J.M.,III, Tuck, A.F., Gordley, I.I., Purcell, P.N., Stone, K.A, Bevilacqua, R.M., Gunson, M.R., Nedoluha, G. and Traub, W.A. 1996. Validation of measurements of water vapor from the HALogen Occultation Experiment (HALOE). J. Geophys. Res. 101: 10,205-10,216.

Hendrick, F., Mueller, R., Sinnhuber, B.-M., Bruns, M., Burrows, J. P., Chipperfield, M. P., Fonteyn, D., Richter, A., Van Roozendael, M. and Wittrock, F. 2000. Simulation of BrO Diurnal Variation and BrO Slant Columns: Intercomparison Exercise Between Three Model Packages. In: Proceedings of the 5th European Workshop on Stratospheric Ozone, Saint Jean de Luz, France, 27 Sept.-1 Oct. 1999. Air Pollution Research Report 73, European Commission - DG XII, Brussels, 2000.

Hermans, C., Vandaele, A. C., Carleer, M., Fally, S., Colin, R., Jenouvrier, A., Mérienne, M.-F., and Coquart B. 1999. Absorption cross-sections of atmospheric constituents: NO_2, O_2, and H_2O. Environ. Sci. & Pollut. Res. 6(3): 151-158.

Hermans, C., Jenouvrier, A., Fally, S., Carleer, M., Vandaele, A. C., Mérienne, M.-F., Coquart, B. and Colin, R. In preparation. Absorption cross-sections of oxygen: the IR and visible bands.

Hintsa, E.J., Weinstock, E.M., Anderson, J.G., May, R.D. and Hurst, D.F. 1999. On the accuracy of *in situ* water vapor measurements in the troposphere and lower stratosphere with the Harvard Lyman-α hygrometer. J. Geophys. Res. 104: 8,183-8,189.

Hofmann, D.J., and Solomon, S. 1989. Ozone destruction through heterogeneous chemistry following the eruption of El Chichon. J. Geophys. Res. 94: 5,029-5,041.

Jäger, H., Uchino, O., Nagai, T., Fujimoto, T., Freudenthaler, V. and Homburg, F. 1995. Ground-based remote sensing of the decay of the Pinatubo eruption cloud at three northern hemisphere sites. Geophys. Res. Lett. 22: 607-610.

Jaquinet-Husson, N., Arié, E., Barbe, A., Bjoraker, G., Bonnet, B., Brown, L. R., Camy-Peyret, C., Champion, J.-P., Chédin, Chursin, A. A., Clerbaux, C., Duxbury G., Flaud, J.-M., Fourrié, N., Fayt, A., Graner, G., Gamach, R., Goldman, A., Golovko V., Guelachvilli, G., Hartmann, J. M., Hilico, J. C., Hillman, J., Lefèvre, G., Lellouch, E., Mikhaïlenko S. N., Naumenko, O. V., Nemtchninov, V., Newnham, D. A., Nikitin, A., Orphal, J., Perrin, A., Reuter, D. C., Rinsland, C. P., Rosenmann, L., Rothman, L. S., Scott, N. A., Selby, J., Sinitsa, L. N., Sirota, J. M., Smith, A. M., Smith, K. M., Tyuterev, V. G., Tipping, R. H., Urban, S., Varanasi, P. and Weber, M. 1999. The 1997 spectroscopic GEISA databank. J. Quant. Spectrosc. Radiat. Transfer 61: 4,205-4,254.

Jenouvrier, A., Mérienne, M.-F., Coquart, B., Carleer, M., Fally S., Vandaele, A. C., Hermans, C. and Colin R. 1999. Fourier transform spectroscopy of the O_2 Herzberg bands. I. Rotational Analysis. J. Mol. Spectrosc. 198: 136-162.

Kockarts, G. 2000. Aeronomie: Physique et Chimie de l'atmosphere. De Boeck. (Ed), Bruxelles, 2000.

Köpke, P, Bais, A., Balis, D., Buchwitz, M., De Backer, H., de Cabo, X., Eckert, P., Eriksen, P., Gillotay, D., Koskela, T., Lapeta, B., Litynska, Z., Lorente, J., Mayer, B., Renaud, A., Ruggaber, A., Schauberger, G., Seckmeyer, G., Seifert, P., Schmalwieser, A., Schwander, H., Vanicek K. and Weber, M. (1998) Comparison of models used for UV index -calculations, Photochemistry and Photobiology 67 (6): 657-662.

Kurylo, M. J., and Solomon, S. 1999. The Network for the Detection of Stratospheric Change. A Status and Implementation Report. In : NASA Headquarters – Code EEU, 600 Independent Avenue, S.W., Washington, D.C. 20546, USA, January 1999: 1-70.

Kylling, A. 1995. UVspec: a program package for calculation of diffuse and direct UV and visible intensities and flux. Available by anonymous ftp to kaja.gi.alaska.edu, cd pub/arve.

Learner, R. C. M., Zhong, W., Haigh, J. D., Belmiloud, D. and Clarke J. 1999. The contribution of unknown weak water vapor lines to the absorption of solar radiation. Geophys. Res. Lett. 26 (24): 3,609-3,612.

Liley, J.B., Johnston, P.V., McKenzie, R.L., Thomas, A.J. and Boyd, I.S. 2000. Stratospheric NO_2 variations from a long time series at Lauder, New Zealand. J. Geophys. Res. 105: 11,633-11,640.

Madronich, S. 1993. UV radiation in the natural and perturbed atmosphere. In: Environmental Effects of UV (Ultraviolet) Radiation. M. Tevini, (Ed). Lewis Publisher, Boca Raton: 17-69.

Mahieu, E., Zander, R., Gunson, M.R., Toon, G.C., Rinsland, C.P. and Demoulin, P. 1996. Evaluation of the life-time of SF_6 in the Earth's atmosphere based on ATMOS and Jungfraujoch IR solar observations. In: Proceedings of the Atmospheric spectroscopy Applications Workshop, ASA-Reims 96, Reims 4-6 sept. 1996. Barbe, A., Flaud, J.-M., Jacon, M., Mérienne, M.-F. and Rothman, L. (Ed). UFR Sciences Exactes et Naturelles, BP 1039-51687, Reims: 125-128.

Mahieu, E., Zander, R., Mélen, F., Demoulin, P., Servais, C., Delbouille, L. and Roland, G. 1998. Recent Characteristic Budget of Inorganic Chlorine and Fluorine above the Jungfraujoch Station. In: Proceedings of the Fourth European Symposium on Polar Stratospheric Ozone Research, Schliersee, Germany, September 22-26, 1997. European Commission, Air pollution research report 66: 358-361.

Mahieu, E., Zander, R., Demoulin, P., De Mazière, M., Mélen, F., Servais, C., Roland, G., Delbouille, L., Poels, J. and Blomme, R. 2000. Fifteen years-trend characteristics of key stratospheric constituents monitored by FTIR above the Jungfraujoch. In: Proceedings of the Fifth European Symposium on Stratospheric Ozone, St. Jean de Luz, France, September 27 - October 1, 1999. N. R. P. Harris, M. Guirlet and G. T. Amanatidis (Eds). Air pollution Research Report 73 - EUR 19340: 99-102.

McKinlay, A.F; and Diffey, B.L. 1987. A reference action spectrum for Ultraviolet induced erythema in human shin. CIE J. 6 : 17-22.

Mélen, F., Mahieu, E., Zander, R., Rinsland, C. P., Demoulin, P., Roland, G., Delbouille, L. and Servais, C. 1998. Vertical column abundances of COF_2 above the Jungfraujoch station derived from ground-based infrared solar observations. J. Atmos. Chem. 29: 119-134.

Mérienne, M.-F., Jenouvrier A. and Coquart, B. 1995. The NO_2 absorption spectrum. I: Absorption cross-sections at ambient temperature in the 300-500 nm region. J. Geophys. Res. 20: 281-297.

Mérienne, M.-F., Jenouvrier, A., Coquart, B., Carleer, M., Fally, S., Colin, R., Vandaele, A.C., and Hermans, C. 2000. Fourier transform spectroscopy of the O_2 Herzberg bands. II. Band oscillator strengths and transition moments. J. Mol. Spectrosc. 202 (2): 171-193.

Mérienne, M.-F., Jenouvrier, A., Coquart, B., Carleer, M., Fally, S., Colin, R., Vandaele, A.C., and Hermans C. Submitted[a]. Improved data set for the Herzberg band systems of $^{16}O_2$. J. Mol. Spectrosc.

Mérienne, M.-F., Jenouvrier A., Carleer, M., Colin, R., Vandaele, A. C., Bernath P. F., Polyansky, O. L. and Tennyson, J. Submitted[b]. The visible and near ultraviolet rotation-vibration spectrum of HOD. J. Mol. Spectrosc.

Michelsen, H. A., Manney, G. L., Irion, F. W., Toon, G. C., Gunson, M. R., Rinsland, C. P., Zander, R., Mahieu, E., Newchurch, M. J., Purcell, P. N., Remsberg, E. E., Russell III, J. M., Pumphrey, H. C., Waters, J. W., Bevilacqua, R. M., Kelly, K. K. and Webster, C. R. 2001 (in press). ATMOS Version 3 water vapor measurements: comparisons with ATMOS Version 2 retrievals and observations from NOAA and Harvard Lyman-α hygrometers, MkIV, MAS, HALOE, and MLS. J. Geophys. Res.

Mlawer, E. J., Clough, S. A., Brown, P. P., Stephen, T. S., Landry J. C., Goldman, A. and Murcray, F. J. 1998. Observed atmospheric collision-induced absorption in near-infrared oxygen bands. J. Geophys. Res. 103 (D4): 3,859-3,863.

Montzka, S.A., Butler, J.H., Myers, R.C., Thompson, T.M., Swanson, T.H., Clarke, A.D., Lock, L.T. and Elkins, J.W. 1996. Decline in the tropospheric abundance of halogen from halcarbons: implications for stratospheric ozone depletion. Science 272: 1,318-1,322.

Montzka, S.A., Butler, J.H., Elkins, J.W., Thompson, T.M., Clarke, A.D. and Lock, L.T. 1999. Present and future trends in the atmospheric burden of ozone-depleting halogens. Nature 398: 690-694.

Neckel, H., and Labs, D. 1984. The Solar Radiation Between 3300 and 12500 A. Solar Physics. 90: 205-258.

Nevison, C.D., Solomon, S. and Russell III, J.M. 1996. Nighttime formation of N2O5 inferred from the Halogen Occultation Experiment sunset/sunrise NOx ratios. J. Geophys. Res. 101: 6,741-6,748.

Norton, R.H., and Rinsland, C.P. 1991. ATMOS data processing and science analysis methods. Appl. Opt. 30: 389-400.

Plets, H. and Vynckier, C. (2000) A comparative study of statistical total column ozone forecasting models, J. Geophys. Res. 105: 26,503-26,517.

Pougatchev, N.S., Connor, B.J., Jones, N.B., and Rinsland, C.P. 1995. Infrared measurements of the ozone vertical distribution above Kitt Peak. J. Geophys. Res. 100(D8): 16,689-16,698.

Pougatchev, N.S., Connor, B.J. and Rinsland, C.P. 1996. Validation of ozone profile retrievals from ground-based solar spectra. Geophys. Res. Lett. 23(13): 1,637-1,640.

Pumphrey, H.C. 1999. Validation of a new prototype water vapor retrieval from the UARS Microwave Limb Sounder. J. Geophys. Res. 104: 9,399-9,412.

Ramanathan, V. and Vogelmann, A. M. 1997. Greenhouse effect, atmospheric solar absorption and the Earth's radiation budget: form the Arrhenius-Langley era to the 1990's. Ambio 26 (1): 38-46.

Ravishankara, A.R., Solomon, S., Turnipseed, A.A. and Warren, R.F. 1993. Atmospheric lifetimes of long-lived halogenated species. Science 259: 194-199.

Rbaihi, E., Belafhal, A., Vander Auwera, J., Naim, S. and Fayt, A. 1998. Fourier transform spectroscopy of carbonyl sulfide from 4700 to 8000 cm^{-1} and new global analysis of $^{16}O^{12}C^{32}S$. J. Mol. Spectrosc. 191: 32-44.

Richter, A., Wittrock, F., Ladstätter-Weißenmayer, A., and Burrows, J. P. 2001. GOME measurements of stratospheric and tropospheric BrO. Accepted for publication in Adv. Space Res.

Rinsland, C.P., Boughner, R.E., Larsen, J.C., Stokes, G.M. and Brault, J.W. 1984. Diurnal variations of atmospheric nitric oxide: Ground-based infrared spectroscopic measurements and their interpretation with time-dependent photochemical model calculations. J. Geophys. Res. 89: 9,613-9,622.

Rinsland, C.P., Goldman, A., Murcray, F., Blatherwick, R., Kosters, J., Murcray, D., Sze, N.D. and Massie, S. 1990. Long-term trends in the concentrations of SF_6, $CHClF_2$ and COF_2 in the lower stratosphere from analysis of high-resolution infrared solar occultation spectra. J. Geophys. Res. 95: 16,477-16,490.

Rinsland, C.P., Gunson, M.R., Abrams, M.C., Lowes, L.L., Zander, R., Mahieu, E., Goldman, A., Ko, M.K.W., Rodriguez, J.M. and Sze, N.D. 1994. Heterogeneous conversion of N2O5 to HNO3 in the post-Mount Pinatubo eruption stratosphere. J. Geophys. Res. 99: 8,213-8,219.

Rinsland, C. P., Salawitch, R. J., Gunson, M. R., Solomon, S., Zander, R., Mahieu, E., Goldman, A., Newchurch, M. J., Irion, F. W. and Chang, A. Y. 1999. Polar stratospheric descent of NO_y and CO and Arctic denitrification during winter 1992-1993, J. Geophys. Res. 104: 1,847-1,861.

Rinsland, C. P., Goldman, A., Connor, B. J., Stephen, T. M., Jones, N. B., Wood, S. W., Murcray, F. J., David, S. J., Blatherwick, R. D., Zander, R., Mahieu, E. and Demoulin, P. 2000. Correlation relationships of stratospheric molecular constituents from high spectral resolution, ground-based infrared solar absorption spectra. J. Geophys. Res. 105: 14,637-14,652.

Rodgers, C.D. 1976. Retrieval of atmospheric temperature and composition from remote measurements of thermal radiation. Reviews of Geophysics and Space Physics 14(4): 609-624.

Rothman, L. S., Rinsland, C. P., Goldman, A., Massie, S. T., Edwards, D. P., Flaud, J.-M., Perrin, A., Camy-Peyret C., Dana, V., Mandin, J.-Y., Schroeder, J., McCann, A., Gamache, R. R., Wattson, R. B., Yoshino, K., Chance, K. V., Jucks, K. W., Brown, L. R. , Nemtchinov, V. and Varanasi, P. 1996. The HITRAN molecular spectroscopic database and HAWKS: 1996 edition. J. Quant. Spectrosc. Radiat. Transfer 60 : 665.

Russell, J.M. III, Deaver, L.E., Luo, M., Park, J.H., Gordley, L.L., Tuck, A.F., Toon, G.C., Gunson, M.R., Traub, W.A., Johnson, D.G., Jucks, K.W., Murcray, D.G., Zander, R., Nolt, I.G. and Webster, C.R. 1996. Validation of hydrogen chloride measurements made by HALOE from the UARS platform. J. Geophys. Res. 101: 10,151-10,162.

Sander, S. P., Friedl, R. R., DeMore, W. B., Golden, D. M., Kurylo, M. J., Hampson, R. F., Huie, R. E., Moortgat, G. K., Ravishankara, A. R., Kolb, C. E. and Molina, M. L. 2000. Chemical kinetics and photochemical data for use in stratospheric modelling, supplement to evaluation 12: Update of key reactions, evaluation 13. Nasa JPL Publication 00-3.

Sarkissian, A., Roscoe, H. K., Fish, D., Van Roozendael, M., Gil, M., Dahlback, A., Perliski, L., Pommereau, J.-P. and Lenoble, J. 1995. Ozone and NO_2 air-mass factors for zenith-sky spectrometers: intercomparison of calculations with different radiative transfer models. Geophys. Res. Lett. 22: 1,113-1,116.

Sen, B., Toon, G.C., Blavier, J.-F., Fleming, E.L. and Jackman, C.H. 1996. Balloon-borne observations of mid-latitude fluorine abundance. J. Geophys. Res. 101: 9,045-9,054.

Simon, P.C. 1996. Spectroscopic Measurements of Atmospheric Changes (SMAC) – Final Scientific Report to OSTC, Contracts Nrs. GC/35/002, GC/35/003 and GC/35/004, April 1996: 1-185.

Sinnhuber, B.-M., Chipperfield, M., Enell, C.-F., Friess, U., Hendrick, F., Johnston, P., Kreher, K., Pfeilsticker, K., Platt, U., Richter, A., South, A., Toernkvist, K.K., Van Roozendael, M., Wagner, T. and Wittrock, F. (2000) Comparison of ground-based BrO measurements during THESEO with the SLIMCAT chemical transport model. In: Proceedings of the Fifth European Workshop on Stratospheric ozone, St Jean de Luz, France, 27 Sep-1st Oct 1999. Air Pollution Research Report 73, European Commission - DG XII, Brussels, 2000. EUR 19340: 352-355.

Solomon, S., Schmeltekopf, A.L. and Sander, R.W. 1987. On the interpretation of zenith sky absorption measurements. J. Geophys. Res. 92: 8,311-8,319.

Stamnes, K., Tsay, S. C., Wiscombe, W. J. and Jayaweera, K. 1988. Numerically stable algorithm for discrete-ordinate-method radiative transfer in multiple scattering and emitting layered media. Appl. Opt. 27: 2502-2509.

Steinbrecht, W., Claude, H., Köhler, U. and Hoinka, K.P. 1998. Correlations between tropopause height and total ozone: Implications for long-term changes. J. Geophys. Res. 103: 19,183-19,192.

Stolarski, R.S., and Rundel, R.D. 1975. Fluorine photochemistry in the stratosphere. Geophys. Res. Lett. 2: 443-444.

Toon, O. B., Mckay, C. P., Ackerman, T. P. and Santhanam, K. 1989. Rapid calculation of radiative heating rates and photodissociation rates in inhomogeneous multiple scattering atmospheres. J. Geophys. Res. 94: 16,287-16,301.

Toon, G.C., Blavier, J.-F., Sen, B., Margitan, J.J., Webster, C.R., May, R.D., Fahey, D., Gao, R., Del Negro, L., Proffitt, M., Elkins, J., Romashkin, P.A., Hurst, D.F., Oltmans, S., Atlas, E., Schauffler, S., Flocke, F., Bui, T.P., Stimpfle, R.M., Bonne, G.P., Voss, P.B. and Cohen, R.C. 1999. Comparison of MKIV balloon and ER-2 aircraft measurements of atmospheric trace gases. J. Geophys. Res. 104: 26,779-26,790.

Tsouli A. 2000. Mesures de constituants minoritaires de l'atmosphère en milieu urbain par spectroscopie d'absorption UV-visible et modélisation de la chimie de la troposphère en vue de la prévision des concentrations d'ozone à Bruxelles. PhD thesis, Oct. 2000, ULB.

Van Hoosier, M., Bartoe, J.D., Brueckner, G. and Prinz, D. 1988. Absolute solar spectral irradiance 120 nm - 400 nm (Results from the Solar Ultraviolet Spectral Irradiance Monitor - SUSIM- Experiment on board Spacelab 2). Astro. Lett. and Communications. 27: 163-168.

Van Roozendael, M., Lambert, J.-C. and Roscoe, H.K. Temperature dependent spectral resolution effects in SAOZ UV-visible spectrometers. In: Proceedings of the 7th GOME/SCIAMACHY Workshop, Frascati, Italy, 6-7 April, 1998.

Van Roozendael, M., Peeters, P., Roscoe, H. K., De Backer, H., Jones, A. E., Bartlett, L., Vaughan, G., Goutail, F., Pommereau, J.-P., Kyro, E., Wahlstrom, C., Braathen, G. and Simon, P. C. 1998. Validation of ground-based visible measurements of total ozone by comparison with Dobson and Brewer spectrophotometers. J. Atm. Chem. 29: 55-83.

Van Roozendael, M., Fayt, C., Lambert, J.-C., Pundt, I., Wagner, T., Richter, A. and Chance, K. 1999. Development of a bromine oxide product from GOME. In:

Proceedings of the European Symposium on Atmospheric Measurements from Space (ESAMS), ESA/ESTEC, The Netherlands, 18-21 January 1999. ESA WPP-161, Vol. 2: 543-547.

Van Roozendael M., Fayt, C., Hendrick, F., Hermans, C., Lambert, J.-C., Fonteyn, D., Sinnhuber, B.-M. and Chipperfield, M. P. Seasonal and Diurnal Variation of BrO Column Abundances above Harestua (60°N) and Haute Provence (44°N) during THESEO (2000a). In: Proceedings of the 5th European Symposium on Polar Stratospheric Ozone Research, Saint-Jean-de-Luz, September 27-October 1, 1999. Air Pollution Research Report, European Commission - DG XII, Brussels: 332-335.

Vandaele, A. C., Hermans, C., Simon P. C., Van Roozendael, M., Guilmot, J. M., Carleer, M. and Colin, R. 1996. Fourier transform measurement of NO_2 absorption cross-sections in the visible range at room temperature. J. Atmos. Chem. 25: 289-305.

Vandaele, A. C., Hermans,, C., Simon, P. C., Carleer, M., Colin, R., Fally, S., Mérienne, M.-F., Jenouvrier, A. and Coquart, B. 1998. Measurements of the NO_2 absorption cross-section from 42000 cm^{-1} to 10000 cm^{-1} (238-1000 nm) at 220 K and 294 K. J. Quant. Radiat. Transfer 59 (3-5): 171-184.

Vander Auwera, J., Kleffmann, J., Flaud, J.-M., Pawelke, G., Bürger, H. and Pétrisse, R. 2000. Absolute □$_2$ line intensities of HOCl by simultaneous measurements in the infrared with a tunable diode laser and far-infrared region using a Fourier transofrm spectrometer. J. Mol. Spectrosc. 204: 36-47.

Vander Auwera, J. 2000a. Absolute intensities measurements in the □$_4$+□$_5$ Band of $^{12}C_2H_2$: Analysis of Herman-Wallis effects and forbidden transitions. J. Mol. Spectrosc. 201: 143-150.

Vander Auwera, J. 2000b. Infrared absorption cross-sections of two substituted ethanes: 1,1-difluoroethane (HFC-152a) and 1,2dichloroethane. J. Quant. Spectrosc. Radiat. Transfer 66: 143-151.

Wagner, T., and Platt, U. 1998. Satellite mapping of enhanced BrO concentrations in the troposphere. Nature 395: 486-490.

Wagner, T. 1999. Satellite Observations of Atmospheric Halogen Species. PhD thesis, University of Heidelberg.

Waugh, D.W., Considine, D.B. and Fleming, E.L. 2001. Is upper stratospheric chlorine decreasing? Geophys. Res. Lett. 28: 1,187-1,190.

WMO Report 44. 1999. Scientific Assessment of Ozone Depletion: 1998, World Meteorological Organization – Global Ozone Research and Monitoring Project. WMO, 41, Avenue Guiseppe Motta, P.O. Box 2300, Geneva 2, CH 1211, Switzerland.

World Climate Programme (WCP). 1986. A preliminary cloudless standard atmosphere for radiation computation. WMO Report WMO/TD 24, World Meteorological Organisation.

Zander, R., Gunson, M.R., Farmer, C.B., Rinsland, C.P., Irion, F.W. and Mahieu, E. 1992. The 1985 chlorine and fluorine inventories in the stratosphere based on ATMOS observations at 30° North latitude. J. Atmos. Chem.15: 171-186.

Zander, R., Ehhalt, D.H., Rinsland, C.P., Schmidt, U., Mahieu, E., Rudolph, J., Demoulin, P., Roland, G., Delbouille, L. and Sauval, A. J. 1994. Secular trend and seasonal variability of the column abundance of N_2O above the Jungfraujoch station determined from IR solar spectra. J. Geophys. Res. 99: 16,745-16,756.

Zander, R., Mahieu, E., Gunson, M. R., Abrams, M. C., Chang, A. Y., Abbas, M., Aellig, C., Engel, A., Goldman, A., Irion, F. W., Kämpfer, N., Michelsen, H. A., Newchurch, M. J., Rinsland, C. P., Salawitch, R. J., Stiller, G. P. and Toon, G. C. 1996. The 1994 northern midlatitude budget of stratospheric chlorine derived from ATMOS/ATLAS-3 observations. Geophys. Res. Lett. 23: 2,357-2,360.

Zander, R., Mahieu, E., Demoulin, P., Servais, C. and Mélen, F. 2000. Long-term evolution of the loading of CH_4, N_2O, CO, CCl_2F_2, $CHClF_2$ and SF_6 above Central Europe during the last 15 years. In: Proceedings of the Second International Symposium on Non-CO_2 Greenhouse Gases - Scientific Understanding, Control and Implementation. Noordwijkerhout, The Netherlands, September 8-10, 1999. Sp. Vol. Environmental Monitoring and Assessment, 2000 Kluwer Academic Publishers: 211-216.

Zobov, N. F., Belmiloud, D., Polyansky, O. L., Tennyson, J., Shirin, S. V., Carleer, M., Jenouvrier, A., Vandaele, A. C., Bernath, P. F., Mérienne, M.-F. and Colin, R. 2000. The near ultraviolet rotation-vibration spectrum of water. J. Chem. Phys. 113 (4): 1,546-1,552.

ESAC PUBLICATIONS

Aliwell, S.R., Van Roozendael, M., Johnston, P.V., Richter, A., Wagner, T., Arlander, D.W., Burrows, J.P., Fish, D.J., Jones, R.L., Tørnkvist, K.K., Lambert, J.-C., Pfeilsticker K. and Pundt, I. In press 2001. Analysis for BrO in Zenith-Sky Spectra: An Intercomparison Exercise for Analysis Improvement. J. Geophys. Res.

Arijs, E., Simon, P.C., Nevejans, D., De Mazière, M., Lippens, C., Müller, J.F., Fonteyn, D., Fussen, D., Amelynck, C., Neefs, E., Vanderpoorten, W., Van Roozendael, M., Hermans, C., Gillotay, D., Bolsée, D., Vandaele, A.C. 1996. Atmospheric research related to Global Change at the Belgian Institute for Space Aeronomy. Nouvelles de la Science et des Technologies 14: 43-58.

Ballard, J., Knight, R. J., Vander Auwera, J., Herman, M., Di Leonardo, G., Masciarelli, G., Nicolaisen, F. M., Beukes, J. A., Christensen, L. K., McPheat, R., Duxbury, G., Freckleton, R., Shine, K. P. 2000. An intercomparison of laboratory measurements of absorption cross-sections and integrated absorption intensities for HCFC-22. J. Quant. Spectrosc. Radiat. Transfer 66: 109-128.

Barry, J., Locke, G., Scollard, D., Sidebottom, H., Treacy, J., Clerbaux, C., Colin, R., Franklin, J. 1997. 1,1,1,3,3-pentafluorobutane (HFC-365mfc): atmospheric degradation and contribution to radiative forcing. Int. J. Chem. Kinet. 29: 607-617.

Bernath, P., Carleer, M., Fally, S., Jenouvrier, A., Vandaele, A. C., Hermans, C., Mérienne, M.-F., Colin, R. 1998. The Wulf bands of oxygen. Chem. Phys. Letters 297: 293-299.

Carleer, M., Jenouvrier, A., Vandaele, A. C., Bernath, P. F., Mérienne, M.-F., Colin, R., Zobov, N. F., Polyansky, O. L., Tennyson, J., Savin, V. A. 1999. The near infrared, visible, and near ultraviolet overtone spectrum of water. J. Chem. Phys. 111 (6): 2,444-2,450.

Chipperfield, M. P., Burton, M., Bell, W., Paton Walsh, C., Blumenstock, T., Coffey, M. T., Hanningan, J. W., Mankin, W. G., Galle, B., Mellqvist, J., Mahieu, E., Zander, R., Notholt, J., Sen, B., and Toon, G. C. 1997. On the use of HF as a reference for the comparison of stratospheric observations and models. J. Geophys. Res. 102 : 12,901-12,919.

Clerbaux, C, Colin, R. and Simon, P.C. 1997. Le potentiel de rechauffement global d'hydrohalo-carbures. Physicalia Mag. 19: 51-73.

Colin, R., Mégie, G., and Borrell, P. 2000. Instruments, In: Overview and synthesis of the scientific results from EUROTRAC. Borrell, P. (Ed), vol 1, chap 1.

De Backer, H., De Muer D. and De Sadelaer, G. 1998. Comparison of ozone profiles obtained with Brewer-Mast and Z-ECC sensors during simultaneous ascents. J. Geophys. Res. 103: 19,641-19,648.

De Backer, H., Köpke, P., Bais, A., Frei, T., Gillotay, D., Haite, C., Heikkilä, A., Koskela, T., Kyrö, E., Lapeta, B., Lorente, J., Mayer, B., Plets, H., Redondaz, A., Renaud, A., Schmalwieser A.W. and Vanicek, K. 1999a. Comparison of measured and modelled UV indices, Meteorological applications.

De Backer, H., Koepke, P., Bais, A., de Cabo, X., Frei, T., Gillotay, D., Haite, C., Heikkila, A., Kanzantzidis, A., Koskela, T., Kyrö, E., Lapeta, B., Lorente, J., Masson, K., Mayer, B., Plets, H., Redondas, A., Renaud, A., Schauberger, G., Schmawieser, A., Schwander, H. and Vanicek, K. In press, 2001. Comparison of Measured and Modelled UV Indices. Meteorological Applications.

De Backer, H. In Press, 2001. Tropospheric ozone trends in Uccle 1969-1999 after homogenisation of the dataset. In: Proceedings from the EUROTRAC symposium 2000. Midgley, P.M., Reuther, M., Williams M. (Ed). Springer Verlag Berlin, Heidelberg 2001.

De Mazière, M., Van Roozendael, M., Hermans, C., Simon, P.C., Demoulin P. and Roland, G. 1998. Quantitative evaluation of the post-Pinatubo NO_2 reduction and recovery, based on 10 years of FTIR and UV-visible spectroscopic measurements at the Jungfraujoch. J. Geophys. Res. 103: 10,849-10,858.

De Mazière, M., Hennen, O., Van Roozendael, M., Demoulin P. and De Backer, H. 1999. Daily ozone vertical profile model built on geophysical grounds, for column retrieval from atmospheric high-resolution spectra. J. Geophys. Res.104: 23,855-23,869.

De Muer, D., De Backer, H. and Van Haver, Ph. 1995. Analysis of 25 years of regular ozone soundings at Uccle (Belgium). Atmospheric ozone as a Climate gas. Wang, W. and Isaksen, I. (Ed). Springer-Verlag Berlin: 113-129.

De Muer, D., Heylen, R., Van Loey, M. and De Sadelaer, G. 1997. Photochemical ozone production in the convective mixed layer, studied with a tethered balloon sounding system. J. Geophys. Res. 102: 15,933-15,947.

Fally, S., Vandaele, A. C., Carleer, M., Hermans, C., Jenouvrier, A., Mérienne, M.-F., Coquart, B., Colin, R. 2000. Fourier transform spectroscopy of the O_2 Herzberg bands. III. Absorption cross-sections of the collision-induced bands and of the Herzberg continuum. J. Mol. Spectrosc. 204: 10-20.
Gillotay, D., Walravens, B., Bolsée D. and Simon, P.C. 1999. Comparison of erythemal doses based on solar UV measurements from filter- and spectro-radiometers. Adv. Space Res.

Goldman, A., Schoenfeld, W. G., Goorvitch, D., Chackerian C. Jr., Dothe, H., Mélen, F., Abrams, M. C. and Selby, J. E. A. 1998. Update line parameters for OH $X^2\tilde{I}IX^2II$ (v",v') transitions, J. Quant. Spectrosc. Radiat. Transfer 59: 453-470, 1998.

Hamdouni, A., Barbe, A., Demoulin, P. and Zander, R. 1997. Retrieval of ozone vertical column amounts from ground-based high resolution infrared solar spectra. J. Quant. Spectrosc. Radiat. Transfer 57: 11-22.

Hermans, C., Vandaele, A.C., Carleer, M., Fally, S., Colin, R., Jenouvrier, A., Coquart, B., Mérienne, M.-F. 1999. Absorption cross-sections of atmospheric constituents: NO_2, O_2, and H_2O. Environ. Sci. & Pollut. Res. 6 (3): 151-158.

Hermans, C., Jenouvrier, A., Fally, S., Carleer, M., Vandaele, A. C., Mérienne, M.-F., Coquart, B. and Colin R. In preparation. Absorption cross-sections of oxygen: the IR and visible bands.

Inngold, T., Schmid, B., Mätzler, C., Demoulin P. and Kämpfer, N. 2000. Modeled and empirical approaches for retrieving columnar water vapor from solar transmittance measurements in the 0.72, 0.82 and 0.94 μm absorption bands. J. Geophys. Res. 105: 24,327-24,343.

Jaquinet-Husson, N., Arié, E., Barbe, A., Bjoraker, G., Bonnet, B., Brown, L. R., Camy-Peyret, C., Champion, J.-P., Chédin, Chursin, A. A., Clerbaux, C., Duxbury, G., Flaud, J.-M., Fourrié, N., Fayt, A., Graner, G., Gamache, R., Goldman, A., Golovko, V., Guelachvilli, G., Hartmann, J. M., Hilico, J. C., Hillman, J., Lefèvre, G., Lellouch, E., Mikhaïlenko, S. N., Naumenko, O. V., Nemtchninov, V., Newnham, D. A., Nikitin, A., Orphal, J., Perrin, A., Reuter, D. C., Rinsland, C. P., Rosenmann, L., Rothman, L. S., Scott, N. A., Selby, J., Sinitsa, L. N., Sirota, J. M., Smith, A. M.,

Smith, K. M., Tyuterev, V. G., Tipping, R. H., Urban, S., Varanasi, P., Weber, M. 1999. The 1997 spectroscopic GEISA databank. J. Quant. Spectrosc. Radiat. Transfer 61: 4,205-4,254.

Jenouvrier, A., Mérienne, M.-F., Coquart, B., Carleer, M., Fally, S., Vandaele, A. C., Hermans, C., Colin, R. 1999. Fourier transform spectroscopy of the O_2 Herzberg bands. I. Rotational Analysis. J. Mol. Spectrosc. 198: 136-162.

Köpke, P, Bais, A., Balis, D., Buchwitz, M., De Backer, H., de Cabo, X., Eckert, P., Eriksen, P., Gillotay, D., Koskela, T., Lapeta, B., Litynska, Z., Lorente, J., Mayer, B., Renaud, A., Ruggaber, A., Schauberger, G., Seckmeyer, G., Seifert, P., Schmalwieser, A., Schwander, H., Vanicek K. and Weber, M. 1998. Comparison of models used for UV index -calculations, Photochemistry and Photobiology 67 (6): 657-662.

Lambert, J.-C., Van Roozendael, M., De Mazière, M., Simon, P.C., Pommereau, J.-P., Goutail, F., Sarkissian, A. and Gleason, J.F. 1999. Investigation of pole-to-pole performances of space-borne atmospheric chemistry sensors with the NDSC. J. Atm. Sci. GOMAC Special issue 56: 176-193.

Lambert, J.C., Van Roozendael, M., Simon, P.C., Pommereau, J.P., Goutail, F., Gleason, J.F., Andersen, S.B., Arlander, D.W., Buivan, N.A., Claude, H., De La Noe, J., De Maziere, M., Dorokhov, V., Eriksen, P., Green, A., Karlsen Tornqvist, K., Kastad Hoiskar, B.A., Kyro, E., Leveau, J., Merienne, M.F., Milinevsky, G., Roscoe, H.K., Sarkissian, A., Shanklin, J.D., Staehelin, J., Wahlstrom Tellefsen, C. and Vaughan, G. 2000. Combined characterisation of GOME and TOMS total ozone measurements from space using ground-based observations from the NDSC. Adv. Space Res. 26: 1,931-1,940.

Lambert, J.-C., Van Roozendael, M., Simon, P.C., Pommereau, J.-P., Goutail, F., Andersen, S.B., Arlander, D.W., Bui Van, N.A., Claude, H., de La Noë, J., De Mazière, M., Dorokhov, V., Eriksen, P., Gleason, J.F., Karlsen Tørnkvist, K., Kåstad Høiskar, B.A., Kyrö, E., Leveau, J., Merienne, M.-F., Milinevsky, G., Roscoe, H.K., Sarkissian, A., Shanklin, J.D., Staehelin, J., Tellefsen, C.W. and Vaughan, G. In press 2001. Combined characterisation of GOME and TOMS total ozone using ground-based observations from the NDSC. Adv. Space Res.

Lemoine, René and H. De Backer. 2001. Assessment of the Uccle ozone sounding time series quality using SAGE II data. J. Geophys. Res. 106:14,515-14,523.

Mahieu, E., Zander, R., Delbouille, L., Demoulin, P., Roland, G. and Servais, C. 1997. Observed Trends in Total Vertical Column Abundances of Atmospheric Gases from IR Solar Spectra Recorded at the Jungfraujoch. J. Atmos. Chem. 28: 227-243.

Mélen, F., Mahieu, E., Zander, R., Rinsland, C. P., Demoulin, P., Roland, G., Delbouille, L. and Servais, C. 1998. Vertical column abundances of COF_2 above the Jungfraujoch station derived from ground-based infrared solar observations. J. Atmos. Chem. 29: 119-134.

Mérienne, M.F., Jenouvrie, A., Coquart, B., Carleer, M., Fally, S., Colin, R., Vandaele, A.C. and Hermans, C. 2000. Fourier transform spectroscopy of the O_2 Herzberg bands. II. Band oscillator strengths and transition moments. J. Mol. Spectrosc. 202 (2): 171-193.

Mérienne, M.F., Jenouvrier, A., Coquart, B., Carleer, M., Fally, S., Colin, R., Vandaele A.C., Hermans C. Submitted[a]. Improved data set for the Herzberg band systems of $^{16}O_2$. J. Mol. Spectrosc.

Mérienne, M.-F., Jenouvrie, A., Carleer, M., Colin, R., Vandaele, A. C., Bernath, P. F., Polyansky, O. L., Tennyson, J. Submitted[b]. The visible and near ultraviolet rotation-vibration spectrum of HOD. J. Mol. Spectrosc.

Michelsen, H. A., Manney, G. L., Gunson, M. R. and Zander, R. 1998. Correlations of stratospheric abundances of NO_y, O_3, N_2O and CH_4 derived from ATMOS measurements. J. Geophys. Res. 103: 28,347-28,359.

Michelsen, H. A., Manney, G. L., Gunson, M. R., Rinsland, C. P. and Zander, R. 1998. Correlations of stratospheric abundances of CH_4 and N_2O derived from ATMOS measurements, Geophys. Res. Lett. 25: 2,777-2,780.

Michelsen, H. A., Manney, G. L., Irion, F. W., Toon, G. C., Gunson, M. R., Rinsland, C. P., Zander, R., Mahieu, E., Newchurch, M. J., Purcell, P. N., Remsberg, E. E., Russell III, J. M., Pumphrey, H. C., Waters, J. W., Bevilacqua, R. M., Kelly, K. K. and Webster, C. R. In press 2001. ATMOS Version 3 water vapor measurements: comparisons with ATMOS Version 2 retrievals and observations from NOAA and Harvard Lyman-a hygrometers, MkIV, MAS, HALOE, and MLS. J. Geophys. Res.

Pfeilsticker, K., Arlander, D.W., Burrows, J. P., Erle, F., Gil, M., Goutail, F., Hermans, C., Lambert, J.C., Platt, U., Pommereau, J.P., Richter, A., Sarkissian, A., Van Roozendael, M., Wagner, T. and Winterrath, T. 1999. Intercomparison of the

detected influence of tropospheric clouds on UVvisible absorptions detected during the NDSC intercomparison campaign at OHP in June 1996. Geophys. Res. Lett.,26: 1,169-1,172.

Plets, H. and Vynckier, C. 2000. A comparative study of statistical total column ozone forecasting models, J. Geophys. Res. 105: 26,503-26,517.

Pougatchev, N. S., Jones, N. B., Connor, B. J., Rinsland, C. P., Becker, E., Coffey, M. T., Connors, V. S., Demoulin, P., Dzhola, A. V., Fast, H., Grechko, E. I., Hannigan, J. W., Koike, M., Kondo, Y., Mahieu, E., Mankin, W. G., Mittermeier, R. L., Notholt, J., Reichle H. G. Jr., Steele, L. P., Toon, G. C., Yurganov, L. N., Zander, R. and Zhao, Y. 1998. Ground-based Infrared Solar Spectroscopic Measurements of Carbon Monoxide During 1994 MAPS Flights, J. Geophys. Res. 103: 19,317-19,325.

Rbaihi, E., Belafhal, A., Vander Auwera, J., Naim, S., Fayt, A. 1998. Fourier transform spectroscopy of carbonyl sulfide from 4700 to 8000 cm^{-1} and new global analysis of $^{16}O^{12}C^{32}S$, J. Mol. Spectrosc. 191: 32-44.

Rinsland, C. P., Jones, N. B., Connor, B. J., Logan, J. A., Pougatchev, N. S., Goldman, A., Murcray, F. J., Stephen, T. M., Pine, A. S., Zander, R., Mahieu, E. and Demoulin, P. 1998. Northern and southern hemisphere ground-based infrared spectroscopic measurements of tropospheric carbon monoxide and ethane, J. Geophys. Res.103: 28,197-28,217.

Rinsland, C. P., Gunson, M. R., Wang, P. H., Arduini, R. F., Baum, B. A., Minnis, P., Goldman, A., Abrams, M. C., Zander, R., Mahieu, E., Salawitch, R. J., Michelsen, H. A., Irion, F. W. and Newchurch, M. J. 1998a. ATMOS/ATLAS 3 Infrared Profile Measurements of Trace Gases in the November 1994 Tropical and Subtropical upper Troposphere, J. Quant. Spectrosc. Radiat. Transfer 60: 891-901.

Rinsland, C. P., Gunson, M. R., Wang, P.-H., Arduini, R. F., Baum, B. A., Minnis, P., Goldman, A., Abrams, M. C., Zander, R., Mahieu, E., Salawitch, R. J., Michelsen, H. A., Irion, F. W. and Newchurch, M. J. 1998b. ATMOS/ATLAS 3 Infrared Profile Measurements of Clouds in the Tropical and Subtropical upper Troposphere, J. Quant. Spectrosc. Radiat. Transfer 60: 903-919.

Rinsland, C. P., Salawitch, R. J., Gunson, M. R., Solomon, S., Zander, R., Mahieu, E., Goldman, A., Newchurch, M. J., Irion, F. W. and Chang, A. Y. 1999. Polar stratospheric descent of NO_y and CO and Arctic denitrification during winter 1992-1993, J. Geophys. Res. 104: 1,847-1,861.

Rinsland, C. P., Goldman, A., Connor, B. J., Stephen, T. M., Jones, N. B., Wood, S. W., Murcray, F. J., David, S. J., Blatherwick, R. D., Zander, R., Mahieu, E. and Demoulin, P. 2000. Correlation relationships of stratospheric molecular constituents from high spectral resolution, ground-based infrared solar absorption spectra, J. Geophys. Res. 105: 14,637-14,652.

Rinsland, C. P., Mahieu, E., Zander, R., Demoulin, P., Forrer J. and Buchmann, B. 2000. Free tropospheric CO, C_2H_6 and HCN above central Europe: recent measurements from the Jungfraujoch station including the detection of elevated columns during 1998, J. Geophys. Res. 105: 24,235-24,249.

Rinsland, C. P., Salavitch, R. J., Osterman, G. B., Irion, F. W., Sen, B., Zander, R., Mahieu, E. and Gunson, M. R. 2000. Stratospheric CO at Tropical and Mid-Latitudes : ATMOS Measurements and Photochemical Steady-State Model Calculations, Geophys. Res. Lett. 27: 1,395-1,398.

Rinsland, C. P., Goldman, A., Zander, R. and Mahieu, E. 2001. Enhanced Tropospheric HCN Columns above Kitt Peak during the 1982-1983 and 1997-1998 El Niño Warm Phases. J. Quant. Spectrosc. Radiat. Transfer 69: 3-8.

Roscoe, H.K., Johnston, P.V., Van Roozendael, M., Richter, A., Roscoe, J., Preston, K.E., Lambert, J.-C., Dzienus, S., Winterrath, T., Burrows, J., Sarkissian, A., Goutail, F., Pommereau, J.-P., D'Almeida, E., Hottier, J., Coureul, C., Didier, R., Pundt, I., Bartlett, L.M., McElroy, C.T., Kerr, J.E., Elokhov, A., Giovanelli, G., Ravegnani, F., Premuda, M., Kostadinov, I., Erle, F., Wagner, T., Pfeilsticker, K., Kenntner, M., Marquard, L.C., Gil, M., Puentedura, O., Arlander, W., Kaastad-Hoiskar, B.A., Tellefsen, C.W., Heese, B., Jones, R.L., Aliwell, S.R. and Freshwater, R.E. 1999. Slant column measurements of O_3 and NO_2 during the NDSC intercomparison of zenith-sky UV-visible spectrometers in June 1996, J. Atmos. Chem. 32: 281-314.

Sinnhuber, B.-M., Arlander, D.W., Bovensmann, H., Burrows, J.B., Chipperfield, M.P., Enell, C.F., Friess, U., Hendrick, F., Johnston, P.V., Jones, R.L., Kreher, K., Mohamed-Tahrin, N., Muller, R., Pfeilsticker, K., Platt, U., Pommereau, J.-P., Pundt, I., Richter, A., South, A.M., Tørnkvist, K.K., Van Roozendael, M., Wagner, T. and Wittrock, F. Submitted 2001. The global distribution of stratospheric bromine monoxide: Intercomparison of measured and modeled slant column densities, J. Geophys. Res.

Van Roozendael, M., De Mazière, M., Hermans, C., Simon, P. C., Pommereau, J.-P., Goutail, F., Tie, X.X., Brasseur, G., Granier, C. 1997. Ground-Based Observations of Stratospheric NO_2 at High and Mid-Latitudes in Europe After the Mt. Pinatubo Eruption, J. Geophys. Res. 102: 19,171-19,176.

Van Roozendael, M., Peeters, P., Roscoe, H. K., De Backer, H., Jones, A.E., Vaughan, G., Goutail, F., Pommereau, J.-P., Kyro, E., Wahlstrom, C., Braathen, G. and Simon, P.C. 1998. Validation of Ground-Based Visible Measurements of Total Ozone by Comparison With Dobson and Brewer Spectrophotometers, J. Atm. Chem. 29: 55-83.

Van Roozendael, M., Richter, A., Wagner, T., Pundt, I., Arlander, D. W., Burrows, J. P., Chipperfield, M., Fayt, C., Johnston, P. V., Lambert, J.-C., Kreher, K., Pfeilsticker, K., Platt, U., Pommereau, J.-P., Sinnhuber, B.-M., Tørnkvist, K. K. and Wittrock, F. In press 2001. Intercomparison of BrO Measurements From ERS-2 Gome, Ground-Based and Balloon Platforms, Adv. Space Res.

Vandaele, A. C., Hermans C., Simon, P. C., Van Roozendae,l M., Guilmot, J. M., Carleer, M. and Colin, R. 1996. Fourier transform measurement of NO_2 absorption cross-sections in the visible range at room temperature. J. Atmos. Chem. 25: 289-305.

Vandaele, A.C., Hermans, C., Simon, P.C., Carleer, M., Colin, R., Fally, S., Mérienne, M.F., Jenouvrier, A. and Coquart, B. 1997. Measurements of the NO2 absorption cross-section from 42000 cm-1 to 10000 cm-1 (238-1000 nm) at 220 K and 294 K. J.Q.S.R.T. 59: 171-184.

Vandaele, A. C., Hermans, C., Simon, P. C., Carleer, M., Colin, R., Fally, S., Mérienne, M.-F., Jenouvrier, A. and Coquart, B. 1998. Measurements of the NO_2 absorption cross-section from 42000 cm^{-1} to 10000 cm^{-1} (238-1000 nm) at 220 K and 294 K. J. Quant. Radiat. Transfer 59 (3-5): 171-184.

Vandaele, A. C. and Carleer, M. 1999. Development of Fourier transform spectrometry for UV-visible DOAS measurements of tropospheric minor constituents, Applied Optics 38: 2,630-2,639.

Vander Auwera, J., Kleffmann, J., Flaud, J.-M., Pawelke, G., Bürger, H. and Pétrisse, R. 2000. Absolute □$_2$ line intensities of HOCl by simultaneous measurements in the infrared with a tunable diode laser and far-infrared region using a Fourier transofrm spectrometer. J. Mol. Spectrosc. 204: 36-47.

Vander Auwera J. 2000a. Absolute intensities measurements in the $\square_4$:+$\square_5$ Band of $^{12}C_2H_2$: Analysis of Herman-Wallis effects and forbidden transitions. J. Mol. Spectrosc. 201: 143-150.

Vander Auwera J. 2000b. Infrared absorption cross-sections of two substituted ethanes: 1,1-difluoroethane (HFC-152a) and 1,2dichloroethane. J. Quant. Spectrosc. Radiat. Transfer 66: 143-151.

Van Weele, M., Blumthaler, M., Brognier, C., Engelsen, O., Gillotay, D., Lenoble, J., Martin, T., Den Outer, P., Pfister, G., Ruggaber, A., Walravens B. and Wehs, P. 1998. From model intercomparison towards benchmarks UV spectra for real atmospheric cases. ECUV Special Section, J. Geophys. Res.

Vaughan, G., Roscoe, H. K., Bartlett, L. M., O'Connor, F. M., Sarkissian, A., Van Roozendael, M., Lambert, J.-C., Simon, P. C., Karlsen, K., Høiskar, B. A. K, Fish, D. J., Jones, R. L., Freshwater, R., Pommereau, J.-P., Goutail, F., Andersen, S. B., Drew, D. G., Hughes, P. A., Moore, D., Mellqvist, J., Hegels, E., Klupfel, T., Erle, F., Pfeilsticker, K. and Platt, U. 1997. An Intercomparison of ground-based UV-visible sensors of ozone and NO_2, J. Geophys. Res. 102: 1,411-1,422.

Zander, R., Demoulin, P., Mahieu, E., Roland, G., Delbouille, L. and Servais, C. 1997. Total Vertical Column Abundances of Atmospheric Gases Derived from IR Remote Solar Observations made at the Jungfraujoch Station. In: Transport and Chemical Transformation of pollutants in the Troposphere. Vol. 6 - Tropospheric Ozone Research. Østein, H (Ed). Springer-Verlag, Berlin Heidelberg New York: 413-425.

Zerefos, C.S., Balis, D.S., Bais, A.F., Gillotay, D., Simon, P.C., Mayer, B. and Seckmeyer, G. 1997. Variability of UV-B at four stations in Europe, Geophys. Res. Lett. 24: 1,363-1,366.

Zerefos, C.S., Meleti, C., Balis, D.S., Bais, A.F. and Gillotay, D. 1998. On long-term spectral UV-B changes in the 90's in Europe. Adv. Space Res.

Zobov, N. F., Belmiloud, D., Polyansky, O. L., Tennyson, J., Shirin, S. V., Carleer, M., Jenouvrier, A., Vandaele, A. C., Bernath, P. F., Mérienne, M.-F. and Colin, R., 2000. The near ultraviolet rotation-vibration spectrum of water. J. Chem. Phys. 113 (4): 1,546-1,552.

Conference proceedings, abstracts, posters, oral presentations and theses

Adams, F., Brasseur, G., Colin, R., De Muer, D., Gérard, J.-C., Maenhaut, W., Peeters, J., Simon, P. C., Van Cleemput, O., Vander Auwera, J., Vanderstraeten, M., Van Der Werf, A., Van Grieken, R., Vinckier, C. and Zander, R. Belgian Impulse Programme GLOBAL CHANGE 1990-1996: Changes in the chemical Composition of the Atmosphere. Federal Office of Scientific, Technical and Cultural Affairs (OSTC), Brussels, 1997.

Bach, M., Depiesse, C., El Hachtouky, R., El Idrissi, M. I., Herman, M., Herregodts, F., Hurtmans, D., Mellouki, A., Vander Auwera, J. 2000. High resolution laboratory spectroscopy of compounds of atmospheric and astrophysical interest. ATO Advanced Research Workshop Spectroscopy from space, Bratislava, Slovaquie, 31 Oct-4 Nov. 2000.

Bais, A.F., Gardiner, B.G., Slaper, H., Kirsch, P.J., Kazaszis, S., Blumthaler, M., Brognier, C., Eriksen, P., Gillotay, D., Josefsson, W., Kjeldstad, B., Koskela, T., Kuik, F., Leszczynski, K., Mckenzie, R.L., Redondas, A., Reinen, H.A.J.M., Seckmeyer, G., Svenoe, T., Wardle, D.I., Weeb, A.R., Weihs, P., Allabar, W., Bernhard, G., Gay, M., Groebner, J., Huber, M., Johnston, P.V., Karlsson, J.E., Keer, J.B., Kotkamp, M., Manzano, J., Masserot, D., Meleti, C., Pachart, E., Persen, T., Rengarajan, G., Saarinen, E., Schmitt, R., Schreder, J., Thorseth, T.M., Visuri, R., Walravens B. and Wauben, W. 1998. Results from comparisons of global solar UV spectra measured during the SUSPEN intercomparison campaign. Oral presentation at the European Conference on Atmospheric UV Radiation, Helsinki, Finland, June 29 - July 2, 1998.

Barret, B., Mahieu, E., Carleer, M., De Mazière, M., Colin, R. and Zander, R. 1999. Tropospheric boundary layer investigations by differential ground-based solar FTIR spectrometry. In: Environmental Sensing and Applications, SPIE Proceedings 3821: 116-123.

Barret, B., De Mazière, M., Demoulin, P., Mahieu, E., Mélen, F., Connor, B.J. and Jones, N. 2000. Investigation of height-resolved information in ground-based high-resolution infrared solar spectra above the Jungfraujoch. In: Atmospheric Ozone, Proceedings of the Quadrennial Ozone Symposium, Sapporo 2000. 3-8 July 2000, pp; 301-302, 2000.

Bojkov, B.R., De Mazière, M., Krognes, T., Paltiel, R., Walker, S.E. 2000. Metadata guidelines for atmospheric and oceanic sciences: a prototype for NADIR. NILU Report TR-12/2000.

Bojkov, B.R., De Mazière, M., Krognes, T. and Koopman, R. To be published Metadata guidelines for atmospheric and oceanographic sciences: NADIR Index for ESA Envisat Cal/Val HDF files.

Bolsee, D., Gillotay, D. and Walravens, B. Relative spectral response of filter radiometers: an example of calibration facility. 1998. Poster presentation at the European Conference on Atmospheric UV Radiation, Helsinki, Finland, June 29 - July 2, 1998.

Carleer, M., Fally, S., Colin, R., Coquart, B., Jenouvrier, A., Mérienne, M.F., Hermans, C., Vandaele, A.C. and Simon, P.C. O_2 Absorption Cross-sections and Absolute Intensities in the UV-visible using a Fourier Transform Spectrometer. 1996. In: Proceedings of the ASA Symposium 1996, Reims, France, 3-5 September 1996: 87-90.

Carleer M., Jenouvrier, A., Vandaele, A. C., Bernath, P., Colin, R., Mérienne, M.-F., Tennyson, J., Polyansky, L. and Zobov, N. F. 1998. New measurements of the water vapour absorption spectrum in the near-UV to near-IR region. In: Water in the Gas Phase Conference, Paris, France, June 21-24, 1998.

Carleer, M., Colin, R. and Vandaele, A. C. 1998. Using a Fourier transform spectrometer for tropospheric UV-Vis DOAS measurements. In: Spectroscopic Atmospheric Environmental Monitoring Techniques. Proceedings of SPIE, Barcelona, Spain, 21-24 Sept. 1998. Schafer K. (Ed). Europto Series 3493: 11-19.

Carleer, M., Fally, S., Colin, R., Jenouvrier, A., Coquart, B., Mérienne, M.-F., Vandaele, A. C. and Hermans, C. 1998. Fourier transform spectroscopy of atmospheric gases, In: Spectroscopic Atmospheric Environmental Monitoring Techniques. Proceedings of SPIE, Barcelona, Spain, 21-24 Sept. 1998, Schafer K. (Ed). Europto Series 3494: 94-103.

Carleer M. 1999. Tutorial lecture: FTS line shapes and their importance in atmospheric measurements in the UV-VIS and the IR, Europto conference on Environmental Sensing and Applications, Munich, Germany, 14-18 June 1999, SPIE vol. 3821: 70-87.

Carleer M. 2000. A Windows program to measure accurately the line intensities of high resolution Fourier transform spectra. EOS/SPIE symposium on Remote Sensing, Barcelone, 25-29 Sept. 2000.

Chichery, A., Barbe, A., Bourgeois, M. T., Demoulin, P. and Tyuterev, G. 1999. The 3 v_3 bands of isotopic ozone 668 and 686. Proceedings of Atmospheric Spectroscopy Applications 1999, Reims, France, September 1-3, 1999: 147-150.

Coheur, P.-F., Fally, S., Carleer, M., Colin, R., Vandaele, A.C., Hermans, C., Jenouvrie,r A. and Mérienne, M.-F. 2000. Absolute intensities of water vapor lines in the near ultraviolet and visible regions. EOS/SPIE symposium on Remote Sensing, Barcelone, 25-29 Sept. 2000.

Colin R., Carleer, M., Guilmot, J.M., Simon, P.C., Vandaele, A.C., Hermans, C., Dufour, P. and Fayt, C. 1997. The Belgian Contribution to Differential Optical Absorption Studies of the Troposphere between 1990 and 1995. In: Instruments Development for Atmospheric Research and Monitoring. Bösenberg, J., Brassington, D. and Simon, P.C. (Eds). Springer-Verlag, Berlin: 347-354.

Colin R., Carleer, M., Tsouli, A., Simon, P.C., Vandaele, A.C. and Bernath, P. 1998. Ultraviolet spectroscopic measurements of ozone. Journée d'étude "Ozone dans la troposphère", SSTC, Brussels, June 26, 1998.

Coquart, B., Jenouvrier, A., Mérienne, M.F., Hermans, C., Vandaele, A.C., Simon, P.C., Tsouli, A., Carleer M., Fally, S., Rizopoulos, A. and Colin, R. 1997. New Measurements of the NO_2 Absorption Cross-section with a Fourier Transform Spectrometer from 10000 to 42000 cm-1 and its Temperature and Pressure Dependence. In: Proceedings of the ASA Symposium 1996, Reims, France, 3-5 September 1996: 79-82.

De Backer, H. 1999. Homogenisation of ozone vertical profile measurements at Uccle. Wetenschappelijke en technische publicaties van het K.M.I. 7, ISSN D1999/0224/007, KMI, Ukkel: 26.
(ftp://ftp.kmi-irm.be/dist/meteo/hugo/publ/1999/o3prof.ps)

De Backer, H., Köpke, P., Bais, A., Cuevas, E., Gillotay, D., Haite, C., Heikkilä, A., Koskela, T., Kyrö, E., Lapeta, B., Lorente, J., Mayer, B., Plets, H., Renaud, A., Schmalwieser A.W. and Vanicek, K. 1999. Comparison of measured and modelled UV Indices. 24th General assembly of EGS, Geophysical Research Abstracts. Vol. 1, number 2: 477.

De Backer, H. In press, 2001. Tropospheric ozone trends in Uccle 1969-1999 after homogenisation of the dataset. In: Proceedings from the EUROTRAC symposium

2000. Midgley, P.M., Reuther, M., Williams M. (Ed). Springer Verlag Berlin, Heidelberg 2001.

De Mazière, M., Hennen, O., Barbe, A., Mérienne, M.F., Hamdouni, H. and Demoulin, P. 1997. Study of Spectroscopic, Meteorological and Climatological Parameters for the Analysis of O_3 FTIR Spectra: a Case-study for Jungfraujoch Data. In: Proceedings of the ASA Symposium 1996, Reims, France, 3-5 September 1996: 149-152.

De Mazière, M., Hennen, O., Van Roozendael, M., Simon, P. C., Demoulin, P., Roland, G., Zander, R., De Backer, H. and Peter, R. 1998. Towards improved evaluations of total ozone at the Jungfraujoch, using vertical profile estimations based on auxiliary data. In: Proceedings of the XXVIII Quadrennial Ozone Symposium, L'Aquila, Italy, September 12-21, 1996. Bojkov, R. and Visconti G (Eds): 25-28.

De Mazière, M., Van Roozendael, M., Hennen, O., Demoulin, P. and Mahieu, E. 1999. Revision of the O3 trend analysis at the Jungfraujoch station. Poster presentation at the Sixth Scientific Conference of the International Global Atmospheric Chemistry Project (IGAC), Bologna, Sept. 13-17, 1999.

De Mazière, M. 1999. COSE, Compilation of Atmospheric Observations in Support of Satellite Measurements over Europe. In: Proceedings of the European Symposium on Atmospheric Measurements from Space (ESAMS). ESA/ESTEC, The Netherlands, 18-21 January 1999. ESA WPP-161, Vol. 2: 655-659.

De Mazière, M. 1999. Atmospheric observations: synergy between ground, airborne and space-based observations. Invited Lecture at 5ème Colloque ASA, Reims, France, Sept. 1-3, 1999.

De Mazière, M., Mahieu, E., Van Roozendael, M., Lambert, J.C., Peeters, P., Barret, B., Hendrick, F., Hermans, C., Van Daele, A.C., Simon, P.C., Zander, R., Demoulin, P., De Muer, D., De Backer, H., Carleer, M. and Colin, R. 2000. Atmospheric changes at the origin of the environment and climate issue (Atmosfeerveranderingen aan de basis van de milieu- en klimaatproblematiek). Invited speaker op het symposium 'Tussen Onderzoek en beleid', DWTC-SSTC, Congrespaleizen, Brussels, Nov. 24-25, 1999. In: Proceedings, D/2000/1191/23, OSTC: 61-67.

De Mazière, M., Van Roozendael, M., Bojkov, B. R., de la Noë, J., Mahieu, E. and Neuber, R. In press. Archiving of atmospheric data: data formats and database. In:

Proceedings of the International Radiation Symposium 2000, St. Petersburg, July 24-29, 2000.

De Mazière, M. In press 2000. Atmospheric Observations in the perspective of changing climate and environment, and the synergy between ground-based, airborne and space-based measurements. In: Proceedings of the ICTP School on 'Exploring the Atmosphere by Remote Sensing Techniques'. Dirs. Guzzi, R., Furlan, G. and Pfeilsticker K. Trieste, Oct. 18-Nov. 5, 1999. Springer-Verlag.

De Mazière, M. 2001. Trace gas measurements at the Jungfraujoch by Fourier transform infrared and UV-Visible spectrometry. Invited seminar at the Institut für Meteorologie und Klimaforschung, Forschungszentrum Karlsruhe, Jan. 16, 2001.

De Muer, D., and De Backer, H. 1994. Influence of sulfur dioxide trends on Dobson measurements and on electrochemical ozone soundings. In: SPIE proceedings series, Atmospheric ozone conference, Tromsö 28-29 June 1993, Vol. 2047: 18-26.

Demoulin, P., Mahieu, E., Zander, R., Roland, G., Delbouille, L., Servais, C., De Mazière, M. and Van Roozendael, M. 1998. The Current Budget of NO_y above the Jungfraujoch as derived from IR Solar Observations. In: Proceedings of the Fourth European Symposium on Polar Stratospheric Ozone Research, Schliersee, Germany, September 22-26, 1997. European Commission, Air pollution Research Report 66: 427-430.

Demoulin, P., Zander, R., Mélen, F., Mahieu, E. and Servais, C. 1999. Column abundance measurements of formaldehyde above the Jungfraujoch. In: Proceedings of Atmospheric Spectroscopy Applications 1999, Reims, France, September 1-3, 1999: 59-62.

Fally, S., Carleer, M., Hermans, C., Vandaele, A. C., Coquart, B., Jenouvrier, A., Mérienne, M.-F. and Colin, R. 1999. UV and visible absorption cross-sections of O_2. In: Proceedings of the ASA Symposium 1999, Reims, France, September 1-3, 1999. Université de Reims-G.S.M.A. (Eds) : 153-156.

Fally, S., Carleer, M., Hermans, C., Vandaele, A. C., Coquart, B., Jenouvrier, A., Mérienne, M.-F. and Colin, R. Absorption cross-sections of O_2: The Herzberg band systems, the Herzberg continuum, and the collision-induced bands. Inspired by Herberg: Spectroscopy for the year 2000, Cornwall, Ontario, October 30-November 3, 1999.

Fischer, H., Blom, C., Oelhaf, H., Carli, B., Carlotti, M., Delbouille, L., Ehhalt, D., Flaud, J.-M., Isaksen, I., Lopez-Puertas, M., McElroy C. T. and Zander R. 2000. ENVISAT-MIPAS: An Instrument for Atmospheric Chemistry and Climate Research. In: ESA Report SP-1229: 124.

Galle, B., Mellqvist, J., Samuelsson, J., Magnusson, S., Van Roozendael, M., Fayt, C., Hermans, C., Hendrick, F., Chipperfield, M. P. and Bjerke A. 2000. FTIR and UV-Visible Measurements of Stratospheric Trace Species at Harestua, Norway during THESEO and Comparison with a 3-D Model. In: Proceedings of the 5th European Workshop on Stratospheric Ozone, Saint Jean de Luz, France, 27 Sept.-1 Oct. 1999. Air Pollution Research Report 73, European Commission - DG XII, Brussels, 2000.

Gillotay, D., Bolsee, D. and Walravens, B. 1998. UV Effective doses: Comparison of erythemal doses obtained by solar UV measurements with broadband UV meter, filter radiometer and spectro-radiometer. Poster presentation at the European Conference on Atmospheric UV Radiation, Helsinki, Finland, June 29 - July 2, 1998.

Gillotay, D., Müller, J.-F., Walravens, B. and Simon, P.C. 1998. The influence of ozone and clouds on the UV climatology in Uccle, Belgium. Atmospheric Ozone. In Proceedings of the Quadrennial Ozone Symposium at l'Aquila, Italy, 12-21 Sept. 1996. R.J. Bojkov and G. Visconti (Eds): 849-852.

Gillotay, D., Pletz, H., De Backer, H. and Bolsee, D. 1998. Comparison of predicted and measured UV index for the Brussels area Uccle-Belgium (Lat. 50°48'N, Long. 4° 21'E, Alt. 120m asl). Poster presentation at the European Conference on Atmospheric UV Radiation, Helsinki, Finland, June 29 - July 2, 1998.

Gillotay D., Walravens, B. and Simon, P.C. Comparison of erythemal doses based on solar UV measurements from filter- and spectro-radiometers. Oral presentation at the 32nd COSPAR Scientific Assembly, Nagoya, Japan, 12-19 July, 1998.

Hendrick, F., Mueller, R., Sinnhuber, B.-M., Bruns, M., Burrows, J.P., Chipperfield, M. P., Fonteyn, D., Richter, A., Van Roozendael, M. and Wittrock F. 2000. Simulation of BrO Diurnal Variation and BrO Slant Columns : Intercomparison Exercise Between Three Model Packages. In: Proceedings of the 5th European Workshop on Stratospheric Ozone, Saint Jean de Luz, France, 27 Sept.-1 Oct. 1999. Air Pollution Research Report 73, European Commission - DG XII, Brussels, 2000.

Hennen, O., De Mazière, M., Van Roozendael, M., Lambert, J.-C., Mahieu, E., Demoulin, P., Roland, G., Godin, S., De Backer H. 1998. Observations coupled to

the overpasses of the polar vortex over mid-latitude Europe in winter 1995-1996. Polar stratospheric ozone 1997. In: Proceedings of the 4th European Symposium on Stratospheric Ozone Research, Schliersee, Bavaria, Germany, Sept. 22-26, 1997: 451-454.

Hermans C., Vandaele, A.C., Simon, P.C., Carlee, M., Fally, S., Colin, R., Coquart, B., Jenouvrier, A., Mérienne M.F. 1997. NO2 and O2 Absorption Cross-sections for Atmospheric measurements. In: Proceedings of the ASA Symposium 1996, Reims, France, 3-5 September 1996: 83-86.

Hermans C., Vandaele, A. C., Carleer, M., Fally, S., Colin, R., Jenouvrier, A., Coquart, B. and Mérienne, M.-F. 1998. FT Measurements of absorption cross-sections of atmospheric gases. 7th GOME/SCIAMACHY Workshop, Frascati, Italy, 6-7 April 1998.

Hermans C., Vandaele, A. C., Carleer, M., Fally, S., Colin, R., Jenouvrier, A., Coquart, B. and Mérienne, M-F. FT. Measurements of absorption cross-sections of atmospheric gases, SCUVS III Workshop, Paris, France, 28-30 April, 1998.

Hermans, C., Vandaele, A. C., Carleer, M., Fally, S., Colin, R., Jenouvrier, A., Coquart, B. and Mérienne M.-F. FT Measurements of absorption cross-sections of atmospheric gases. In: Proceedings of the 7th GOME/SCIAMACHY Workshop, Frascati, Italy, 6-7 April, 1998.

Hermans, C., Vandaele, A. C., Carleer, M., Fally, S., Colin, R., Bernath P.F., Jenouvrier, A., Coquart, B. and Mérienne, M.-F. FT Absorption Cross-Sections of Atmospheric Constituents: NO2, O2 and H2O. 1998. Poster presentation at the 6th FECS Conference on Chemistry and the Environment, Copenhagen, August 26 to 28, 1998.

Hermans, C., Vandaele, A.C., Coquart, B., Jenouvrier, A., Mérienne M.-F., Fally S., Carleer, M., Colin, R. 2000. Absorption Bands of O_2 and its Collision Induced Bands in the 30000-7700 cm^{-1} wavenumber Region. In: Proceedings of the International Radiation Symposium IRS 2000, St Petersbourg, 24-29 July. 2000.

Jenouvrier, A., Mérienne, M.-F., Coquart, B., Fally, S., Carleer, M., Colin, R., Hermans, C. and Vandaele A. C. 1999. Reinvestigation of the molecular oxygen transitions in the 42000-75000 cm-1 wavenumber region. In: Proceedings of the ASA Symposium 1999, Reims, France, September 1-3, 1999. Université de Reims-G.S.M.A. (Eds): 157-160.

Kelder, H., Platt, U., Simon, P.C., Timmermans, R., Aben, I., Burrows, J.P., Camy-Peyret, C., Hilsenrath, E., Kerridge, B., Künzi, K., Lambert, J.-C., Lelieveld, J., Levelt, P., McKenna, D., Perner, D., Piters, A., Attema, E., Balzer, W., Bruzzi, S., Durville, M. and Friker, A. 1999. SCIAMACHY Validation. In: Proceedings of the European Symposium on Atmospheric Measurements from Space (ESAMS), ESA/ESTEC, The Netherlands, 18-21 January 1999. ESA WPP-161, Vol. 2: 643-647.

Koepke, P., Bais, A.F., Balis, D.S., Buchwitz, M., De Backer, H., De Cabo, X., Eckert, P., Eriksen, P., Gillotay, D., Heikkila, A., Koskela, T., Lapeta, B., Litynska, Z., Lorente, J., Mayer, B., Renaud, A., Ruggaber, A., Schauberger, G., Seckmeyer, G., Schmalwieser, A.W., Schwander, H., Vanicek K. and Weber, M. 1998. UV index calculations: absolute and relative agreement of models with different complexity. Oral presentation at the European Conference on Atmospheric UV Radiation, Helsinki, Finland, June 29-July 2, 1998.

Kurylo, M. J. and Zander, R. J. 2000. The NDSC-Its status after ten years of operation. In: Proceedings of the the International Quadrennial Ozone Symposium, Sapporo, Japan, 3-8 July 2000: 167-168.

Lambert, J.-C., Van Roozendael, M., Simon, P.C., De Mazière, M., Pomereau, J.-P., Goutail, F., Sarkissian, A., Denis, L., Dorokhov, V., Eriksen, P., Kyro, E., Leveau, J., Roscoe, H.K., Tellefsen, C.W., Vaughan, G. Validation of ERS-2 GOME total ozone measurements with the SAOZ ground-based network during the period 28 June-17 August 1996. Atmospheric Ozone. In: Proceedings of the Quadrennial Ozone Symposium at l'Aquila, Italy, 12-21 Sept. 1996. R.J. Bojkov and G. Visconti (Eds): 297-300.

Lambert, J.-C., Van Roozendael, M., Simon, P.C., De Mazière, M., Pomereau, J.-P., Goutail, F., Sarkissian, A., Andersen, S.B., Dorokhov, V., Eriksen, P., Kaastad Hoiskar, B.A. and Kyro, E. 1998. GOME and TOMS total ozone in northern winter 1996-1997: comparison with SAOZ/UV-visible ground-based measurements in the Arctic and at mid-latitude, in Polar stratospheric ozone 1997. In: Proceedings of the 4th European Symposium on Stratospheric Ozone Research, Schliersee, Bavaria, Germany, Sept. 22-26, 1997: 696-699.

Lambert, J.-C., Van Roozendael, M., Granville, J., Gérard, P., Simon, P.C., Claude, H., Staehelin, J. 1998. Comparison of the GOME ozone and NO2 total amounts at mid-latitude with ground-based zenith-sky measurements. Atmospheric Ozone. In: Proceedings of the Quadrennial Ozone Symposium at l'Aquila, Italy, 12-21 Sept. 1996. R.J. Bojkov and G. Visconti (Eds): 301-304.

Lambert, J.-C., Van Roozendael, M., Simon, P.C., Pommereau, J.-P., Goutail, F., Andersen, S.B., Arlander, D.W., Bui Van, N. A., Claude, H., de La Noë, J., De Mazière, M., Dorokhov, V., Eriksen, P., Gleason, J.F., Karlsen Tørnkvist, K., Kåstad Høiskar, B.A., Kyrö, E., Leveau, J., Merienne, M.-F., Milinevsky, G., Roscoe, H.K., Sarkissian, A., Shanklin, J.D., Staehelin, J., Tellefsen, C.W. and Vaughan, G. 1998. Combined characterisation of GOME and TOMS total ozone using ground-based observations from the NDSC. Poster presentation at the 32nd COSPAR Scientific Assembly, Nagoya, Japan, 12-19 July, 1998.

Lambert, J.-C. and De Mazière, M. 1999. Satellite observations of tropospheric ozone-related constituents. In: Proceedings of the 'Ozone in the troposphere: research and policies', Palais des Congrès, Bruxelles, June 26, 1998. DWTC-SSTC publications: 83-90.

Lambert, J.-C., De Mazière, M., Simon, P.C. and Van Roozendael, M. 1999. ESMOS, SCUVS, COSE, and THESEO-BrO: Some EC-sponsored field projects including satellite validation activities. Oral presentation by J.-C. Lambert at the NASA Planning Workshop for Integration of Satellite Cal/Val and Research-Oriented Field Missions in the Next Decade, Snowmass Village, Colorado, USA, 23-27 August 1999.

Lambert, J.-C., Granville, J., Van Roozendael, M., Müller, J.-F., Pommereau, J.-P., Goutail, F. and Sarkissian, A. 1999. A pseudo-global correlative study of ERS-2 GOME NO2 data with ground-, balloon-, and space-based observations. In: Proceedings of the European Symposium on Atmospheric Measurements from Space (ESAMS), ESA/ESTEC, The Netherlands, 18-21 January 1999. ESA WPP-161, Vol. 1: 217-224.

Lambert, J.-C., Granville, J., Van Roozendael, M., Sarkissian, A., Goutail, F., Müller, J.-F., Pommereau, J.-P. and Russell III, J. M. 1999. A climatology of NO2 profile for improved Air Mass Factors for ground-based vertical column measurements. Poster presented at the 5th European Workshop on Stratospheric Ozone, Saint-Jean-de-Luz, France, September 27-October 1, 1999.

Lambert, J.-C., Simon, P.C., De Mazière, M., Van Roozendael, M., Pommereau, J.-P., Goutail, F., Gleason, J.F. and Russell III, J.M. 1999. Integrated use of ground-based network, balloon, satellite and field campaigns data for the validation of ERS-2 GOME. Poster presentation by J.-C. Lambert at the NASA Planning Workshop for Integration of Satellite Cal/Val and Research-Oriented Field Missions in the Next Decade, Snowmass Village, Colorado, USA, 23-27 August 1999.

Lambert, J.-C., Van Roozendael, M., Granville, J., Gerard, P., Simon, P.C., Pommereau, J.-P., Goutail, F. and Sarkissian, A. 1999. Geophysical validation of ERS-2 GOME ozone products by means of correlative observations from the NDSC. In: Proceedings of the European Symposium on Atmospheric Measurements from Space (ESAMS), ESA/ESTEC, The Netherlands, 18-21 January 1999. ESA WPP-161, Vol. 2: 595-601.

Mahieu, E., Zander, R., Mélen, F., Demoulin, P., Servais, C., Delbouille, L. and Roland, G. 1998. Recent Characteristic Budget of Inorganic Chlorine and Fluorine above the Jungfraujoch Station. In: Proceedings of the Fourth European Symposium on Polar Stratospheric Ozone Research, Schliersee, Germany, September 22-26, 1997. European Commission, Air pollution research report 66: 358-361.

Mahieu, E., Zander, R., Demoulin, P., De Mazière, M., Mélen, F., Servais, C., Roland, G., Delbouille, L., Poels, J. and Blomme, R. 2000. Fifteen years-trend characteristics of key stratospheric constituents monitored by FTIR above the Jungfraujoch. In: Proceedings of the Fifth European Symposium on Stratospheric Ozone, St. Jean de Luz, France, September 27 - October 1, 1999. N. R. P. Harris, M. Guirlet and G. T. Amanatidis (Eds). Air pollution Research Report 73 - EUR 19340: 99-102.

Mahieu, E., Zander, R., Mélen, F., Demoulin, P., Rinsland C. P. and Russel III, J. M. 2000. Monitoring the stratospheric chlorine budget during the past decades: the Montreal Protocol at work. In: Proceedings of the International Quadrennial Ozone Symposium, Sapporo, Japan, 3-8 July 2000: 149-150.

Mélen, F., Mahieu, E., Demoulin, Ph., Servais, C. and Zander, R. 1999. Vertical column abundances of COF_2 above the Jungfraujoch Station: update and consolidation of the database with measurements in the ν_4 band region. In: Proceedings of the Atmospheric Spectroscopy Applications 1999, Reims, France, September 1-3, 1999: 77-1 to 77-4.

Paton Walsh, C., Bell, W., Blumenstock, T., Chipperfield, M. P., Galle, B., Mellqvist, J., Notholt, J., Zander, R., Demoulin, P. and Mahieu, E. 1998. Ground-based FTIR Measurements from a Series of European sites during the Winter of 1995/96 and a Comparison with a 3D Chemical Transport Model: Evidence of Chlorine Activation and Ozone Depletion. In: Proceedings of the Fourth European Symposium on Polar Stratospheric Ozone Research, Schliersee, Germany, September 22-26, 1997. European Commission, Air pollution research report 66: 305-308.

Peeters, P., Muller, J.F., Simon, P.C., Gillotay, D., Menklaus, A., Weber, M., Haite, C. and Burrows, J. 1998. Estimation of surface UV dose from satellite data; Comparison with mid-latitude ground measurements. Poster presentation at the European Conference on Atmospheric UV Radiation, Helsinki, Finland, June 29 - July 2, 1998.

Plets, H. 2000. UV index forecasts in Uccle, Wetenschappelijke en technische publicaties van het K.M.I. no 9, ISSN D1999/0224/009, K.M.I., Ukkel: 21.

Prinn, R. G., Zander, R., Elkins, J. W., Fraser, P. J., Ko, M. K. W., Cunnold, D., Engel, A., Gunson, M.R., Mahieu, E., Midgley, P. M., Russell III, J. M. and Weiss, R. F. 1999. Long-lived ozone-related compounds, Scientific Assessment of Ozone Depletion: 1998. In: WMO Report 44: I-1 to I-54. World Meteorological Organization, P.O. Box 2300, Geneva 2, CH 1211, Swizerland, ISBN: 92-807-1722-7.

Pundt, I., T. Wagner, M. Van Roozendael, A. Richter, M.P. Chipperfield, M.P., Burrows, J.P., Fayt, C., Hendrick, F., Pfeilsticker, K., Platt U. and Pommereau J.P. 2000. Simultaneous UV-visible measurements of BrO from balloon, satellite and ground: Implications for tropospheric BrO. In: Proceedings of the fifth European Workshop on Stratospheric Ozone, EUR19340: 316-319.

Richter, A., Van Roozendael, M., Wagner, T., Lambert, J.-C., Arlander, D.W., Burrows, J.P., Fayt, C., Johnston, P.V., Jones, R., Toernkvist, K.K., Kreher, K., Pfeilsticker, K., Platt, U., Pundt, I., South, A., Wittrock, F. 2000. BrO measurements from GOME and from the ground: An intercomparison study. In: Proceedings of the Fifth European Workshop on Stratospheric ozone, St Jean de Luz, France, 27 Sep-1st Oct 1999. EUR 19340: 324-327.

Sarkissian, A., Goutail, F., Pommereau, J.-P., Lambert, J.-C., Van Roozendael, M., Vandenberghe, J.-M., Richter, A., Buchwitz, M., Høiskar, B.A.K., Fløisand, I. and Tørnkvist, K. Improved Air Mass Factors for ground-based total NO2 measurements: A sensitivity study. 5th European.Workshop on Stratospheric Ozone, Saint-Jean-de-Luz, France, 27 September - 1 October 1999.

Schmidt, U., H. K. Roscoe, N. R. P. Harris, K. Künzi, L. Stefanutti, and R. Zander. 1997. Instrument Development and Deployment. In European Research in the Stratosphere - The contribution of EASOE and SESAME to our current understanding of the ozone layer, European Commission - DGXII, Ref. EUR16986/ISBN 92-827-9719-8, 1997: 201-241.

Sinnhuber, B.-M., Chipperfield, M., Enell, C.-F., Friess, U., Hendrick, F., Johnston, P., Kreher, K., Pfeilsticker, K., Platt, U., Richter, A., South, A., Toernkvist, K.K., Van Roozendael, M., Wagner, T. and Wittrock, F. 2000. Comparison of ground-based BrO measurements during THESEO with the SLIMCAT chemical transport model. In: Proceedings of the Fifth European Workshop on Stratospheric ozone, St Jean de Luz, France, 27 Sep-1st Oct 1999. Air Pollution Research Report 73, European Commission - DG XII, Brussels, 2000. EUR 19340: 352-355.

Tsouli A., Vandaele, A.C., Colin, R. and Simon, P.C. 1997. Urban Monitoring during Spring and Summer 1995 in Brussels, Belgium. In: Proceedings of the ASA Symposium 1996, Reims, France, 3-5 September 1996: 143-146.

Tsouli A. 2000. Mesures de constituants minoritaires de l'atmosphère en milieu urbain par spectroscopie d'absorption UV-visible et modélisation de la chimie de la troposphère en vue de la prévision des concentrations d'ozone à Bruxelles, PhD thesis, Oct. 2000, ULB.

Van Roozendael, M., Fayt, C., Hermans, C., Lambert, J.-C. 1998b. Ground-based UV-visible measurements of BrO, NO2, O3 and OClO at Harestua (60°N) since 1994, in Polar stratospheric ozone 1997. In: Proceedings of the 4th European Symposium on Stratospheric Ozone Research, Schliersee, Bavaria, Germany, Sept. 22-26, 1997. Air pollution research report 66, 510-513.

Van Roozendael, M., Lambert, J.-C. and Roscoe, H.K. Temperature dependent spectral resolution effects in SAOZ UV-visible spectrometers. In: Proceedings of the 7th GOME/SCIAMACHY Workshop, Frascati, Italy, 6-7 April, 1998.

Van Roozendael, M., Lambert, J.-C., Simon, P.C., Hansen, G., Dahlback, A., De Muer, D., Schoubs, E., Koopman, R., Vanderwoerd, H., Pieters, A., Barbe, A., Claude, H., de La Noë, J., Merienne, M.-F., Staehelin, J. 1998. Ground-based validation of GOME total ozone measurements by means of Dobson, Brewer and GUV instruments, in Atmospheric Ozone. In: Proceedings of the Quadrennial Ozone Symposium at l'Aquila, Italy, 12-21 Sept. 1996. R.J. Bojkov and G. Visconti (Eds): 665-668.

Van Roozendael, M. et al. THESEO - Stratospheric ozone destruction by bromine: project's overview and first results. Oral communication at the EGS Assembly, Apil 19-23, 1999, Den Hague, The Netherlands.

Van Roozendael, M., Arlander, D. W., De Maziere, M., Fricke, K.H., Goutail, F., Hendrick, F., Klein, U., Oelhaf, H., Pommereau, J.-P., Pundt, I., Richter, A., Sinnhuber, B.M., Toernkvist, K.K. and Wagner, T. 1999. Observations in the high latitude stratosphere during THESEO. Oral presentation at the Fifth European Workshop on Stratospheric ozone, St Jean de Luz, France, 27 Sep.-1st Oct. 1999.

Van Roozendael, M., Fayt, C., Lambert, J.-C., Pundt, I., Wagner, T., Richter, A. and Chance, K. 1999. Development of a bromine oxide product from GOME. In: Proceedings of the European Symposium on Atmospheric Measurements from Space (ESAMS), ESA/ESTEC, The Netherlands, 18-21 January 1999. ESA WPP-161, Vol. 2: 543-547.

Van Roozendael M., Fayt, C., Hendrick, F., Hermans, C., Lambert, J.-C., Fonteyn, D., Sinnhuber, B.-M. and Chipperfield, M. P. Seasonal and Diurnal Variation of BrO Column Abundances above Harestua (60°N) and Haute Provence (44°N) during THESEO (2000a). In: Proceedings of the 5th European Symposium on Polar Stratospheric Ozone Research, Saint-Jean-de-Luz, September 27-October 1, 1999. Air Pollution Research Report, European Commission - DG XII, Brussels: 332-335.

Van Roozendael, M., Arlander, D. W., Burrows, J. P., Chipperfield, M. P., Fayt, C., Hendrick, F., Hermans, C., Johnston, P., Jones, R. L., Kreher, K., Lambert, J.-C., Tahrin, N. M., Newnham, D., Pfeilsticker, K., Platt, U., Pommereau, J.-P., Pundt, I., Richter, A., Sinnhuber, B.-M., South, A., Tørnkvist, K.K. and Wagner, T. 2000b. Lessons learned from 2 years coordinated multi-platform UV-visible observations of atmospheric bromine monoxide. In: Proceedings of the Quadriennal Ozone Symposium, Sapporo, Japan, 3-8 July 2000: 157-158.

Van Weele, M., Blumthaler, M., Brognier, C., Engelsen, O., Gillotay, D., Lenoble, J., Martin, T., Den Outer, P., Pfister, G., Ruggaber, A., Walravens, B. and Wehs, P. 1998. From model intercomparison towards benchmarks UV spectra for real atmospheric cases. Oral presentation at the European Conference on Atmospheric UV Radiation, Helsinki, Finland, June 29 - July 2, 1998.

Vandaele, A.C., Hermans, C., Carleer, M., Tsouli,A. and Colin, R. 1998. Urban Pollution Measurements by UV-Visible DOAS. Poster presentation for the 6th FECS Conference on Chemistry and the Environment, Copenhagen, August 26 - 28, 1998.

Vandaele, A. C., Hermans, C., Fayt, C., Fally, S., Carlee, M., Colin R., Mérienne, M.-F. and Jenouvrier, A. 2000. High resolution Fourier transform measurements of the NO_2 visible absorption cross-section: Temperature and pressure influences on its

atmospheric detection, Proceedings of the International Radiation Symposium IRS 2000, St Petersbourg, 24-29 July 2000.

Zander, R., Demoulin, P., Mahieu, E., Delbouille, L., Roland, G., Mélen, F., Servais, C., De Mazière, M. and Van Roozendael, M. 1998. An overview of NDSC-related activities at the Jungfraujoch through high-resolution infrared solar observations. In: Proceedings of the XXVIII Quadrennial Ozone Symposium, L'Aquila, Italy, September 12-21, 1996. R. Bojkov and G. Visconti (Eds): 1,005-1,008.

Zander, R. 1999. Experimental Studies of Atmospheric Changes and Contribution to the Study of the Earth's Atmosphere from Space (ATMOS). Scientific Report Nr 2 to the OSTC-Research Contract Nr. CG/DD/01D: 1-11.

Zander, R., Mahieu, E., Demoulin, P., Servais, C., Mélen, F., Roland, G. and Delbouille, L. 1999. Spectrometric Solar Observations at the Jungfraujoch for Long-term Atmospheric Monitoring. Actes du Colloque "Ozone dans la Troposphère: la Recherche et la Politique", Bruxelles, 26 juin 1998. SSTC-D/1999/1191/3 : 69-76.

Zander, R., Midgley, P. M. and Kurylo, M. J. 1999. The NDSC in support of satellite data validation and calibration. In: Proceedings of the ESA "European Symposium on Atmospheric Measurements from Space", ESTEC-Nordwijk, The Netherlands, January 18-22, 1999. WPP-161, Vol. 2: 649-654.

Zander, R., Mahieu, E, Mélen, F. and Elkins, J. 2000. An evaluation of the northern mid-latitude tropopause heightening, based on N_2O column abundance measurements above the Jungfraujoch. In: Proceedings of the Fifth European Symposium on Stratospheric Ozone, St. Jean de Luz, France, September 27 - October 1, 1999. N. R. P. Harris, M. Guirlet and G. T. Amanatidis (Eds): 135-138.

Zander, R., Mahieu, E., Demoulin, P., Servais, C., Mélen, F. 2000. Long-term evolution of the loading of CH_4, N_2O, CO, CCl_2F_2, $CHClF_2$ and SF_6 above Central Europe during the last 15 years. In: Proceedings of the Second International Symposium on Non-CO_2 Greenhouse Gases - Scientific Understanding, Control and Implementation, Noordwijkerhout, The Netherlands, September 8-10, 1999. Sp. Vol. Environmental Monitoring and Assessment, 2000. Kluwer Academic Publishers: 211-216.

Zerefos, C.S., Meleti, C., Balis, D.S., Bais, A.F. and Gillotay, D. 1998. On long-term spectral UV-B changes in the 90's in Europe. Oral presentation at the 32nd COSPAR Scientific Assembly, Nagoya, Japan, 12-19 July, 1998